NUREG/CR--3320-Vol.3
DE88 001716

NUREG/CR-3320, Vol. 3
HEDL-TME 87-3
R5

LWR PRESSURE VESSEL SURVEILLANCE DOSIMETRY IMPROVEMENT PROGRAM:

PSF PHYSICS-DOSIMETRY PROGRAM

Edited by:
W.N. McElroy
R. Gold

Manuscript Completed: July 1987
Date Published: October 1987

Hanford Engineering Development Laboratory
Operated by Westinghouse Hanford Company
P.O. Box 1970 Richland, WA 99352
A Subsidiary of Westinghouse Electric Corporation

Prepared for Division of Engineering
Office of Nuclear Regulatory Research
U.S. Nuclear Regulatory Commission
Washington, DC 20555
NRC FIN B5988

ABSTRACT

The metallurgical irradiation experiment at the Oak Ridge Research Reactor Poolside Facility (ORR-PSF) is one of the series of benchmark experiments in the framework of the Light Water Reactor Pressure Vessel Surveillance Dosimetry Improvement Program (LWR-PV-SDIP). The goal of this program is to test, against well-established benchmarks, the methodologies and data bases that are used to predict the irradiation embrittlement and fracture toughness of pressure vessel and support structure steels. The prediction methodology includes procedures for neutron physics calculations, dosimetry and spectrum adjustment methods, metallurgical tests, and damage correlations. The benchmark experiments serve to validate, improve, and standardize these procedures. The results of this program are implemented in a set of ASTM Standards on pressure vessel surveillance procedures. These, in turn, may be used as guides for the nuclear industry and for the Nuclear Regulatory Commission (NRC).

To serve as a benchmark, a very careful characterization of the ORR-PSF experiment is necessary, both in terms of neutron flux-fluence spectra and of metallurgical test results. Statistically determined uncertainties must be given in terms of variances and covariances to make comparisons between predictions and experimental results meaningful. Detailed descriptions of the PSF physics-dosimetry program and its results are reported.

CONTENTS

CONTENTS (Cont'd)

FOREWORD

The Light Water Reactor Pressure Vessel Surveillance Dosimetry Improvement Program (LWR-PV-SDIP) has been established by NRC to improve, test, verify, and standardize the physics-dosimetry-metallurgy, damage correlation, and associated reactor analysis methods, procedures, and data used to predict the integrated effect of neutron exposure to LWR pressure vessels and their support structures. A vigorous research effort attacking the same measurement and analysis problems exists worldwide; and strong cooperative links between US NRC-supported activities at HEDL, ORNL, NBS, and MEA and those supported by CEN/SCK (Mol, Belgium), EPRI (Palo Alto, CA, USA), KFA (Jülich, Germany), and several UK laboratories have been extended to other countries. These cooperative links are strengthened by the active membership of the scientific staff from many countries and laboratories in the ASTM E10 Committee on Nuclear Technology and Applications. Several ASTM E10 subcommittees are responsible for preparation of LWR surveillance standards.

The primary objective of this multilaboratory program is to prepare an updated and improved set of physics-dosimetry-metallurgy, damage correlation, and associated reactor analysis ASTM standards for LWR pressure vessel and support structure irradiation surveillance programs. Supporting this objective are a series of analytical and experimental validation and calibration studies in "Standard, Reference, and Controlled Environment Benchmark Fields," research reactor "Test Regions," and operating power reactor "Surveillance Positions."

These studies will establish and certify the precision and accuracy of the measurement and predictive methods recommended in the ASTM standards and used for the assessment and control of present and end-of-life (EOL) conditions of pressure vessel and support structure steels. Consistent and accurate measurement and data analysis techniques and methods, therefore, will be developed, tested, and verified along with guidelines for required neutron field calculations to correlate changes in material properties with characteristics of the neutron radiation field. Application of established ASTM standards should permit the reporting of measured materials property changes and neutron exposures to an accuracy and precision within 10% to 30%, depending on the measured metallurgical variable and neutron environment.

Assessment of the radiation-induced degradation of material properties in a power reactor requires accurate definition of the neutron field from the outer region of the reactor core to the outer boundaries of the pressure vessel. The accuracy of measurements on neutron flux and spectrum is associated with two distinct components of LWR irradiation surveillance procedures: 1) proper application of calculational estimates of the neutron exposure at in- and ex-vessel surveillance positions, various locations in the vessel wall and in ex-vessel support structures, and 2) understanding the relationship between material property changes in reactor vessels and their support structures, and in metallurgical test specimens irradiated in test reactors and at accelerated neutron flux positions in operating power reactors.

The first component requires verification and calibration experiments in a variety of neutron irradiation test facilities, including LWR-PV mockups, power reactor surveillance positions, and related benchmark neutron fields. The benchmarks serve as a permanent reference measurement for neutron flux and fluence detection techniques. The second component requires serious extrapolation of an observed neutron-induced mechanical property change from research reactor "Test Regions" and operating power reactor "Surveillance Positions" to locations inside the body of the pressure vessel wall and to ex-vessel support structures. The neutron flux at the vessel inner wall is up to one order of magnitude lower than at surveillance specimen positions and up to two orders of magnitude lower than at test reactor positions. At the vessel outer wall, the neutron flux is one order of magnitude or more lower than at the vessel inner wall. Further, the neutron spectra at, within, and leaving the vessel are substantially different.

To meet reactor pressure vessel radiation monitoring requirements, a variety of neutron flux and fluence detectors are employed, most of which are passive. Each detector must be validated for application to the higher flux and harder neutron spectrum of the research reactor "Test Region" and to the lower flux and degraded neutron spectrum at "Surveillance Positions." Required detectors must respond to neutrons of various energies so that multigroup spectra can be determined with accuracy sufficient for adequate damage response estimates. Detectors being used, developed, and tested for the program include radiometric (RM) sensors, helium accumulation fluence monitor (HAFM) sensors, solid state track recorder (SSTR) sensors, and damage monitor (DM) sensors.

The necessity for pressure vessel mockup facilities for physics-dosimetry investigations and for irradiation of metallurgical specimens was recognized early in the formation of the NRC program. Experimental studies associated with high- and low-flux versions of a pressurized water reactor (PWR) pressure vessel mockup are in progress in the US, Belgium, France, and United Kingdom. The US low-flux version is known as the ORNL Poolside Critical Assembly (PCA) and the high-flux version is known as the Oak Ridge Research Reactor (ORR) Poolside Facility (PSF), both located at Oak Ridge, Tennessee. As specialized benchmarks, these facilities provide well-characterized neutron environments where active and passive neutron dosimetry, various types of LWR-PV and support structure neutron field calculations, and temperature-controlled metallurgical specimen exposures are brought together.

The two key low-flux pressure vessel mockups in Europe are known as the Mol-Belgium-VENUS and Winfrith-United Kingdom-NESDIP facilities. The VENUS Facility is being used for PWR core source and azimuthal lead-factor studies, while NESDIP is being used for PWR cavity and azimuthal lead-factor studies. A third and important low-fluence pressure vessel mockup in Europe is identified with a French PV-simulator at the periphery of the Triton reactor. It served as the irradiation facility for the DOMPAC dosimetry experiment to study surveillance capsule perturbations and through-PV-wall radial fluence and damage profiles (gradients) for PWRs of the Fessenheim 1 type.

Results of measurement and calculational strategies outlined here will be made available for use by the nuclear industry as ASTM standards. Code of Federal Regulations 10CFR50 (Cf83) already requires adherence to several ASTM standards that establish a surveillance program for each power reactor and incorporate metallurgical specimens, physics-dosimetry flux-fluence monitors, and neutron field evaluation. Revised and new standards in preparation will be carefully updated, flexible, and, above all, consistent.

This is the third of six planned NUREG reports on the ORR-PSF Experiments and Blind Test. Summary information on each of these six documents follows:

NUREG/CR-3320
PSF Physics-Dosimetry-Metallurgy Experiments:

Vol. 1 (Date Published: July 1986)
PSF Experiments Summary and Blind Test Results - W. N. McElroy, Editor

This document provides PSF experiment summary information and the results of the comparison of measured and predicted physics-dosimetry-metallurgy results for the PSF experiment. This document contains (in an appendix) each final report of participants.

Vol. 2 (Probable Date Published: Fall 1987)
PSF Startup Experiment - W. N. McElroy and R. Gold, Editors

Beyond scope of title, this document supports analysis of the PSF Blind Test and provides experimental conditions, as-built documentation, and PSF physics-dosimetry results for the Startup, SSC-1, and SSC-2 experiments.

Vol. 3 (Date Published: August 1987)
PSF Physics-Dosimetry Program - W. N. McElroy and R. Gold, Editors

Beyond scope of title, this document supports analysis of the PSF Experiment and Blind Test and provides experimental conditions, as-built documentation, and final PSF physics-dosimetry results for SSC, SPVC, and SVBC.

Vol. 4 (Probable Date Published: Fall 1987)
PSF Metallurgy Program - W. N. McElroy and R. Gold, Editors

Beyond scope of title, this document supports analysis of the PSF Experiments and Blind Test and provides experimental conditions, as-built documentation, and final metallurgical data on measured property changes in different pressure vessel steels for SSC-1 and -2 positions, and the (SPVC) simulated PV locations at the 0-T (inner surface), 1/4-T, and 1/2-T positions of the 4/12 PWR PV wall mockup. The corresponding SSC-1, SSC-2, and SPVC locations' neutron exposures are $\sim 2 \times 10^{19}$, $\sim 4 \times 10^{19}$, $\sim 4 \times 10^{19}$, $\sim 2 \times 10^{19}$, and $\sim 1 \times 10^{19}$ n/cm^2, respectively, for a ~550°F irradiation temperature. It contains and/or references available damage analysis results for SVBC using the Vol. 5 metallurgical data base.

Vol. 5 (Date Published: August 1986)
PSF Simulated Void Box Capsule (SVBC) Charpy and Tensile Metallurgical Test Results - J. S. Perrin

Beyond scope of title, this document provides experimental conditions, as-built documentation, and final Charpy and tensile specimen measured property changes in PV support structure and reference steels for the ex-vessel SVBC simulated cavity (void box) for a neutron exposure on the order of 5×10^{16} n/cm^2 (E > 1.0 MeV) for ~95°F irradiation temperature.

Vol. 6 (Probable Date Published by CEN/SCK: 1988)
PSF Simulated Surveillance Capsule (SSC) Results - CEN/SCK/MEA - Ph. Van Asbroech, A. Fabry, and R. Hawthorne, Editors

This document, to be issued by CEN/SCK, provides CEN/SCK/MEA metallurgical data and results from the Mol, Belgium PV steel irradiated in the SSC position for the ORR-PSF physics-dosimetry-metallurgy experiments.

ACKNOWLEDGMENTS

The success of the LWR Pressure Vessel Surveillance Dosimetry Improvement Program (LWR-PV-SDIP) continues to depend on the efforts and the free exchange of ideas and views by representatives of a large number of research, service, regulatory, vendor, architect/engineer, and utility organizations. The information reported herein could not have been developed without the continuing support of the respective funding organizations and their management and technical staffs. Special acknowledgment is due to C. Z. Serpan of NRC for having identified the need for an international program such as the LWR-PV-SDIP and for making it possible by taking a strong overall support and management lead.

The encouragement, help, and contributions of T. U. Marston of EPRI; C. Z. Serpan of NRC; E. B. Norris of SwRI; J. R. Hawthorne of MEA; G. R. Odette of UCSB; D. Pachur of KFA; and A. F. Thomas, T. J. Williams, and R. Squire of RR&A in helping to formulate plans and providing information and guidance for Parts I, II, and III of the PSF Experiments and Blind Test require special and separate acknowledgment.

The dedication and professional skills of the ORR-PSF operations team at ORNL contributed significantly to the success of the PSF experimental program. The authors are indebted to staff members of the ORNL Operating Division Technical Service Group for their contributions and for their support to individual experimenters.

Additional acknowledgment is due to A. Taboada, the NRC Program Manager, and to R. L. Knecht, H. H. Yoshikawa, and L. D. Blackburn of HEDL for their constructive comments and help in program management and the preparation and review of program documentation. Contributions to this document resulting from interactions with other LWR-PV-SDIP participants, who are not identified as authors in this report, are also acknowledged. Very special acknowledgment is given to J. M. Dahlke, who edited this document; to D. C. Smith of the HEDL Irradiation Environment Group; and to the HEDL Technical Publications, Word Processing, Graphics, and Duplicating personnel who contributed to its preparation.

Woody Norris died on February 3, 1986, without having seen the final form of this publication. The authors of this third volume of the PSF Experiments, therefore, would like to dedicate it to his memory as a permanent remembrance of his many contributions, as a scientist-engineer, as the Vice-Chairman of the ASTM E10.05 subcommittee on Nuclear Radiation Metrology, as an officer of the ASTM-EURATOM Symposia Program Committee, and as a good and trusted friend.

ACRONYMS

ANO-1	Arkansas Nuclear One Reactor
ASTM	American Society for Testing and Materials
BC	Battelle Columbus
BMI	Battelle Memorial Institute, Columbus, Ohio
BSR	Bulk Shielding Reactor
BWR	Boiling Water Reactor
B&W	Babcock & Wilcox
CE	Combustion Engineering; Consensus Evaluation
CEN/SCK	Centre d'Etude de l'Energie Nucleaire, Mol, Belgium
CT	Compact Tension
DM	Damage Monitor
DOE	Department of Energy
DOMPAC	Triton Reactor Thermal Shield and Pressure Vessel Mockup, Fontenay-aux-Roses, France
EFPY	Effective Full-Power Years
EIR	Eidgendossisches Institut für Reaktorforschung, Switzerland
ENDF	Evaluated Nuclear Data File
EOL	End-of-Life
EPRI	Electric Power Research Institute, Palo Alto, California
FERRET	Least-Squares Adjustment Code
GE	General Electric Company
HAFM	Helium Accumulation Fluence Monitor
HEDL	Hanford Engineering Development Laboratory, Richland, WA
HSST	Heavy Section Steel Technology
IAEA	International Atomic Energy Agency, Vienna, Austria
IKE	Institut für Kernenergetik und Energiesysteme der Universität Stuttgart, Federal Republic of Germany
KFA	Kernforschungsanlage Jülich GmbH, Federal Republic of Germany
LWR	Light Water Reactor
MEA	Materials Engineering Associates Inc, Oxen Hill, Maryland
MOL	Mol, Belgium
NBS	National Bureau of Standards, Gaithersburg, Maryland
NDC	National Dosimetry Center (at PNL)
NDTT	Nil Ductility Transition Temperature
ΔNDTT	Nil Ductility Transition Temperature Shift
NESDIP	NESTOR Shielding and Dosimetry Improvement Program, UK

ACRONYMS (Cont'd)

NRC	Nuclear Regulatory Commission
NRDC	National Reactor Dosimetry Center (at HEDL)
NRL	Naval Research Laboratory, Washington, DC
NUREG	Nuclear Regulatory Commission Report Designation
ORNL	Oak Ridge National Laboratory
ORR	Oak Ridge (Research) Reactor (at ORNL)
ORR-PSF	Oak Ridge (Research) Reactor - Poolside Facility
PCA	Poolside Critical Assembly (at ORNL)
PSF	Poolside Facility (at ORNL)
PTS	Pressurized Thermal Shock
PV	Pressure Vessel
PVS	Pressure Vessel Simulator
PWR	Pressurized Water Reactor
RM	Radiometric Monitor
RPV	Reactor Pressure Vessel
RT_{NDT}	Reference Temperature, Nil-Ductility Transition
SAND II	Spectrum Analysis by Neutron Detectors, Version II (A Multiple-Foil Adjustment Code)
SDIP	Surveillance Dosimetry Improvement Program
SDM	Sapphire Damage Monitor
SDMF	Simulated Dosimetry Measurement Facility
SPVC	Simulated Pressure Vessel Capsule
SSC	Simulated Surveillance Capsule
SSTR	Solid State Track Recorder
SUNY-NSTF	State University of New York - Nuclear Science and Technology Facilities, Buffalo, NY
SVBC	Simulated Void Box Capsule
SwRI	Southwest Research Institute, San Antonio, Texas
UCSB	University of California at Santa Barbara
UK	United Kingdom
US	United States
USE	Upper Shelf Energy
VB	Void Box
VENUS	PV Mockup (at Mol, Belgium)
West	Westinghouse

S.0 SUMMARY

W. N. McElroy,* R. Gold (HEDL),* F. B. K. Kam (ORNL), A. Fabry (CEN/SCK), E. D. McGarry (NBS), M. Austin (RR&A), and W. Schneider (KFA)

S.1 INTRODUCTION

The metallurgical irradiation experiment at the Oak Ridge Research Reactor Poolside Facility (ORR-PSF) is one of the series of benchmark experiments in the framework of the Light Water Reactor Pressure Vessel Surveillance Dosimetry Improvement Program (LWR-PV-SDIP) (Figure S.1) (Mc87). The goal of this program is to test, against well-established benchmarks, the methodologies and data bases that are used to predict the irradiation embrittlement and fracture toughness of pressure vessel steels in commercial power reactors at the end of their service life and to determine safe operating limits for these vessel steels. Knowledge of pressure vessel steel embrittlement and fracture toughness is also essential to determine the resistance of the vessel under thermal shock conditions and to determine if and when annealing of the vessel is needed. It is also needed for establishing temperature/pressure limits for normal startup and shutdown operating curves. The prediction methodology, as practiced in pressure vessel surveillance programs, includes procedures for neutron physics calculations, dosimetry and spectrum adjustment methods, metallurgical tests, and damage correlations. The benchmark experiments in the framework of the LWR-PV-SDIP serve to validate, improve, and standardize these procedures. The results of this program are implemented in a set of ASTM Standards (Figure S.2) on pressure vessel surveillance procedures, which are in various stages of completion (Mc87). These, in turn, may be used as guides for the nuclear industry and for the regulatory procedures of the Nuclear Regulatory Commission (NRC).

The ORR-PSF experiment was specifically designed to simulate the surveillance capsule-pressure vessel configuration in power reactors and to test the validity of procedures that determine the radiation damage in the vessel from test results of surveillance capsules. Emphasis was on radiation embrittlement and fracture toughness of reactor vessel steels and on damage correlation to test current embrittlement and fracture toughness prediction methodologies. For this purpose, a PSF metallurgical Blind Test was initiated (Mc83d). Experimental results were withheld from the participants; only the information normally contained in surveillance reports was given. The goal was to predict from this limited information the metallurgical test results in the pressure vessel wall capsule. Of particular interest was what effects, if any, differences in fluence rate and fluence spectrum in the surveillance capsule and in the pressure vessel wall may have on the embrittlement and fracture toughness predictions.

To serve as a benchmark, a very careful characterization of the ORR-PSF experiment is necessary, both in terms of neutron flux-fluence spectra and of metallurgical test results. Statistically determined uncertainties must be given in terms of variances and covariances to make comparisons between predictions and experimental results meaningful. Detailed descriptions of the PSF physics-dosimetry program and its results are reported in this volume of the NUREG/CR-3320 series of reports.

*As a result of the consolidation of Hanford contractors on June 29, 1987, WN McElroy, R. Gold, LS Kellogg, and CC Preston, who are authors of subsequent sections, are now staff members of Battelle, Pacific Northwest Laboratories.

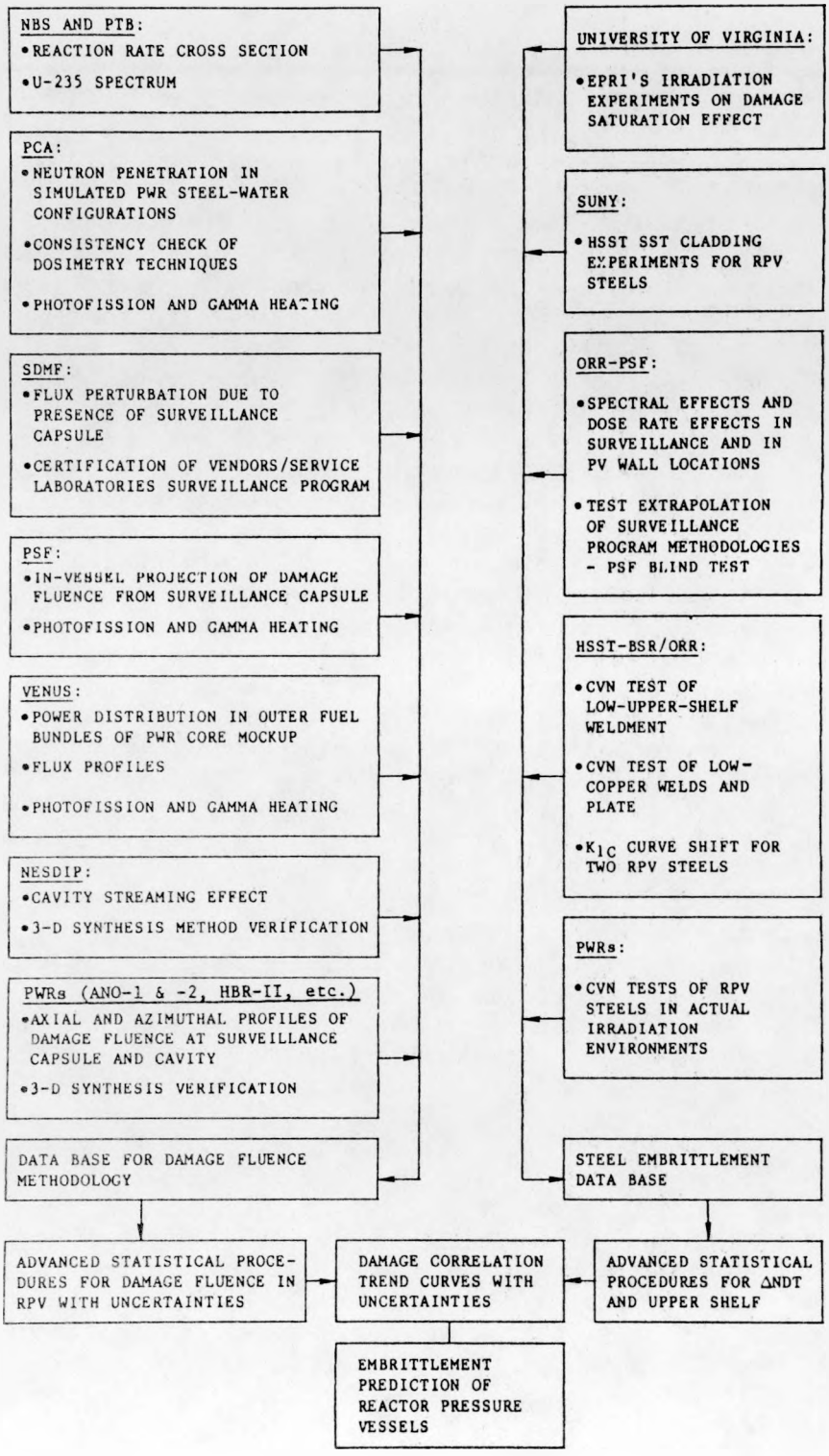

FIGURE S.1. Benchmark Experiments in the Framework of the LWR Pressure Vessel Surveillance Dosimetry Improvement Program.

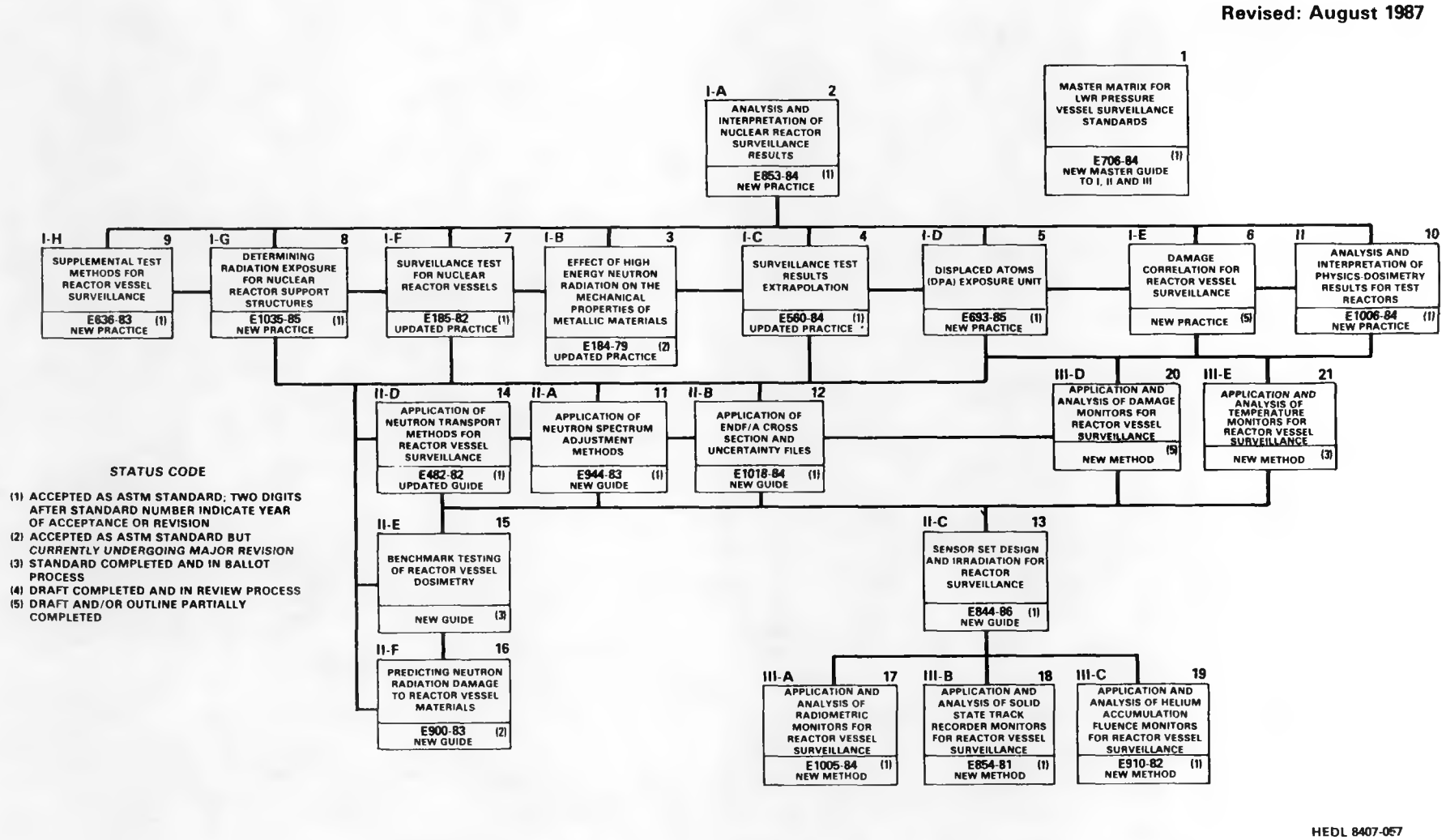

FIGURE S.2. ASTM Standards for Surveillance of LWR Nuclear Reactor Pressure Vessels and Their Support Structures.

S.2 NEUTRON TRANSPORT CALCULATIONS

Flux, fluence, and reaction rate calculations were performed by ORNL for each of the three exposures (two surveillance capsules, a pressure vessel capsule, and a void box capsule) performed during the two-year metallurgical experiment at the ORR-PSF. Motivation for these calculations was prompted by differences of up to 25% between dosimetry measurements performed in the earlier startup scoping experiment and the two-year experiment (see Appendix A).

Following the same simplified calculational methods used in a re-analysis of the startup experiment, fission source distributions were obtained from three-dimensional diffusion theory for most of the 52 cycles active during the course of the complete experiment, combined in small groups, and the resultant ex-core group fluxes calculated by two-dimensional discrete ordinate transport theory. More details can be found in Refs. (Ma84a,Ma84b).

Comparisons of the ORNL-calculated dosimeter end-of-irradiation activities with HEDL measurements agree generally within 15% for the first surveillance capsules, 5% for the second, and 10% for three locations in the pressure vessel capsule, which are as good as, if not somewhat better than, comparisons in the startup experiment. The calculations thus validate the trend of the measurements in both the startup and the two-year experiments and confirm a significant cycle-to-cycle variation in the core leakage. The ORNL tape containing the unadjusted spectral fluences for each of the three exposures that can be used in the metallurgical analysis is thus considered to be accurate to within about 10%.

Details are provided of the calculational methods and data used and the results obtained by RR&A in the successful validation of ANISN methodology and the subsequent calculation of the PSF 4/12 irradiation facility using both the ANISN and MCBEND techniques. These RR&A ANISN (1-D) and MCBEND (3-D Monte Carlo) results provide a further basis for comparison and verification of the overall reliability of the ORNL and RR&A transport calculational results.

S.3 DOSIMETRY AND ADJUSTMENT PROCEDURES

A 10% accuracy, as quoted in the preceding section, for the damage parameter values of the metallurgical specimen is quite sufficient for most metallurgical damage correlation studies. However, since the ORR-PSF experiment is intended to be a benchmark, higher accuracies and a more thorough study of the uncertainties are required. Thus, comprehensive statistical analyses with the use of adjustment procedures were made by program participants to obtain complete three-dimensional fluence-spectrum maps (Figure S.3). These maps included not only the damage parameter values of thermal fluence, $\phi t > 1.0$ MeV, $\phi t > 0.1$ MeV (ϕt = fluence), and dpa in iron, but also reaction rate values for all major broad energy and threshold reactions. Final HEDL dosimetry measurement and exposure parameter results are documented in Appendices A, B, and C; and the results of other LWR-PV-SDIP participants are discussed and, when appropriate, are referenced in Sections 2.0 through 4.0.

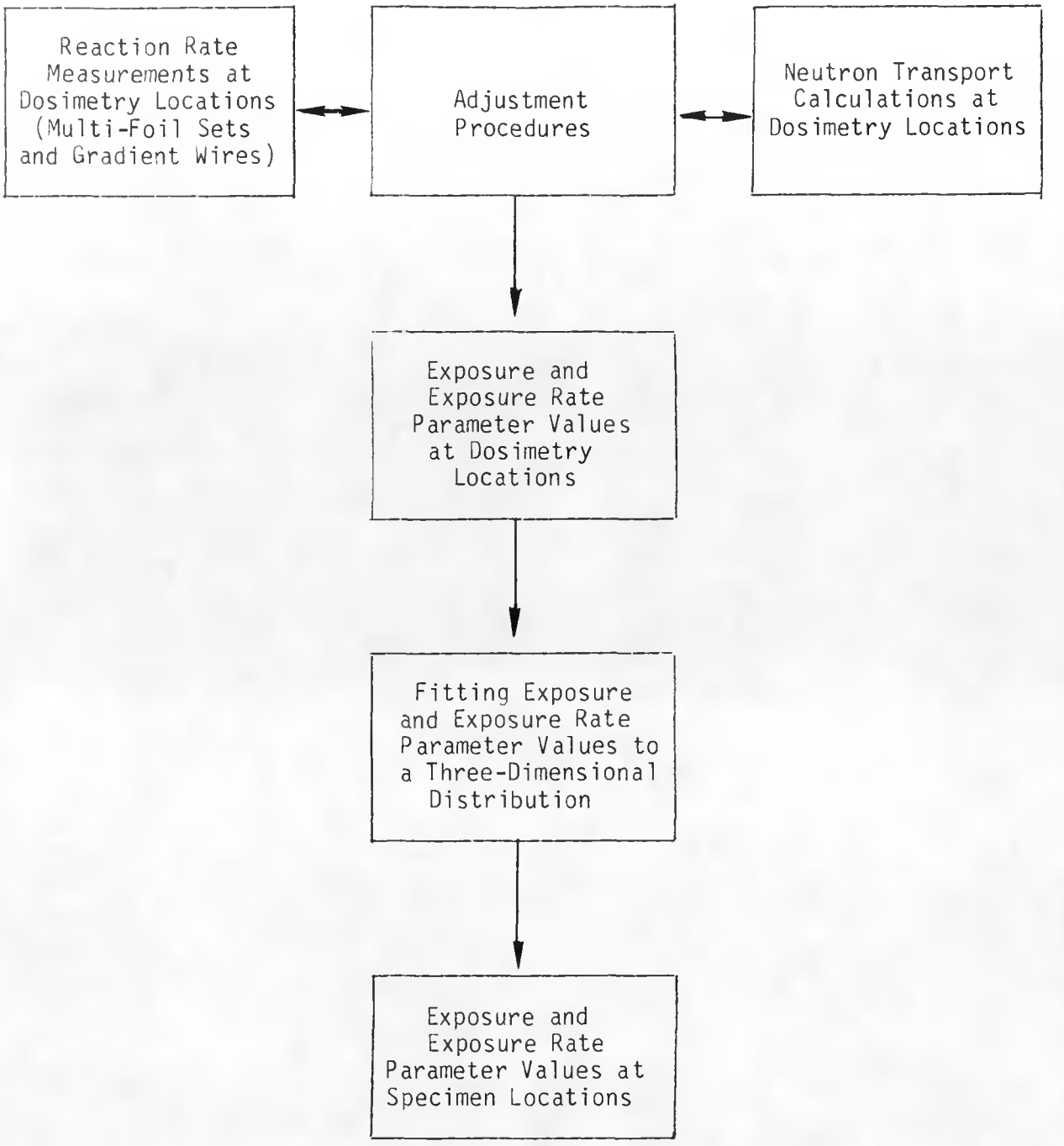

FIGURE S.3. Methodology for the Determination of Exposure and Exposure Rate Parameter Values and Uncertainties.

1.0 DESCRIPTION OF THE EXPERIMENTAL FACILITY - SUMMARY

L. F. Miller (ORNL)

The Simulated Surveillance Capsules (SSC-1 and SSC-2), the Simulated Pressure Vessel Capsule (SPVC), and the Simulated Void Box Capsule (SVBC) provide valuable metallurgical data relative to the changes in properties due to exposure of fast neutrons. This exposure is accomplished by placing the irradiation test specimens adjacent to the Oak Ridge Research Reactor (ORR) in the Pool Side Facility (PSF). Note from Figure 1.0.1 in the exploded portion of the illustration that the SPVC is located behind the SSC and the thermal shield. The void box and SVBC are located directly behind the SPVC. Positioning of the SPVC relative to the SSC and to the face of the ORR core is described in NUREG/CR-3320, Vol. 2, Section 1.1.

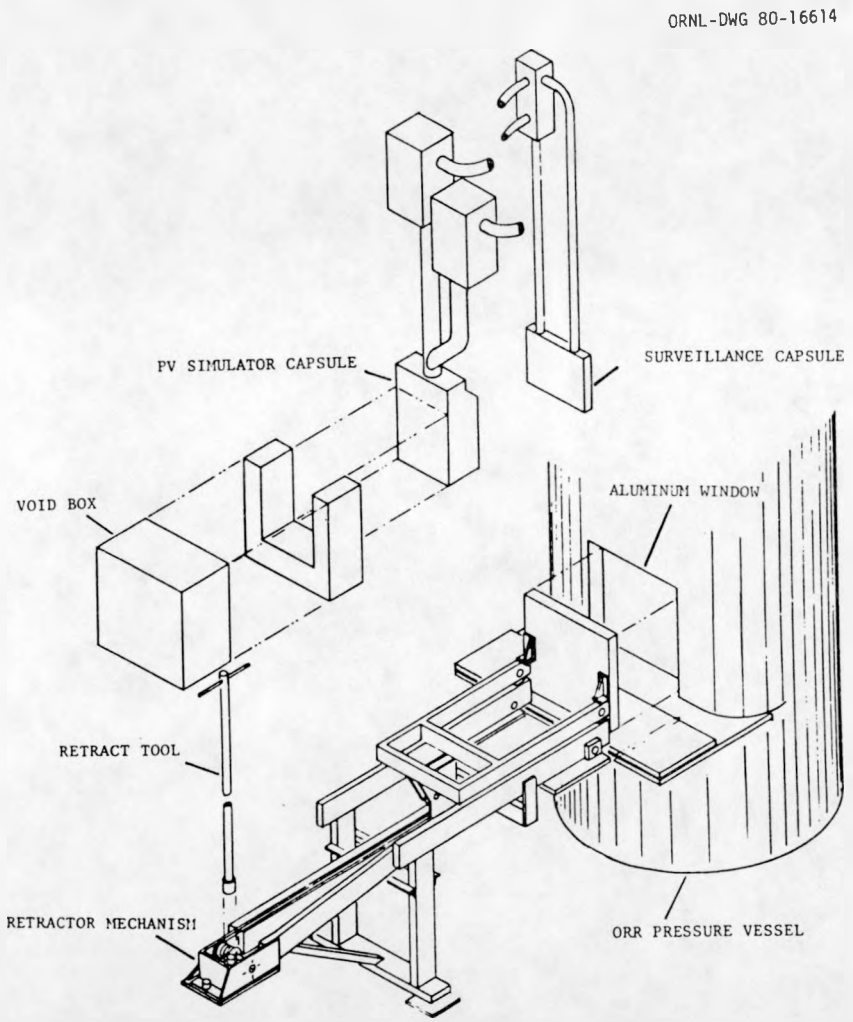

FIGURE 1.0.1. Illustration of the Pool Side Facility and the Oak Ridge Research Reactor Pressure Tank.

1.1 PHYSICAL DESCRIPTION OF THE SSC, SPVC, AND SVBC

L. F. Miller (ORNL)

The locations of the SSC, SPVC, and SVBC relative to the ORR core and aluminum window are illustrated by an elevation view given in Figure 1.1.1. Note that the outside dimensions of the SPVC, or Pressure Vessel Simulator (PVS), PVS are 22.48 cm in depth and 68.58 cm in height and that the outside dimensions of the Void Box (VB) are 30.48 cm in depth and 68.58 cm in height. Also note from Figure 1.1.1 that there is no space between the SPVC and the VB and that there is a water gap of 0.08 cm between the VB and the SVBC. The elevation views, shown in Figures 1.1.2 through 1.1.4, illustrate the overall width to be 40.64 cm.

Internal dimensions and components of the SSCs, SPVC, and SVBC are shown in Figures 1.1.3 through 1.1.8. Note that in the SPVC there are three separate regions for specimens that are separated by heating and cooling regions. Locations of these specimen correspond to the zero (0-T), one-fourth, (1/4-T), and one-half (1/2-T) thickness positions of a reactor pressure vessel. Typical dimensions for a 1-in. (2.54-cm) Charpy specimen are also illustrated at the 1/2-T position. The nichrome electrical heater wires are embedded in steel plate that supports each specimen face, and the regions between specimens are cooled by water flowing through pipes. Internal heat conduction rates can be changed significantly by adjusting the mixture of the neon-helium cover gas maintained in the SPVC that surrounds each capsule and fills gas gaps on the SPVC front and back faces. A more detailed physical description of the SSCs, SPVC, and SVBC is given in Section 1.1 of NUREG/CR-3320, Vol. 4.

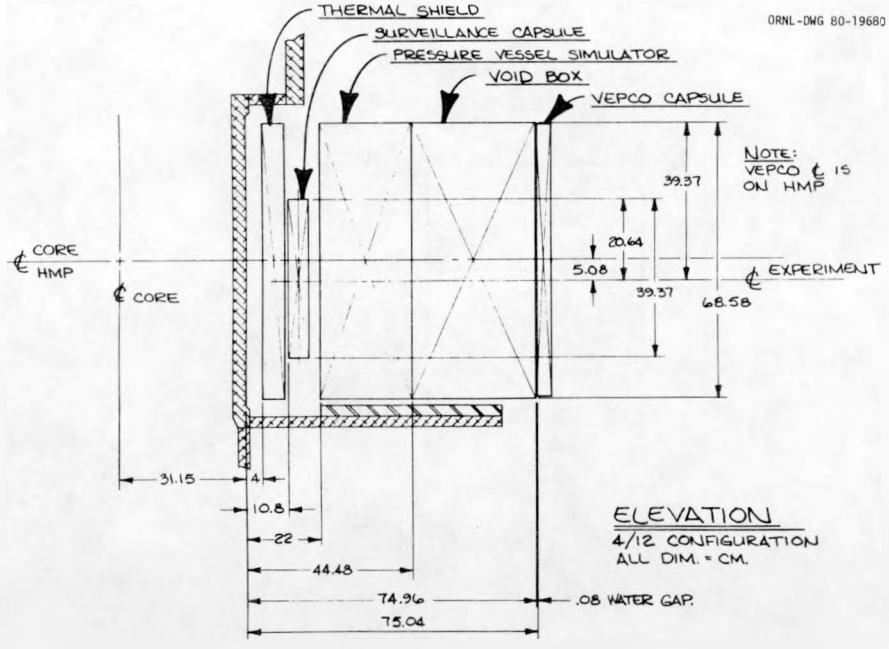

FIGURE 1.1.1. Elevation View Schematic of the Pool Side Facility with Component Identifications and External Dimensions.

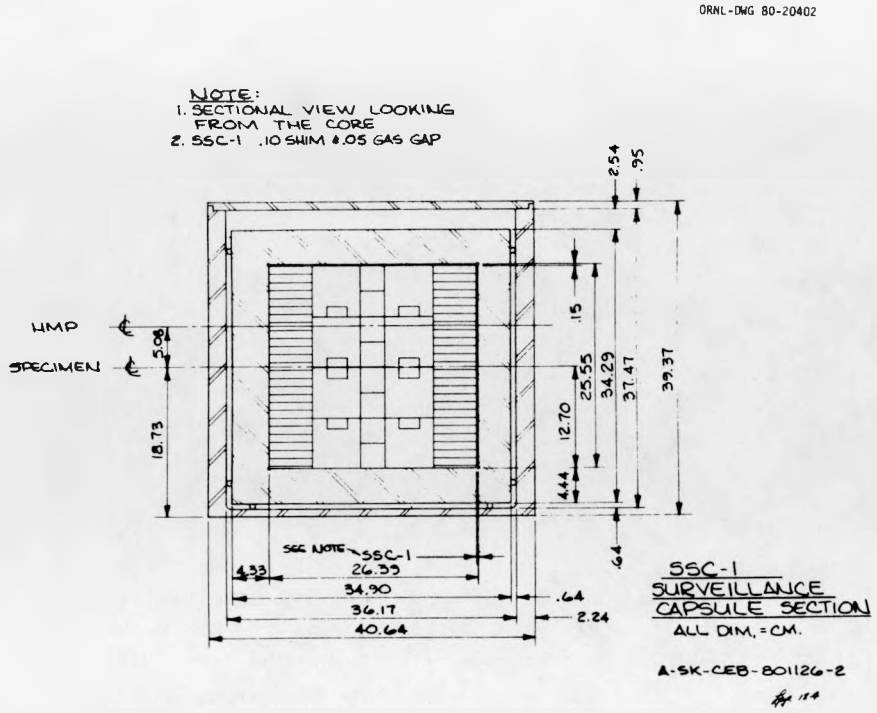

FIGURE 1.1.2. Front Elevation Sectional of the SSC-1 with External Dimensions.

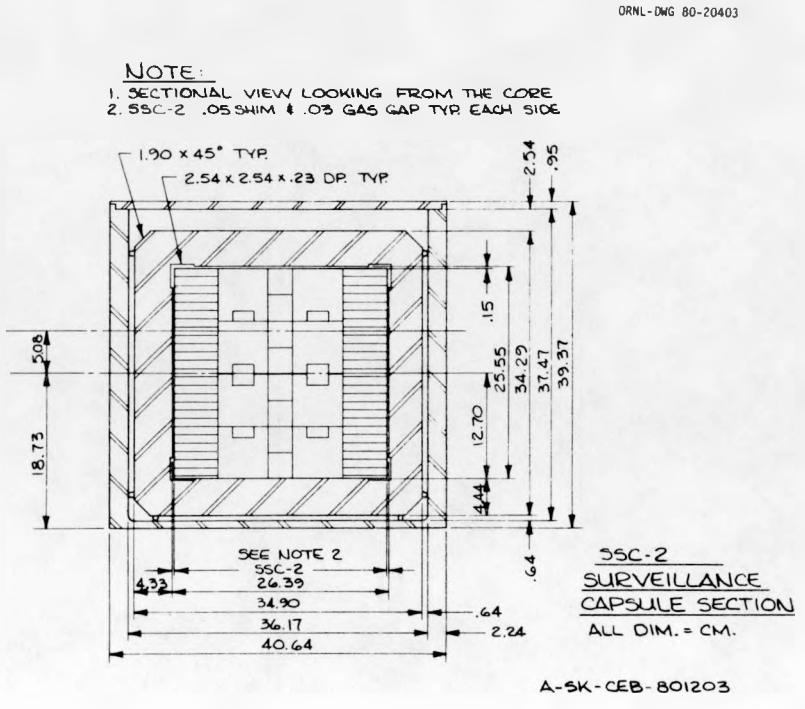

FIGURE 1.1.3. Front Elevation Sectional of the SSC-2 with External Dimensions.

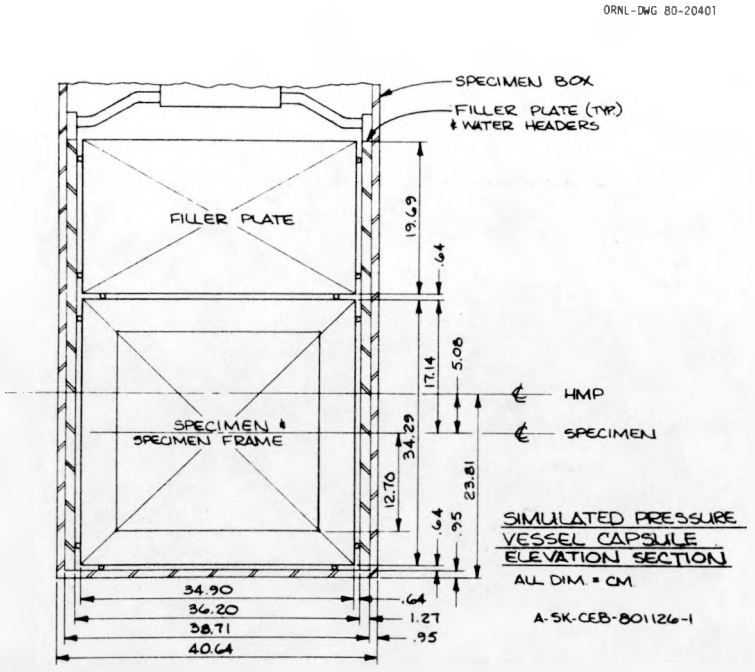

FIGURE 1.1.4. Front Elevation Sectional of the Pressure Vessel Capsule.

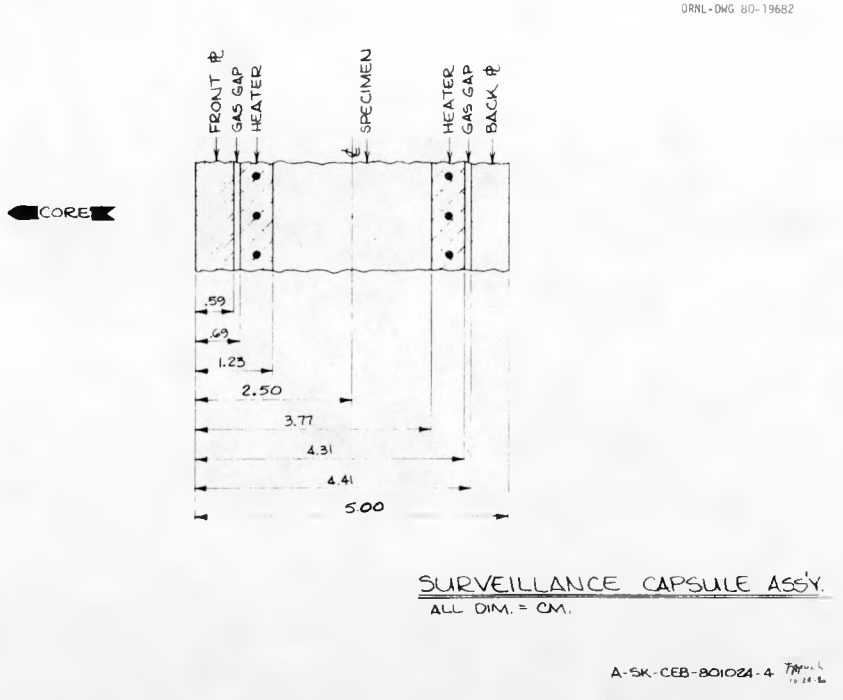

FIGURE 1.1.5. Internal Dimensions and Components of the Simulated Surveillance Capsules.

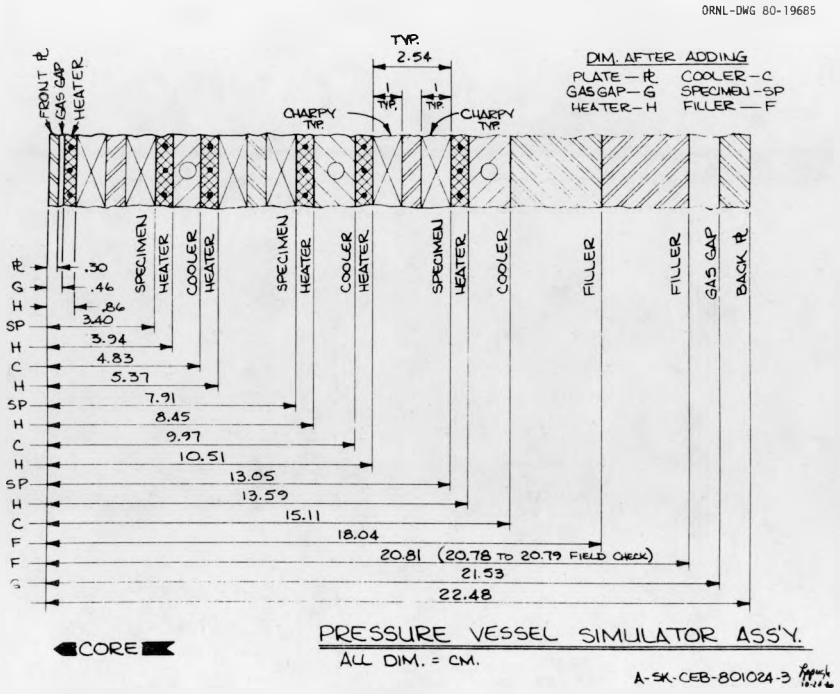

FIGURE 1.1.6. Internal Dimensions and Components of the Pressure Vessel Simulator.

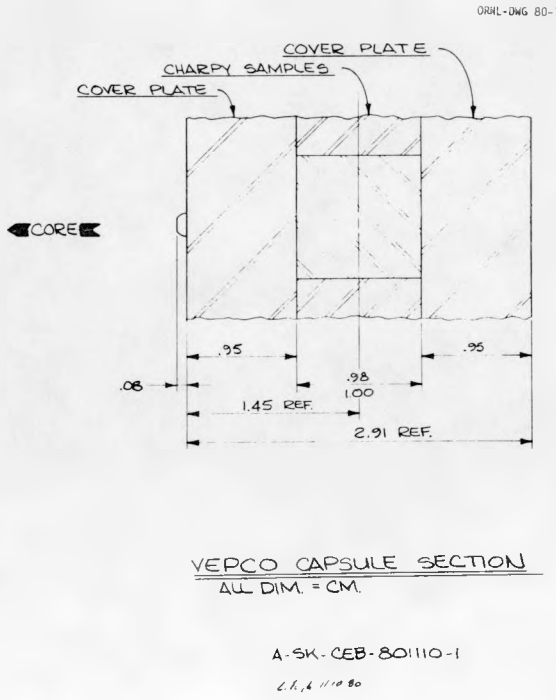

FIGURE 1.1.7. Internal Dimensions of the Void Box Capsule.

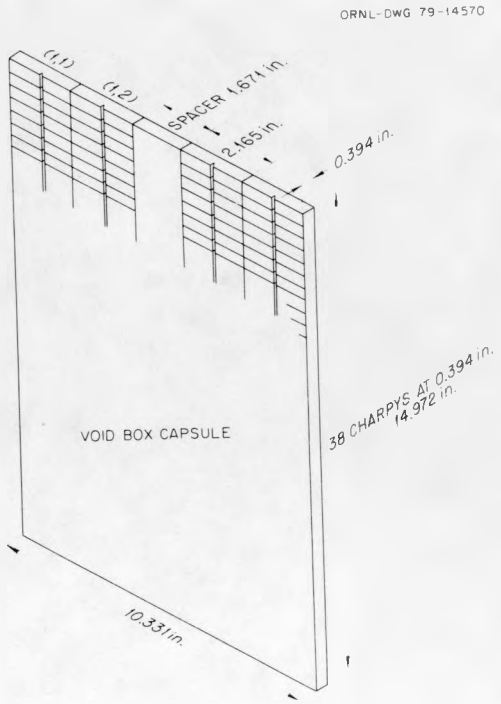

FIGURE 1.1.8. Illustration of the Void Box Capsule with External Dimensions.

1.2 POSITIONS OF PARTICIPANT DOSIMETER PACKAGES

L. F. Miller (ORNL)

Dosimetry materials were placed in a variety of positions in the SSCs, in each of the three sets of mechanical test specimens in the SPVC and in the SVBC. The numbered locations, illustrated in Figure 1.2.1, are the same for the SSCs and for the SPVC except that the location numbers are followed by -1, -2, or -3 to designate locations in the 0-T, 1/4-T, or 1/2-T mechanical test specimens. Locations of dosimeters in the SVBC are shown in Figure 1.2.2. Holes for dosimetry in some of the numbered locations are identified by exploded views in Figure 1.2.1. Designations for the organization utilizing a particular location and the type of dosimetry are also shown. A more complete list of designations of contents, cognizant organizations, and locations is given by Table 1.2.1. Organization and content specifications are essentially the same for the SSCs, each of the SPVC locations, and the SVBC; hence, listings are not provided for each specimen set. Detailed dosimetry component designations identifications are not included because this information is needed only for the initial counting and analysis of the dosimeters.

Positions of the numbered dosimeter locations, shown in Figures 1.2.1 and 1.2.2, can be identified from the coordinate systems illustrated by Figure 1.2.3 and from locations listed in Table 1.2.2. Dimensions of the 1/2-T and 1-T compact tensile specimens are given in Figures 1.2.4 and 1.2.5, and dimensions of the Charpy specimens are given by Figure 1.2.6. Details relative to dimension and drilling patterns for plugs 29 through 36 are given by Figures 1.2.7 through 1.2.11. Similar information applicable to plugs 37 through 38 is given in Figures 1.2.12 and 1.2.13.

More details on dosimeter specifications, cognizant organizations, fluences, and locations of dosimeters are given in Section 2.0 and References (Li81,Mc86b,Sc86a).

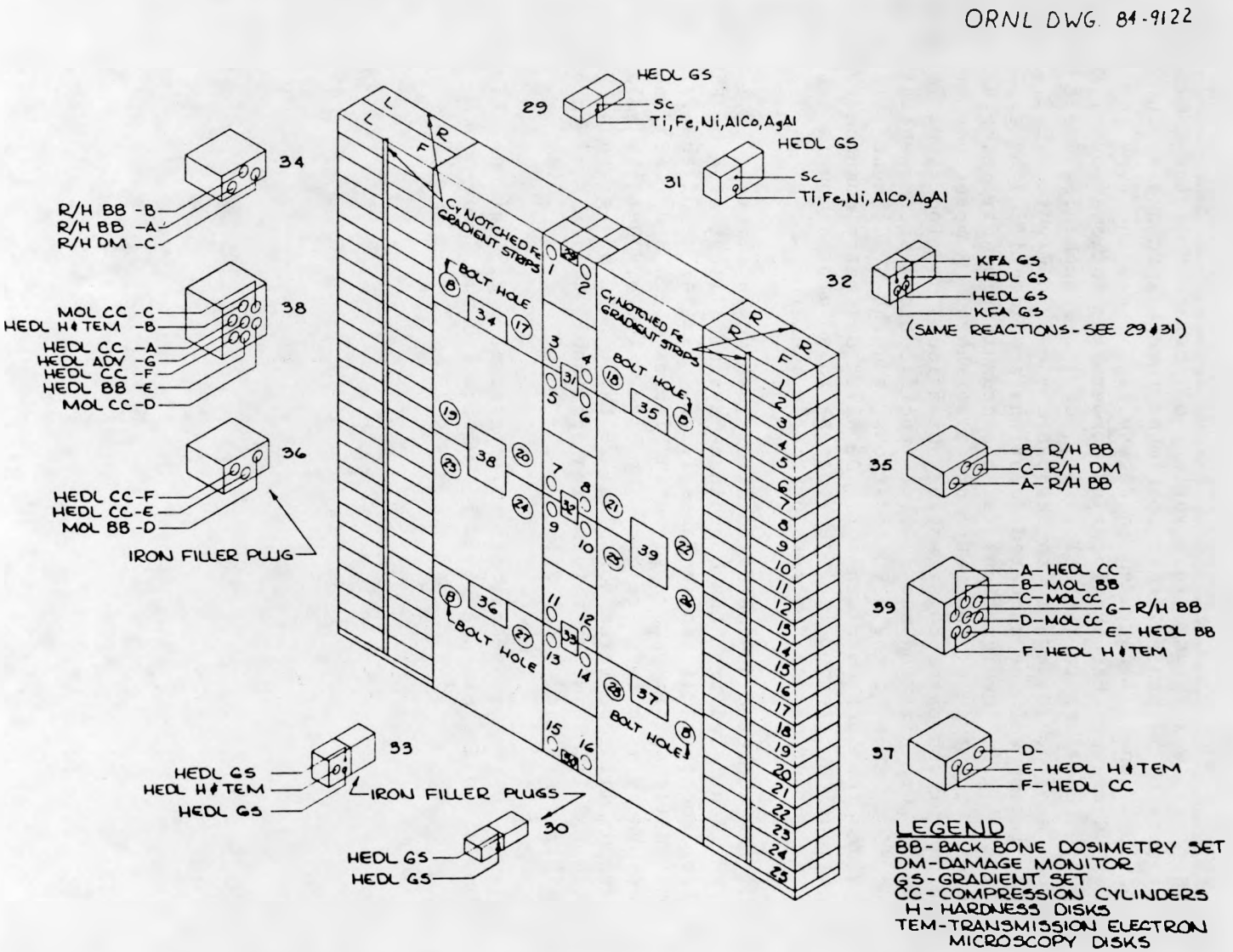

FIGURE 1.2.1. Illustration of Dosimeter Locations in the SSCs and the SPVC. The 0-T, 1/4-T, and 1/2-T location designations for the SPVC are followed by -1, -2, or -3, respectively.

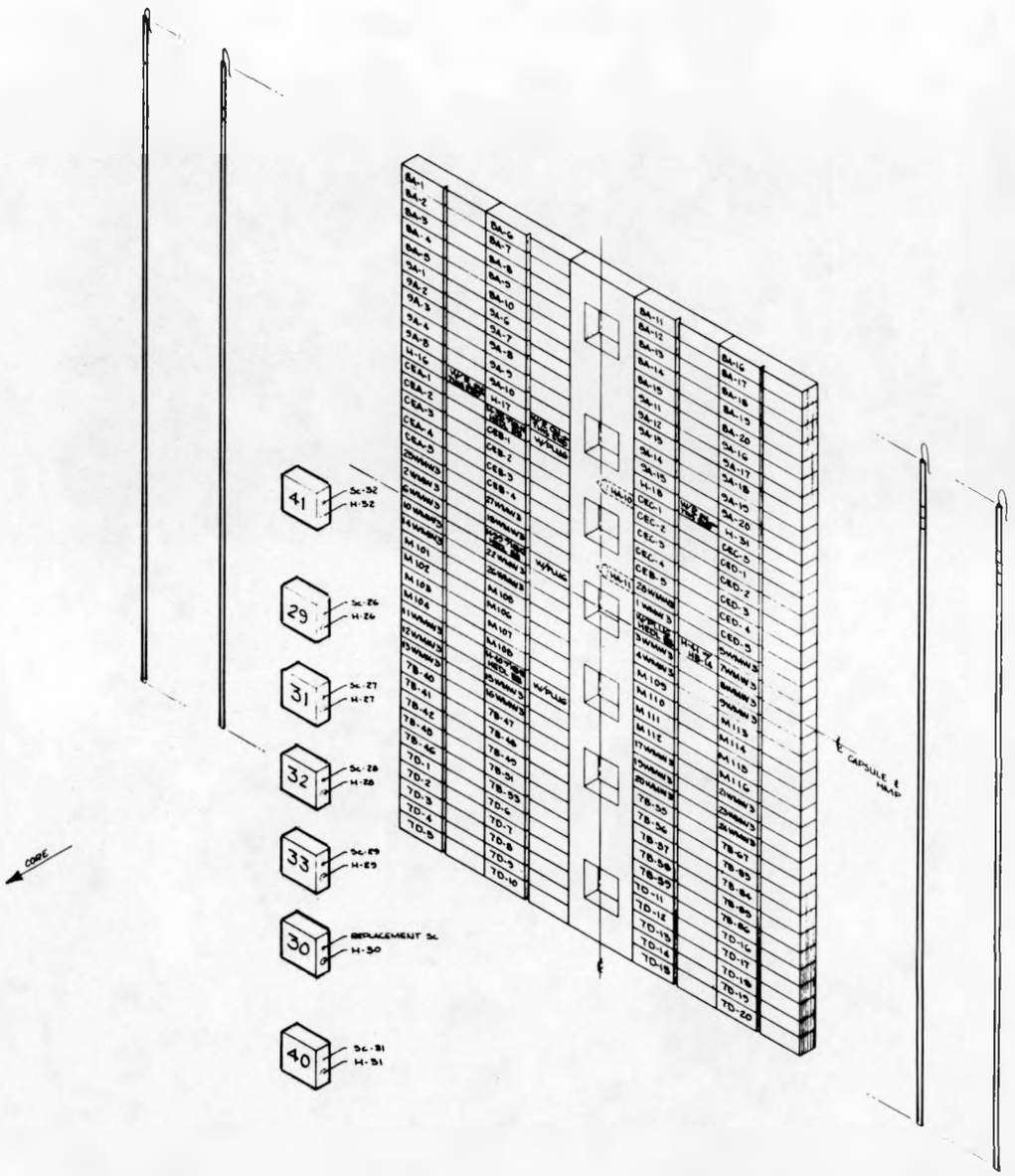

FIGURE 1.2.2. Identification of the Metallurgical Test Specimens and Dosimeter Locations in the SVBC.

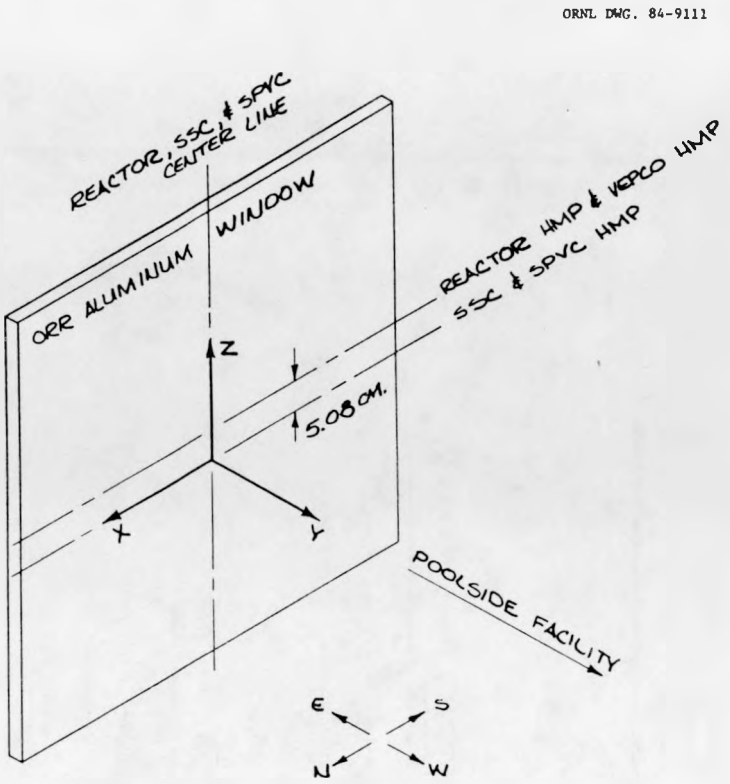

FIGURE 1.2.3. Coordinate System for Locating Dosimetry Positions Relative to the ORR Aluminum Window.

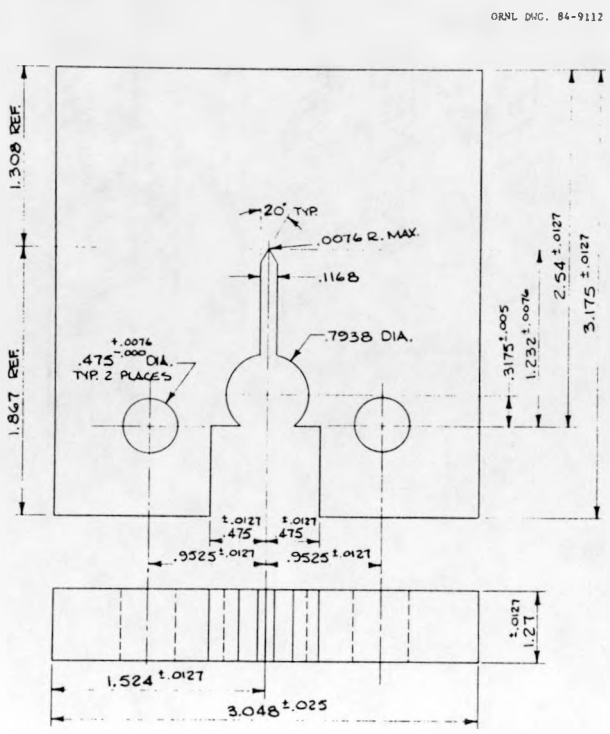

FIGURE 1.2.4. Dimensions of the 1/2-T Compact Tensile Specimens.

ORNL DWG 84-9113

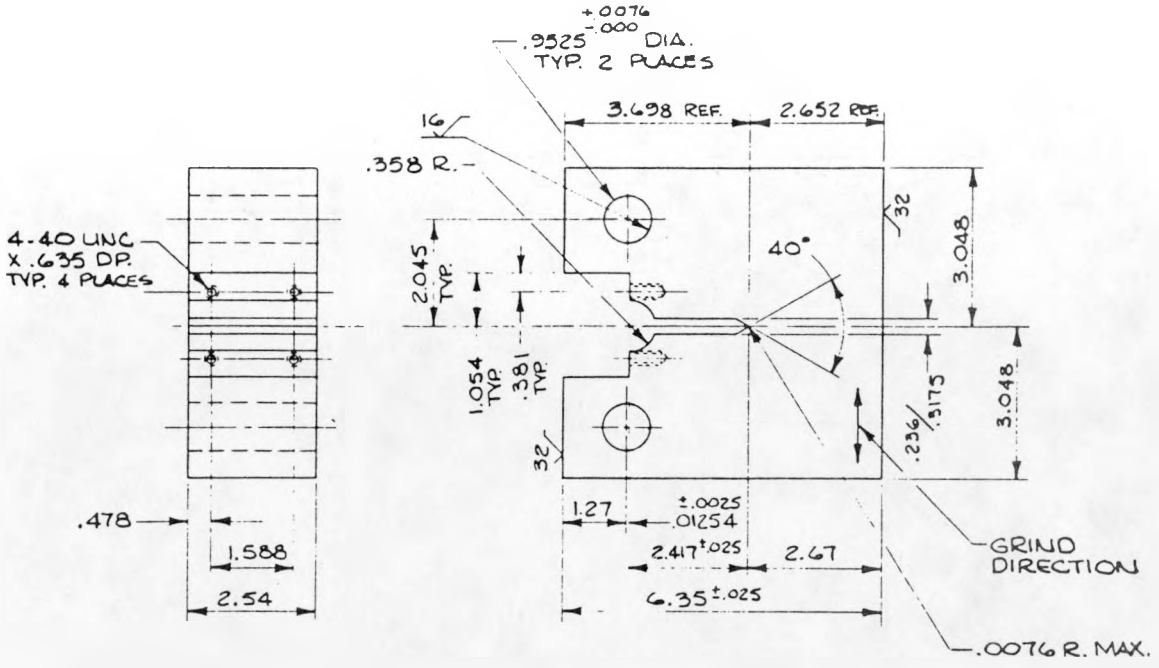

FIGURE 1.2.5. Dimensions of the 1-T Compact Tensile Specimens.

ORNL DWG. 84-9114

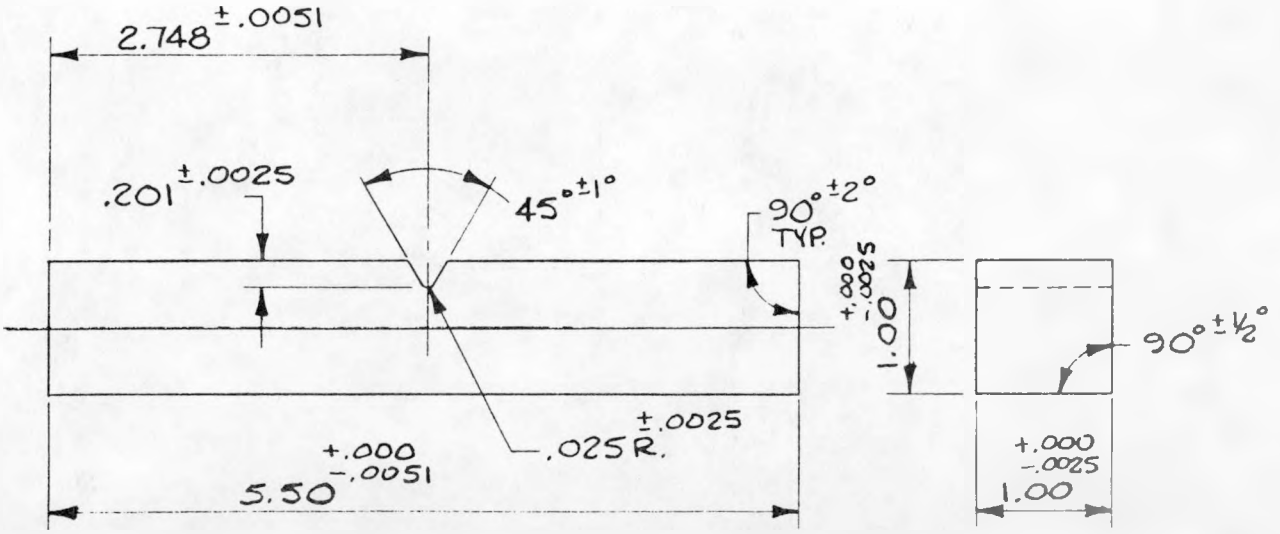

FIGURE 1.2.6. Dimensions of the V-Notched Charpy Specimens.

ORNL DWG. 84-9115

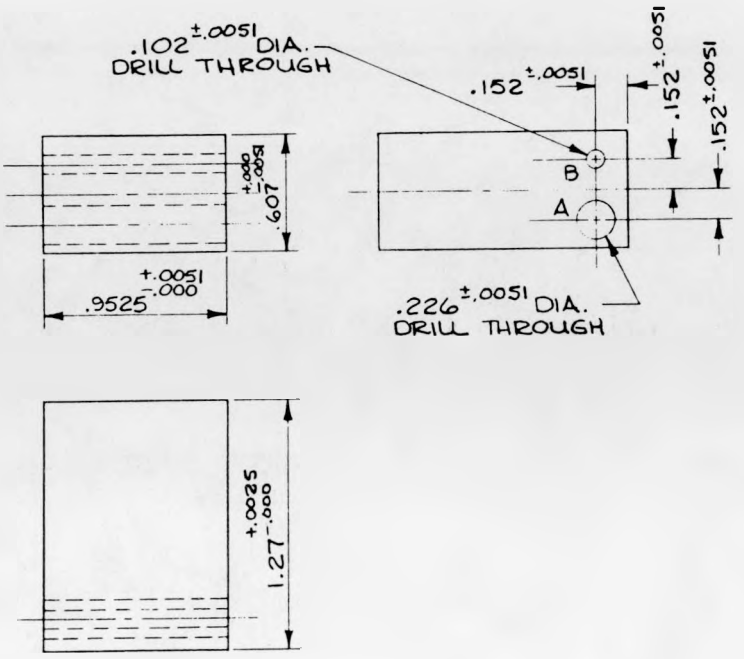

FIGURE 1.2.7. Dimensions and Drilling Patterns for Plugs 29 and 30.

ORNL DWG. 84-9116

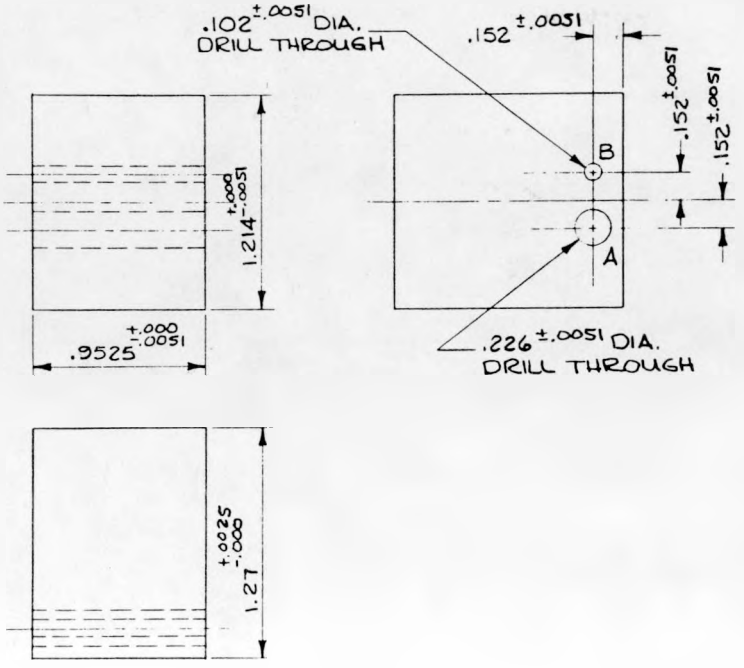

FIGURE 1.2.8. Dimensions and Drilling Pattern for Plug 31.

ORNL DWG. 84-9117

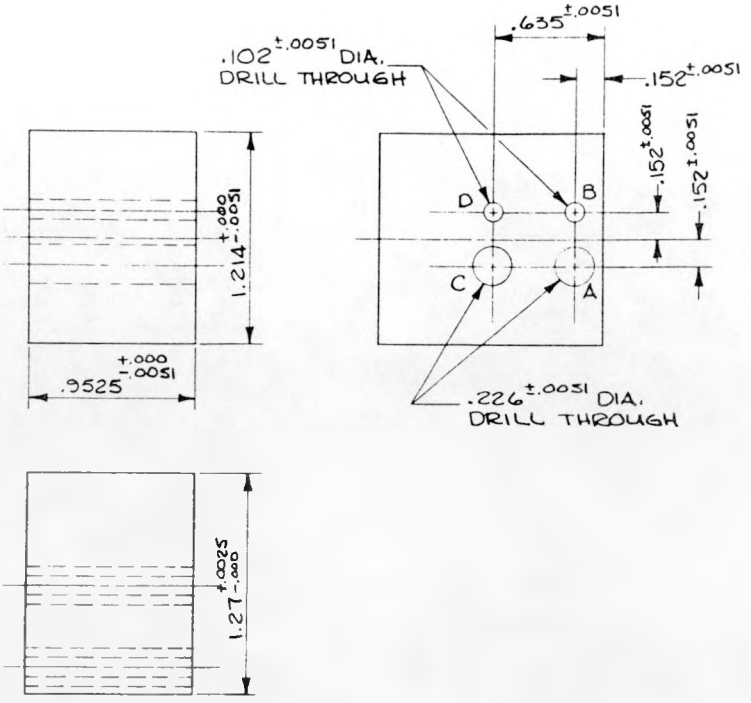

FIGURE 1.2.9. Dimensions and Drilling Pattern for Plug 32.

ORNL DWG. 84-9118

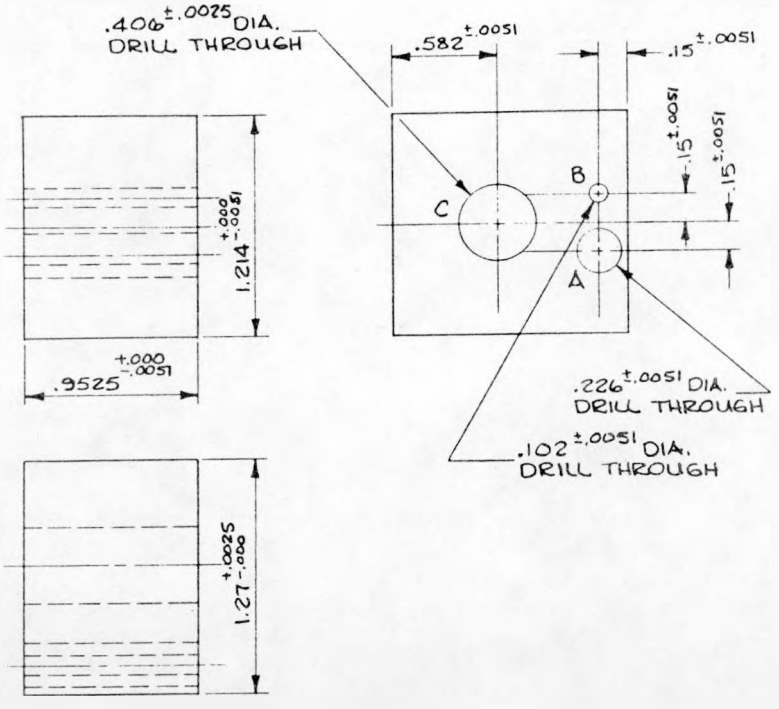

FIGURE 1.2.10. Dimensions and Drilling Pattern for Plug 33.

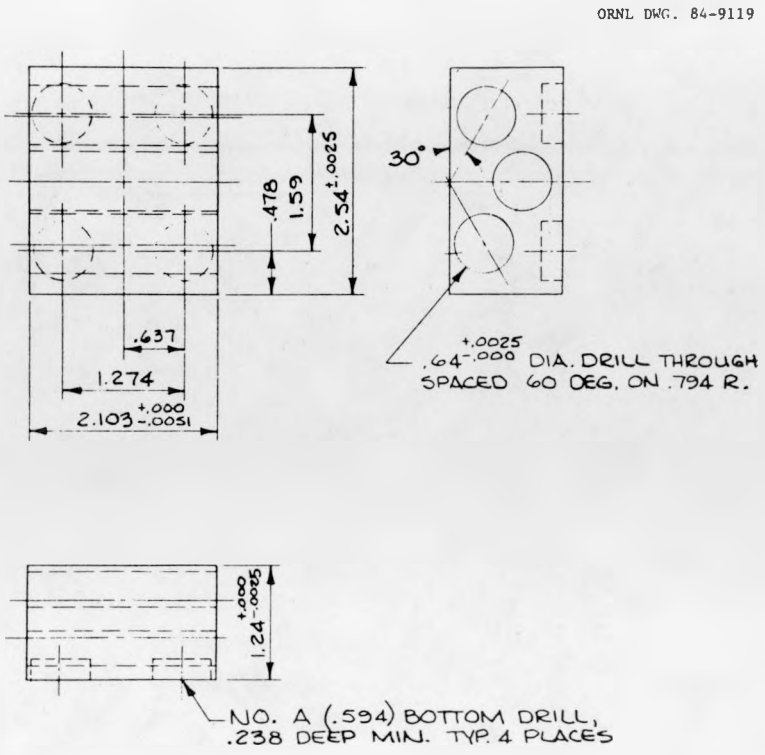

FIGURE 1.2.11. Dimensions and Drilling Patterns for Plugs 34, 35, and 36.

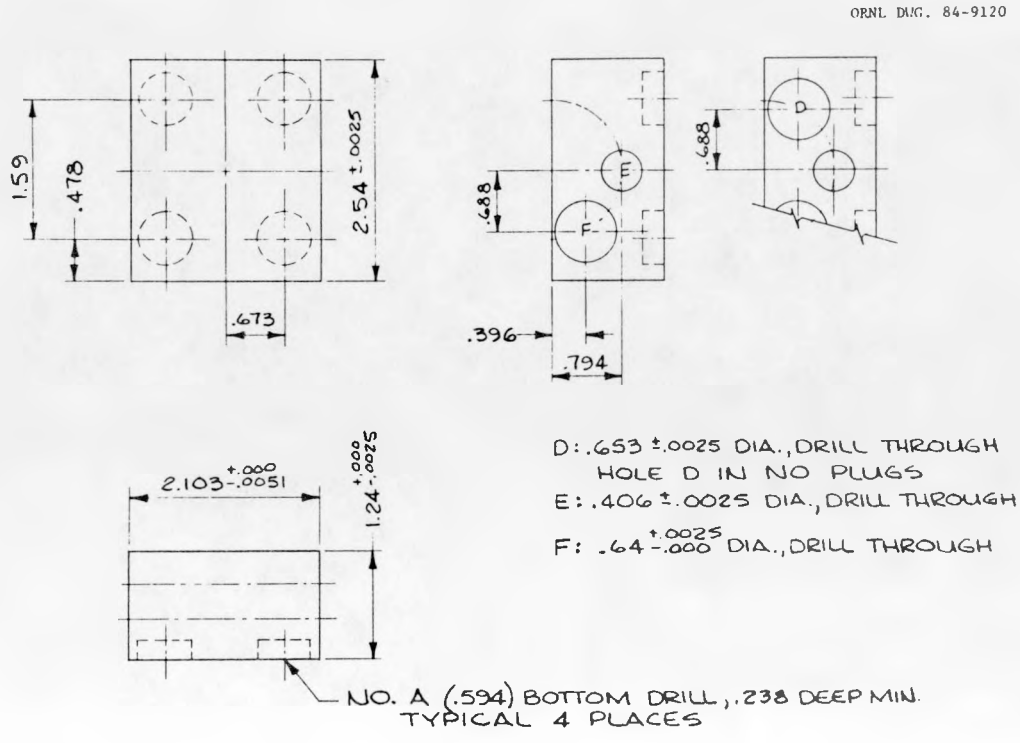

FIGURE 1.2.12. Dimensions and Drilling Pattern for Plug 37.

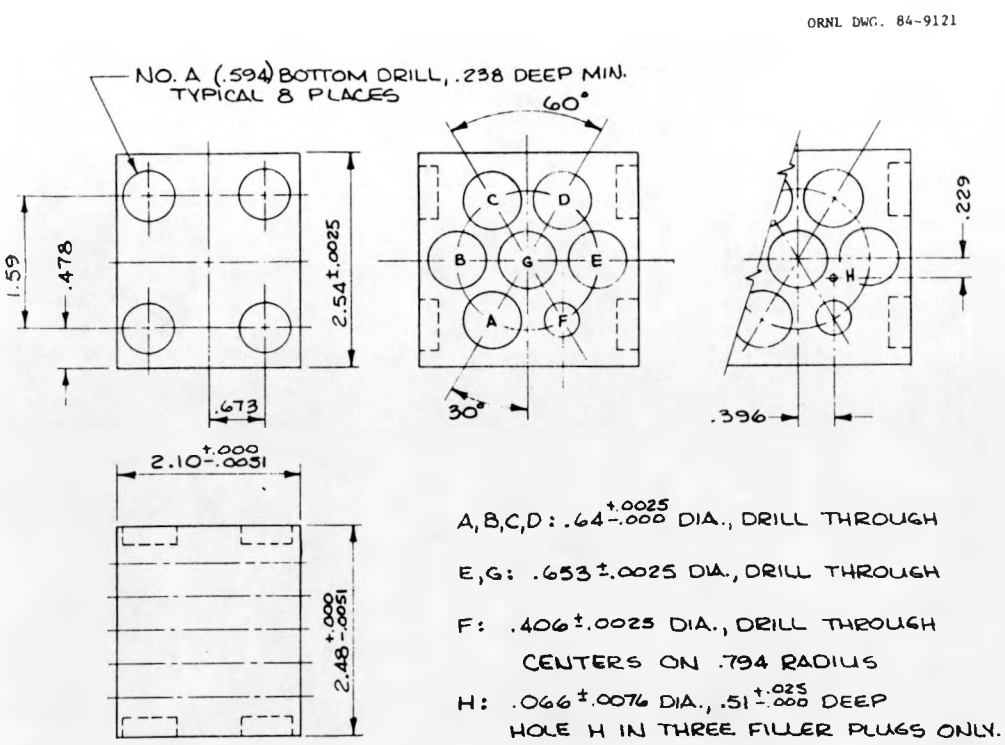

FIGURE 1.2.13. Dimensions and Drilling Patterns for Plugs 38 and 39.

TABLE 1.2.1

DESIGNATIONS OF CONTENTS AND COGNIZANT ORGANIZATION
AT LOCATIONS ILLUSTRATED BY FIGURE 1.2.1
FOR THE SSCs, SPVC, AND SVBC

Location	Hole	Organization	Contents
17	N/A	RRA	CC & TEM
18	N/A	RRA	CC & TEM
19	N/A	GE	Capsule
20	N/A	CE	Capsule
21	N/A	Blank	N/A
22	N/A	B&W	Capsule*
23	N/A	Blank	N/A
24	N/A	Blank	N/A
25	N/A	Blank	N/A
26	N/A	Blank	N/A
27	N/A	HEDL	H & TEM
28	N/A	HEDL	H & TEM
29	N/A	HEDL	GS
30	N/A	HEDL	GS
31	N/A	HEDL	GS
32	N/A	HEDL & KFA	GS
33	N/A	HEDL	GS, H & TEM
34	A	RRA	BB
	B	RRA	BB
	C	RRA	BB (DM @ OT)
35	A	RRA	BB
	B	RRA	BB
	C	RRA	BB (DM @ OT)
36	D	MOL	BB
	E	HEDL	533-CC
	F	HEDL	533-CC
37	D	Blank	N/A
	E	HEDL	H & TEM
	F	HEDL	533-CC
38	A	HEDL	302-CC
	B	HEDL	H & TEM
	C	MOL	CC
	D	MOL	CC
	E	HEDL	BB
	F	HEDL	302-CC
	G	HEDL	ADV DOS
39	A	HEDL	302-CC
	B	MOL	BB
	C	MOL	CC
	D	MOL	CC
	E	HEDL	BB
	F	HEDL	H & TEM
	G	RRA	BB
40	N/A	MOL	GS
41	N/A	MOL	GS
CVRF(13)	N/A	KFA	BB

BB - Back bone dosimetry set
DM - Damage monitor
GS - Gradient set
CC - Compression cylinders
RRA - Rolls-Royce & Assoc. Ltd.
HEDL- Hanford Engineering Development Laboratory
GE - General Electric
ADV DOS - Advanced dosimetry
H - Harness disks
TEM - Transmission electron microscopy disks
CVRF(13) - Charpy specimen location 13
N/A - Not applicable
CE - Combustion Engineering Inc.
B&W - Babcock & Wilcox Co.
MOL - Centre d'Etude de l'Energie Nucleaire

*A report prepared by B&W provides as-built documentation for the B&W dosimetry capsules (Gr79).

TABLE 1.2.2

COORDINATE LOCATIONS OF SELECTED NUMBERED DOSIMETRY POSITIONS ILLUSTRATED IN FIGURE 1.2.1. THE X-Z CORDINATE LOCATIONS LISTED ARE RELATIVE TO THE COORDINATE SYSTEM SHOWN IN FIGURE 1.2.2. THESE COORDINATE LOCATIONS APPLY TO THE SCCs, SPVC, AND THE SVBC.

Description of Location	Coordinate Locations (cm) X	Z
Center of dosimetry location 32	0.0	0.0
Vertical lines that separate the 1/2-T and 1-T specimens	±1.524	---
Vertical lines that separate the 1-T and Charpy specimens	±7.62	
Horizontal lines that separate the 1/2-T specimens	---	0.0, ±3.175 ±6.35, ±9.525
Horizontal lines that separate the 1-T specimens	---	0.0, ±6.35
Vertical lines through centers of locations 2, 4, 6, 8, 10, 12, 14, and 16 (and through location 1, 3, 5, 7, 9, 11, 13, and 15)	0.9525 (-0.9525)	---
Vertical lines through centers of locations 18, 21, and 25 and (through locations 17, 20, 24, and 27)	2.527 (-2.527)	---
Vertical lines through centers of locations 22, and 26 (and through locations 19 and 23)	6.617 (-6.617)	---
Horizontal lines through centers of locations 7 and 8 (and through locations 9 and 10)	---	0.635 (-0.635)
Horizontal lines through centers of locations 5 and 6 (and through locations 11 and 12)	---	5.715 (-5.715)
Horizontal lines through centers of locations 3 and 4 (and through locations 13 and 14)	---	6.985 (-6.985)
Horizontal lines through centers of locations 1 and 2 (and through locations 15 and 16)	---	12.065 (-12.065)
Horizontal lines through locations 19, 20, 21, and 22 (and through locations 23, 24, 25, and 26)	---	1.27 (-1.27)
Horizontal lines through locations 17 and 18 (and through locations 27 and 28)	---	7.62 (-7.62)
Horizontal lines through locations 31, 29, and 41 (and through locations 33, 30, and 40)	6.35, 12.70, 19.05 (-6.35, -12.70, -19.05)	

1.3 CALCULATED CORE POWER SOURCE

L. F. Miller (ORNL)

During the two-year irradiation of the simulated surveillance capsules (SSC-1 and SSC-2) and the simulated pressure vessel capsule (SPVC), the Oak Ridge Research Reactor (ORR) underwent 52 fuel cycles. The time history of the capsule irradiation and in-core fuel distribution for each cycle is essentially unique. Hence, the exposure parameters in irradiation capsules vary for different cycles even when they are normalized to a unit of energy release (megawatt-hours). Thus, it becomes necessary to determine the neutron source distribution for each cycle. Calculations for exposure parameters are accomplished by properly accounting for the time history of the irradiation as well as the spatial distribution of the neutron source. Details relative to these calculations are reported by Maerker and Worley (Ma84a).

Table 1.3.1 lists essential details relative to the irradiation history of SSC-1, SPVC, and SSC-2. The calculated effective multiplication constant (k_{eff}) is listed for ORR core configurations for which three-dimensional (3-D) diffusion theory results are available. Data listed in Table 1.3.2 demonstrate variations in calculated saturated activities for selected fuel cycles. Note that the variation is as much as 40% among cycle groups 158C+158D and 161C. Thus, it is apparent that an accurate determination of the neutron source distribution, for specific core configurations, is needed to accurately calculate the saturated activities at any particular time. The spectrum remains essentially unaltered, however, as indicated in the last column which represents the ratio of two markedly different detector responses.

Neutron source distributions were calculated for 46 ORR core configurations. The source distributions for the remaining six fuel cycles are obtained from the 46 calculated, since some of the core configurations and fuel cycles (154H, 155D, 155G, 155H, 156A, and 156B) are essentially equivalent to the others. These results are on an IBM magnetic tape and may be obtained from F. B. K. Kam at the Oak Ridge National Laboratory (ORNL). Table 1.3.3 documents the correspondence between the file number on the tape and the fuel cycle. Table 1.3.4 defines interval boundaries for the source distribution calculations. A typical neutron source distribution, the one calculated for the PSF Startup Experiment, is reported in Section 1.2 of NUREG/CR-3320, Vol. 2. This distribution is reported as two 2-D neutron sources, one vertical (on the centerline) and one horizontal (on the midplane). Each of these distributions is obtained by integrating the calculated 3-D neutron source distributions in the appropriate transverse direction. These results can be used directly in 2-D ex-core neutron transport calculations so that 3-D flux distributions can be synthesized in the irradiation capsules.

Results from the 3-D source distribution calculations (using diffusion theory) for various ORR core configurations and subsequent 2-D ex-core neutron transport calculations, are used to calculate spectral fluences in the irradiation capsules. These spectral fluences are, in turn, utilized to calculate exposure parameters and for input to dosimetry data analyses. Applicable ORNL analyses results are documented in Section 4.2 of this report.

TABLE 1.3.1

IRRADIATION HISTORY AND CYCLE PARAMETERS

Cycle	k_{eff}	Date and Time Inserted		Date and Time Retracted		Down-Time After Previous Irradiation Δt_d (hr)	t(inserted) (hr)	t(retracted) (hr)	Δtup (hr)	Setback Δt_s (hr)	Average Power Including Setback (MW)
						Start Irradiation of SSC-1, SPVC, and SVBC					
153B	1.0242	4/30/80	13:34	5/08/80	7:00		0	185.43	185.43	1.00	29.822
153C	1.0251	5/08/80	16:43	5/14/80	13:30	9.72	195.14	335.90	140.76	0	29.800
153C	1.0251	5/16/80	9:57	5/21/80	2:17	44.45	380.35	492.68	112.33	0	29.957
153D	1.0162	5/22/80	10:49	6/06/80	24:00	32.53	525.21	898.39	373.18	2.55	29.657
153F	1.0224	6/12/80	9:20	6/23/80	12:55	129.33	1027.72	1295.30	267.58	0.43	29.377
						End Irradiation of SSC-1					
153G	1.0042	6/27/80	18:30	7/05/80	3:30	101.58	1396.88	1573.88	177.00	2.32	28.855
153G	1.0042	7/07/80	13:55	7/08/80	9:40	58.42	1632.30	1652.05	19.75	0.18	29.058
153G	1.0042	7/08/80	15:18	7/13/80	8:00	5.63	1657.68	1770.38	112.70	1.01	29.565
154A	1.0047	7/18/80	17:00	7/18/80	18:32	129.00	1899.38	1900.70	1.32	0.82	3.712
154A	1.0047	7/18/80	22:50	7/21/80	4:26	4.30	1905.00	1958.60	53.60	1.26	28.319
154A	1.0047	7/22/80	10:05	7/31/80	7:00	29.65	1988.25	2201.17	212.92	13.39	28.200
154B	1.0066	7/31/80	18:20	8/12/80	19:02	11.33	2212.50	2501.20	288.70	0.33	30.335
154C	1.0019	8/15/80	14:48	8/15/80	16:07	67.77	2568.97	2570.29	1.32	0.05	28.977
154D	1.0024	8/21/80	10:55	8/26/80	16:00	138.80	2709.09	2834.17	125.08	0.39	28.849
154E	1.0016	8/27/80	14:30	9/01/80	3:29	22.50	2856.67	2965.62	108.95	0	29.799
154E	1.0016	9/3/80	9:53	9/09/80	8:00	54.40	3020.02	3162.14	142.12	0.57	30.031
154F	1.0007	9/10/80	11:22	9/23/80	4:00	27.37	3189.51	3494.14	304.63	1.73	29.471
154G	0.9993	9/23/80	13:52	10/05/80	21:32	9.87	3504.01	3799.68	295.67	0.44	29.909
154H	1.0190	10/7/80	13:46	10/17/80	17:50	40.23	3839.91	4083.95	244.04	0	29.905
154I	0.9858	10/21/80	12:48	10/29/80	4:00	90.97	4174.92	4359.05	184.13	1.00	29.486
154J	0.9890	10/29/80	18:47	11/08/80	8:00	14.78	4373.83	4603.05	229.22	0.29	29.223
155B	0.9983	12/03/80	14:51	12/09/80	0:26	606.85	5209.90	5339.48	129.58	0.90	28.786
155C	0.9920	12/10/80	12:54	12/18/80	5:15	36.47	5375.95	5560.30	184.35	0	28.247
155D	0.9936	12/18/80	17:46	12/30/80	8:00	12.52	5572.82	5851.59	278.77	0.54	27.832
155E	0.9891	12/30/80	16:11	1/07/81	8:00	8.18	5859.77	6043.59	183.82	0.29	26.823
155F	0.9922	1/07/81	21:55	1/15/81	4:00	13.92	6057.51	6231.59	174.08	0.22	27.115
155G		1/16/81	11:41	1/19/81	20:22	31.68	6263.27	6343.95	80.68	0.21	30.066
155H		1/21/81	9:02	1/22/81	7:16	36.67	6380.62	6402.85	22.23	0.89	29.311
155H		1/22/81	16:18	2/02/81	8:00	9.03	6411.88	6667.58	255.70	0.61	30.346
156A		2/09/81	13:35	2/24/81	8:00	173.58	6841.16	7195.58	354.42	2.92	27.279
156B		2/24/81	15:00	3/13/81	8:04	7.00	7202.58	7603.65	401.07	2.19	27.223
156B		3/13/81	8:47	3/16/81	3:00	0.72	7604.37	7670.59	66.22	0.61	27.168
156C	1.0052	3/19/81	10:13	3/30/81	22:40	79.22	7749.81	8026.26	276.45	0	30.447
156C	1.0052	3/31/81	11:33	4/02/81	4:00	12.88	8039.14	8079.59	40.45	1.08	29.598
156D	1.0076	4/02/81	16:10	4/19/81	8:00	12.17	8091.76	8491.60	399.84	0	30.290
157A	1.0021	4/27/81	11:12	5/11/81	3:12	194.20	8585.80	9013.80	328.00	2.50	30.174
157B	1.0184	5/11/81	17:24	5/27/81	4:00	14.20	9028.00	9398.60	370.60	0	30.335

TABLE 1.3.1

(CONTINUED)

Cycle	k_{eff}	Date and Time Inserted		Date and Time Retracted		Down-Time After Previous Irradiation Δt_d (hr)	t(inserted) (hr)	t(retracted) (hr)	Δtup (hr)	Setback Δt_s (hr)	Average Power Including Setback (MW)
						Start Irradiation of SSC-2					
157C	1.0166	5/29/81	11:39	5/29/81	20:45	55.65	9454.25	9463.35	9.10	0	30.048
157C	1.0166	6/01/81	11:49	6/09/81	8:10	63.07	9526.42	9714.77	188.35	0.94	29.997
157D	1.0127	6/10/81	8:15	6/23/81	4:23	24.08	9738.85	10046.98	308.13	0	30.352
157E	0.9756	6/25/81	12:20	7/10/81	12:00	55.95	10102.93	10462.60	359.67	0	30.044
158C	1.0018	7/22/81	13:47	8/06/81	6:30	289.78	10752.38	11105.10	352.72	0.15	27.082
158D	0.9997	8/07/81	19:05	8/20/81	4:00	36.58	11141.68	11438.61	296.93	0	27.008
158E	1.0101	8/21/81	15:17	8/30/81	24:00	35.28	11473.89	11698.61	224.72	0	30.354
158F	1.0076	9/02/81	19:01	9/08/81	16:52	67.02	11765.63	11907.48	141.85	0.22	30.136
158G	1.0274	9/11/81	8:17	9/25/81	2:00	63.42	11970.90	12300.62	329.72	0	30.260
						End Irradiation of SSC-2					
158H	1.0126	9/25/81	23:10	10/13/81	3:20	21.17	12321.79	12733.96	412.17	0.12	30.180
158I	1.0206	10/13/81	20:30	10/23/81	3:00	17.17	12751.13	12973.63	222.50	0.57	30.174
158J	1.0142	10/23/81	13:28	10/26/81	20:13	10.47	12984.10	13063.85	79.75	0.12	29.819
158J	1.0142	10/27/81	9:41	11/04/81	4:00	13.47	13077.32	13263.64	186.32	1.43	30.267
158K	1.0173	11/04/81	16:10	11/15/81	8:00	12.17	13275.81	13531.64	255.83	0.09	30.311
159A	1.0156	11/24/81	14:12	12/12/81	6:00	222.20	13753.84	14177.64	423.80	0	30.287
159B	1.0037	12/18/81	9:47	12/28/81	13:20	147.78	14325.42	14568.97	243.55	0.43	30.009
159C	1.0054	12/31/81	21:21	1/06/82	8:36	80.02	14648.99	14780.24	131.25	0.71	29.794
159C	1.0054	1/06/82	14:18	1/14/82	3:00	5.70	14785.94	14966.64	180.70	0.37	30.234
159D	1.0121	1/21/82	15:36	2/01/82	2:58	180.60	15147.24	15398.61	251.37	0	30.256
159E	1.0025	2/01/82	16:56	2/07/82	8:00	13.97	15412.58	15547.65	135.07	0	30.126
160A	1.0020	2/12/82	17:33	2/18/82	9:00	129.55	15677.20	15812.65	135.45	0.07	29.987
160B	1.0064	2/18/82	18:59	3/08/82	8:20	9.98	15822.63	16243.98	421.35	0.14	30.173
160C	1.0175	3/09/82	15:33	3/25/82	3:00	31.22	16275.20	16646.65	371.45	1.44	30.113
160D	1.0166	3/26/82	18:55	4/05/82	3:00	39.92	16686.57	16910.65	224.08	0.34	30.223
160E	1.0108	4/04/82	18:40	4/16/82	15:05	15.67	16926.32	17186.74	260.42	0.69	29.856
161B	1.0149	4/29/82	17:42	5/24/82	3:30	313.62	17500.36	18086.16	585.80	0.88	30.062
161C	1.0223	5/27/82	22:28	6/22/82	24:00	90.97	18177.13	18802.66	625.53	1.73	30.116
						End Irradiation of SPVC and SVBC					

TABLE 1.3.2

CYCLE GROUP-TO-CYCLE GROUP VARIATION OF SOME SATURATED ACTIVITIES AT THE 1/2-T LOCATION, X = -53.7, Y = 337.8, AND Z = -8.5 mm

Cycles	Capsules Irradiated	$^{54}Fe(n,p)$	$^{63}Cu(n,\alpha)$	$^{237}Np(n,f)$	Np/Cu
153B+153C	SSC-1 +	7.59-15*	5.87-17	6.17-13	1.05+4
153D	SPVC +	7.58-15	5.87-17	6.16-13	1.05+4
153F	SVBC	7.83-15	5.71-17	5.99-13	1.05+4
153G-154C	SPVC	7.83-15	6.05-17	6.35-13	1.05+4
154D-154J	and	7.47-15	5.79-17	6.06-13	1.05+4
155B-155F	SVBC	9.15-15	7.06-17	7.42-13	1.05+4
156C-157B		8.65-15	6.68-17	6.99-13	1.05+4
157C-157E	SSC-2 +	8.82-15	6.80-17	7.14-13	1.05+4
158C+158D	SPVC +	9.65-15	7.45-17	7.83-13	1.05+4
158E-158G	SVBC	8.24-15	6.36-17	6.64-13	1.04+4
158H-158K	SPVC	8.14-15	6.33-17	6.50-13	1.03+4
159A-159C	and	8.42-15	6.54-17	6.73-13	1.03+4
159D-160C	SVBC	7.83-15	6.10-17	6.24-13	1.02+4
160D+160E		7.27-15	5.69-17	5.76-13	1.01+4
161B		7.14-15	5.62-17	5.65-13	1.01+4
161C		6.86-15	5.40-17	5.41-13	1.00+4
Startup (151A)	SSC + SPVC	8.84-15	7.05-17	7.04-13	1.00+4

*Read 7.59×10^{-15} reactions per atom per second at 30 MW, etc.

TABLE 1.3.3

CORRESPONDENCE BETWEEN FILE NUMBER ON TAPE AND FUEL CYCLE IDENTIFICATION. THE FOOTNOTE DOCUMENTS THE FILE STRUCTURE OF DATA

ICYCLE	CYCLE	ICYCLE	CYCLE	ICYCLE	CYCLE	ICYCLE	CYCLE
1	153B	13	154I	25	157E	37	159C
2	153C	14	154J	26	158C	38	159D
3	153D	15	155B	27	158D	39	159E
4	153F	16	155C	28	158E	40	160A
5	153G	17	155E	29	158F	41	160B
6	154A	18	155F	30	158G	42	160C
7	154B	19	156C	31	158H	43	160D
8	154C	20	156D	32	158I	44	160E
9	154D	21	157A	33	158J	45	161B
10	154E	22	157B	34	158K	46	161C
11	154F	23	157C	35	159A		
12	154G	24	157D	36	159B		

```
*  DØ  4  ICYCLE=1,46
   READ(5,3)ICYCLE,LØG,IXMAX,JYMAX
   DØ  1  KZ=1,41
 1 READ(5,2)((PFS(IX,JY),IX=1,43),JY=1,36)
 4 CØNTINUE
 2 FØRMAT(6E12.5)
 3 FØRMAT(4I4)
```

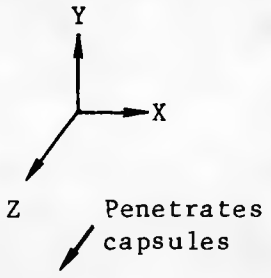

Note that, relative to the capsules, the X-coordinate intervals (IX) are horizontal and parallel, the Y-coordinate intervals (JY) are vertical and perpendicular, and the Z-coordinate intervals (KZ) are perpendicular and horizontal. The footnote example places interval 41 in the PFS matrix. Interval boundaries are reported in Table 1.3.4. Note also that the coordinate system location and orientation is different for the source distribution and ex-core calculations.

TABLE 1.3.4

INTERVAL BOUNDARIES FOR THE THREE-DIMENSIONAL SOURCE DISTRIBUTIONS CITED IN TABLE 1.3.3

X (cm) (43 intervals)	Y (cm) (36 intervals)	Z (cm) (45 intervals)
0.0	0.0	0.0
5.92	6.35	5.92
11.85	12.70	11.85
17.78	15.24	17.78
20.32	17.78	20.32
22.86	20.32	22.86
25.40	22.86	25.40
27.94	25.40	27.94
30.48	27.94	30.48
33.02	30.48	33.02
35.56	33.02	35.56
38.10	35.56	38.10
40.64	38.10	40.64
43.18	40.64	43.18
45.72	43.18	45.72
46.55	45.72	46.55
46.90	48.26	56.90
49.53	50.80	49.53
52.15	53.34	52.15
52.50	55.88	52.50
53.34	58.42	53.34
55.88	60.96	55.88
58.42	63.50	58.42
60.96	66.04	60.96
61.79	68.58	61.79
62.14	71.12	62.14
64.77	73.66	64.77
67.39	76.20	67.39
67.74	78.74	67.74
68.58	81.28	68.58
71.12	83.82	69.85
73.66	86.36	71.12
76.20	88.90	72.39
78.74	91.44	73.66
81.28	93.98	74.93
83.82	100.33	76.20
86.36	106.68	76.70
88.90		79.24
91.44		81.78
93.98		84.32
96.52		86.86
102.44		89.86
108.37		92.86
114.30		95.86
		98.86
		101.86

The origin is located in the upper left-aft corner of the ORR core when viewed upright from the irradiation capsules. Details on the ORR core geometry and composition can be obtained from F. B. K. Kam at ORNL.

2.0 SSC, SPVC, AND SVBC DOSIMETRY AND MEASUREMENTS - SUMMARY

W. N. McElroy, L. S. Kellogg, and Raymond Gold (HEDL)

An 18-Day Simulated Dosimetry Measurement Facility (SDMF-1) "Startup Experiment" with dummy metallurgical capsules containing only dosimeters was performed prior to the PSF metallurgical experiments to accurately determine the irradiation times needed to reach the target fluences (see Appendix A and NUREG/CR-3320, Vol. 2). This experiment was also used to test the accuracy of a preliminary ORNL neutron transport calculation. Comparison of dosimetry results between the startup and the two-year PSF experiment showed significant differences, which were traced to differences in core loadings (Ma84b,To82a). A new set of transport calculations (described in Section 1.3) was performed to account for 52 different core loadings. Not including the SDMF-1 and other startup tests, six test irradiations have been performed in the ORNL ORR-PSF Benchmark Facility in support of the NRC LWR-PV-SDIP Program. These tests are identified in Appendix A. The information presented in Sections 2.1 through 2.7 is restricted to discussions of the design, fabrication, irradiation, and measurements of dosimetry sensor reaction products from the SSC-1, SSC-2, SPVC, and SVBC metallurgical experiments.

2.1 DOSIMETRY SYSTEM DESIGN

W. N. McElroy, L. S. Kellogg, and Raymond Gold (HEDL)

The ORR-PSF (Figure 1.1.1) in Ref. (Mc86b) consists of the ORR reactor core and the ex-core components that are used to mock up pressure vessel surveillance configurations for light water reactors (LWRs). The ex-core components are the thermal shield (TS), the simulated surveillance capsule (SSC), the simulated pressure vessel capsule (SPVC), and the simulated reactor cavity [void box (VB)]. The aluminum window is the part of the ORR pressure vessel that separates the core from the ex-core components.

Five metallurgical specimen assemblies were prepared for the SPVC irradiation experiment. Each assembly (Figures 2.1.1 and 2.1.2) contains the same mix of plate, forging, and weld material specimens (Ha84,Ha84a). Dosimeters are distributed throughout each assembly to monitor the neutron exposures received by the specimens (Li81). Two capsules were fabricated for irradiation in sequence at the simulated surveillance locations (SSC-1 and SSC-2) to target fluences ($E > 1.0$ MeV) of about 2×10^{19} and 4×10^{19} neutrons/cm^2, respectively. Each SSC contained one of the metallurgical specimen assemblies. The SPVC contained the other three assemblies, which were positioned corresponding to the inner surface (0-T), the quarter thickness (1/4 T), and the half thickness (1/2 T) of a pressure vessel. The fluences for SSC-1 and SSC-2 are approximately equal to the 1/4-T and 0-T positions, respectively. The total irradiation times for SSC-1 and SSC-2 are ∿46 days and ∿92 days while the irradiation time for the SPVC is ∿600 days. The temperature of the specimens was tightly controlled to 288° ± 7°C during the irradiation (Mi81).

Appendices A and B provide information on the design, fabrication, irradiation and results of the physics-dosimetry analysis for the simulated void box capsule (SVPC) irradiation experiment. The metallurgical results for this experiment are given and discussed by Perrin in Ref. (Pe86).

A "startup experiment" with dummy capsules containing only dosimeters was performed prior to the PSF metallurgical experiments to accurately determine the irradiation times needed to reach the target fluences (NUREG/CR-3320, Vol. 2). This experiment was also used to test the accuracy of a preliminary ORNL neutron transport calculation. Comparison of dosimetry results between the startup and the two-year PSF experiment showed significant differences, which were traced to differences in core loadings (Ma84b,To82a). A new set of transport calculations, described Section 1.3, was performed to account for 52 different core loadings.

2.1.1 HEDL Dosimetry

Extensive dosimetry was included in the PSF LWR-PV mockup irradiation to accurately characterize the fluence for each specimen. The dosimetry was contained in available space in each metallurgical capsule. Locations of the dosimetry materials are shown in Figures 2.1.1 and 2.1.2.

The dosimetry was of several types designed to determine the neutron fluence spectrum and the fluence gradient to allow extrapolation and interpolation

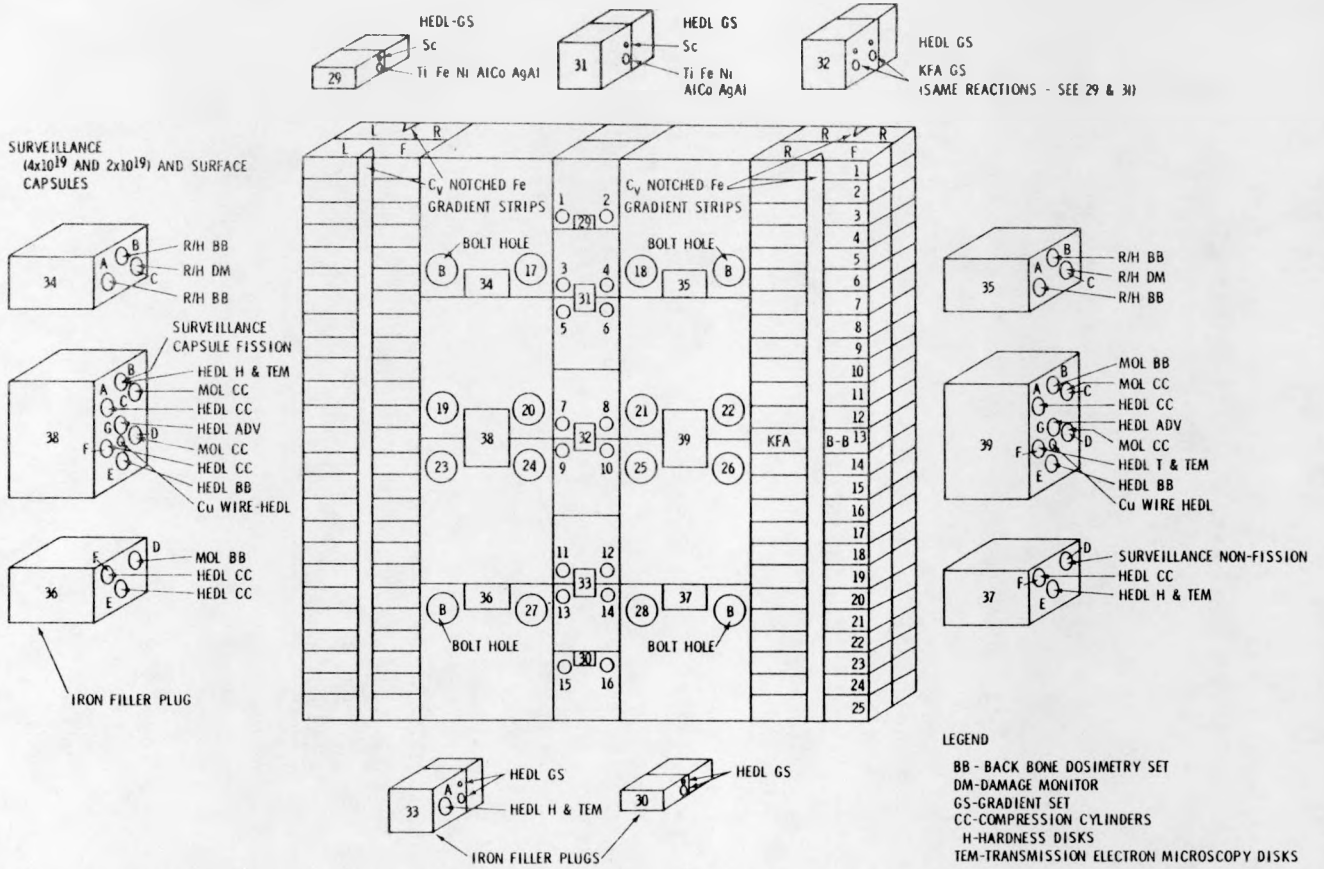

PT#	HOLE	LAB	CONTENTS
17	RRA-	HARWELL	CC & TEM
18	"	"	"
19	AVAILABLE FOR UP TO THREE GE DOSIMETRY SETS		
20	" " " " " CE	"	"
21	" " " " " WEST.	"	"
22	" " " " " BW	"	"
23	" " " " " OTHERS	"	"
24	4x10^19 SURV. AND SURFACE CAPS.	HEDL	EXPLORATORY SSTR-DM
25	"	"	"
26	AVAILABLE FOR UP TO THREE OTHERS DOSIMETRY SETS		
27		HEDL	H & TEM
28		"	"

PT#	HOLE	LAB	CONTENTS
29		HEDL	GS
30		"	"
31		"	"
32		HEDL & KFA	"
33		HEDL	(GS+(H&TEM IN A)
34	A	RRA/HAR (R/H)	BB
	B	"	BB
	C	"	DM
35	A	"	BB
	B	"	BB
	C	"	DM
36	D	MOL	BB

PT#	HOLE	LAB	CONTENTS
36	E	HEDL	533-CC
	F	HEDL	533-CC
37	D	BLANK	
	E	HEDL	H&TEM
	F	HEDL	533-CC
38	A	HEDL	302-CC
	B	HEDL	H&TEM
	C	MOL	CC
	D	MOL	CC
	E	HEDL	BB
	F	HEDL	302-CC
	G	HEDL	ADV DOS

PT#	HOLE	LAB	CONTENTS
39	A	HEDL	302-CC
	B	MOL	BB
	C	MOL	CC
	D	MOL	CC
	E	HEDL	BB
	F	HEDL	H&TEM
	G	HEDL	ADV DOS
CVRF-13		KFA	BB
CVLF Fe		NOTCHED △	
CVLR Fe		" "	
CVRF "		" "	
CVRR "		" "	

HEDL 7906-170.1

FIGURE 2.1.1. Layout of Surveillance and Surface Capsules.

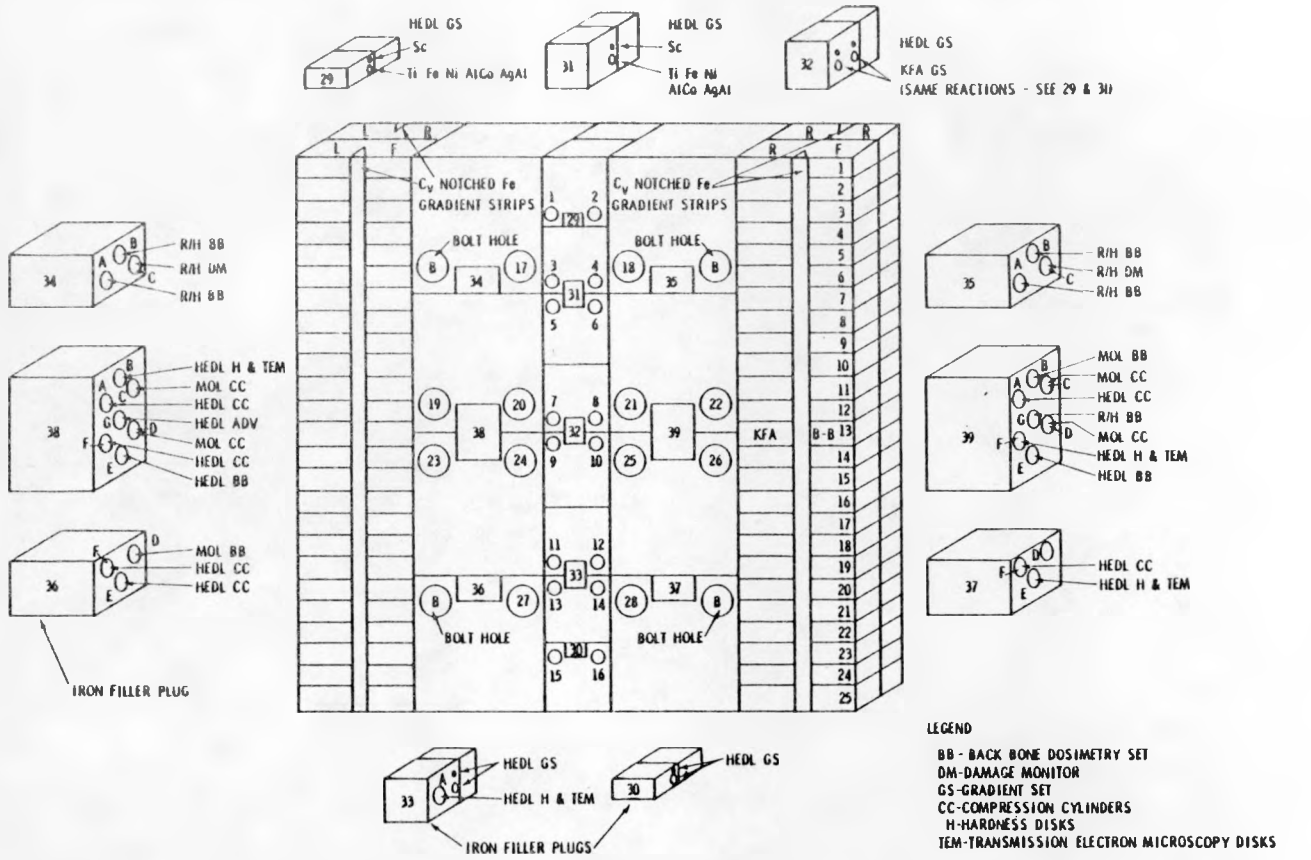

PT#	HOLE	LAB	CONTENTS
17	RRA-	HARWELL	CC & TEM
18	"	"	"
19	AVAILABLE FOR UP TO THREE GE DOSIMETRY SETS		
20	" " " " " GE	"	"
21	" " " " " WEST.	"	"
22	" " " " " BW	"	"
23	" " " " " OTHERS*	"	"
24	" " " " " " "	"	"
25	" " " " " " "	"	"
26	" " " " " " "	"	"
27		HEDL	H & TEM
28		"	"

PT#	HOLE	LAB	CONTENTS
29		HEDL	GS
30		"	"
31		"	"
32		HEDL & KFA	"
33		HEDL	(GS+LH&TEM IN A)
34	A	RRA/HAR (R/H)	BB
	B	"	BB
	C	"	BB
35	A	"	BB
	B	"	BB
	C	"	DM
36	D	MOL	BB

PT#	HOLE	LAB	CONTENTS
36	E	HEDL	533-CC
	F	HEDL	533-CC
37	D	BLANK	
	E	HEDL	H&TEM
	F	HEDL	533-CC
38	A	HEDL	302-CC
	B	HEDL	H&TEM
	C	MOL	CC
	D	MOL	CC
	E	HEDL	BB
	F	HEDL	302-CC
	G	HEDL	ADV DOS

PT#	HOLE	LAB	CONTENTS
39	A	HEDL	302-CC
	B	MOL	BB
	C	MOL	CC
	D	MOL	CC
	E	HEDL	BB
	F	HEDL	H&TEM
	G	RH	BB
CVRF-13		KFA	BB
CVLF Fe		NOTCHED Δ	
CVLR Fe		" "	
CVRF "		" "	
CVRR "		" "	

HEDL 7904-170.2

FIGURE 2.1.2. Layout of Pressure Vessel 1/4 T and 1/2 T Capsules.

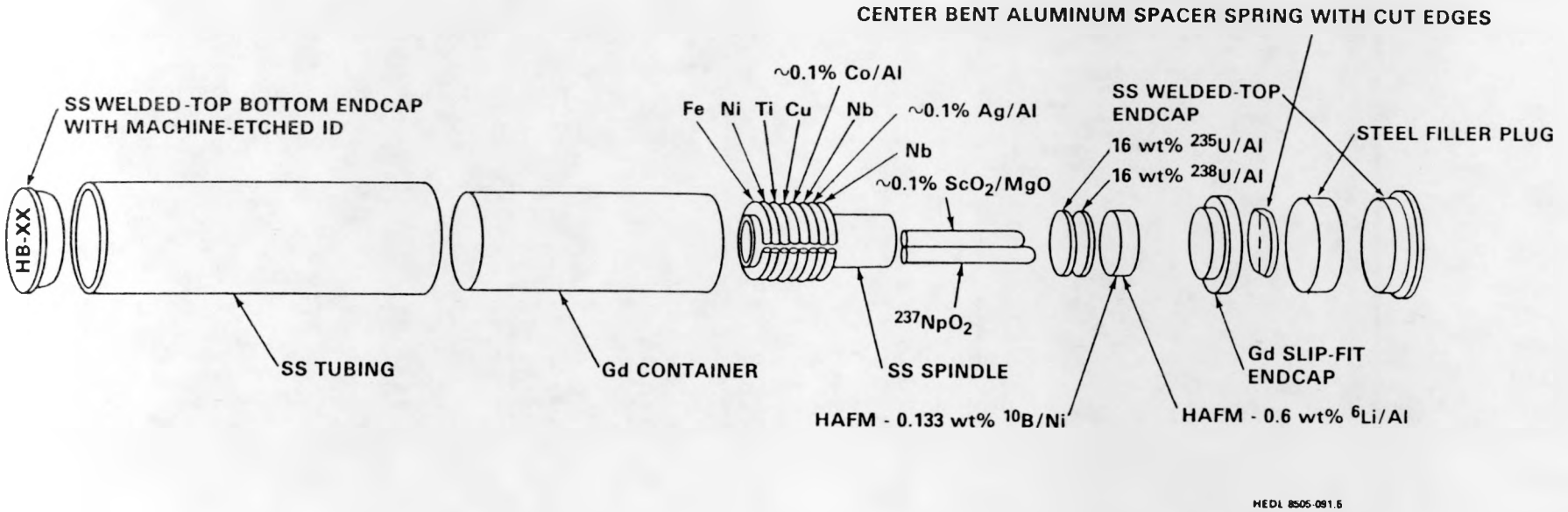

FIGURE 2.1.3. PSF LWR-PV Mockup: Backbone Dosimetry Sets.

in each specimen position. The neutron spectrum determination was mainly influenced by the HEDL gadolinium-covered backbone dosimetry sets. A description of these sets is shown in Figure 2.1.3. Two backbone sets (positioned in Holes 38E and 39E) were included in each metallurgical capsule.

Gradient data were provided by HEDL gradient capsules (Figure 2.1.4) located near the vertical centerline in Blocks 29 through 33 and by four 0.010-in. iron wires located in the Charpy V notches. HEDL also provided additional experimental dosimetry in advanced and exploratory sets (see Figures 2.1.5 and 2.1.6). Those sets included additional radiometric, SSTR, HAFM, and damage monitors.

Dosimetry was also supplied by CEN/SCK (Mol), RRA, KFA, GE, and CE and was placed as shown in Figures 2.1.1 and 2.1.2; also see Table 1.2.1.

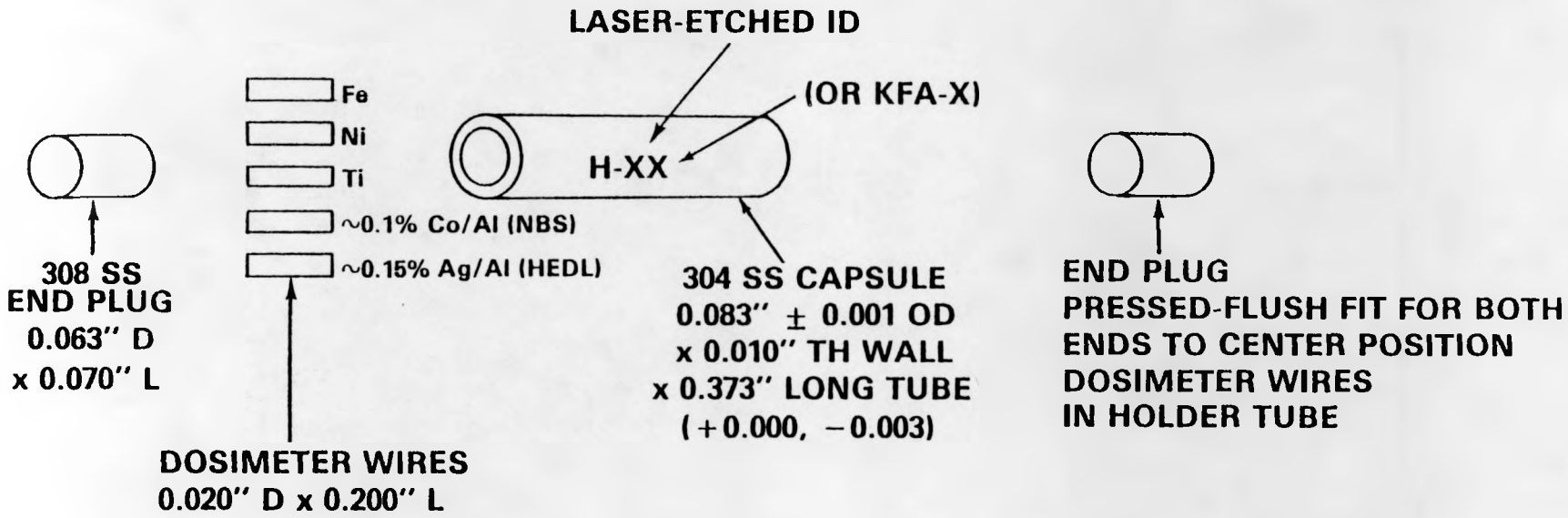

FIGURE 2.1.4. Metal and Metal Alloy Wires and Stainless Steel Capsule Gradient Sets.

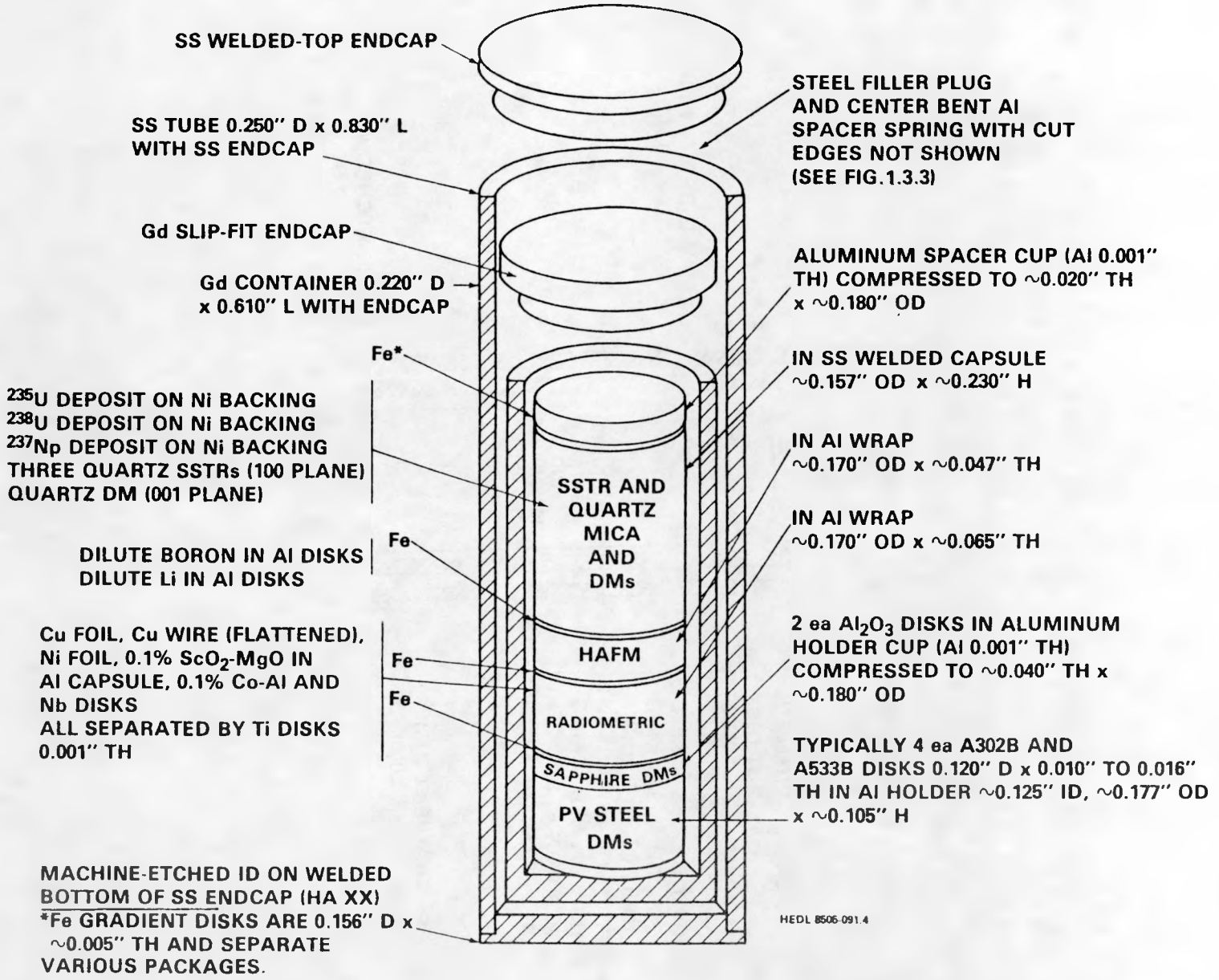

FIGURE 2.1.5. PSF LWR-PV Mockup: Advanced Dosimetry Set Showing Gadolinium Liner and Contents.

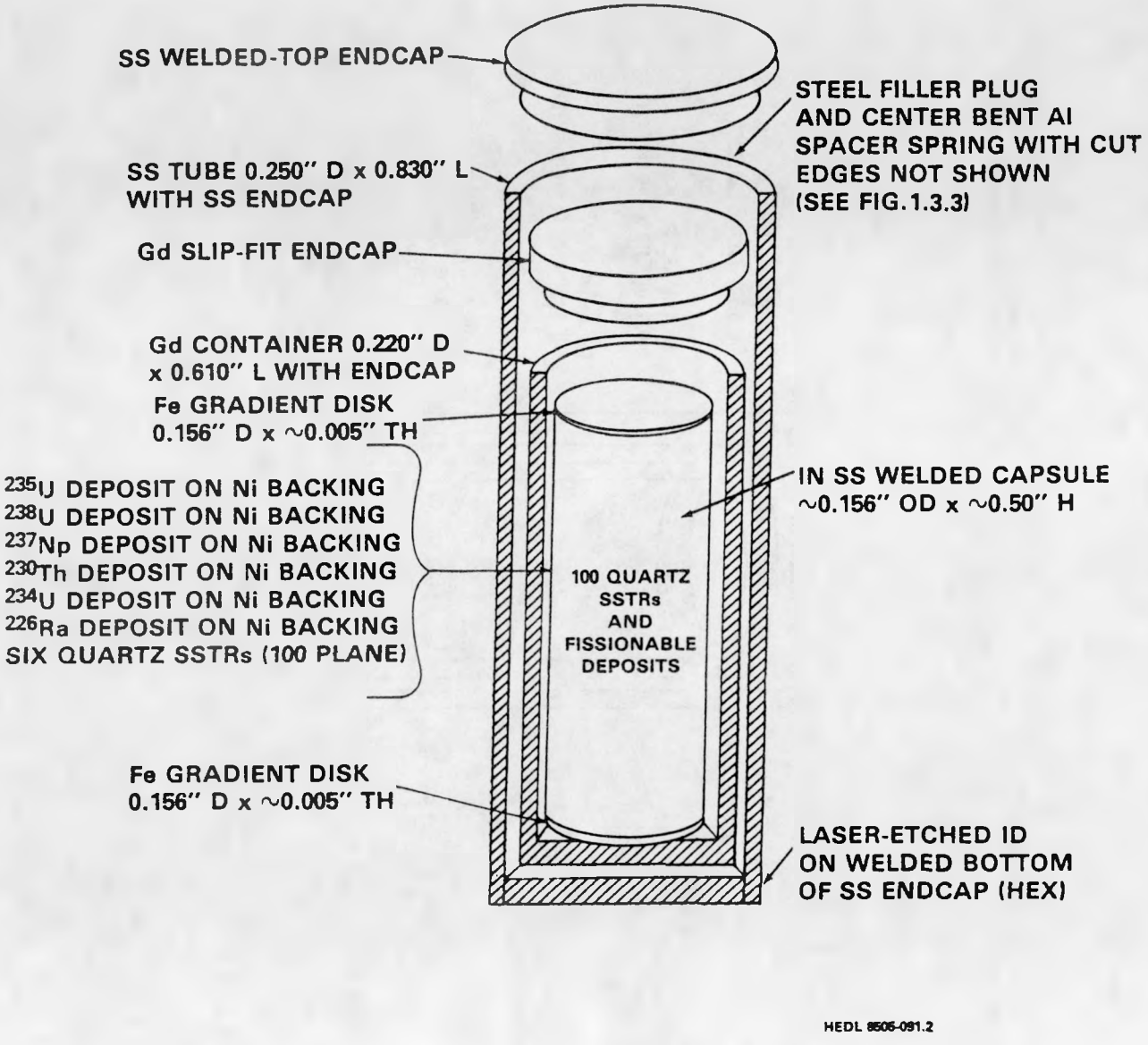

FIGURE 2.1.6. PSF LWR-PV Mockup: Exploratory SSTR Dosimetry Set Showing Gadolinium Liner and Contents.

2.1.2 CEN/SCK Dosimetry

H. Tourwé and J. Lacroix (CEN/SCK)

The results of the CEN/SCK analysis and comparison of the Mol and HEDL dosimetry measurements and the derivation of exposure parameter values of neutron fluence (E > 1 MeV) and dpa in iron are documented in Appendix A.5 of Reference (Mc86b). The reader is referred to Appendix A.5 for more detailed information and a tabulation of the Mol results for the six PV steels.

2.1.3 RR&A/Harwell Dosimetry

A. F. Thomas (Rolls-Royce and Associates Ltd, UK)
A. J. Fudge (AERE Harwell, UK)

2.1.3.1 Activation Detectors

The design of the UK activation dosimetry on all the ORR/PSF LWR simulator capsules was based on the then current AERE standard dosimetry capsule supplied for use in the Rolls-Royce and Associates MTR Steels Irradiation Programme. This comprised a welded tubular stainless steel capsule of 6.25-mm OD and 20-mm length containing either a nickel or gadolinium "box" into which small disks or wires of various activation foils were placed (see Figure 2.1.3.1a). For the purposes of the PSF metallurgical irradiation, AERE fabricated an equal number of nickel and gadolinium box capsules containing iron, nickel, titanium, niobium, cobalt/aluminum, and copper foils in a similar manner to that described in NUREG/CR-3320, Vol. 2, Section 2.3.1. In the case of SSC and SPVC capsules, these were allocated to the dosimetry locations 34 and 35 shown in Figure 2.1.3.2, which were the locations closest to the Rolls-Royce and Associates steel Charpy specimens. The construction of these locations is also shown in detail in Figure 2.1.3.2. As described elsewhere, there are steel filler plugs within the Compact Tension (CT) specimens in which three 6.5-mm diameter holes have been bored perpendicular to both the thickness and the vertical planes of the metallurgical capsule (i.e., minimal flux gradient). The 34-A and 35-A holes were filled by the gadolinium-lined dosimetry capsules, and the 34-B and 35-B holes by the nickle-lined dosimetry capsules.

2.1.3.2 Damage Monitors

At the time of the design of the PSF metallurgical irradiations, the Sapphire Damage Monitor (SDM) was still in the development stages and had not been incorporated as a standard feature of the AERE Standard Dosimetry Capsules, such as those incorporated in the PSF 18-Day Start-Up irradiation (see NUREG/CR-3320, Vol. 2, Section 2.3.1). The SDMs in the PSF metallurgical irradiations were, therefore, fabricated into separate capsules (see Figure 2.1.3.1b) whose external dimensions were compatible with insertion into the bolt holes in the CT specimens. The locations assigned to the SDM capsules in SSC and SPVC were holes 17 and 18, which were situated close to the UK activation dosimetry positions 34 and 35 (see Figure 2.1.3.2).

Since it had been realized that the SDM capsules would probably experience a small but significant difference in neutron flux from that at the activation detector locations, it was decided to incorporate iron activation foils into the SDM capsules, which could be used to correct for flux gradients between the SDM and the activation dosimetry capsules in locations 34 and 35.

Each of the SDM capsules was fabricated from a pair of hollowed-out rectangular stainless steel sections that, after loading, were dowelled together at each end. The assembled capsules were then machined to cylinders to 9.5-mm diameter. This lack of a water-tight seal proved a weakness since, after irradiations, it was found that coolant water had, in fact, penetrated the metallurgical capsules and then also found its way inside the SDM capsules. The consequence of this was that the iron activation foils had corroded away and could not be used.

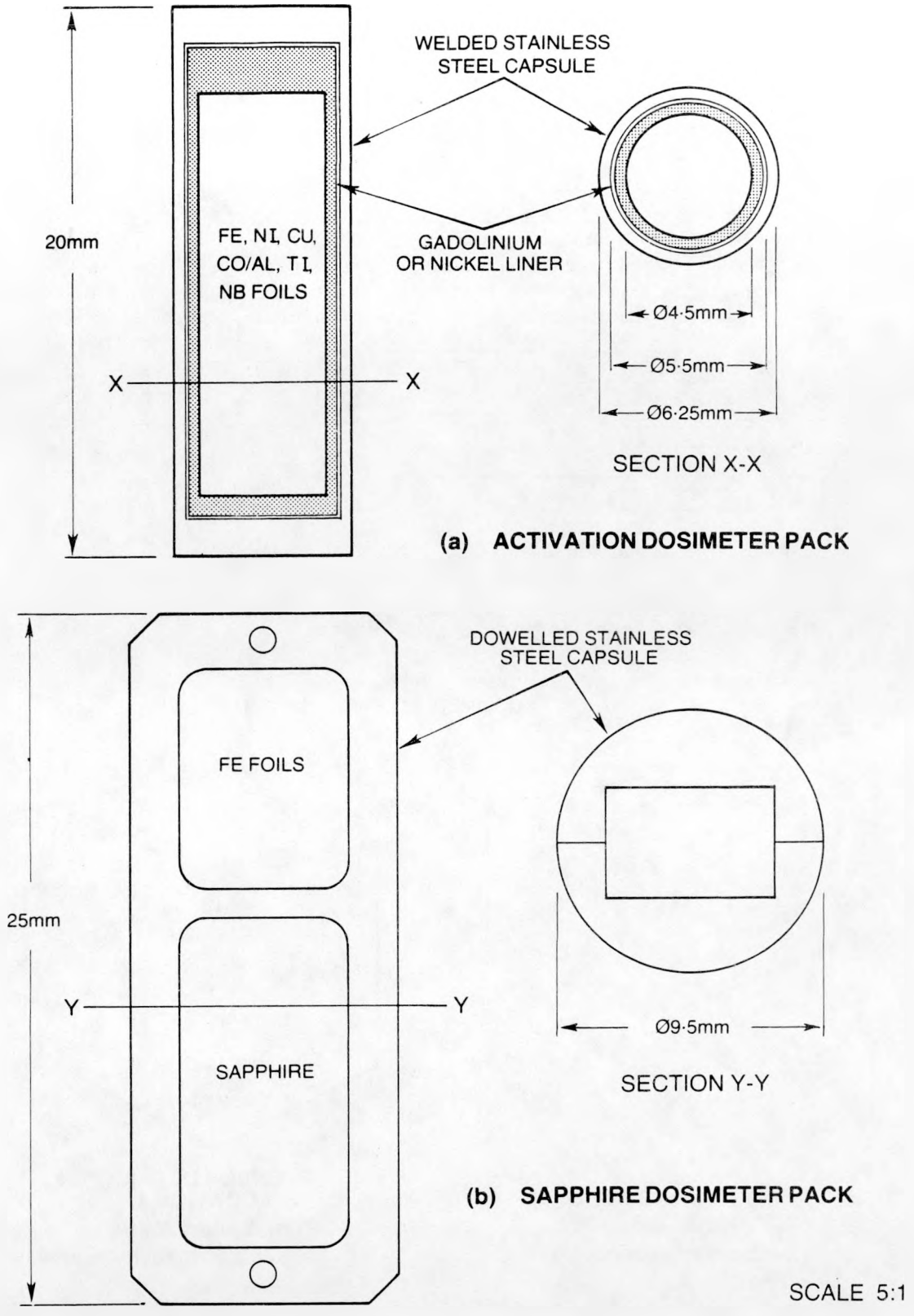

FIGURE 2.1.3.1. Design and Assembly of UK (Rolls-Royce and Associates) Dosimetry in ORR/PSF Metallurgical Capsules.

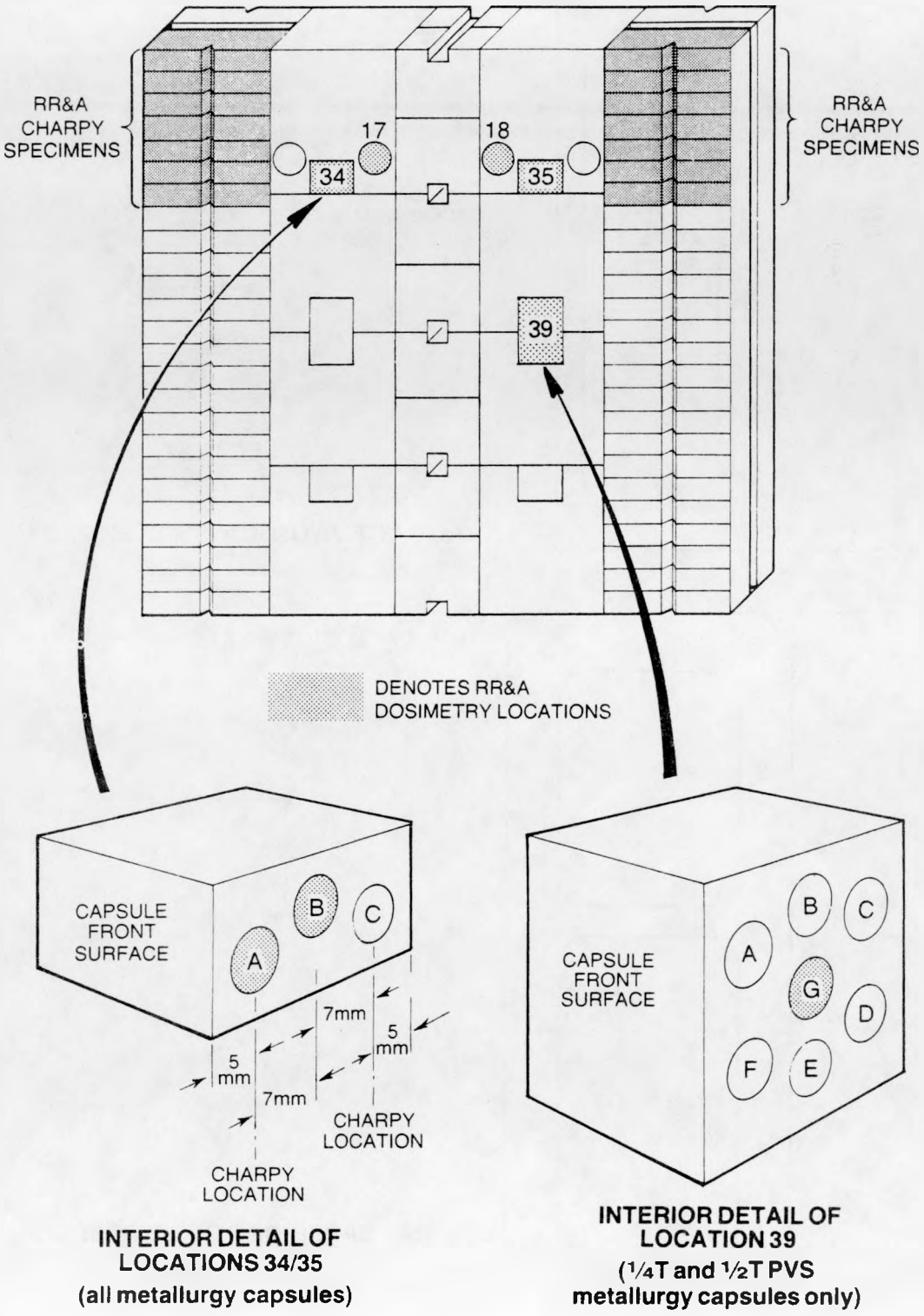

FIGURE 2.1.3.2. Location of UK (Rolls-Royce and Associates) Dosimeter Packs in ORR/PSF Metallurgical Capsules.

2.1.4 KFA Dosimetry

W. Schneider (KFA)

The results of the KFA dosimetry measurements and analysis are provided in Sections 2.3.4 and 4.5. The reader is referred to Reference (Sc86a) for the most recent and complete documentation of the final results of the KFA PSF experiments physics-dosimetry study.

2.1.5 Other Dosimetry

W. N. McElroy (HEDL)

The results of the physics-dosimetry analysis of the PSF experiments by other LWR-PV-SDIP participants will be found in Appendices A.1, A.2, A.3, A.4, A.6, A.7, and A.8 of Reference (Mc86b).

As stated in Section 3.0 of Reference (Mc86b): "None of the quoted figures for damage parameter values differed by more than 30% in either direction from the recommended HEDL and ORNL consensus evaluations, and 65% of the values were within $\pm$10%.

2.2 BENCHMARK FIELD REFERENCING

E. D. McGarry (NBS)

The bases for benchmark field referencing are usually taken to be irradiations performed in neutron fields of known energy spectra and intensities. The reason for this is that measured responses can be interpreted in absolute terms of spectrum-averaged cross sections and certified neutron fluences. There are, however, other aspects of benchmarking which rely upon relative intercomparisons, such as the comparison of different methods or comparisons of interlaboratory consistency in measuring and evaluating some quantity. Finally, there are neutron fields that are designed to mockup those nuclear reactor environments which are frequently not accessible for measurement. When these mockups are suitably characterized they are referred to as benchmark fields.

All three aspects of benchmarking, or benchmark field referencing, have been utilized in the LWR-PV-SDIP work discussed in this report. In particular, emphasis is on the use of the ORR-PSF, high-powered, benchmark-mockup of a power reactor pressure vessel.

2.2.1 Radiometric Dosimetry

Table 2.2.1 shows the results of an NBS round-robin benchmark on counting of nickel fluence standards from the $^{58}Ni(n,p)^{58}Co$ reaction induced in the ^{235}U fission spectrum. This was a measure of capabilities as of 1980. Half of the results were within the ±2.5% range of agreement; 75% of the results were within the ±5% range. Of the larger discrepancies, the 13% disagreement on sample "CI" reduced to 3% when a second fluence standard was evaluated by the laboratory involved. A subsequent round-robin test of this type has not been conducted. Instead, individual fluence standards, together with a report of the certified standard-neutron-field fluence, have been distributed for a number of radiometric reactions. Table 2.2.2 lists the fluence standards supplied to ORNL in support of the dosimetry for the start-up experiments.

Irradiations were performed at the ORR-PSF for 18 days at a reactor power of 30 MW in the SDMF-1, 4/12 SSC engineering mockup of a power reactor pressure vessel. Therein, actual surveillance dosimetry sets were exposed in the simulated surveillance capsule (SSC) and in tubes inserted into holes at 1/4, 1/2 and 3/4 thicknesses of the pressure vessel simulator block. The following laboratories participated in radiometric analyses of the dosimeters: HEDL; ORNL; CEN/SCK (Mol); KFA (Jülich); Harwell (England - counting for Rolls Royce Assos. Ltd.); PTB (Federal Republic of Germany); Petten (Netherlands). Table 2.2.3 lists the NBS Certified Fluence Standards that were supplied to these laboratories. Unfortunately, with the exception of Harwell and KFA, there has been no official communication with NBS on the results or use of these fluence standards. Although this is not strictly necessary (because a certification of the fluence which activated the particular

TABLE 2.2.1

COMPARISON OF INTERLABORATORY CONSISTENCY IN

MEASURING NICKEL FLUENCE STANDARDS[a]

Nickel Foil I.D.	^{235}U Fission Spectrum Fluence in Units of 10^{15} n/cm^2 Reported Value	NBS Value[d]	Ratio of Reported to NBS Value
AP	1.48 ± 5.5 %	1.51 ± 2.5%	0.98
AR	1.479 ± 0.84%	1.47 ± 2.7%	1.01
AS	1.491 ± 1.2 %	1.49 ± 2.7%	1.00
AU	1.672 ± 2.8 %	1.58 ± 3.6%	1.06
BK	2.74 ± 2.6 %	2.74 ± 2.4%	1.00
BL	2.85 ± 4.0 %	2.66 ± 2.5%	1.07
BM	2.60 ± 2.26%	2.65 ± 2.7%	0.98
BN	2.388 ± 0.07%	2.74 ± 2.8%	0.87
BV	2.479 ± ---	2.36 ± 2.8%	1.05
BW	2.25 ± 2.0 %	2.23 ± 3.0%	1.01
BY	2.17 ± 4.0 %	2.23 ± 3.2%	0.97
BX(1)[b]	2.286 ± 3.1 %	2.20 ± 3.2%	1.04
BX(2)	2.232 ± 1.2 %	(2.20 ± 3.2%)	1.01
CA	1.964 ± ---	2.10 ± 3.2%	0.94
CD(1)[c]	2.08 ± (1.8 %)	2.12 ± 3.5%	0.98
CD(2)	2.10 ± (1.7 %)	(2.12 ± 3.5%)	0.99
CD(3)	2.13 ± (1.7 %)	(2.12 ± 3.5%)	1.00
CG	1.61 ± 3.0 %	1.66 ± 2.9%	0.97
CI	1.96 ± 1.6 %	1.73 ± 3.2%	1.13
CJ	2.14 ± ---	2.30 ± 2.7%	0.93
CL	2.26 ± 3.3 %	2.23 ± 2.9%	1.01

Footnotes:

[a] Prepared by activation of the $^{58}Ni(n,p)^{58}Co$ reaction in the NBS Cavity ^{235}U Fission Spectrum.

[b] Two values reported by one laboratory: one for Ge(Li) and one for NaI counting.

[c] Three different groups counted this foil but did not report fluence but specific activity on 29 January 1979: Group 1 reported 8164 ± 1.7% dps; Group 2 reported 8257 ± 1.8% dps; Group 3 reported 8373 ± 1.8% dps. Fluence values were derived using a cross section of 102 mb.

[d] Accuracies differ within various sets because of positioning uncertainties in foil stacks and flux gradients.

TABLE 2.2.2

NBS NEUTRON-FLUENCE STANDARDS SUPPLIED TO ORNL TO BENCHMARK THE SDMF START-UP EXPERIMENTS* AND ORNL DOSIMETRY ACCOMPLISHED IN SUPPORT OF THE SURVEILLANCE CAPSULE PERTURBATION EXPERIMENTS**

Irradiation's I.D.	EOI	Exposure Time	Standard's I.D.	Approximate Date Supplied
^{252}Cf-11-80	11/23/80	42.3h	Indium 1 & 10	11/23/80
^{235}U-6-81	06/20/81	42.5h	Nickel AA	09/27/81
^{235}U-7-81	07/01/81	28.8h	Iron F32	09/27/81
^{252}Cf-9-81	09/27/81	39.6h	Indium K1 & K2	09/27/81
^{252}Cf-4-82	04/19/82	48.3h	Aluminum FA & FB	04/20/81
^{235}U-5-82	05/16/82	55.2h	Aluminum FA	05/17/82

*SDMF Experiment Designations and Dates

SDMF Designation	ORR Core Cycle	Dates Start	Dates Stop	Description of Purpose
1	151-A	10/27/79	11/14/79	Start Up Expt.*
2	152-A	10/31/80	02/09/80	West. Pert Expt.**
3	162-B	08/26/82	09/07/82	B&W Pert Expt.**
4-1	166-D	11/23/83	12/07/83	Radiometric & Advanced Sensor Calibration Expt.
4-2	166-E	12/09/83	12/14/83	

TABLE 2.2.3

^{235}U NEUTRON-FLUENCE STANDARDS SUPPLIED BY NBS TO BENCHMARK REFERENCE RADIOMETRIC DOSIMETRY IN THE ORR-SDMF EXPERIMENTS*

Irradiation's I.D.	EOI	Exposure Time	Standard's I.D.	Approximate Date Supplied
(Fluence standards supplied to HEDL, Richland)				
^{235}U-12-81	12/06/81	53.2h	Nickel BG	08/82
Ti-Ni-1	01/25/83	96.9h	Nickel Ni-B	03/83
Ti-Ni-1	01/25/83	96.9h	Titanium Ti-14	03/83
Fe/Ni-1	02/06/83	72.3h	Iron Fe-GB	03/83
Fe/Ni-1	02/06/83	72.3h	Nickel Ni-R	01/84
Ti/Fe-1	03/01/83	95.0h	Iron Fe-GD	01/84
U/Fe-2	11/20/83	97.8h	Alloy Fe/Ni-C	01/84
U/Fe-2	11/20/83	97.8h	^{238}U-5-27	01/84
U/Fe-3	08/30/84	149 h	^{238}U(NAT)-52	09/84
(Fluence standards supplied to KFA, Jülich)				
U/Fe-1	11/14/81	94.6h	Alloy Fe/Ni-B	12/83
U/Fe-1	11/14/81	94.6h	^{238}U-5-21	12/83
Fe/Ni-1	02/06/83	72.3h	Iron Fe-GA	12/83
Fe/Ni-1	02/06/83	72.3h	Nickel Ni-P	12/83
(Fluence standards supplied to CEN/SCK, Mol)				
Ti/Fe-1	03/01/83	95.0h	Nickel Ni-S	05/83
Ti/Fe-1	03/01/83	95.0h	Titanium Ti-15	05/83
Ti/Fe-1	03/01/83	95.0h	Iron Fe-GC	05/83
Ti/Fe-2	08/26/83	94.2h	Titanium 46A	09/83
Ti/Fe-2	08/26/83	94.2h	Titanium 46B	09/83
U/Fe-3	08/30/84	149 h	Nickel Ni-T	10/84
(Fluence standards supplied to Westinghouse, NTD, Pittsburgh)				
Ti/Fe-3	08/06/84	95.0h	Titanium Ti-2	01/85
Ti/Fe-3	08/06/84	95.0h	Iron Fe-GH	01/85
Ti/Fe-3	08/06/84	95.0h	Nickel Ni-G	01/85
(Fluence standards supplied to Harwell, England)				
^{235}U-11-78	11/14/78	15.8h	Nickel Ni-CK	02/79
^{235}U-12-81	12/06/81	53.2h	Nickel Ni-BJ	10/82
(Fluence standards supplied to ORNL, Oak Ridge)*				
Ti/Ni-1	01/25/83	96.9h	Nickel Ni-B	03/83
Ti/Fe-1	03/01/83	95.0h	Titanium Ti-16	08/83

*In addition to those specified for ORNL in Table 2.2.2

fluence standard is supplied with the standard), it would be instructive to have such results compiled for program use. For example, to relate the fluence to a measured specific activity, a fission spectrum-average cross section must be used. As can be seen in Table 2.2.4, exactly which cross section is chosen (experimental or calculated,) can make significant differences. The most notable example is the $^{63}Cu(n,\alpha)$ reaction, whose ^{235}U experimental value is currently under investigation at NBS, following a 30-day irradiation in the ^{235}U fission spectrum.

A measure of the consistency of results from various laboratories is given in Table 2.2.5 where spectral indicies relative to the $^{58}Ni(n,p)$ reaction for the SSC-1 and 1/4T SDMF-1 locations are tabulated for four of the above mentioned laboratories.

Appendix A addresses the issue of observed higher uncertainties (by a factor of two) which are associated with fissile radiometric (RM) dosimetry, as opposed to non-fissile, threshold RM dosimeters. In particular, it is noted that there is no fundamental reason for these higher uncertainties. In fact, the ^{237}Np and ^{238}U fission reactions exhibit more accurate integral cross sections in standard fission spectra than most of the threshold reactions. See Table 2.2.4 which shows observed and calculated spectrum-averaged cross sections in the ^{252}Cf and ^{235}U fission spectra. This implies that systematic effects for which corrections are methodically made are impacting the accuracy of these fission dosimeters. Problems can come from neglecting to adequately account for effects such as those caused by impurities, ^{239}Pu in ^{237}Np or ^{235}U in ^{238}U; burn-in of ^{239}Pu atoms by low energy neutron capture in ^{238}U; resonance neutron fission of ^{237}Np, perturbation of the fluence in the vicinity of the ^{237}Np detector and to a lesser extent the ^{238}U dosimeters during irradiation. Because the ^{237}Np fission reaction has the lowest threshold of all reactions, it is most sensitive to local spectrum perturbations.

2.2.2 Use of Benchmark Fields to Calibrate New Sensor Methodology

As new sensor technology is developed, it is necessary to perform definitive and easily interpretable experiments in benchmark fields with representative dosimeter sensors. Where possible, these should be performed in the standard benchmark fields and/or with direct reference to other types of previously tested sensors. Because of the inherent flux limitations in standard neutron fields, other benchmark facilities have been used; e.g., the SDMF (Mc84b) and benchmarked power reactors such as H. B. Robinson, Turkey Point, Maine Yankee, and ANO-1 and ANO-2.

2.2.2.1 Benchmark Referencing of HEDL-SSTR Technology

Following successful validation-of-method work in standard neutron fission spectra at NBS and parallel fission chamber and SSTR measurements at PCA (which further validated the SSTR technique for deposits with microgram masses and identified a NBS fission chamber field perturbation effect), SSTR technology had to extend the mass scales from microgram to nano-picogram

TABLE 2.2.4

CALCULATED-TO-OBSERVED RATIOS OF SPECTRUM-AVERAGED CROSS SECTIONS IN FISSION SPECTRA

REACTION TYPE	INTEGRAL CROSS SECTIONS (IN MILLIBARNS) Observed	Calculated	Calculated-to-Observed
(For a ^{235}U Fission Spectrum)*			
^{238}U(n,f)	312 ± 2.3%	305.2	0.978
^{237}Np(n,f)	1359 ± 2.1%	1347	0.991
^{115}In(n,n')	190 ± 2.1%	179.3	0.970
^{58}Ni(n,p)	111 ± 2.4%	105.0	0.946
^{54}Fe(n,p)	81.7 ± 2.7%	81.0	0.991
^{46}Ti(n,p)	11.8 ± 3.5%	11.2	0.949
^{63}Cu(n,α)	0.60 ± 7.0%	0.558	0.930
^{27}Al(n,α)	0.720± 3.5%	0.719	0.999
(For a ^{252}Cf Fission Spectrum)			
^{238}U(n,f)	326 ± 2.0%	313.6	0.962
^{237}Np(n,f)	1365 ± 2.0%	1352	0.990
^{115}In(n,n')	195 ± 1.9%	182	0.933
^{58}Ni(n,p)	119.4± 1.5%	114	0.955
^{54}Fe(n,p)	87.8± 2.2%	88.3	1.006
^{46}Ti(n,p)	14.2± 2.5%	13.5	0.951
^{63}Cu(n,α)	0.696± 3.0%	0.758	1.089
^{27}Al(n,α)	1.024± 2.5%	1.059	1.034

* ^{235}U spectrum is that from the ENDF/BV file

TABLE 2.2.5

EXPERIMENTAL SPECTRAL INDICIES RELATIVE TO THE $^{58}Ni(n,p)^{58}Co$ REACTION FOR THE PSF START UP EXPERIMENTS

SSC-1 (Experimental Data from Indicated Laboratory)

	Harwell	PTB	CEN/SCK	HEDL	Average
$^{63}Cu/Ni$	4.63-3	4.85-3	4.63-3	4.83-3	$4.74\pm0.15)\times10^{-3}$
$^{46}Ti/Ni$	0.0998	0.0971	0.0898	0.0936	0.095 ± 0.004
$^{54}Fe/Ni$	0.711	0.718	0.731	0.712	0.72 ± 0.01
$^{238}U/Ni$	-	-	3.78	3.95	3.87 ± 0.15
$^{237}Np/Ni$	-	-	32.0	32.3	32.2 ± 0.5

1/4T (Experimental Data from Indicated Laboratory)

$^{63}Cu/Ni$	5.74-3	5.96-3	5.65-3	5.71-3	$5.77\pm0.17)\times10^{-3}$
$^{46}Ti/Ni$	0.107	0.105	0.0985	0.103	0.103 ± 0.004
$^{54}Fe/Ni$	0.735	0.694	0.726	0.722	0.725 ± 0.02
$^{238}U/Ni$	-	-	4.14	4.32	4.23 ± 0.08
$^{237}Np/Ni$	-	-	38.7	39.1	39.0 ± 1

deposits in order to limit fission-track density in the high-powered SDMF irradiation and in ex-vessel cavity dosimetry in power reactors. As discussed in Sect. 2.4 of this document, the use of ultra-low-mass deposits has not yet been adequately benchmarked, but work is in progress. Furthermore, benchmark efforts are needed to extend validation for track densities above 5×10^5 tracks/cm^2. Consequently, SDMF and other experiments to benchmark the use of ultra-low-mass SSTRs against the older, accepted radiometric technique have yet to be completed.

2.2.2.2 Benchmark Referencing of HAFM Technology

SDMF experimental results, as well as intercomparisons from H. B. Robinson and Turkey Point irradiations are helping to confirm the applicability of the Helium Accumulation Fluence Monitoring (HAFM) Technique for the $^{27}A\ell(n,\alpha)$, $^{63}Cu(n,\alpha)$ and other reactions for surveillance capsule and cavity measurements, see Section 2.5.

2.2.3 Benchmark Coupling of PCA, PSF and HSST Measurements

In March, 1980, Fabry (Ref: Intra-Laboratory Correspondence, to F. B. K. Kam from A. Fabry, 11 March 1980, Subject: "Neutronic Characterization of the Heavy Section Steel Technology 1T-CT Capsule A: Results of Dosimetry Measurements in the Capsule A Mock-up at the BSR"), provided benchmark-referenced dosimetry measurements of neutron fluence rates, $\phi > 1$ MeV, in the HSST 1T-CT Capsule A Mock-up from fission equivalent fluence rates obtained with five reactions; $^{103}Rh(n,n')^{103}Rh$, $^{115}In(n,n')^{115}In$, $^{58}Ni(n,p)^{58}Co$, $^{27}A\ell(n,\alpha)^{24}Na$ and $^{54}Fe(n,p)^{54}Mn$. These measurements were made at the BSR at a reactor power level of 2MW, to benchmark the Heavy-Section Steel Tests at ORNL to the LWR-PV-SDIP PCA measurements. Fluence standards were made in the NBS ^{235}U and ^{252}Cf standard neutron fields to calibrate two transportable $NaI(\tau\ell)$ gamma counters from the CEN/SCK Laboratory, Mol. The methods and techniques were the same as those applied for radiometric measurements in the various PCA configurations, including the 4/12 SSC configuration that served as the critical facility for other ORNL PSF benchmark fields. This physics-dosimetry benchmarking is important because the metallurgical results obtained from irradiation in the PSF and BSR facilities are being used together with other test and power reactor data in establishing the NRC embrittlement data base (EDB).

2.3 RADIOMETRIC MEASUREMENTS

L. S. Kellogg, W. N. McElroy, R. L. Simons, Raymond Gold (HEDL)

The PSF Experiments' radiometric measurements were performed by staff members associated with the National Dosimetry Center (NDC) at HEDL and by staff members at counting laboratories at Mol (CEN/SCK), ORNL, KFA, RRA/Harwell, AEEW, ECN, PTB, GE, CE, W, B&W, SwRI, and BMI. The results of these measurements are discussed and referenced in Sections 2.3.1 through 2.3.5.

2.3.1 HEDL Results

L. S. Kellogg, W. Y. Matsumoto, J. M. Ruggles, W. N. McElroy, Raymond Gold (HEDL)

The necessary references and/or documentation for all HEDL-NDC radiometric (RM) measurements associated with the PSF Experiments are reported in Appendix A. The radiometric analysis procedures used by the NDC at HEDL are well documented in the FTR Dosimetry Handbook, MG-166. Section A1 provides a listing and brief discussion of all PSF test irradiations and discusses the results of a study of the current state-of-the-art of RM neutron dosimetry for LWR-PV surveillance. Section A2 provides and/or discusses the documentation for SSC, SPVC, SVBC, and the series of SDMF-1 through -4 experiments. Section A3 discusses the SVBC dosimetry measurement results in relation to the perturbation and reduction in magnitude of the SVBC fluence-spectra resulting from the flooding of the void box. The possible effect of the SVBC perturbations on the SSC and SPVC are also addressed by a study and comparison of measured vertical axial gradients for selected measured reaction rates. Reference is also made to the results of a set of ORNL RM measurements related to a simulated surveillance capsule perturbation experiment (Ba84a).

The flooding of the void box and possible neutron streaming effects at the top upper-most locations of the SSC, SPVC, and SVBC should be considered when comparisons and correlations are made among the results of the PCA (Mc81,Mc84i), PCA Replica (Bu84) and PSF Experiments. The availability of the RM results from all of these PSF test irradiations, therefore, should help in resolving and understanding differences between measured and calculated quantities for the PCA, PCA Replica and the PSF series of dosimetry experiments.

2.3.2 CEN/SCK RESULTS

H. Tourwé and J. Lacroix (CEN/SCK)

The results of the CEN/SCK analysis and comparison of the Mol and HEDL dosimetry measurements and the derivation of exposure parameter values of neutron fluence (E > 1 MeV) and dpa in iron are documented in Appendix A.5 of Reference (Mc86b). The reader is referred to Appendix A.5 for more detailed information and a tabulation of the Mol results for the six PV steels.

2.3.3 RR&A/HARWELL RESULTS

2.3.3.1 UK Radiometric Measurements in SSC-1 and SSC-2

A. F. Thomas (Rolls-Royce and Associates Ltd, Derby, UK)
M. Wilkins (AERE, Harwell, UK)
M. E. Foy (AERE, Harwell, UK)

2.3.3.1.1 Activation Measurements

Following removal of the activation foils from the UK dosimetry capsules in SSC-1 and SSC-2, the activity on each of the copper, iron, nickel, titanium, niobium, and cobalt/aluminum foils was measured using similar techniques to those described in NUREG/CR-3320, Vol. 2, Section 2.3.1 for the 18-Day PSF Start-Up Experiment. On this occasion, however, all activation measurements were made by AERE Harwell, including the ^{93m}Nb activity of the niobium foil that was measured by means of a silicon (Li-drifted) detector rather than the pure germanium detector used by AEE Winfrith for the niobium measurements in the 18-Day PSF Start-Up Experiment. In the case of the SSC-1 and SSC-2 analysis, the production of the sources of ^{93m}Nb* activity from the niobium foils used the same methods as those used by AEE Winfrith, but both sources and calibration standards were placed only 20 mm from the detector head. The detector efficiency calibration for the ^{93m}Nb activity was carried out by interpolation from an efficiency curve generated by means of standard sources of ^{109}Cd, ^{57}Co, ^{133}Ba, ^{139}Ce, and ^{241}Am over an energy range of 7.06 to 59.54 keV. The detector efficiency for the other activities were determined from an efficiency curve calibrated by means of standard sources of the activity being measured (i.e., ^{59}Fe, ^{58}Co, ^{60}Co, ^{55}Mn, and ^{46}Sc).

The nuclear data used in the determination of absolute activities from count rates were the same as those given in Table 2.3.1.5 of NUREG/CR-3320, Vol. 2, Section 2.3.1.

The values of absolute activity are given in Table 2.3.3.2 and are quoted in terms of disintegrations per second per milligram of dosimeter material.

2.3.3.1.2 Measurement Uncertainties

The breakdown of the activity uncertainties for all measured specific activities has been stated by AERE Harwell to be:

Source of Error	Uncertainty (1σ)
Foil weight	±0.2%*
Count rate (cps)	±2.0% (max)
γ-ray abundance	±2.0% (max)
Isotopic half-life	±0.2% (max)
Detector efficiency	±5.0%

*For the ^{93}Nb activity, see Section 2.3.3.1.4.

Table 2.3.3.1 Absolute Activities Measured on Rolls-Royce and Associates Ltd Dosimeters Used in ORR/PSF SSC-1 and SSC-2 Metallurgical Capsule

	Active Nuclide (Foil)	Activity dps/mg at End Irradiation*			
		CAPSULE 34-A	CAPSULE 34-B	CAPSULE 35-A	CAPSULE 35-B
SSC1	^{60}Co(Cu	3.275E2	2.976E2	3.042E2	2.900E2
	^{46}Sc(Ti)	2.016E4	1.765E4	1.887E4	1.783E4
	^{54}Mn(Fe)	2.776E4	2.441E4	2.859E4	2.442E4
	^{58}Co(Ni)	1.348E6	1.177E6	1.396E6	1.213E6
	^{93m}Nb(Nb)	4.378E4	3.938E4	4.832E4	3.905E4
	^{60}Co(Co/Al)	1.654E7	2.500E7	1.766E7	2.625E7
	^{59}Fe(Fe)	-	-	-	-
SSC2	^{60}Co(Cu)	6.122E2	5.487E2	5.942E2	5.278E2
	^{46}Sc(Ti)	3.191E4	2.884E4	3.129E4	2.738E4
	^{54}Mn(Fe)	5.216E4	4.447E4	5.172E4	4.656E4
	^{58}Co(Ni)	2.033E6	1.768E6	1.996E6	1.739E6
	^{93m}Nb(Nb)	9.480E4	6.453E4	8.917E4	6.003E4
	^{60}Co(Co/al)	3.132E7	4.938E7	3.131E7	4.906E7
	^{59}Fe(Fe)	3.210E4	8.102E4	3.232E4	8.207E4
	LINER	Gd	Ni	Gd	Ni

*^{58}Co activity 14 days after end of irradiation.

This can be summarized as 3% (1σ) random errors on each activity measured and 5% (1σ) systematic error on each set of activities from a given capsule.

2.3.3.1.3 Activation Analysis

The measured activities shown in Table 2.3.3.1 and the irradiation power histories given in Ref. (Mc84c) were processed by means of the Rolls-Royce and Associates computer code, ADA, described in NUREG/CR-3320, Vol. 2, Section 2.3.1.4 to produce reaction rates at a nominal ORR core power of 30 MW. These reaction rates are tabulated in Table 2.3.3.2. For convenience, only the absolute reaction rate values for the reaction rates in the 34-A capsule locations are shown; all the other reaction rates are relative to the appropriate activity in the 34-A capsule. The ratio of measured reactor rates (SSC-1/SSC-2) is given in Table 2.3.3.3.

Table 2.3.3.2 Reaction Rates Measured on Rolls-Royce and Associates Ltd. Dosimeters in ORR/PSF SSC1 and SSC2 Metallurgical Capsules

	REACTION	REACTION RATE (s^{-1} atom $^{-1}$) (30MW)*			
		CAPSULE 34-A	CAPSULE 34-B	CAPSULE 35-A	CAPSULE 35-B
SSC1	$^{63}Cu(n,\alpha)^{60}Co$	3.133E-15	0.91	0.93	0.89
	$^{46}Ti(n,p)^{46}Sc$	6.679E-14	0.88	0.94	0.88
	$^{54}Fe(n,p)^{54}Mn$	4.755E-13	0.88	1.03	0.88
	$^{54}Ni(n,p)^{58}Co$	6.690E-13	0.87	1.04	0.90
	$^{93}Nb(n,n')^{93m}Nb$	1.309E-12	0.90	1.10	0.89
	$^{59}Co(n,\gamma)^{60}Co$	1.015E-10	0.51	1.07	1.59
	$^{58}Fe(n,\gamma)^{59}Fe$	-	-	-	-
SSC2	$^{63}Cu(n,\alpha)^{60}Co$	2.955E-15	0.90	0.97	0.86
	$^{46}Ti(n,p)^{46}Sc$	6.544E-14	0.90	0.98	0.86
	$^{54}Fe(n,p)^{54}Mn$	4.758E-13	0.85	0.99	0.89
	$^{58}Ni(n,p)^{58}Co$	6.532E-13	0.87	0.98	0.86
	$^{93}Nb(n,n')^{93m}Nb$	1.420E-12	0.68**	0.94	0.63**
	$^{59}Co(n,\gamma)^{60}Co$	9.700E-11	1.58	1.00	1.57
	$^{58}Fe(n,\gamma)^{59}Fe$	1.513E-12	2.52	1.01	2.56
	LINER	Gd	Ni	Gd	Ni

* Reaction rates in capsules 34B, 35A, 35B are relative to 34A
** Probable counting errors.

Table 2.3.3.3 Comparison of Measured Reaction Rates in Rolls-Royce and Associates Ltd. Dosimetry in SSC1 and SSC2

REACTION	RATIO OF SSC REACTION RATES (SSC1/SSC2)				
	CAPSULE 34-A	CAPSULE 34-B	CAPSULE 35-A	CAPSULE 35-B	MEAN
$^{63}Cu(n,\alpha)^{60}Co$	1.06	1.07	1.02	1.10	1.06±0.03
$^{46}Ti(n,p)^{46}Sc$	1.02	1.00	0.98	1.04	1.01±0.03
$^{54}Fe(n,p)^{54}Mn$	1.00	1.03	1.04	0.99	1.02±0.02
$^{58}Ni(n,p)^{58}Co$	1.02	1.02	1.09	1.07	1.05±0.04
$^{93}Nb(n,n')^{93m}Nb$	0.92	(1.22)*	1.08	(1.30)*	1.00±0.11
$^{59}Co(n,\gamma)^{60}Co$	1.05	1.00	1.12	1.06	1.06±0.05
$^{58}Fe(n,\gamma)^{59}Fe$	-	-	-	-	-
MEAN	1.01±0.05	1.02±0.03	1.06±0.05	1.05±0.04	1.04±0.02

*Probable counting errors in SSC2

2.3.3.1.4 Discussion

Results of reaction rate measurements using the threshold (fast neutron) detectors indicate that in both the SSC-1 and SSC-2 irradiations the fast neutron flux intensity was symmetrical about the capsule vertical axis (i.e., the 34-A and 35-A reaction rates are very similar, given the size of the measurement errors). Similarly, the differences in reaction rates in the A locations are 10% to 15% higher than those in the B locations, which is consistent with the deeper penetration of the B location by about 7 mm (see Figure 1.2.1).

Results of the resonance reaction rates (i.e., $^{59}Co(n,\gamma)$ and $^{58}Fe(n,\gamma)$ in gadolinium box capsules 34-A and 35-A) reflect the lateral symmetry of the flux profile observed in the threshold detector reaction rates. However, the uncovered reaction rates measured on these detectors in the nickel box capsules in locations 34-B and 35-B were some 55% higher than those in the 34-A and 35-A locations (i.e., the gadolinium box capsules) for the $^{59}Co(n,\gamma)$ reaction and 160% higher for the $^{58}Fe(n,\gamma)$ reaction. On the assumption that the resonance reaction rate in the B locations is also 10% to 15% less than in the A locations, this implies a so-called 'gadolinium ratio' (i.e., covered-to-uncovered reaction rate) of 1.9 for $^{59}Co(n,\gamma)$ and 3.0 for $^{58}Fe(n,\gamma)$ in the 34-B and 35-B locations in the SSC-1 and SSC-2 irradiations.

Comparison of reaction rates in the SSC-1 and SSC-2 irradiations indicated that the flux levels were a few percent higher in SSC-1 than in SSC-2, which might easily occur as the result of changes in power distribution in the ORR core over the two irradiation periods. However, within this general observation it may be noted that the $^{93}Nb(n,n')$ reaction rates are not so consistent, particularly in the case of the $^{93}Nb(n,n')$ reaction rates in capsules 34-B and 35-B in SSC-2 and, to a lesser extent, in capsule 35-A in SSC-1. This inconsistency can be probably ascribed to inherent difficulties in determining the specific activity of ^{93m}Nb using the method described in NUREG/CR-3320, Vol. 2, Section 2.3.1.3 since the dissolution of the niobium foil can sometimes prove less than satisfactory. For the purposes of data analysis, therefore, it is recommended that the random errors on the ^{93m}Nb activity should be assumed to be $\pm$10%.

2.3.3.2 UK Radiometric Measurements in the Surface, 1/4 T and 1/2 T PVS Capsules

A. F. Thomas (Rolls-Royce and Associates)
M. Wilkins and M. E. Foy (AERE Harwell)

2.3.3.2.1 Dosimetry Design

The design of the UK dosimetry in the PVS block was identical in all major respects to the UK dosimetry in the SSC-1 and SSC-2 capsules (see Section 1.2 and NUREG/CR-3320, Vol. 1, Section 1.3). This involved placing the UK activation dosimetry capsule in locations 34-A, 34-B, 35-A and 35-B and the Sapphire Damage Monitor capsules in locations 17 and 18. In addition, in the 1/4 T and 1/2 T capsules additional UK activation dosimetry packs were placed in the 39-G locations to serve as an intercomparison point with the HEDL and CEN/SCK dosimetry in the 39-E and B locations, respectively, and the KFA dosimetry in the Charpy-V right-front 13 position [CVRF (13)]; see Table 1.2.1.

2.3.3.2.2 Activation Measurements

The methods used to measure the UK dosimetry in the PVS block were also identical in all major respects to those used to measure the UK dosimetry in the SSC-1 and SSC-2 capsules (see NUREG/CR-3320), Vol. II, Section 2.3.1). The measured activities of all the dosimetry foils irradiated in the PVS block are shown in Table 2.3.3.4.

2.3.3.2.3 Measurement Uncertainties

The uncertainties in the measurement of activities are stated by AERE Harwell to be the same as those quoted for the SSC-1 and SSC-2 UK dosimetry measurements (see NUREG/CR-3320, Vol. 2), i.e., 3% (1σ) random errors and 5% (1σ) systematic errors. However, discrepancies in the analysis of the ^{93m}Nb activities indicate (as was noted in the case of the SSC-1 and SSC-2 niobium activities) that the random errors on this activity are nearer to $\pm$10% (1σ).

2.3.3.2.4 Activation Analysis

The activation analysis of the measured activities from the UK dosimeters in the PVS block was conducted in the same manner as for those in the SSC-1 and SSC-2 capsules (see NUREG/CR-3320, Vol. 2). Power history corrections were made using the power histories given in (Gu82c), and reaction rates at a nominal 30-MW core power were calculated. These are given in Table 2.3.3.5.

Table 2.3.3.4 Absolute Activities Measured on Rolls-Royce and Associated Ltd Dosimeters Used in ORR/PSF Pressure Vessel Simulator (PVS)

	Active Nuclide (Foil)	Activity dps/mg at End Irradiation*				
		CAPSULE 34A	CAPSULE 34B	CAPSULE 35A	CAPSULE 35B	CAPSULE 39G
OT	^{60}Co(Cu)	5.720E2	5.288E2	5.690E2	5.117E2	-
	^{46}Sc(Ti)	7.004E3	5.915E3	6.700E3	6.141E3	-
	^{54}Mn(Fe)	2.326E4	2.078E4	2.376E4	2.102E4	-
	^{58}Co(Ni)	3.632E5	3.557E5	3.666E5	3.527E5	-
	^{93m}Nb(Nb)	6.441E4	5.173E4	5.812E4	5.695E4	-
	^{60}Co(Co/Al)	2.687E7	6.670E7	2.634E7	6.853E7	-
	^{59}Fe(Fe)	4.997E3	2.159E4	4.972E3	2.346E4	-
¼T	^{60}Co(Cu)	2.517E2	2.427E2	2.498E2	2.304E2	2.254E2
	^{46}Sc(Ti)	3.134E3	2.524E3	3.143E3	2.606E3	2.723E3
	^{54}Mn(Fe)	1.047E4	9.065E3	1.084E4	9.124E3	9.488E3
	^{58}Co(Ni)	1.761E5	1.526E5	1.772E5	1.549E5	1.618E5
	^{93m}Nb(Nb)	3.697E4	3.428E4	3.579E4	3.280E4	3.326E4
	^{60}Co(Co/Al)	1.358E7	1.547E7	1.341E7	1.460E7	1.158E7
	^{59}Fe(Fe)	2.214E3	3.134E3	2.423E3	3.324E3	2.043E3
½T	^{60}Co(Cu)	9.691E1	9.005E1	9.686E1	9.053E1	8.734E1
	^{46}Sc(Ti)	1.225E3	1.057E3	1.159E3	1.016E3	1.038E3
	^{54}Mn(Fe)	4.143E3	3.694E3	4.272E3	3.337E3	3.707E3
	^{58}Co(Ni)	6.940E4	6.354E4	6.971E4	6.199E4	6.324E4
	^{93m}Nb(Nb)	1.027E4**	1.579E4	1.678E4	1.336E4	1.676E4
	^{60}Co(Co/Al)	6.626E6	6.727E6	6.437E6	6.496E6	5.706E6
	^{59}Fe(Fe)	1.130E3	1.286E3	1.196E3	1.164E3	1.038E3
	LINER	Gd	Ni	Gd	Ni	Gd

*^{58}Co activity 14 days after end of irradiation.
**Probable counting error.

Table 2.3.3.5 Reaction Rates Measured on Rolls-Royce and Associated Ltd Dosimeters in ORR/PSF Pressure Vessel Simulator (PVS)

	REACTION	REACTION RATE ($s^{-1}.atom^{-1}$) (30MW)*				
		CAPSULE 34A	CAPSULE 34B	CAPSULE 35A	CAPSULE 35B	CAPSULE 39G
	$^{63}Cu(n,\alpha)^{60}Co$	4.816E-16	0.92	0.99	0.89	-
	$^{46}Ti(n,p)^{46}Sc$	8.580E-15	0.85	0.96	0.88	-
	$^{54}Fe(n,p)^{54}Mn$	5.836E-14	0.89	1.02	0.90	-
OT	$^{58}Ni(n,p)^{58}Co$	7.370E-14	0.98	1.01	0.98	-
	$^{93}Nb(n,n')^{93m}Nb$	1.509E-13	0.80	0.90	0.88	-
	$^{59}Co(n,\gamma)^{60}Co$	1.400E-11	2.49	0.98	2.56	-
	$^{58}Fe(n,\gamma)^{59}Fe$	1.858E-13	4.30	1.00	4.71	-
	$^{63}Cu(n,\alpha)^{60}Co$	2.051E-16	0.96	0.99	0.92	0.90
	$^{46}Ti(n,p)^{46}Sc$	3.839E-15	0.81	1.00	0.83	0.87
	$^{54}Fe(n,p)^{54}Mn$	2.627E-14	0.87	1.04	0.87	0.91
¼T	$^{58}Ni(n,p)^{58}Co$	3.573E-14	0.87	1.00	0.88	0.92
	$^{93}Nb(n,n')^{93m}Nb$	8.662E-14	0.93	0.97	0.89	0.90
	$^{59}Co(n,\gamma)^{60}Co$	7.107E-12	1.14	0.99	1.08	0.85
	$^{58}Co(n,\gamma)^{59}Fe$	8.265E-14	1.42	1.09	1.50	0.92
	$^{63}Cu(n,\alpha)^{60}Co$	7.897E-17	0.93	1.00	0.93	0.90
	$^{46}Ti(n,p)^{46}Sc$	1.501E-15	0.86	0.95	0.83	0.85
	$^{54}Fe(n,p)^{54}Mn$	1.039E-14	0.89	1.03	0.81	0.90
½T	$^{58}Ni(n,p)^{58}Co$	1.408E-14	0.91	1.00	0.89	0.91
	$^{93}Nb(n,n')^{93m}Nb$	3.931E-14**	0.94	1.00	0.80	1.00
	$^{59}Co(n,\gamma)^{60}Co$	3.465E-12	1.01	0.97	0.98	0.86
	$^{58}Fe(n,\gamma)^{59}Fe$	4.218E-14	1.14	1.06	1.03	0.91
	LINER	Gd	Ni	Gd	Ni	Gd

*Capsules 34-B, 35-A, 35-B, and 39-G normalized to values in 34-A.
**Reaction rate actually measured was 2.406E-14, but this appears to be in error. The value measured in 35-A has, therefore, been quoted as the normalization value since there is no apparent left-to-right bias.

2.3.3.2.5 Discussion

The trends in reaction rate measurements follow a similar pattern to that noted in the SSC-1 and SSC-2 capsules, i.e.,

- There is no significant left-to-right bias from the 34-A/-B locations to the 35-A/-B locations.
- The threshold (i.e., fast neutron) detector reaction rate measurements in the 34-A and 35-A locations are 10% to 15% higher than those in the 34-B and 35-B locations.

Results from the resonance reaction rates [i.e., $^{59}Co(n,\gamma)$ and $^{58}Fe(n,\gamma)$ in the gadolinium box capsules 34-A and 35-A] and the thermal reaction rates [i.e., $^{59}Co(n,\gamma)$ and $^{58}Fe(n,\gamma)$ in the nickel box capsules 34-B and 35-B] indicate that the "gadolinium ratios" in the PVS location are as follows:

	$^{59}Co(n,\gamma)$	$^{58}Fe(n,\gamma)$
PSV (0 T)	3.0	5.3
PSV (1/4 T)	1.3	1.7
PSV (1/2 T)	1.2	1.3

The only obvious discrepancy in the measured reaction rates was that of the $^{93}Nb(n,n')$ reaction in the 34-A location in the PVS (1/2 T) capsule. This is probably due to the problems encountered in the SSC-1 and SSC-2 analyses in which difficulties can sometimes arise in determining the specific activity of the dissolved niobium foils prior to counting. In view of the lateral symmetry of the capsule reaction rates, it is, therefore, recommended that the $^{93}Nb(n,n')$ reaction rate measured in 35-A be used as the normalization point in Table 2.3.3.5.

It is also worth noting that, due to the long (2+ years) duration of the PVS capsules irradiations, the ratio of activation product half-life to irradiation time for several of the detectors was less than optimal. This lack of optimization would manifest itself as an additional uncertainty in the integrated reaction rate of such a detector in the case of an unknown and variable source intensity. Such source variations may not only result from changes in reactor power, which can be monitored, but also from changes in local power distributions that may be of equal importance but not be so readily monitored. This might clearly be true in the case of the changes in the power distributions over the 52 reactor cycles that occurred in the Oak Ridge Reactor (ORR) during the PVS irradiation. As far as the reaction rates in the PVS capsules are concerned, therefore, those of $^{58}Ni(n,p)$, $^{46}Ti(n,p)$ and $^{58}Fe(n,\gamma)$, whose product half-lives are, respectively, only 11%, 13% and 7% of the lengths of the irradiation, and are probably a reflection of the reaction rates in the PVS only during the last 10 to 20 cycles of irradiation.

In order to investigate any such differences, the comparison of measured reaction rates in the 18-Day Start-Up (SU), SSC-1, SSC-2 and PVS capsules was made. The results of the comparison indicated that no significant discrepancies exist between reactions of different product half-lives. However, while the SSC-1, SSC-2, and SU (SSC) reaction rates are very similar, those in the SU (1/4 T) and SU (1/2 T) are about 10% higher than those in the PVS (1/4 T) and PVS (1/2 T). Such systematic differences could well be due to parallel differences in time-averaged local source distributions. However, in the case of the PVS capsules, the lack of differential effects between reactions may signify that time-averaged local source distribution over the last 10 to 20 cycles was typical of the total 52-cycle irradiation.

2.3.4 KFA RESULTS

W. Schneider (Kernforschungsanlage Jülich GmbH)

2.3.4.1 Introduction

About the program and the experiments mentioned here in (Sc86a), we refer to the relevant publications (Ka82,Mo78,Ro80,Sc86a), to the HEDL dosimeter preparation report (Li81), and to the LWR-PV-SDIP meeting results. Besides the general description of the purpose, procedure, and arrangements made for the experiments, in these references are given the locations of the individual specimens and dosimeters belonging to all participants for the different irradiations. So among others the particular arrangement of the KFA dosimeter is given in the positions "Cube 32" and "KFA Charpy" for all irradiations (see Table 1.2.1). The data of the irradiations carried out (SSC-1, SSC-2, and the others) are given in (Cu78,Ho79,Mu76,Sc86a,Se81,Zi79).

2.3.4.2 Measurement of the Dosimeters

Arriving at Jülich after irradiation, the dosimeters were recapsuled for measurement. Since all dosimeters were radiometric, all were measured with the aid of two (Ge-Li) gamma-ray spectrometers, both of them calibrated (and cross-calibrated). The two spectrometers are different in sensitivity to higher and lower radioactivity regions. For determining the wanted activities, for each radionuclide at least two gamma-ray full-energy peaks were measured, either simultaneously (if several peaks were available) or by repetition after a decay time long enough to help to identify the nuclide being sought. Further details of the measurement procedure will not be reported here because they are of no special interest.

2.3.4.3 Evaluation of the Measurements

About the evaluation, we restrict ourselves here to saying that from the measured gamma-ray peaks the radioactivities of the nuclides in question have been determined in the usual way. From the activities, the reaction rates per atom of the original nuclide of the different measuring reactions have been evaluated, relative to the start of the irradiation. For this evaluation, the dosimeter data were taken from Lists 1a and 1b and the corrections applied as given in List 2. The neutron and nuclide data have been taken mainly from (Zi79) and in special cases from (Cu78,Ho79,Mu76,Se81).

The measured neutron reactions and the evaluated reaction rates are presented in Lists 3a and 3b. Comparisons, further evaluation of these data, and their discussion will be given in Section 4.5.

2.3.4.4 Acknowledgements

All names given here belong to coworkers of the Kernforschungsanlage Jülich, Division ZBB. The preparation of the dosimeters before irradiation was executed by G. Segelhorst, the recuperation and recapsulation of the irradiated dosimeters by O. Hampe. The evaluation of the single gamma-ray peaks (with resulting activities, including the time corrections) was done by G. Borchardt, applying his evaluation code.

Date: Jan.1984 List No.: 1a

Dosimeter description and measurement results from KFA Jülich to LWR-PV-SDIP PSF Specimen Set: SSC-1

Material, composition	Size (mm)	Mass (mg)	Dosimeter	Irradiation Position
Metal, Ti el.:99.917% /*/	. 5Øx .5	4.438	Ti	
Metal, Fe el.:99.975% /*/	. 5Øx 5	8.035	Fe	
				Cube "32"
Metal, Ni el.:99.999% /*/	. 5Øx 5	9.072	Ni	
				(Dosi-
Ceramic,Sc el.:64.63% /*/	. 5Øx2.5	.8382	Sc_2O_3	meters
Ceramic,Sc el.:.1272% /*/	. 5Øx 6	3.007	Sc/MgO	without Gd
				cover)
Co-Al alloy,Co el.:.116% /*/	. 5Øx 5	2.484	Co	[Location 32,
Ag-Al alloy,Ag el.:.145% /*/	. 5Øx 5	2.557	Ag	Table 1.2.1]
Metal, Cu el.:99.999%, [1]	1.0Øx 5	35.33	Cu	
Metal, Ti el.:99.917%, [2]	. 3Øx 5	3x1.085	Ti	
Metal, Fe el.:99.999%,	. 5Øx 5	7.940	Fe	
				KFA
Metal, Ni el.:99.95 %	. 5Øx 5	8.430	Ni	Charpy
Ceramic,U(depl.)O_2,U238 i.U: 99.999%, in V capsule [3]	1.3Øx8.6	U:7.950	U-238	(Dosi-
" ,ThO_2,Th232 i.Th:100%	1.3Øx7.1	Th:5.123	Th	meters
" ,NpO_2,Np237 i.Np: 99.99%	1.3Øx8.6	Np:7.794	Np	with Gd
Metal, Sc el.: 99.9 %	1.2Øx2.5	7.150	Sc	cover)
Metal, Co el.: 99.99%	. 1Øx 5	.3795	Co	[CVRF (13),
Metal, Ag el.: 99.999%	. 5Øx 5	10.14	Ag	Table 1.2.1]
Ceramic, U(enr.)O_2, [4] in V capsule	1.3Øx 8	U:8.573	U-235	

/*/ Dosimeters provided by HEDL; data in reference (Li81) related to the atomic weight of the elemental substance

1) Co <1ppm 2) 3 wires of 3) U235 in U:.0012 %

4) U235 i.U: 99.89 %

Date: Jan.1984 List No.: 1b

Dosimeter description and measurement results from KFA Jülich to LWR-PV-SDIP PSF Specimen Set: SSC-2

Material, composition	Size (mm)	Mass (mg)	Dosimeter	Irradiation Position
Metal, Ti el.:99.917% /*/	. 5Øx 5	4.506	Ti	
Metal, Fe el.:99.975% /*/	. 5Øx 5	8.234	Fe	
				Cube "32"
Metal, Ni el.:99.99% /*/	. 5Øx 5	8.815	Ni	
				(Dosi-
Ceramic,Sc el.:64.63% /*/	. 5Øx2.5	.7856	Sc_2O_3	meters
Ceramic,Sc el.:.1272% /*/	. 5Øx 6	3.349	Sc/MgO	without Gd
				cover)
Co-Al alloy,Co el.:.116% /*/	. 5Øx 5	2.474	Co	[Location 32,
Ag-Al alloy,Ag el.:.145% /*/	. 5Øx 5	2.508	Ag	Table 1.2.1]
Metal, Cu el.:99.999%, 1)	1.0Øx 5	34.76	Cu	
Metal, Ti el.:99.917%, 2)	. 3Øx 5	3x1.085	Ti	
Metal, Fe el.:99.999%,	. 5Øx 5	7.940	Fe	
				KFA
Metal, Ni el.:99.95 %	. 5Øx 5	8.430	Ni	Charpy
Ceramic,U(depl.)O_2,U238 i.U: 99.999%, 3) in V capsule	1.3Øx8.6	U:8.377	U-238	(Dosi-
" ,ThO_2,Th232 i.Th:100%	1.3Øx7.1	Th:5.130	Th	meters
" ,NpO_2,Np237 i.Np: 99.99%	1.3Øx8.6	Np:7.691	Np	with Gd cover)
Metal, Sc el.: 99.9 %	1.2Øx2.5	7.330	Sc	[CVRF (13).
Metal, Co el.: 99.99%	. 1Øx 5	.3795	Co	Table 1.2.1]
Metal, Ag el.: 99.999%	. 5Øx 5	10.14	Ag	
Ceramic, U (enr.)O_2, 4) in V capsule	1.3Øx 8	U:8.401	U-235	

/*/ Dosimeters provided by HEDL; data in reference (Li81) related to the atomic weight of the elemental substance

1) Co <1ppm 2) 3 wires of 3) U235 in U:.0012 %

4) U235 i.U: 99.89 %

Date: Jan.1984 List No.: 2

Dosimeter description and measurement results from KFA Jülich

to LWR-PV-SDIP PSF Specimen Set: SSC-1, SSC-2

Corrections applied to the measured activity for systematic errors (disturbing activities) caused by: the dosimeter element or nuclide	impurities	Dosimeter	Irradiation Position
		Ti	
		Fe	
			Cube "32"
Co58m(n,γ) Co59 Co58g(n,γ)		Ni	
			(Dosimeters without Gd cover)
		Sc_2O_3	
		Sc/MgO	
		Co	[Location 32, Table 1.2.1]
		Ag	
	Co59(n,γ)Co60	Cu	
	Ta 182	Ti	
		Fe	
			KFA Charpy
Co58m(n,γ) Co59 Co58g(n,γ)		Ni	
U238(γ,f)/ * /; Pu239(n,f)	U235(n,f)	U-238	(Dosimeters with Gd cover)
Th232(γ,f)/ * /;U233(n,f)		Th	
Np237(γ,f)/ * /;Np238(n,f)		Np	
		Sc	[CVRF (13), Table 1.2.1]
		Co	
		Ag	
U235(γ,f)/ * /		U-235	

*References (Cu78,Ho79,Mu76,Se81,Zi79).

Date: Jan.1984 List No.: 3a

Dosimeter description and measurement results from KFA Jülich to LWR-PV-SDIP PSF Specimen Set: SSC-1

Measured Reaction	Reaction Rate 1/s		+(1σ) Uncert. %	Dosimeter	Irradiation Position
Ti (n,x)Sc46	6.573	E-14 ±	2.8	Ti	
Fe54 (n,p)Mn54	5.024	E-13 ±	2.9	Fe	
Fe58 (n,γ)Fe59	4.504	E-12 ±	10.4		Cube "32"
Ni58 (n,p)Co58	6.931	E-13 ±	2.6	Ni	
Sc45 (n,γ)Sc46	5.147	E-11 ±	3.0	Sc_2O_3	(Dosimeters without Gd cover)
Sc45 (n,γ)Sc46	7.715	E-11 ±	2.6	Sc/MgO	
Co59 (n,γ)Co60	2.101	E-10 ±	3.0	Co	Location 32, Table 1.2.1]
Ag109 (n,γ)Ag110m	1.226	E-10 ±	2.5	Ag	
Cu63 (n,α)Co60	2.918	E-15 ±	2.5	Cu	
Ti (n,x)Sc46	5.920	E-14 ±	2.3	Ti	
Fe54 (n,p)Mn54	4.416	E-13 ±	3.0	Fe	
Fe58 (n,γ)Fe59	1.544	E-12 ±	10.5		KFA Charpy (Dosimeters with Gd cover) [CVRF (13), Table 1.2.1]
Ni58 (n,p)Co58	6.131	E-13 ±	2.7	Ni	
U 238(n,f)F.P.	2.243	E-12 ±	3.1	U-238	
Th232(n,f)F.P.	5.970	E-13 ±	4.9	Th	
Np237(n,f)F.P.	1.701	E-11 ±	3.8	Np	
Sc45 (n,γ)Sc46	1.657	E-11 ±	2.8	Sc	
Co59 (n,γ)Co60	7.332	E-11 ±	2.8	Co	
Ag109(n,γ)Ag110m	2.052	E-11 ±	1.6	Ag	
U 235(n,f)F.P.	3.880	E-10 ±	3.5	U-235	

Date: Jan.1984 List No.: 3b

Dosimeter description and measurement results from KFA Jülich to LWR-PV-SDIP PSF Specimen Set: SSC-2

Measured Reaction	Reaction Rate 1/s		± (1σ) Uncert. %		Dosimeter	Irradiation Position
Ti (n,x)Sc46	6.211	E-14	±	2.7	Ti	
Fe54 (n,p)Mn54	5.032	E-13	±	3.0	Fe	
Fe58 (n,γ)Fe59	4.464	E-12	±	10.8		Cube "32"
Ni58 (n,p)Co58	6.678	E-13	±	2.8	Ni	
Sc45 (n,γ)Sc46	7.781	E-11	±	1.8	Sc_2O_3	(Dosimeters without Gd cover)
Sc45 (n,γ)Sc46	8.154	E-11	±	2.6	Sc/MgO	
Co59 (n,γ)Co60	2.067	E-10	±	3.0	Co	[Location 32, Table 1.2.1]
Ag109 (n,γ)Ag110m	1.206	E-10	±	2.4	Ag	
Cu63 (n,α)Co60	2.855	E-15	±	2.5	Cu	
Ti (n,x)Sc46	5.951	E-14	±	2.8	Ti	
Fe54 (n,p)Mn54	4.450	E-13	±	2.4	Fe	
Fe58 (n,γ)Fe59	1.482	E-12	±	10.5		KFA Charpy
Ni58 (n,p)Co58	5.781	E-13	±	2.7	Ni	(Dosimeters with Gd cover)
U 238(n,f)F.P.	2.342	E-12	±	3.1	U-238	
Th232(n,f)F.P.	6.067	E-13	±	5.6	Th	
Np237(n,f)F.P.	1.580	E-11	±	3.1	Np	
Sc45 (n,γ)Sc46	1.281	E-11	±	2.3	Sc	[CVRF (13), Table 1.2.1]
Co59 (n,γ)Co60	not recuperated				Co	
Ag109(n,γ)Ag110m	2.018	E-11	±	1.3	Ag	
U 235(n,f)F.P.	3.685	E-10	±	2.6	U-235	

By means of the code SAND-MX2 the reaction rates from the SSC-1, KFA Charpy position [CVRF (13), Table 1.2.1] were used by L. Weise for neutron spectrum unfolding (We83), starting with an approximation spectrum provided by H. Tourwe obtained with the one-dimensional transport code ANISN. The reaction rates used in (We83) are almost completely identical with those given here in List 3a; however, for ^{238}U a re-evaluation (for improved corrections) lead to a somewhat (~10%) higher value, which should cause no remarkable spectrum distortion, all the more as the SAND-MX2 code did shift the ^{238}U reaction rate as first reported already in the correct direction.

2.3.5 OTHER RESULTS

W. N. McElroy (HEDL)

The results of the physics-dosimetry analysis of the PSF experiments by other LWR-PV-SDIP participants will be found in Appendices A.1, A.2, A.3, A.4, A.6, A.7, and A.8 of Reference (Mc86b).

As stated in Section 3.0 of Reference (Mc86b): "None of the quoted figures for damage parameter values differed by more than 30% in either direction from the recommended HEDL and ORNL consensus evaluations, and 65% of the values were within $\pm$10%.

2.4 SOLID STATE TRACK RECORDER EXPERIMENTS

R. Gold, C. C. Preston and L. S Kellogg (HEDL) and
J. H. Roberts (MC^2)

2.4.1 INTRODUCTION

The ASTM E854 "Standard Method for Analysis of Solid State Track Recorder (SSTR) Monitors for Reactor Surveillance," E706(IIIB) (see Figure S.2) describes the use of SSTRs for neutron dosimetry in light-water reactor applications (As82b). In support of this standard, SSTRs were inserted in the PSF Experiments to demonstrate applications at fluences and temperatures typical of power reactor surveillance conditions.

SSTR observations provide time-integrated reaction rates. Therefore, SSTR are truly passive-fluence detectors. They provide permanent records of dosimetry experiments without the need for time-dependent corrections, such as decay factors that arise with radiometric monitors. Also, the SSTRs cause minimal perturbations to the neutron environment and do not require neutron self-shielding corrections; i.e., they provide a direct measurement of infinitely dilute fission rates.

The useful range of the SSTR method in manual counting is limited by upper and lower bounds on track density that arise in practice. These upper and lower bounds are roughly 5×10^5 tracks/cm^2 and 5 tracks/cm^2, respectively. These are representative bounds for manual scanning work at high accuracy levels; and as such, they depend upon many factors, such as the type of SSTR, etching conditions, deposit range, and method of track scanning. For high accuracy automated track scanning, the lower and upper bounds are currently, about 5×10^4 and 5×10^5 tracks/cm^2, respectively (for uniform track density SSTR).

The design, fabrication, and placement of SSTR in combination with HAFM, RM, Sapphire DM, and PV steel DM sensors in the PSF-SSC and -SPVC experiments are discussed in Section 2.1.1. Appendix A discusses the PSF experiments' radiometric (RM) measurements and the documentation of RM results that are or will be available for comparison and evaluation of SSTR, HAFM, and DM results. Application of the SSTR technique at the fluence levels encountered in the PSF Experiments represented a severe challenge to extend the fluence range of applicability. This extension involved development of ultra-low-mass fission deposits and advanced automated track counting techniques (Go82a). Preliminary efforts generated optimism that these developments would be successful and the high fluence experiments were planned accordingly.

Limitations associated with the fabrication and application of ultra-low-mass SSTRs were:

- Difficulties associated with deposit mass calibration.
- Defining the background from trace level of fissionable materials.

- Assessing the possibility of SSTR contamination.

- Difficulties associated with controlling and checking overall deposit quality.

These limitations led to an experimental design that produced very high track densities (in the 10^6 to 10^7 track/cm^2 and beyond). Analysis of these high track densities, while possible, would require considerable further development and it is probable that high accuracy results would still not be obtained. Therefore, no further efforts on the analysis of the PSF Experiments high fluence ultra-low-mass SSTRs are anticipated.

Discussion of the problems involved in the analysis of the PSF Experiments' SDMF-3 and SDMF-4 irradiations is presented in Section 2.4.2. These two tests are considered here because they provide results that are representative of the problems that arose and would have to be resolved to obtain high-quality and high-accuracy SSTR fission rate results for the PSF-SSC and -SPVC experiments.

2.4.2 SSTR OBSERVATIONS IN SDMF-3 AND SDMF-4

Solid state track recorders (SSTRs) were irradiated in the SDMF-3 test along with RM dosimeters to evaluate the perturbation effect of a B&W surveillance capsule. In this B&W perturbation experiment, mica SSTRs were used with electrodeposits of ^{235}U, ^{238}U, and ^{237}Np.

In the SDMF-4 test, SSTRs were irradiated in an attempt to ascertain the photofission contribution in fissile neutron dosimeters. SSTRs with deposits of ^{232}Th, ^{235}U, ^{238}U, ^{237}Np, and ^{239}Pu were located both fore and aft of a tungsten photofission gauge (Ve80) in the SDMF void box.

After recovery and processing, SSTRs from the SDMF-3 and SDMF-4 tests were qualitatively inspected to determine whether accurate track scanning data could be obtained from these irradiations. Unfortunately, these ultra-low mass-SSTRs are plagued with problems that have already surfaced for LWR cavity surveillance dosimetry (Go87c,Ke85,Li87). As a result, scanning of these SSTRs ranges from difficult to impossible because of one or more of the following: 1) track densities that vary from high to completely out of range, 2) extremely nonuniform track density, and 3) the existence of clusters of tracks (possibly from impurities or contamination).

Problems that have arisen with these SDMF-3 and -4 ultra low-mass deposits are depicted in Figures 2.4.1 through 2.4.5. Here track density obtained from qualitative manual scans of these irradiated SSTR are graphically presented for ultra-low-mass deposits of ^{235}U, ^{238}U, ^{232}Th, ^{237}Np, and ^{239}Pu.* In most cases, the track density is so high that it is out of range for manual and even automated scanning, at least for existing systems. Nonuniformity is the rule, rather than the exception. This is equally true for track clusters or "stars," the existence of which implies the presence of impurities or contamination.

---

* The actual track densities are very much higher than those depicted in the Figures 2.4.1 through 2.4.5 hand drawn simulations.

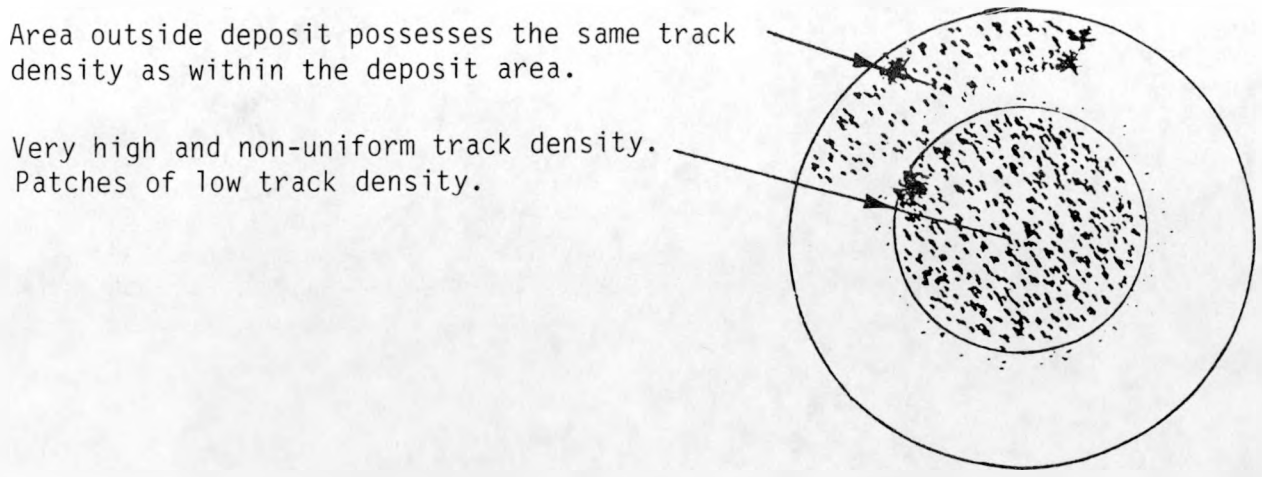

Figure 2.4.1. Qualitative scan of U-235 deposits No. 930.

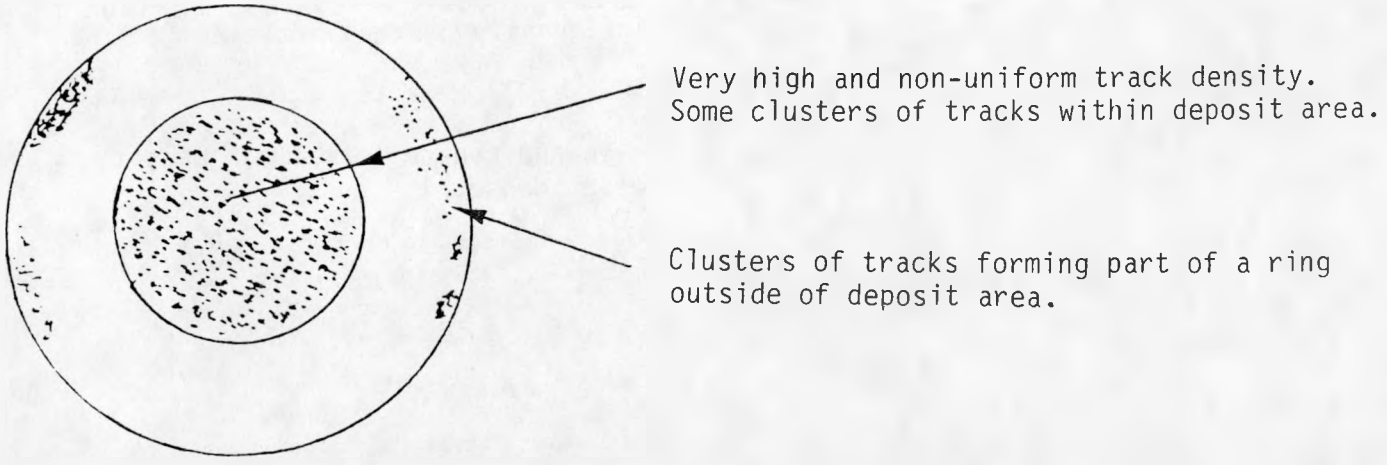

Figure 2.4.2. Qualitative scan of U-238 deposit No. 904.

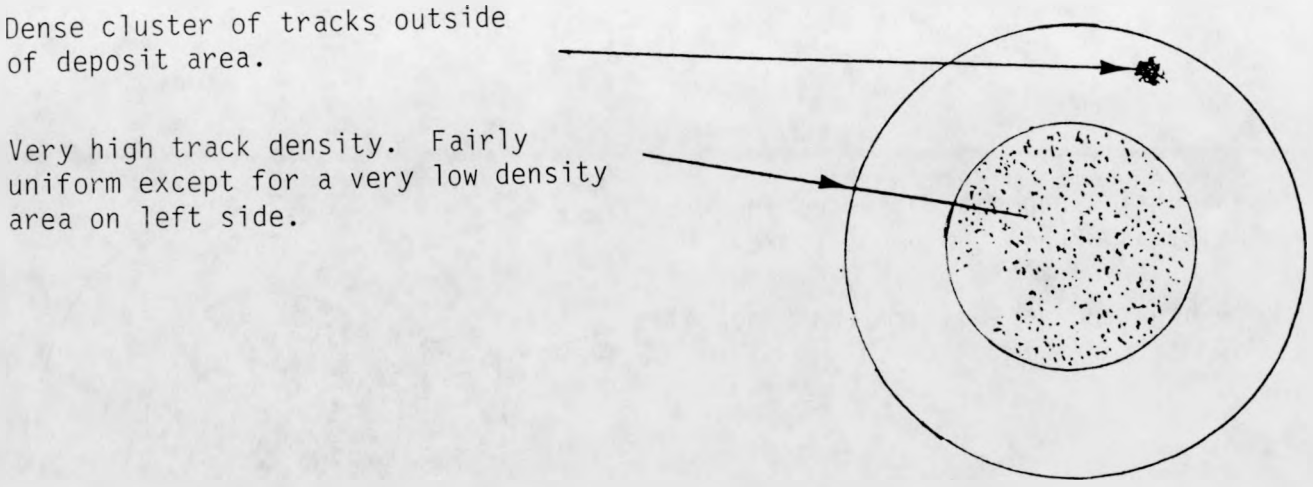

Figure 2.4.3. Qualitative scan of Th-232 deposit No. 1082.

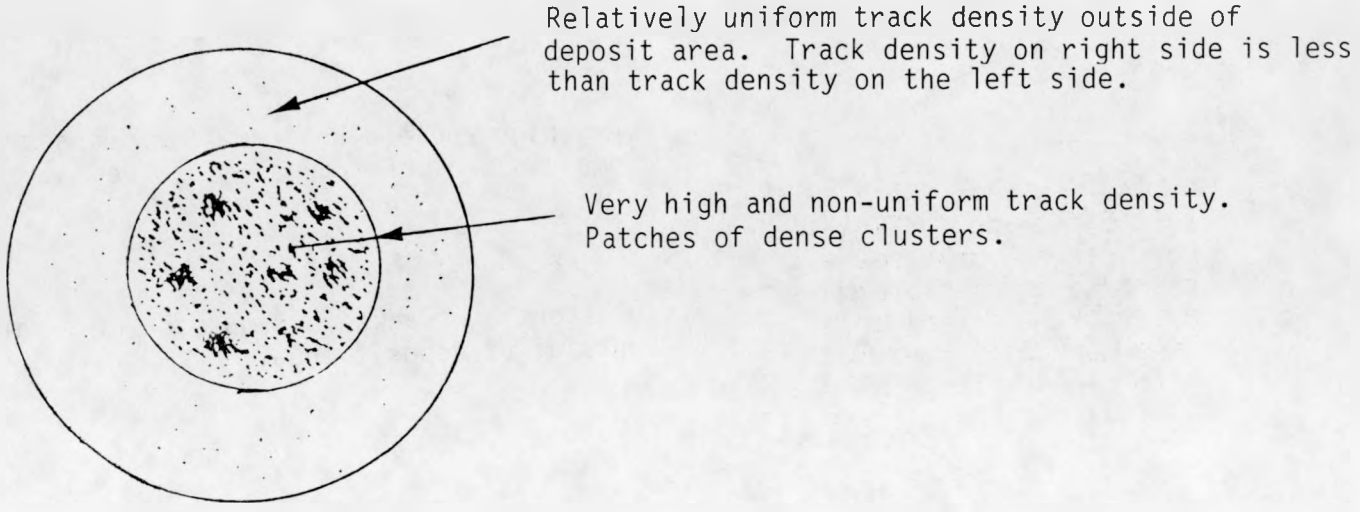

Figure 2.4.4. Qualitative scan of Np-237 deposit No. 1011.

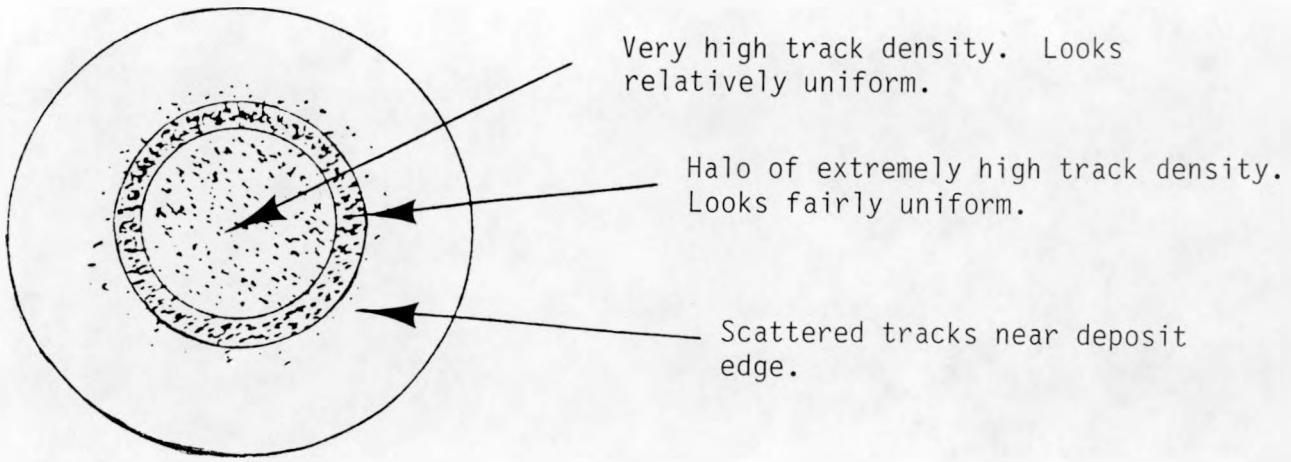

Figure 2.4.5. Qualitative scan of Pu-239 deposit No. 1055.

On the basis of these qualitative scans, it is clear that SSTR dosimetry in the SDMF-3 and SDMF-4 experiments has been seriously compromised. Moreover, the scanning problems associated with the existing SSTRs would entail an enormous effort to extract data, that at best would possess only marginal accuracy. In view of these serious problems, together with the present lower priority need for these specific SSTR results, further LWR-PV-SDIP efforts to salvage SSTR data from the series of PSF experiments (SSC, SPVC, SDMF-3, and SDMF-4) are not justified.

2.5 HELIUM ACCUMULATION FLUENCE MONITOR MEASUREMENTS

B. M. Oliver (RI-RD), L. S. Kellogg and W. N. McElroy (HEDL)

2.5.1 Introduction

An ASTM Standard, E910 [E706-III-C], Figure S.2, on Application and Analysis of Helium Accumulation Fluence Monitors for Reactor Vessel Surveillance has been established. Dosimetry wires, capsules, and Charpy steel specimens can be used as Helium Accumulation Fluence Monitors (HAFM) for the direct determination of fluence-spectra without a knowledge of the irradiation flux time-history; see References (As83a,Li87).

The PSF Experiments are being used to help establish the reliability and accuracy of using the HAFM technique for 1) surveillance capsule dosimetry wires, capsules, and Charpy specimen measurements, 2) PV steel, cladding, and mirror insulation scrappings, 3) copper and aluminum electrical component scrappings, and 4) support structure and shield tank scrappings for a postiori dosimetry measurements. Another aspect of this work is to measure the boron and helium (B/He) content of irradiated PV steels (C_V specimens) to help determine the effect of the He generation rate (as one of the contributing environmental variables) in the calculation of plant specific end-of-life and life-extension-range material dependent trend curves.

The design, fabrication, and placement of HAFM in combination with SSTR, RM, Sapphire DM, and PV steel DM sensors in the PSF-SSC and -SPVC experiments are discussed in Section 2.1.1. Appendix A discusses the PSF experiments' radiometric (RM) measurements that are or will be available for comparison and evaluation of HAFM, SSTR, and DM results.

To date, helium analyses have been conducted on most of the SDMF-4 HAFMs irradiated in the SSC position. The results of these analyses are presented and discussed in Section 2.5.2. These results are representative of those that would be obtained from the analyses of the PSF-SSC-1 and -SSC-2 experiments. Resource limitations have prevented any analyses to be performed on the HAFMs irradiated during the PSF-SSC-1, -SSC-2, -0T, -1/4T, and -1/2T tests.

2.5.2 HAFM Measurements in SDMF-4

A total of 235 HAFM samples were included by Rockwell in the fourth SDMF experiment at Oak Ridge National Laboratory. These consisted of 166 encapsulated HAFMs and 68 bare wire HAFMs. The encapsulating material was a 70%Au-30%Pt alloy specially fabricated for LWR surveillance dosimetry applications. The encapsulated HAFMs included the following sensor elements and compounds: Be, TiN, Nb_2O_5, SiO_2, PbF_2, $PbCl_2$, KI, and CaF_2. Empty Au-Pt capsules were also included to verify negligible helium generation from the encapsulating material. The bare wire HAFMs included the elements Al, Fe, Ni, Cu and Au, and the alloys Al-0.7% ^{6}Li and Al-0.5% B.

The HAFMs in SDMF were located at six different positions ranging from the SSC to the void box. To date, helium analyses have been conducted on most of the SSC HAFMs. The results of these analyses are given in Tables 2.5.1 and 2.5.2.

The helium content of each HAFM was obtained at Rockwell by isotope-dilution mass spectrometry (Fa86). Each analysis involved vaporizing the HAFM sample (including capsule for the encapsulated HAFMs) in a resistance-heated tungsten-wire or graphite crucible in one of the high temperature vacuum furnaces of the mass spectrometer system. The absolute amount of ^{4}He released was then measured relative to an accurately known amount of ^{3}He "spike". The ^{3}He spike was obtained by expanding and partioning a known quantity of ^{3}He gas through a succession of calibrated volumes (Ol84a). The mass spectrometer was calibrated for mass sensitivity during each series of runs by analyzing known mixtures of ^{3}He and ^{4}He.

The helium analysis results in Tables 2.5.1 and 2.5.2 are given as total atoms of helium released, and as helium concentrations in atomic parts per billion (10^{-9} atom fraction) with respect to the total number of atoms or molecules in each sample. The helium concentrations are given in this manner to simplify later adjustments for helium generation from any carrier material present (e.g., Ti in TiN) and from any boron impurity. Helium concentrations in Table 2.5.2 for the Al-Li and Al-B alloys are with respect to ^{6}Li and ^{10}B respectively. The measured helium data in column 6 have been corrected for background helium released by the tungsten-wire or graphite crucibles and the vacuum furnaces. In addition, the measured helium data for the encapsulated HAFMs in Table 2.5.1 have also been corrected for very small amounts of measured helium in the irradiated empty Au-Pt capsules.

All of the samples were etched prior to helium analysis to remove surface material which may have been affected by helium recoil either out of the samples or into the samples from adjacent materials. The encapsulated HAFMs were then analyzed as a single unit, whereas the bare wires were segmented to yield additional gradient information. Each wire was segmented into either 4 or 6 pieces, at approximately equal spaced intervals along the length of the wire. The variation in mass for the individual wire specimens in Table 2.5.2 is a result of etching variations along the wire, and spacing variations.

In general, the data in Tables 2.5.1 and 2.5.2 show good consistency between the multiple samples for the various sensor elements irradiated at immediately adjacent locations in the same dosimetry capsule. A few of the data, however, showed unexpectedly large variations. Four of these data show values which are too high, possibly explained by an unmeasured increase in the mass spectrometer system background for these particular runs. The three cases where the data seem too low could be the result of incomplete vaporization. Although either of these explanations are unlikely, based on the vast experience gained with the analysis system, no other explanations for these variations have yet been formulated.

The mean values for the various HAFM sensor elements are given in the last column of Tables 2.5.1 and 2.5.2. For the HAFM capsules, this value represents the mean and standard deviation of the multiple analyses. For the unencapsulated wire HAFMs, the mean value was obtained from a linear

least squares fit to the data evaluated at the midpoint of the wire. The uncertainty for these latter values was obtained from the estimated standard deviations in the two fitting parameters. The helium analysis results for those data which are suspect are not included in the mean values.

Notwithstanding the discussion above, uncertainty in the measured helium concentration values, based on the cumulative uncertainties of sensor mass, helium isotopic ratio measurement, spike size, and material composition, is estimated to be <2% of the concentration values. The results of the correlation of these HAFM dosimetry results with other dosimetry results from the SDMF-4 experiment will be reported in NUREG/CR-3321 on "Service Laboratory Procedure Verification and Surveillance Capsule Perturbations".

2.5.3 Other Results

The results of using selected dosimetry wire materials (Fe, Cu, Al, ...) as HAFM dosimeters in Maine Yankee, H. B. Robinson, and Turkey Point have been addressed elsewhere (Oi83, Li87, and Ke85) and will be further addressed in NUREG/CR-3321.

The status of work to determine the boron and helium content of irradiated PV steels, including the six PSF irradiated steels, is discussed in Section I of Reference (Mc87) and in References (Oi83,Oi84a). The PSF irradiated steel specimens selected for boron and helium analyses are identified in Table 2.5.3.

The results of the above work will help to demonstrate the value and potential for the routine dosimetry application of the HAFM monitoring technique for complementing, supplementing, and expanding on the value of conventional RM dosimetry.

TABLE 2.5.1

HELIUM CONCENTRATIONS IN SDMF HAFMs - SSC
(Encapsulated)

HAFM Number	Sensor Material	Sensor Mass (mg)[a]	SS/Gd Capsule	Sample Layer	Measured ^4He (10^{11} atoms)	Helium Concentration (appb)[b] Measured	Helium Concentration (appb)[b] Average[c]
Be-L2	Be	0.859	16/32	1	1534	2673	
-Y2		0.932		1	1574	2527	2570 (90)
-71		1.100		1	1839	2502	
TiN-87	TiN	1.329	16/32	1	105.0	813.9	
-R8		2.410		1	202.2	864.8	840 (25)
-2Y		2.411		1	196.7	840.9	
NbO-2C	Nb_2O_5	1.788	16/32	1	16.86	413.2	
-HZ		1.933		1	26.29	597.5[d]	400 (20)
-6A		2.055		2	18.13	386.8	
SiO-5R	SiO_2	0.684	9/33	2	12.74	184.1	
-5A		0.833		2	14.56	173.0	177 (6)
-D5		0.864		2	15.08	172.8	
PbF-5Z	PbF_2	3.705	16/32	2	26.40	288.8	
-DV		3.930		2	27.15	280.0	284 (6)
-7A		4.210		2	36.04	347.4[d]	
PbS-H8	PbS	5.778	9/33	1	91.24	626.5	
-B7		6.157		1	97.71	629.7	630 (4)
-H3		6.409		1	102.4	634.0	
PbCl-I7	$PbCl_2$	4.210	16/32	1	24.86	271.4	
-BJ		4.647		1	32.46	321.4	300 (35)
-E7		4.722		1	12.15	117.7[d]	
KI-IC	KI	2.874	9/33	1	4.29	39.9[d]	
-R5		3.076		1	19.94	177.6	178 (1)
-E5		3.043		1	19.87	178.9	
CaF-7A	CaF_2	2.836	9/33	1	126.1	575.9	
-J5		2.872		1	144.4	651.3[d]	581 (8)
-7H		2.936		2	133.0	586.8	

[a]Mass uncertainty is ±1μg.
[b]Helium concentration in atomic parts per billion (10^{-9} atom fraction) with respect to the total number of atoms or molecules of sensor material.
[c]Mean and standard deviation (in parentheses) of multiple analyses.
[d]Data not included in average value (see text).

TABLE 2.5.2

HELIUM CONCENTRATIONS IN SDMF HAFMs - SSC
(Unencapsuled Bare Wires)

HAFM Number	Sensor Material	Sensor Mass (mg)[a]	SS/Gd Capsule	Sample Layer	Measured ^{4}He (10^{11} atoms)	Helium Concentration[b] Measured	Helium Concentration[b] Average[c]
AlLi-2A	Al-0.7%^{6}Li	0.918	16/32	2	3915	614.3	
-2B		1.033			4565	636.6	
-2C		1.125			5225	669.0	689 (6)
-2D		1.140			5561	702.7	
-2E		0.743			3816	739.8	
-2F		0.936			5041	775.8	
AlB-2A	Al-0.5%B	0.101	16/32	2	139.1	2552	
-2B		0.157			225.7	2664	
-2C		0.135			207.5	2848	2870 (45)
-2D		0.119			185.0	2884	
-2E		0.106			173.9	3041	
-2F		0.140			244.1	3231	
Al-2A	Al	2.682	16/32	2	3.465	5.789	
-2B		2.456			2.390	4.360[d]	6.30 (7)
-2C		2.353			3.380	6.436	
-2D		2.327			3.559	6.853	
Fe-2A	Fe	8.554	16/32	2	2.378	2.578	
-2B		6.669			1.982	2.756	2.84 (5)
-2C		8.331			2.669	2.971	
-2D		7.957			2.632	3.068	
Cu-2A	Cu	3.573	9/33	2	1.213	3.582	
-2B		3.875			1.462	3.981[d]	
-2C		4.403			1.245	3.249	3.13 (7)
-2D		4.709			1.319	2.955	
-2E		4.710			1.280	2.867	
-2F		4.697			1.219	2.738	

[a]Mass uncertainty is ±1μg.
[b]Helium concentration in atomic parts per million (10^{-6} atom fraction) for Al-Li and Al-B and atomic parts per billion (10^{-9} atom fraction) for Al, Fe, and Cu; all with respect to the total number of atoms or molecules of sensor material. Values for the Al-Li and Al-B alloys are with respect only to the ^{6}Li or ^{10}B content.
[c]Mean and standard deviation (in parentheses) of multiple analyses.
[d]Data not included in average value (see text).

TABLE 2.5.3

PSF-IRRADIATED CV SPECIMENS* FOR BORON AND HELIUM ANALYSES

Material	Heat Code	Specimens	Supplier	Thickness (mm)	Yield** Strength (MPa)	Heat Treatment
A533-B Plate (HSST Plate 03)	3PS, 3PU, 3PT	3PU-22	NRL	305	454	843 to 899°C - 4 h, water quenched 649 to 655°C - 4 h, air cooled 607 to 636°C - 20 h, furnace cooled
A302-B Plate (ASTM Reference Plate)	F23	F23-85	NRL	152	482	899°C - 6 h, water quenched 649°C - 6 h, air cooled
Submerged Arc Weld (Single Vee type, A533-B Base Plate)	R	R-54	RR&A	160	489	920°C ± 15°C - 6 h, water spray quenched 600°C ± 6 h, air cooled 600°C - 36 h, air cooled 600°C - 6 h, air cooled
Submerged Arc Weld (Single Vee type, A533-B Base Plate)	EC	EC-16	EPRI	235	456	621°C ± 28°C - 50 h, furnace cooled
22NiMoCr37 Forging	K	K414	KFA	295	407	Not reported to MEA or ORNL
A508-3 Forging	MO	MO-14	Mol	238	462	900 to 955°C - 12.8 h, air cooled 630 to 665°C - 14 h, furnace cooled 610°C ± 10°C - 24 h, furnace cooled
A537-2 Plate (Lukens Steel Base Plate)	D0662		CEN-Saclay			885 to 913°C 556 to 593°C

*The six PSF CV specimens were selected by F. Kam of ORNL.
**Ambient temperature strength.

2.6 SAPPHIRE DAMAGE MONITOR MEASUREMENTS

G. P. Pells, A. J. Fudge and M. J. Murphy (AERE, Harwell, UK)
and S. Watt (Rolls-Royce and Associates, Ltd., UK)

2.6.1 Introduction

The final damage state of any material subjected to fast neutron irradiation is governed by the neutron spectrum and fluence, the irradiation temperature, the chemical composition of the material and possibly the neutron flux or dose rate. The neutron spectrum and fluence determine the number of displacements per atom (dpa) that occur in the irradiated material although the final damage state can be influenced by quite small variations in chemical composition and irradiation temperature. This has been found to be particularly true of PWR pressure vessel steels where radiation embrittlement has been found to vary widely. In the light of these variations it has become increasingly important for accurate neutron dosimetry that takes account of the entire neutron spectrum and can be expressed in terms of dpa. Such extensive measurements using neutron activation monitors are expensive in terms of both time and money. This has led to several attempts to use solid state dpa monnitors in which one measurement of some physical parameter can be related to total dpa (Ni72,Al79a). Most of these have had limited success due to the irradiation-induced defects annealing out at reactor operating temperatures.

Sapphire, a single crystal α-Al_2O_3, has a number of properties which allow it to be used as a dpa monitor as described by Pells et al. (Pe82). The main features are that the displacement cross-section as a function of neutron energy is similar for Al in Al_2O_3 to that of Fe in steel; the defects produced by neutron collisions have reasonable thermal stability and the defect concentration can be measured by optical absorption spectroscopy. The techniques by which the dpa response curve was established and the results from the PSF and other experiments and the range of applicability of sapphire as a dpa monitor are described in subsequent sections (Pe87). The design and fabrication of Sapphire Damage Monitor (SDM) capsules for the PSF test irradiations are described in Section 2.1.3.2.

2.6.2 Experimental Procedure and Results

2.6.2.1 Optical Response of Sapphire to Irradiation

The single crystal sapphire was supplied by Union Carbide as rectangular blocks 10mm x 3mm x 2mm with the 3mm x 10 mm faces polished to optical standards. An analysis of the impurity content of the sapphire showed that the major impurity was 25 appm Si, with all other impurities <10 appm. The optical absorption spectrum of each "as received" specimen was measured on either a Cary 14 or Perkin Elmer Lambda 9 spectrophotometer. Neutron irradiation introduced a number of overlapping absorption bands as shown in Figure 2.6.1. The aluminum vacancy, the V centre, produced a broad absorption band peaking near 400 nm that was partly masked by a series of superposed absorption bands due to various oxygen vacancy centres. The electronic state of the V centre changed slowly with time after irradiation and to ensure that all aluminum vacancies were optically active every specimen was X-irradiated by a Philips 3kW tube run at 80kV, 35mA for

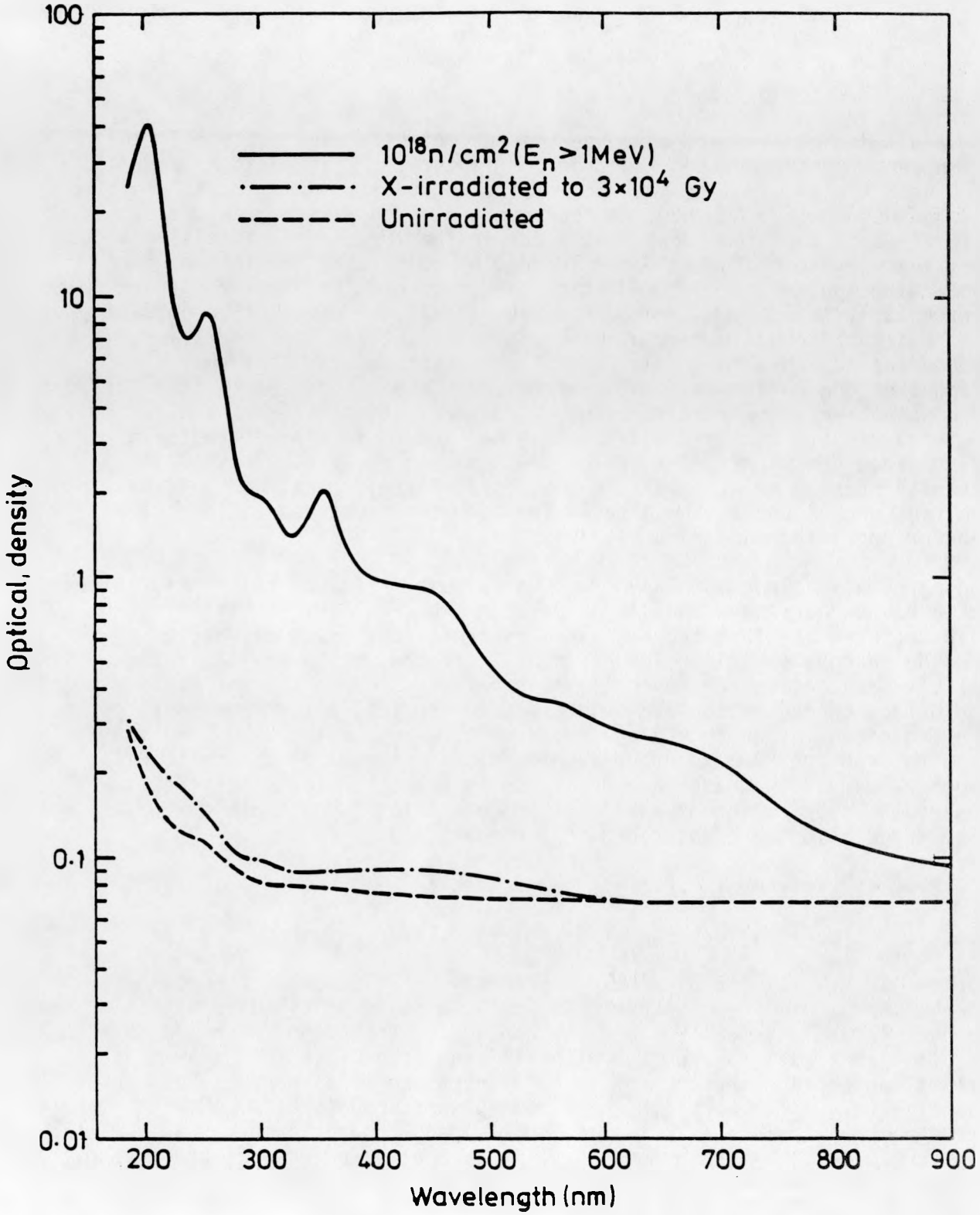

FIGURE 2.6.1. Optical Absorption Spectra of Irradiated Union Carbide, UV Grade Sapphire as a Function of Wavelength.

30 minutes to give an absorbed X-ray dose of ~5 x 10^4 Gy. The strength of the V band was measured near the peak of the band at 400 nm. It should be noted that the peak wavelength and half-width of the V band changed with neutron dose making it impractical to use curve resolving techniques to isolate the band from overlapping absorption bands on a routine basis. However, the resolved bands, an example is given in Figure 2.6.2, show that interference from overlapping bands at 400 nm was small and, at the highest neutron fluence, was ~6%.

2.6.2.2 Reactor Irradiation

Following measurement of the optical density of the "as received" sapphires, they were wrapped in aluminum foil and sealed in helium filled stainless steel cans along with standard Fe, Ni, Cu, Co/Al, Ti and Nb neutron activation monitors. The aluminum foil wrapping served to provide good thermal contact between the sapphire and the stainless steel can. An exploded view of the capsule is given in Figure 2.6.3. Some sapphires supplied for the ORNL poolside facility (PSF) light water reactor pressure vessel mock-up irradiations had less sophisticated encapsulation and dosimetry.

The majority of the measurements were obtained by irradiation at various positions and temperatures within the core of the HERALD reactor. The irradiation facility has been described by Collins (Co83) and consisted of water cooled positions operating at the reactor pool temperature of ~60°C or rigs heated by gamma and neutron irradiation with gas-gap temperature control using helium/nitrogen gas mixtures to temperatures of 220-310°C. Temperature control was quoted as ±1°C short term but with slow drifts requiring manual correction giving maximum errors of ±5°C. The fast neutron flux (E > 1 MeV) varied between 3.6-5.8 x 10^{12} n/cm^2/s depending on the exact location in the core. Sapphires were included in the PSF dosimetry intercomparison exercise (Mc86b) both in the 18-day irradiations at pool temperature and in the full power run at 290°C. These irradiations provided a wide range of neutron spectra depending on the dosimeter position with respect to the reactor core and within the pressure vessel steel mock-up.

2.6.2.3 Dosimetry

In order to obtain values of the sapphire damage dose that are consistent in a variety of irradiation environments, an estimate is required of the neutron energy spectrum within the irradiation facility that can be combined with the differential displacement cross-section of aluminum. The following methodology (illustrated in Fig. 2.6.4) was adopted to determine a consistent estimate of neutron dose. The neutron energy spectrum was first calculated for the environment of interest using neutron transport computer codes and then adjusted in the light of measurements obtained from a multiple foil activation (MFA) experiment. Such an adjustment removed errors incorporated in the original spectrum, caused by uncertainties in the transmission cross-sections and approximations in geometrical modelling in the neutron source term, to give a definitive neutron energy spectrum. Long-term irradiations of sapphires were then made in the standard dosimetry pack. Analysis of the reaction rates derived from the activities induced in

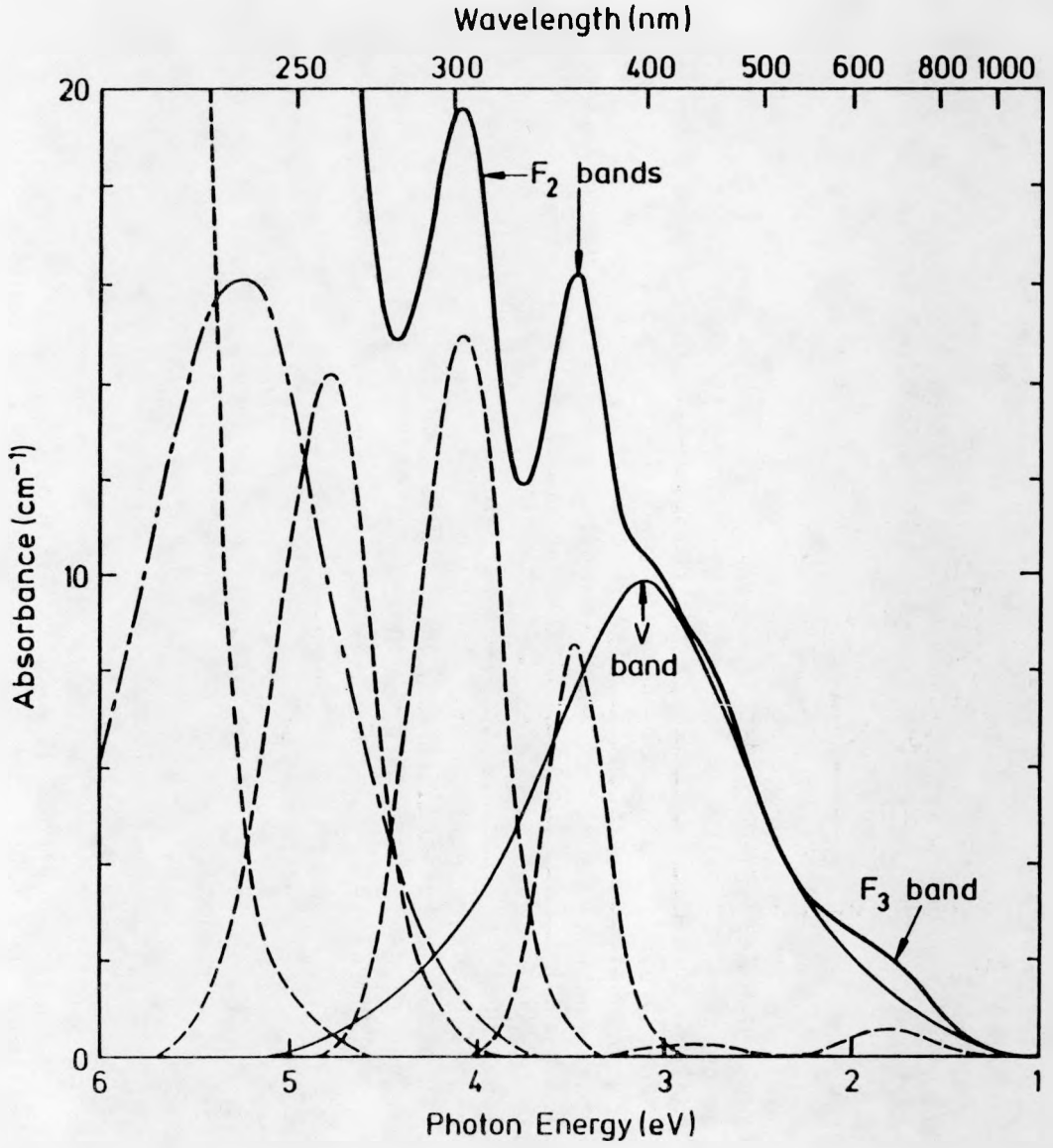

FIGURE 2.6.2. Resolved Optical Absorption Bands of Sapphire Neutron-Irradiated to $\sim 3 \times 10^{18}$ n/cm^2 (E > 1 MeV) at 250°C.

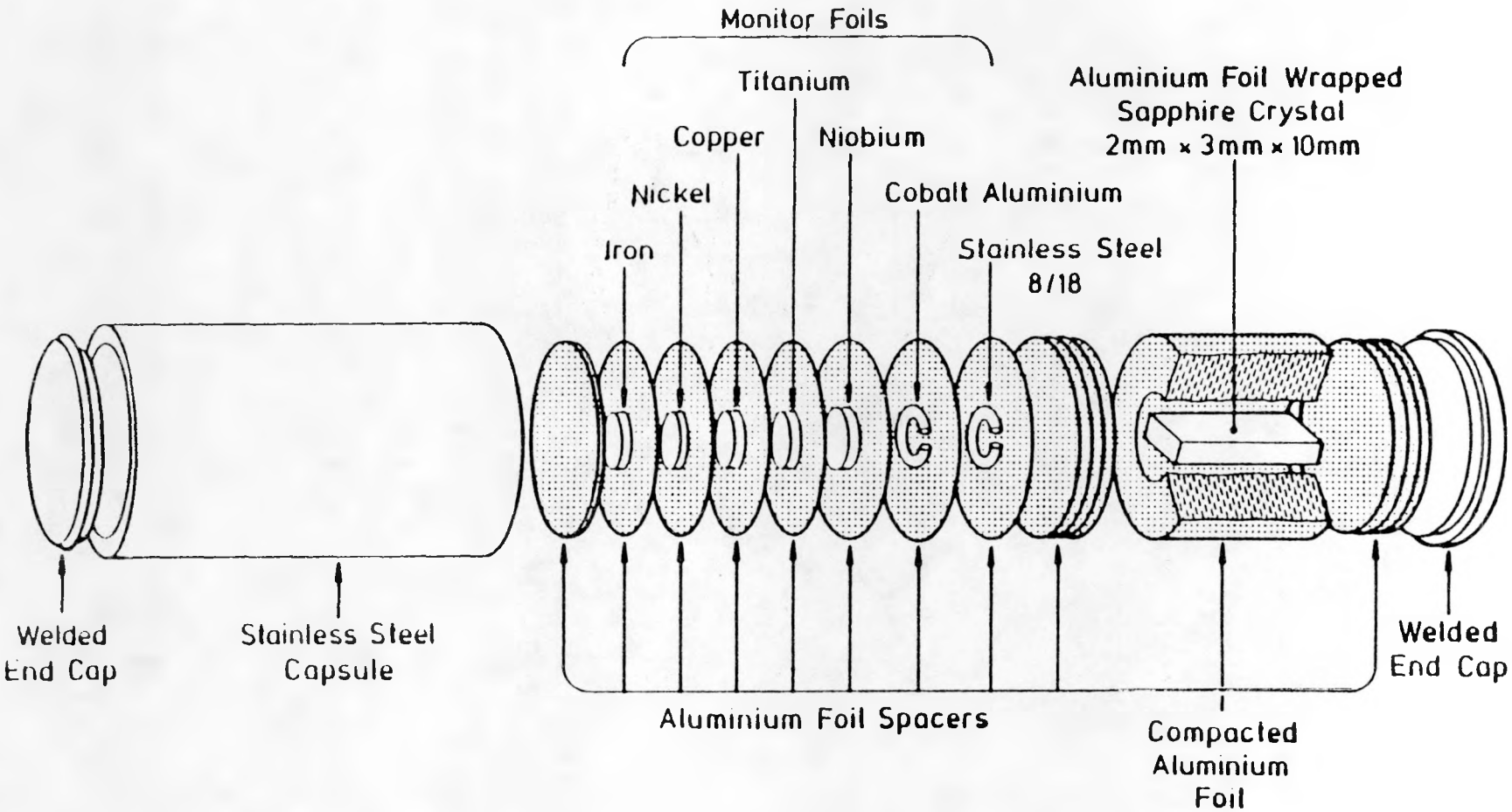

FIGURE 2.6.3. Exploded View of Dosimetry Capsule Containing Sapphire Damage Monitor and Activation Monitors.

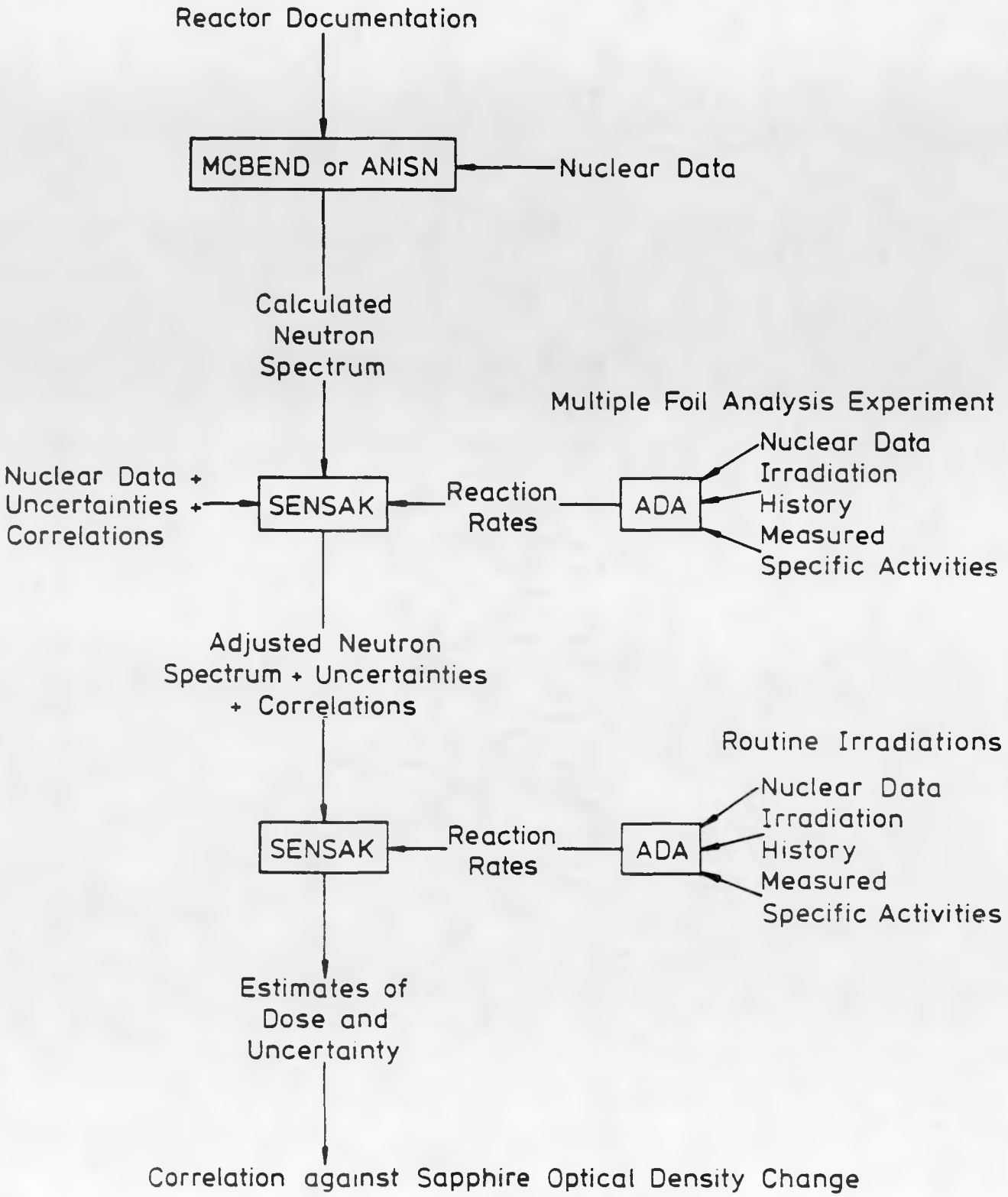

FIGURE 2.6.4. Block Diagram of the Methodology Used to Determine a Consistent Estimate of Neutron Dose.

the monitors was used, together with the MFA adjusted spectrum, in a least-squares data adjustment to produce an estimate of the dose rates within the irradiation rig.

The neutron energy spectrum was calculated using the Monte Carlo neutron transport code MCBEND (Be82), although in some applications the discrete ordinates Sn transport code ANISN (En67) was utilized. A standard EUROLIB-40 energy group scheme covering the energy range from 10^{-10} MeV to 14.86 MeV was employed for all calculations. The activation monitors used in a typical MFA experiment are given in Table 2.6.1. They can be divided into those sensitive to thermal neutrons and those that exhibit an effective energy threshold in or above the region at which displaced atom damage in LWR environments is a maximum, typically 0.5 MeV to 2.0 MeV. The MFA experiment consisted of a short-duration, full-power irradiation. As the dpa differential cross-sections include a response from the recoil atoms following radiative thermal neutron capture reactions (n,γ), the thermal neutron monitors enable this contribution (which may be of critical importance in heavy water moderated reactors) to be accounted for.

The spectral analysis of the various MFA measurements used the least-squares data adjustment code SENSAK (Mc83g). The specific activities determined from the activation monitors were first converted into reaction rates normalized to peak reactor power using the irradiation power history in conjunction with activation and decay corrections using the code ADA (Zi83). These were then used as input to SENSAK along with the calculated estimate of the neutron energy spectrum in the form of group fluxes together with sets of group-averaged activation and response cross-sections (dpa, ϕ > 1.0 MeV, ϕ > 0.1 MeV) each with associated variance-convariance data. SENSAK then combines the various sets of disparate data such that the integral measurements of reaction rates from differential data are consistent in that their joint probability distribution is maximized within the limits established by the uncertainties in the data. A consequence of the generalised linear least-squares technique is that an updated estimate of the neutron spectrum is obtained. Once this experimentally adjusted spectrum was obtained from the MFA experiment, it could be used in the analysis of all further irradiations in that irradiation locality. Figure 2.6.5 compares a neutron spectrum calculated using the 1-dimensional transport code ANISN with that produced from the adjustments performed using the code SENSAK from the MFA experiment. Clearly, other than scaling the neutron spectrum by ~14%, no significant spectral adjustment was made that would indicate the original calculated spectral shape was incorrect.

The irradiation dose from a routine irradiation in a characterized position was determined in an identical way to the MFA analysis with the difference that the standard dosimetry pack contained fewer activation monitors and had only one threshold monitor with a response significantly lower than 1.0 MeV, namely $^{93}Nb(n,n)^{93m}Nb$. Having produced an adjusted spectrum, the standard activation monitors were used to normalize the MFA adjusted spectrum with no significant flux adjustments being sought or expected. The scaled spectrum was then used to produce estimates of material dose in terms of dpa of aluminum in sapphire using the aluminum displacement cross-sections derived from the RECOIL code (Ga76).

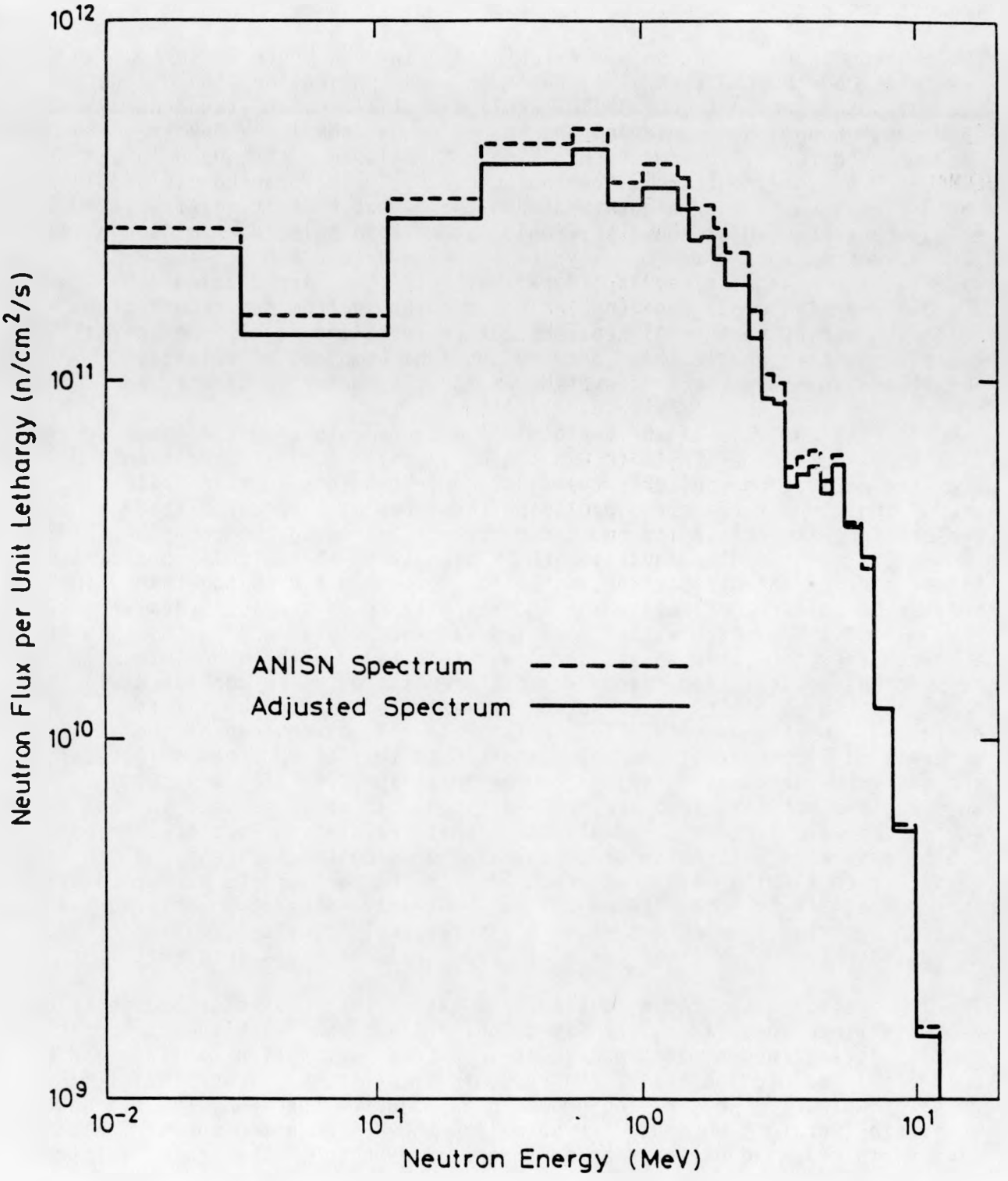

FIGURE 2.6.5. Comparison of ANISN Calculated Spectrum and MFA Adjusted Spectrum for the HERALD VT4 Irradiation Location. (The ANISN spectrum is shown prior to scaling by SENSAK.)

TABLE 2.6.1

DETECTORS AND REACTIONS EMPLOYED

TYPE	DETECTOR AND REACTION	EFFECTIVE ENERGY THRESHOLD (MeV)
THERMAL	Co59(n,γ)Co60	Thermal
	Fe58(n,γ)Fe59	Thermal
	Cu63(n,γ)Cu64	Thermal
FISSION	Np237(n,f)FP	0.67
	U238(n,f)FP	1.51
	Th232(n,f)FP	1.52
THRESHOLD	Nb93(n,n')Nb93m	0.50
	In115(n,n')In115m	0.95
	Ti47(n,p)Sc47	1.90
	Ni58(n,p)Co58	2.10
	Fe54(n,p)Mn54	2.50
	Ti46(n,p)Sc46	3.90
	Ti48(n,p)Sc48	5.70
	Cu63(n,α)Co60	6.10
	Al27(n,α)Na24	6.50

2.6.2.4 Results

Over one hundred sapphires have been irradiated for which the dose has been accurately determined. The optical absorbance as a function of dose is given in Figure 2.6.6. The majority of the irradiations were at known temperatures, but those HERALD irradiations described as "walking stick" had ill-defined irradiation temperatures, although they were probably <150°C. It can be seen that there are two distinct response curves. The lower curve gives the response for all irradiations within the temperature range 220-310°C and within this temperature band there is no discernable temperature dependence. For irradiation temperatures below 200°C, there is clearly a temperature effect with larger optical densities being recorded for a given dose and the response curve tends towards saturation at $\sim 10^{-2}$ dpa.

Some of the sapphires from both HERALD and PSF irradiations were annealed at 290°C for times up to 4 years. The variations in optical density at 400 nm with annealing time are given in Figure 2.6.7. The specimens irradiated at 250°C and 290°C showed a small reduction in optical absorbance with annealing time. The rise and subsequent decay in the first few weeks were due to the interfering aggregate oxygen vacancy bands. The specimens irradiated at 60°C exhibited a much more rapid initial decay except at the highest doses. If the optical absorbances for the 290°C annealed specimens are replotted against dpa in sapphire along with those for specimens irradiated at temperatures above 200°C as shown in Figure 2.6.8 then all the points fall on a common curve. The initial response is linear but rapidly becomes sublinear until at doses above 10^{-3} dpa the optical absorbance appears to vary as the cube root of dose.

2.6.3 Discussion

The optical absorption of neutron irradiated sapphire has been shown to give a useful response over a wide range of damage dose. At doses of $<10^{-4}$ dpa the response appears to be linear which is consistent with displacements being produced in discrete cascades. At higher neutron fluences cascade overlap will increase the number of vacancy-interstitial recombinations thus giving a sublinear response leading to eventual saturation as was observed for the low-temperature irradiations. However, at temperatures above 200°C saturation was not observed and for damage doses of $>10^{-3}$ dpa the absorbance increased as the cube root of dose. Similar behavior has been observed for the V centre in MgO irradiated at ~150°C, which extended to neutron fluences $>10^{20}$ n/cm^2 (E > 1 MeV) (He71). The reason for this behavior is not known but must involve the stabilization of cation interstitials in some way. The most obvious sink for interstitials would be interstitial dislocation loops, but previous work (Wi68) suggests that both higher irradiation temperatures and doses are required to produce such loops.

Despite a lack of detailed understanding of how the colour centres produced at high doses and temperatures are stabilized, it is now clear that the response curve given in Figure 2.6.8 represents a stable situation for irradiation conditions in which the irradiation temperature was between 210-310°C and for neutron dose rates varying between that in HERALD of 5×10^{12} n/cm^2/s and that in the steel pressure vessel mock-up of PSF at $\sim 2 \times 10^{11}$ n/cm^2/s where the irradiation lasted for a year. The long-term annealing curves in Figure 2.6.7, whilst not truly representative of thermal

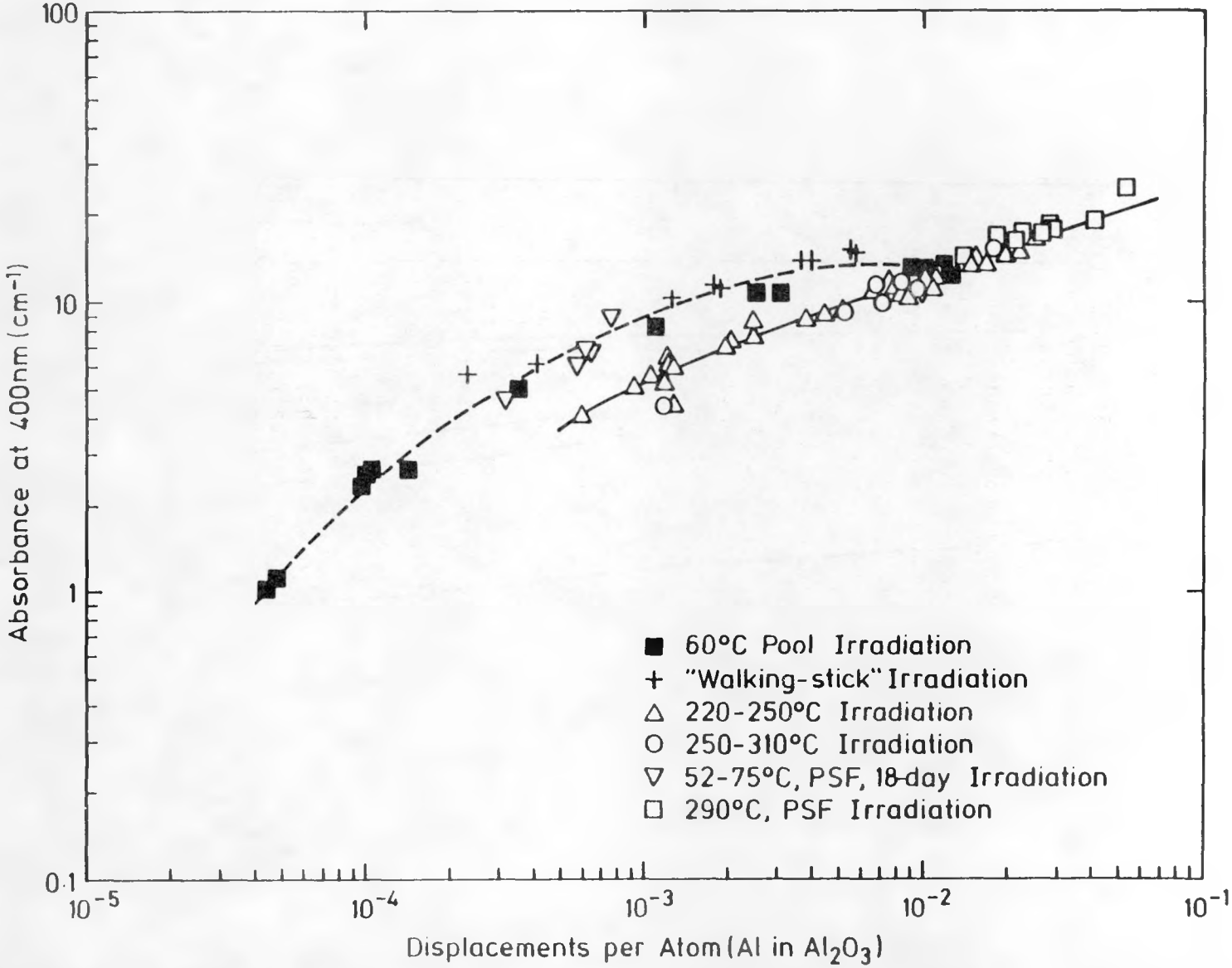

FIGURE 2.6.6. Optical Absorbance of Sapphire, Neutron Irradiated in a Variety of Locations and at Temperatures from 60-310°C, as a Function of Calculated dpa Dose for Aluminum in Sapphire.

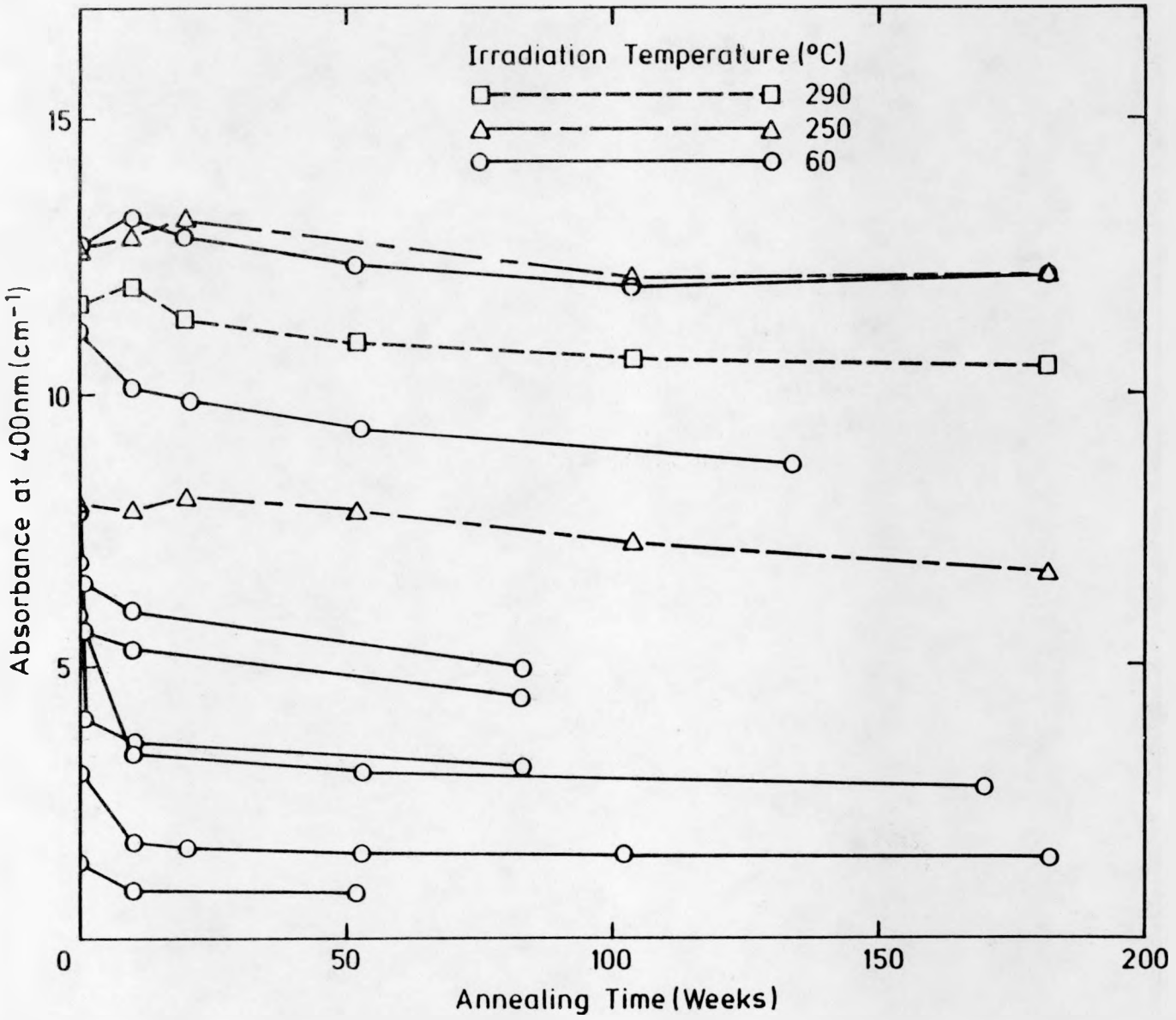

FIGURE 2.6.7. Optical Absorbance of Neutron Irradiated Sapphires Following Long-Term Annealing at 290°C.

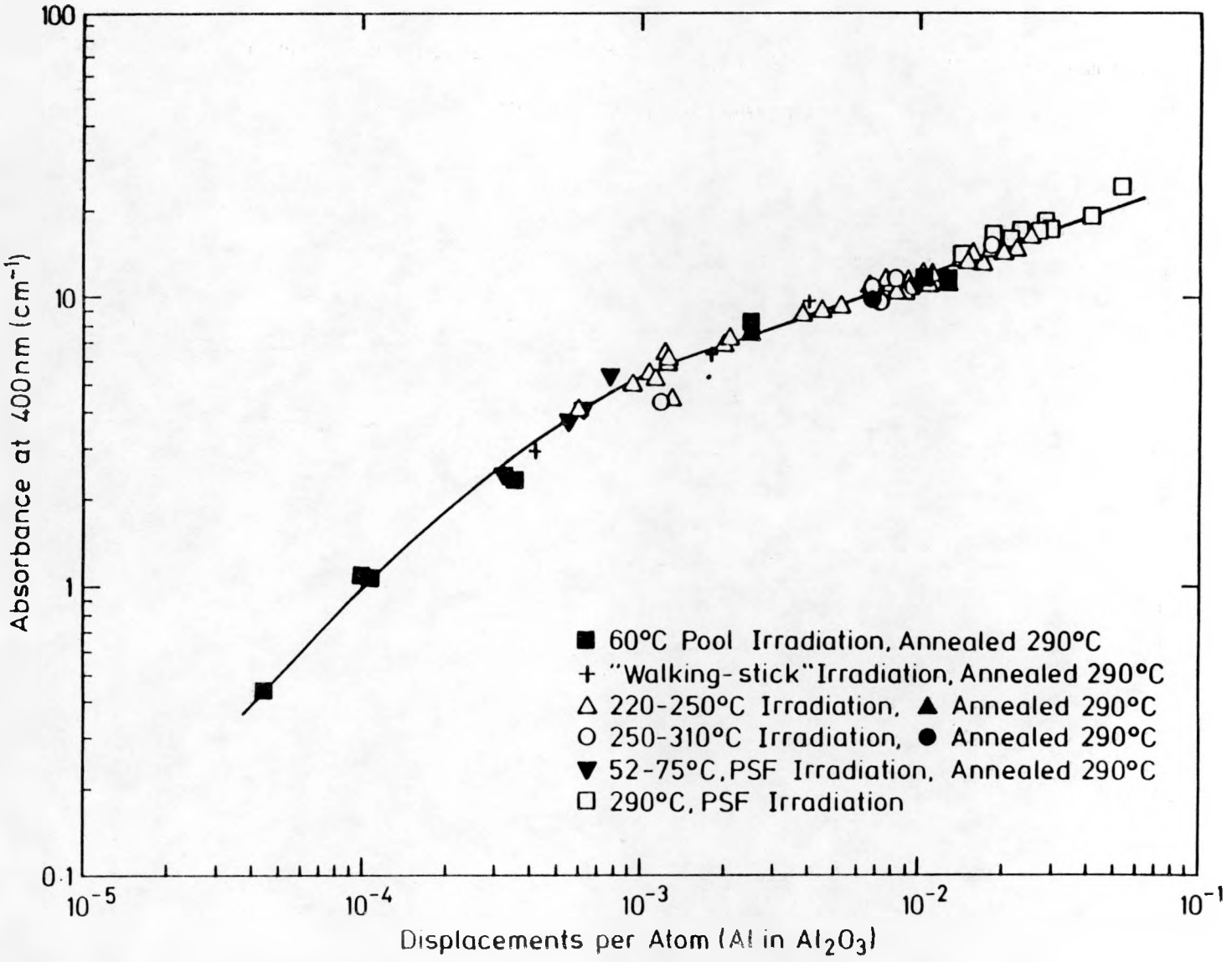

FIGURE 2.6.8. Optical Absorbance of Neutron Irradiated Sapphires as a Function of Damage Dose for Specimens That Have Either Been Irradiated at Temperatures >200°C or Postirradiation Annealed at 290°C.

conditions in-reactor, do demonstrate the general thermal stability of the V centres particularly for sapphires that have received high damage doses. The annealing curves for the 60°C irradiated sapphires show an initial rapid reduction in optical absorbance that may be associated with next-nearest-neighbor recombination of vacancy-interstitial pairs. The subsequent long term annealing behaviour is then similar to that exhibited by sapphires that have been irradiated at 250°C and 290°C. Therefore, the inclusion in Figure 2.6.8 of long-term, 290°C annealed sapphires along with specimens irradiated at different dose rates at temperatures >200°C enables a response curve to be established for a wide range of conditions.

The calculation of damage dose used the most modern computation techniques to take account of all the errors in the calculation of neutron spectra in the various irradiation positions. The success of the procedures, which can be used to calculate damage dose for any material, has been validated by the self-consistency with which the dose measured by optical absorbance in sapphire corresponds with dpa dose calculated for a wide range of neutron spectra. Furthermore, damage doses determined from sapphires irradiated in locations whose neutron spectra had not been subject to MFA adjustments were found to be in good agreement with the calculated dose, thus demonstrating the overall soundness of the present dosimetry calculations. By the same token this also demonstrates that the response curve given in Figure 2.6.8 will allow the optical absorbance of neutron irradiated sapphire to be used to determine damage dose of aluminum in sapphire. From this value the damage dose of any other material irradiated in the same location can be obtained from the relative displacement cross-sections of that material to aluminum.

2.6.4 Conclusions

The optical absorption at 400 nm of aluminum vacancy centres produced by neutron irradiation in high-purity, single crystal α-Al_2O_3 (sapphire) has been shown to increase in a reproducible manner with damage dose for irradiations at temperatures between 200-310°C in a variety of neutron spectra. The constancy of this behaviour has been used to validate the procedures used to calculate the neutron energy spectrum and damage dose in irradiated LWR pressure vessel steels.

The thermal stability of the aluminum vacancy centre in sapphire and the fact that sapphire responds to the entire neutron spectrum in a manner similar to that of steels makes it superior to conventional, high-threshold energy, activation monitors in irradiation locations for which a detailed neutron energy spectrum is not available.

2.6.5 Acknowledgements

The authors wish to thank the staff at Aldermaston and Oak Ridge for irradiation facilities, M. Wilkins for some of the activity measurements, and A. Thomas for his support and encouragement.

2.7 METALLURGICAL CORRELATION AND OTHER DAMAGE MONITOR MEASUREMENTS

W. N. McElroy (HEDL)

The PSF and other benchmark experiments in the framework of the LWR-PV-SDIP serve to validate, improve, and standardize the damage analysis and correlation procedures and data recommended in the set of 21 LWR ASTM Standards. The ASTM E706-IIID Standard on Application and Analysis of Damage Monitors (DM) for Reactor Vessel Surveillance, Figure S.2, is still in the development stage. The status of this work is that W. N. McElroy and R. Gold are expected to prepare a first draft of the E706-IIID Standard and it will provide a general discussion and overview on the use of available DM dosimetry techniques for LWR surveillance applications. Currently, it is planned to have three separate ASTM Method Standards that are recommended for use in the E706-IIID Standard:

E706-IIID.1) ASTM Standard Method for Application and Analysis of Standard Reference Materials Data in Nuclear Reactor Pressure Vessel Surveillance

E706-IIID.2) ASTM Standard Method for Applications and Analysis of Sapphire Damage Monitors

E706-IIID.3) ASTM Standard Method for Application and Analysis of Graphite and Tungsten Damage Monitors

M. Manahan (BMI, Columbus Laboratories) has completed a first draft of the E706-IIID.1 Standard. It concentrates on the use of the ASTM A302B, HSST 01, and HSST 02 steel plate materials currently being used in PWR surveillance capsules. Results on the use of the ASTM A302B and HSST 03 steel plate materials in the PSF experiments are provided in NUREG/CR-3220, Volumes 1 and 4.

G. Pells, A. Fudge, and M. Murphy (AERE, Harwell) and S. Watt (RRA) have provided results in Section 2.6 on the use of Sapphire Damage Monitors in test reactor irradiations, including the PSF experiments. A. Fudge is expected to prepare a first draft of the new E706-IIID.2 Standard.

A. Albermann, M. Benoist, and M. Thierry have provided results in NUREG/CR-3320, Volume 2, Section 2.2. on the use of the Graphite and Tungsten Damage Monitors measurements in the PSF experiments. They have provided experimentally derived exposure parameter results for the SSC, OT, 1/4T, 1/2T, and 3/4T locations based on measurements in the 18-day startup test (SDMF-1); see Appendix A. A. Alberman is expected to prepare a first draft of the new E706-IIID.2 Standard.

3.0 TRANSPORT CALCULATION RESULTS - SUMMARY

L. F. Miller (ORNL)

Neutron diffusion theory and transport theory calculations were performed to determine the neutron fluence at a variety of locations in the irradiation capsules. The source distribution calculations were accomplished with three-dimensional diffusion theory calculations, and the ex-core results were obtained by a synthesis of two-dimensional and one-dimensional transport calculations (Ma84a).

Calculated results generally agreed well with measurements. Discrepancies between measurements and calculations near the void box led to a later confirmation that the void box contained water.

The neutronics calculations involved numerous detailed procedures and extensive computations. In particular, the ORR underwent 52 fuel cycles with startups and shutdowns during each cycle. Predicting the activity required that the power history of the reactor, as well as the fuel loading changes, be accurately modeled by the neutronics calculation. Details associated with these efforts are documented in Section 3.1.

3.1 ORNL Analysis

L. F. Miller (ORNL)

The neutronics analysis of the two-year irradiation of metallurgical test specimens at the ORR-PSF involved an extensive set of neutron diffusion, neutron transport, and data-handling calculations. In particular, 52 fuel cycles (or core loadings) were utilized during the irradiation, and since significant cycle-to-cycle variations in core leakage were observed, diffusion and transport theory calculations were performed for most of the fuel cycles. Furthermore, the determination of saturated activities at any particular time required that the reactor power history be accurately known so that the accumulation and decay (and buildup) of activity could be properly treated. These calculations are documented by Maerker and Worley (Ma84a) and are briefly described herein.

Figure 3.1.1 illustrates the coordinate system for the neutronics calculations, and Figure 3.1.2 provides an overview illustration. Major steps associated with the calculations include:

1. preparation of input for a three-dimensional (3-D) diffusion theory calculation based on a specific core loading,

2. execution of the 3-D diffusion theory calculation,

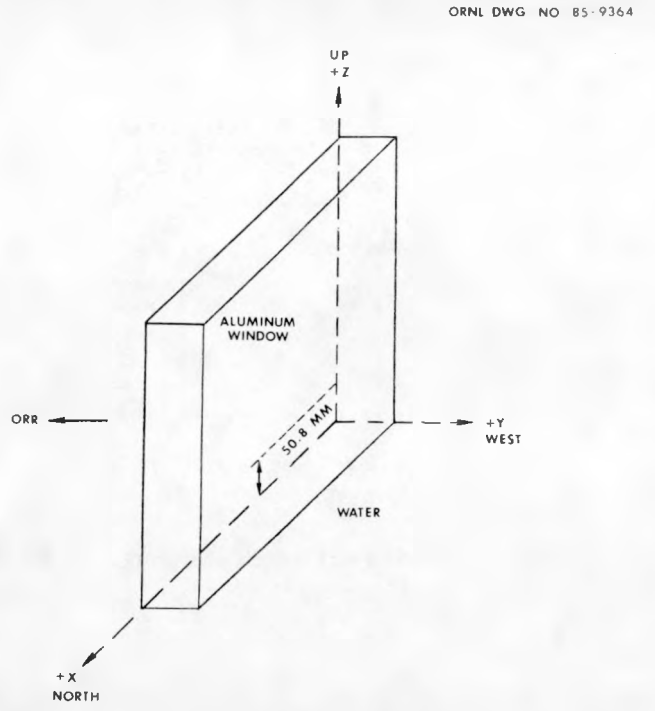

FIGURE 3.1.1. Definition of the Cartesian Coordinate System. The Origin is Located 50.8 mm below the Reactor Horizontal Midplane on the Outside Surface of the Aluminum Window.

ORNL DWG.84-9508

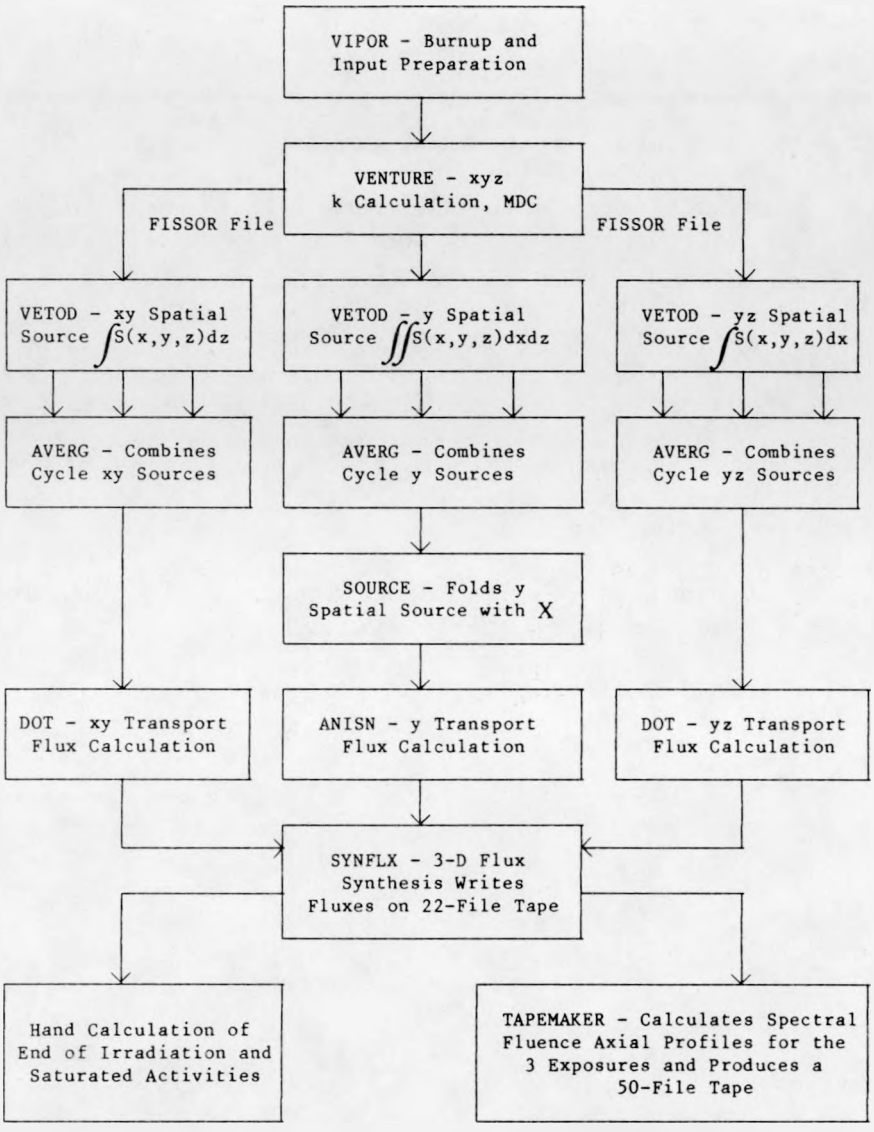

FIGURE 3.1.2. Sequence of Calculations.

3. processing of the neutron source distribution from the 3-D diffusion theory calculation for two 2-D (XY and YZ) transport calculations and for one 1-D (Y) calculation,

4. execution of three neutron transport calculations (two 2-D and one 1-D) for selected (specific or combination of) fuel cycles,

5. synthesis of the three transport calculations to obtain a 3-D neutron flux distribution in the reactor core and in the experimental facility,

6. repetition of steps 1 through 3 for each unique reactor core configuration and of steps 4 and 5 for applicable groups of fuel cycles during the irradiations, and

7. calculation of end-of-irradiation saturated activities and spectral-fluence axial profiles.

During the course of the two-year irradiation, the reactor core was partially reloaded 52 times and underwent 64 startups (and shutdowns). Thus, the calculation of the saturated activities required that the flux distribution in the irradiation specimens for applicable fuel cycles (c.f., Ma84a) be appropriately combined with the time history of reactor power and the applicable isotopic half-lives. Table 3.1.1 provides essential details relative to reactor core loadings, the time history of reactor power, insertion and retraction times of the capsules, automatic reductions in power (setbacks), and average reactor power.

One may appreciate the need to account for cycle-to-cycle variations in reactor operation by noting the associated effects on saturated activities for several fuel cycles listed in Table 3.1.2. In particular, cycle-to-cycle fluence variations of 25% and spectral variations of 5% are apparent. Saturation activities may be obtained for any irradiation cycle from data and computational methods provided by Maerker and Worley (Ma84a).

It is expected that fluence spectra should be sufficient for performing analyses relative to damage correlations for metallurgical specimens; thus, these data are provided for selected locations rather than fluxes for all 50 core configurations. Table 3.1.3 provides fluence spectra on the Y axis (c.f., Figure 3.1.1) for the complete irradiation at the centers of SSC-1 and SSC-2 and at the 0-T, 1/4-T, and 1/2-T locations in the SPVC. These results are obtained from synthesized 3-D fluences and cover neutron energies from 0.098 MeV to 17.33 MeV.

The effect of water in the void box on exposure calculations for the SSC and SPVC, reported by Stallmann (St84), is negligible for fluences above 1.35 MeV as can be noted from Table 3.1.4. Derived exposure parameters, reported in Section 4.2, are based on neutronics calculations and on dosimetry measurements. In particular, calculations for the derived exposure parameters use measurements and calculations in conjunction with applicable uncertainty data to obtain a best estimate for the exposure parameters. Thus, the derived exposure values should be significantly more accurate than would be indicated by ratios listed in Table 3.1.4. In effect, results given by Table 3.1.4 confirm the claim that neutronics calculations performed with no water in the void box are suitable for input to an adjustment calculation for the derived exposure parameters. This claim may not be valid, however, relative to the void box specimens. Large perturbations are apparent for all energies in the void box. These results are obtained from two 1-D neutron transport calculations with and without water in the void box and with no transverse leakage.

TABLE 3.1.1

IRRADIATION HISTORY AND CYCLE PARAMETERS

Cycle	k_{eff}	Date and Time Inserted		Date and Time Retracted		Down-Time After Previous Irradiation Δt_d (hr)	t(inserted) (hr)	t(retracted) (hr)	Δtup (hr)	Setback Δt_s (hr)	Average Power Including Setback (MW)
						Start Irradiation of SSC-1, SPVC, and SVBC					
153B	1.0242	4/30/80	13:34	5/08/80	7:00		0	185.43	185.43	1.00	29.822
153C	1.0251	5/08/80	16:43	5/14/80	13:30	9.72	195.14	335.90	140.76	0	29.800
153C	1.0251	5/16/80	9:57	5/21/80	2:17	44.45	380.35	492.68	112.33	0	29.957
153D	1.0162	5/22/80	10:49	6/06/80	24:00	32.53	525.21	898.39	373.18	2.55	29.657
153F	1.0224	6/12/80	9:20	6/23/80	12:55	129.33	1027.72	1295.30	267.58	0.43	29.377
						End Irradiation of SSC-1					
153G	1.0042	6/27/80	18:30	7/05/80	3:30	101.58	1396.88	1573.88	177.00	2.32	28.855
153G	1.0042	7/07/80	13:55	7/08/80	9:40	58.42	1632.30	1652.05	19.75	0.18	29.058
153G	1.0042	7/08/80	15:18	7/13/80	8:00	5.63	1657.68	1770.38	112.70	1.01	29.565
154A	1.0047	7/18/80	17:00	7/18/80	18:32	129.00	1899.38	1900.70	1.32	0.82	3.712
154A	1.0047	7/18/80	22:50	7/21/80	4:26	4.30	1905.00	1958.60	53.60	1.26	28.319
154A	1.0047	7/22/80	10:05	7/31/80	7:00	29.65	1988.25	2201.17	212.92	13.39	28.200
154B	1.0066	7/31/80	18:20	8/12/80	19:02	11.33	2212.50	2501.20	288.70	0.33	30.335
154C	1.0019	8/15/80	14:48	8/15/80	16:07	67.77	2568.97	2570.29	1.32	0.05	28.977
154D	1.0024	8/21/80	10:55	8/26/80	16:00	138.80	2709.09	2834.17	125.08	0.39	28.849
154E	1.0016	8/27/80	14:30	9/01/80	3:29	22.50	2856.67	2965.62	108.95	0	29.799
154E	1.0016	9/3/80	9:53	9/09/80	8:00	54.40	3020.02	3162.14	142.12	0.57	30.031
154F	1.0007	9/10/80	11:22	9/23/80	4:00	27.37	3189.51	3494.14	304.63	1.73	29.471
154G	0.9993	9/23/80	13:52	10/05/80	21:32	9.87	3504.01	3799.68	295.67	0.44	29.909
154H	1.0190	10/7/80	13:46	10/17/80	17:50	40.23	3839.91	4083.95	244.04	0	29.905
154I	0.9858	10/21/80	12:48	10/29/80	4:00	90.97	4174.92	4359.05	184.13	1.00	29.486
154J	0.9890	10/29/80	18:47	11/08/80	8:00	14.78	4373.83	4603.05	229.22	0.29	29.223
155B	0.9983	12/03/80	14:51	12/09/80	0:26	606.85	5209.90	5339.48	129.58	0.90	28.786
155C	0.9920	12/10/80	12:54	12/18/80	5:15	36.47	5375.95	5560.30	184.35	0	28.247
155D	0.9936	12/18/80	17:46	12/30/80	8:00	12.52	5572.82	5851.59	278.77	0.54	27.832
155E	0.9891	12/30/80	16:11	1/07/81	8:00	8.18	5859.77	6043.59	183.82	0.29	26.823
155F	0.9922	1/07/81	21:55	1/15/81	4:00	13.92	6057.51	6231.59	174.08	0.22	27.115
155G		1/16/81	11:41	1/19/81	20:22	31.68	6263.27	6343.95	80.68	0.21	30.066
155H		1/21/81	9:02	1/22/81	7:16	36.67	6380.62	6402.85	22.23	0.89	29.311
155H		1/22/81	16:18	2/02/81	8:00	9.03	6411.88	6667.58	255.70	0.61	30.346
156A		2/09/81	13:35	2/24/81	8:00	173.58	6841.16	7195.58	354.42	2.92	27.279
156B		2/24/81	15:00	3/13/81	8:04	7.00	7202.58	7603.65	401.07	2.19	27.223
156B		3/13/81	8:47	3/16/81	3:00	0.72	7604.37	7670.59	66.22	0.61	27.168
156C	1.0052	3/19/81	10:13	3/30/81	22:40	79.22	7749.81	8026.26	276.45	0	30.447
156C	1.0052	3/31/81	11:33	4/02/81	4:00	12.88	8039.14	8079.59	40.45	1.08	29.598
156D	1.0076	4/02/81	16:10	4/19/81	8:00	12.17	8091.76	8491.60	399.84	0	30.290
157A	1.0021	4/27/81	11:12	5/11/81	3:12	194.20	8585.80	9013.80	328.00	2.50	30.174
157B	1.0184	5/11/81	17:24	5/27/81	4:00	14.20	9028.00	9398.60	370.60	0	30.335

TABLE 3.1.1

(CONTINUED)

Cycle	k_{eff}	Date and Time Inserted		Date and Time Retracted		Down-Time After Previous Irradiation Δt_d (hr)	t(inserted) (hr)	t(retracted) (hr)	Δtup (hr)	Setback Δt_s (hr)	Average Power Including Setback (MW)
						Start Irradiation of SSC-2					
157C	1.0166	5/29/81	11:39	5/29/81	20:45	55.65	9454.25	9463.35	9.10	0	30.048
157C	1.0166	6/01/81	11:49	6/09/81	8:10	63.07	9526.42	9714.77	188.35	0.94	29.997
157D	1.0127	6/10/81	8:15	6/23/81	4:23	24.08	9738.85	10046.98	308.13	0	30.352
157E	0.9756	6/25/81	12:20	7/10/81	12:00	55.95	10102.93	10462.60	359.67	0	30.044
158C	1.0018	7/22/81	13:47	8/06/81	6:30	289.78	10752.38	11105.10	352.72	0.15	27.082
158D	0.9997	8/07/81	19:05	8/20/81	4:00	36.58	11141.68	11438.61	296.93	0	27.008
158E	1.0101	8/21/81	15:17	8/30/81	24:00	35.28	11473.89	11698.61	224.72	0	30.354
158F	1.0076	9/02/81	19:01	9/08/81	16:52	67.02	11765.63	11907.48	141.85	0.22	30.136
158G	1.0274	9/11/81	8:17	9/25/81	2:00	63.42	11970.90	12300.62	329.72	0	30.260
						End Irradiation of SSC-2					
158H	1.0126	9/25/81	23:10	10/13/81	3:20	21.17	12321.79	12733.96	412.17	0.12	30.180
158I	1.0206	10/13/81	20:30	10/23/81	3:00	17.17	12751.13	12973.63	222.50	0.57	30.174
158J	1.0142	10/23/81	13:28	10/26/81	20:13	10.47	12984.10	13063.85	79.75	0.12	29.819
158J	1.0142	10/27/81	9:41	11/04/81	4:00	13.47	13077.32	13263.64	186.32	1.43	30.267
158K	1.0173	11/04/81	16:10	11/15/81	8:00	12.17	13275.81	13531.64	255.83	0.09	30.311
159A	1.0156	11/24/81	14:12	12/12/81	6:00	222.20	13753.84	14177.64	423.80	0	30.287
159B	1.0037	12/18/81	9:47	12/28/81	13:20	147.78	14325.42	14568.97	243.55	0.43	30.009
159C	1.0054	12/31/81	21:21	1/06/82	8:36	80.02	14648.99	14780.24	131.25	0.71	29.794
159C	1.0054	1/06/82	14:18	1/14/82	3:00	5.70	14785.94	14966.64	180.70	0.37	30.234
159D	1.0121	1/21/82	15:36	2/01/82	2:58	180.60	15147.24	15398.61	251.37	0	30.256
159E	1.0025	2/01/82	16:56	2/07/82	8:00	13.97	15412.58	15547.65	135.07	0	30.126
160A	1.0020	2/12/82	17:33	2/18/82	9:00	129.55	15677.20	15812.65	135.45	0.07	29.987
160B	1.0064	2/18/82	18:59	3/08/82	8:20	9.98	15822.63	16243.98	421.35	0.14	30.173
160C	1.0175	3/09/82	15:33	3/25/82	3:00	31.22	16275.20	16646.65	371.45	1.44	30.113
160D	1.0166	3/26/82	18:55	4/05/82	3:00	39.92	16686.57	16910.65	224.08	0.34	30.223
160E	1.0108	4/04/82	18:40	4/16/82	15:05	15.67	16926.32	17186.74	260.42	0.69	29.856
161B	1.0149	4/29/82	17:42	5/24/82	3:30	313.62	17500.36	18086.16	585.80	0.88	30.062
161C	1.0223	5/27/82	22:28	6/22/82	24:00	90.97	18177.13	18802.66	625.53	1.73	30.116
						End Irradiation of SPVC and SVBC					

TABLE 3.1.2

CYCLE GROUP-TO-CYCLE GROUP VARIATION OF SOME SATURATED ACTIVITIES
AT THE 1/2-T LOCATION, X = -53.7, Y = 337.8, AND Z = -8.5 mm

Cycles	Capsules Irradiated	$^{54}Fe(n,p)$	$^{63}Cu(n,\alpha)$	$^{237}Np(n,f)$	Np/Cu
153B+153C	SSC-1 +	7.59-15*	5.87-17	6.17-13	1.05+4
153D	SPVC +	7.58-15	5.87-17	6.16-13	1.05+4
153F	SVBC	7.83-15	5.71-17	5.99-13	1.05+4
153G-154C	SPVC	7.83-15	6.05-17	6.35-13	1.05+4
154D-154J	and	7.47-15	5.79-17	6.06-13	1.05+4
155B-155F	SVBC	9.15-15	7.06-17	7.42-13	1.05+4
156C-157B		8.65-15	6.68-17	6.99-13	1.05+4
157C-157E	SSC-2 +	8.82-15	6.80-17	7.14-13	1.05+4
158C+158D	SPVC +	9.65-15	7.45-17	7.83-13	1.05+4
158E-158G	SVBC	8.24-15	6.36-17	6.64-13	1.04+4
158H-158K	SPVC	8.14-15	6.33-17	6.50-13	1.03+4
159A-159C	and	8.42-15	6.54-17	6.73-13	1.03+4
159D-160C	SVBC	7.83-15	6.10-17	6.24-13	1.02+4
160D+160E		7.27-15	5.69-17	5.76-13	1.01+4
161B		7.14-15	5.62-17	5.65-13	1.01+4
161C		6.86-15	5.40-17	5.41-13	1.00+4
Startup (151A)	SSC + SPVC	8.84-15	7.05-17	7.04-13	1.00+4

*Read 7.59 x 10^{-15} reactions per atom per second at 30 MW, etc.

TABLE 3.1.3

FLUENCE SPECTRA AT VARIOUS LOCATIONS IN THE SSC AND SPVC
OBTAINED FROM A 3-D SYNTHESIS OF TWO 2-D AND ONE 1-D TRANSPORT CALCULATIONS

Group Boundary (eV)	Location in Capsule				
	SSC-1	SSC-2	0-T	1/4-T	1/2-T
1.733+07	7.411+14	1.706+15	2.174+15	9.719+14	4.881+14
1.419+07	3.610+15	8.308+15	1.081+16	4.936+15	2.520+15
1.221+07	5.853+15	1.350+16	1.616+16	7.278+15	3.664+15
1.105+07	1.304+16	3.005+16	3.592+16	1.599+16	7.951+15
1.000+07	4.363+16	1.007+17	1.147+17	5.043+16	2.473+16
8.607+06	2.322+16	5.364+16	5.801+16	2.509+16	1.211+16
8.187+06	6.730+16	1.555+17	1.649+17	7.010+16	3.328+16
7.408+06	4.393+16	1.016+17	1.022+17	4.312+16	2.031+16
7.047+06	2.048+17	4.738+17	4.771+17	1.956+17	8.982+16
6.065+06	4.377+17	1.015+18	9.339+17	3.709+17	1.659+17
4.966+06	6.797+17	1.579+18	1.338+18	5.243+17	2.318+17
4.066+06	3.975+17	9.253+17	7.126+17	2.846+17	1.277+17
3.679+06	1.105+18	2.576+18	1.937+18	8.023+17	3.703+17
3.012+06	8.537+17	1.990+18	1.571+18	6.765+17	3.203+17
2.725+06	5.190+17	1.210+18	9.578+17	4.291+17	2.086+17
2.592+06	4.973+17	1.160+18	9.313+17	4.044+17	1.929+17
2.466+06	5.228+17	1.218+18	9.835+17	4.337+17	2.087+17
2.365+06	1.419+17	3.304+17	2.802+17	1.331+17	6.721+16
2.346+06	7.046+17	1.641+18	1.363+18	6.530+17	3.333+17
2.231+06	6.380+17	1.487+18	1.206+18	5.797+17	2.962+17
2.123+06	1.231+18	2.869+18	2.297+18	1.103+18	5.627+17
1.921+06	7.207+17	1.679+18	1.273+18	6.586+17	3.521+17
1.827+06	1.671+18	3.892+18	3.041+18	1.632+18	9.027+17
1.653+06	1.583+18	3.689+18	2.888+18	1.535+18	8.433+17
1.496+06	1.890+18	4.402+18	3.365+18	1.904+18	1.090+18
1.353+06	1.883+18	4.387+18	3.270+18	1.918+18	1.128+18
1.225+06	4.549+18	1.060+19	7.434+18	4.858+18	3.097+18
1.003+06	2.261+18	5.268+18	3.603+18	2.558+18	1.735+18
9.072+05	2.381+18	5.547+18	3.879+18	2.672+18	1.808+18
8.209+05	2.171+18	5.059+18	3.728+18	2.324+18	1.488+18
7.427+05	6.617+18	1.541+19	1.210+19	9.674+18	7.144+18
6.081+05	5.201+18	1.212+19	9.602+18	7.446+18	5.504+18
4.979+05	5.842+18	1.361+19	1.148+19	9.288+18	7.037+18
3.688+05	4.974+18	1.158+19	9.597+18	8.665+18	7.054+18
3.020+05	5.763+18	1.342+19	1.034+19	8.102+18	6.156+18
2.128+05	1.943+18	4.526+18	3.661+18	2.686+18	1.974+18
1.832+05	6.706+18	1.562+19	1.253+19	1.008+19	7.788+18
1.111+05	9.916+17	2.310+18	1.898+18	1.341+18	9.919+17
9.804+04					

Results are based on transport calculations for each fuel cycle during the two-year irradiation. Location designations are at the centers of the two simulated surveillance capsules (SSC-1 and SSC-2) and at the surface (0-T), one-fourth thickness (1/4-T), and one-half thickness (1/2-T) of the simulated pressure vessel capsule.

TABLE 3.1.4

FLUENCE PERTURBATION DUE TO WATER IN THE VOID BOX

Upper energy (eV)	Fluence ratio water/void					
	SSC	0-T	1/4-T	1/2-T	3/4-T	Void Box
1.7333 E+7	1.00	1.00	1.00	1.00	1.00	0.59
8.6071 E+6	1.00	1.00	1.00	1.00	1.00	0.53
4.9659 E+6	1.00	1.00	1.00	1.00	0.99	0.33
2.5924 E+6	1.00	1.00	1.00	1.00	0.98	0.23
2.1225 E+6	1.00	1.00	1.00	1.00	0.97	0.14
1.3534 E+6	1.00	1.00	1.00	0.99	0.95	0.06
7.4274 E+5	1.00	0.98	0.96	0.93	0.86	0.03
2.1280 E+5	1.00	0.97	0.94	0.89	0.80	0.03
6.7379 E+4	1.00	0.96	0.93	0.88	0.80	0.04
2.1875 E+4	1.00	0.97	0.94	0.88	0.79	0.06
3.3546 E+3	1.00	0.99	0.98	0.95	0.93	0.17

The reason that fluxes in the SPVC are smaller with water (rather than gas-filled) in the void box is probably due to inelastic scattering of the steel (i.e., void box specimens) behind the void box. In particular, the water in the void box attenuates neutrons reflected by the steel, which is apparently more effective in reflecting high-energy neutrons than water. Geometric effects are not accounted for by these calculations. If spatial attenuation effects were accounted for, the perturbation effect may be somewhat less significant since moving the water closer to the SPVC should slightly decrease transverse leakage.

Selected results from neutronics calculations reported herein should be accurate within 10% [c.f., Maerker (Ma84a)] and may be used with significant confidence for input to damage correlation analyses.

3.2 RR&A ANALYSIS

A.F. Thomas, S.P. Walley (Rolls-Royce and Associates Limited, U.K.)

3.2.1 Introduction

As part of the USNRC-LWR-PV-SDIP, neutronics calculations of the experimental facilities were required in support of the dosimetry analysis of the metallurgical specimens. Detailed calculational and experimental data had previously been generated on the low power Pool Critical Assembly (PCA) mock up of the high-power Oak Ridge Reactor Poolside Facility (PSF) which simulates the core/thermal shield/pressure vessel/cavity of a typical civil LWR. These included 3D MCBEND Monte Carlo calculations carried out by RR&A which generally proved successful in predicting the experimentally determined neutron reaction rates (Mc81).

In order to facilitate the analysis of the dosimetry measurements from the PSF metallurgical irradiations (including the 18-day full-power thermal and physics "Start-Up" experiment) which took place in an optimised but different configuration from that of the PCA, neutron spectral shape information throughout the PSF array was required, as well as best estimates of calculated parameters at locations of particular importance in the SSC and PVS. In order to achieve this a calculational methodology was defined which incorporated both a 1-D deterministic neutron transport calculational technique (ANISN) and a 3-D Monte Carlo neutron transport calculational technique (MCBEND). Initially the use of the 1-D ANISN method was considered to be a simple and cheap way of achieving the objective of providing systematic spectral information providing it could be shown that the methodology and data used could be validated against a reliable and relevant benchmark, such as the PCA experiments. In contrast, the 3-D MCBEND method is much more expensive but allows a more exact representation of the problem, and is capable of providing accurate estimates of both neutron spectrum shapes and flux intensities within predefined error targets. However since economics dictate that only a few specific locations can be characterised, the ANISN and MCBEND methods were, in effect, considered to be complementary.

This section thus details the methods and data used and the results obtained by RR&A in the successful validation of ANISN methodology and the subsequent calculation of the PSF 4/12 irradiation facility using both the ANISN and MCBEND techniques.

3.2.2 Calculational Methodology - ANISN

For the purpose of the ANISN (En67) calculations, 40 neutron energy groups were used (Table 3.2.1) in conjunction with a third order Legendre polynomial expansion of transmission cross section and eight angular flux quadratures (P3/S8), which have in the past been shown to give sufficient accuracy for shielding calculations in support of dosimetry analyses. The calculations were carried out assuming slab geometry since this closely approximated to the geometry of the experimental facility itself, and assumed a fixed source of neutrons in the core which were reflected at the core centre. Reaction rates were computed from the neutron flux spectra at all mesh points initially using the ENDF/B-IV dosimetry cross section file but later using the IRDF82 file which is ENDF/B-V based (Cu82).

TABLE 3.2.1

ANISN AND MCBEND 40 GROUP ENERGY BOUNDARIES

Group Number	Upper Energy (MeV)	Group Number	Upper Energy (MeV)
1	0.149E+2	21	0.135E+1
2	0.122E+2	22	0.100E+1
3	0.100E+2	23	0.743E+0
4	0.819E+1	24	0.550E+0
5	0.704E+1	25	0.247E+0
6	0.638E+1	26	0.111E+0
7	0.549E+1	27	0.318E-1
8	0.497E+1	28	0.912E-2
9	0.449E+1	29	0.335E-2
10	0.407E+1	30	0.961E-3
11	0.368E+1	31	0.354E-3
12	0.333E+1	32	0.101E-3
13	0.301E+1	33	0.373E-4
14	0.272E+1	34	0.176E-4
15	0.247E+1	35	0.504E-5
16	0.235E+1	36	0.306E-5
17	0.203E+1	37	0.186E-5
18	0.183E+1	38	0.113E-5
19	0.165E+1	39	0.625E-6
20	0.149E+1	40	0.414E-6
			0.100E-9

The use of the buckling option is ANISN to simulate 3-D geometry has a significant effect on both computed flux intensity and neutron energy spectrum. Therefore, for the purpose of the validation, calculations were performed with and without buckling corrections, to establish which produced the more accurate spectral information for the purposes of later PSF 4/12 calculation.

Similarly, since the resulting calculations of the PSF 4/12 facility were required with as high an accuracy as the methodology would allow, considerable effort was spent on verifying that the correct input data were supplied.

3.2.3 ANISN Validation Calculations

3.2.3.1 Methodology

Since the later MCBEND calculational route had been earlier studied using the PCA 12/13 benchmark (Mc81) it seemed appropriate and elegant to use the same calculational benchmark to validate the ANISN calculations of the PSF 4/12 array. The data used are briefly detailed below.

Geometry

The geometry mesh structure for the PCA 12/13 is shown in Figure 3.2.1 and is based on the data given in (Mc81). The total number of meshes used was 58 and no ex-core mesh interval was allowed to be greater than 2-3cm (5cm in the void box).

Materials

The material compositions used in the various zones are shown in Table 3.2.2. A mesh was computed for the fuel element and the thermal shield (18/8 stainless steel).

Source Representation

The source distribution in the core was taken from the centre line power distribution of the MCBEND Monte Carlo calculation of the PCA 12/13 benchmark. This gave:

Fuel Element	Mesh Point	Relative Power
C5	1	1.480
B5	2	1.440
B5	3	1.320
A5	4	1.030
A5	5	0.855

The Watt-Cranberg fission spectrum in the 40 group scheme that was used is given in Table 3.2.3.

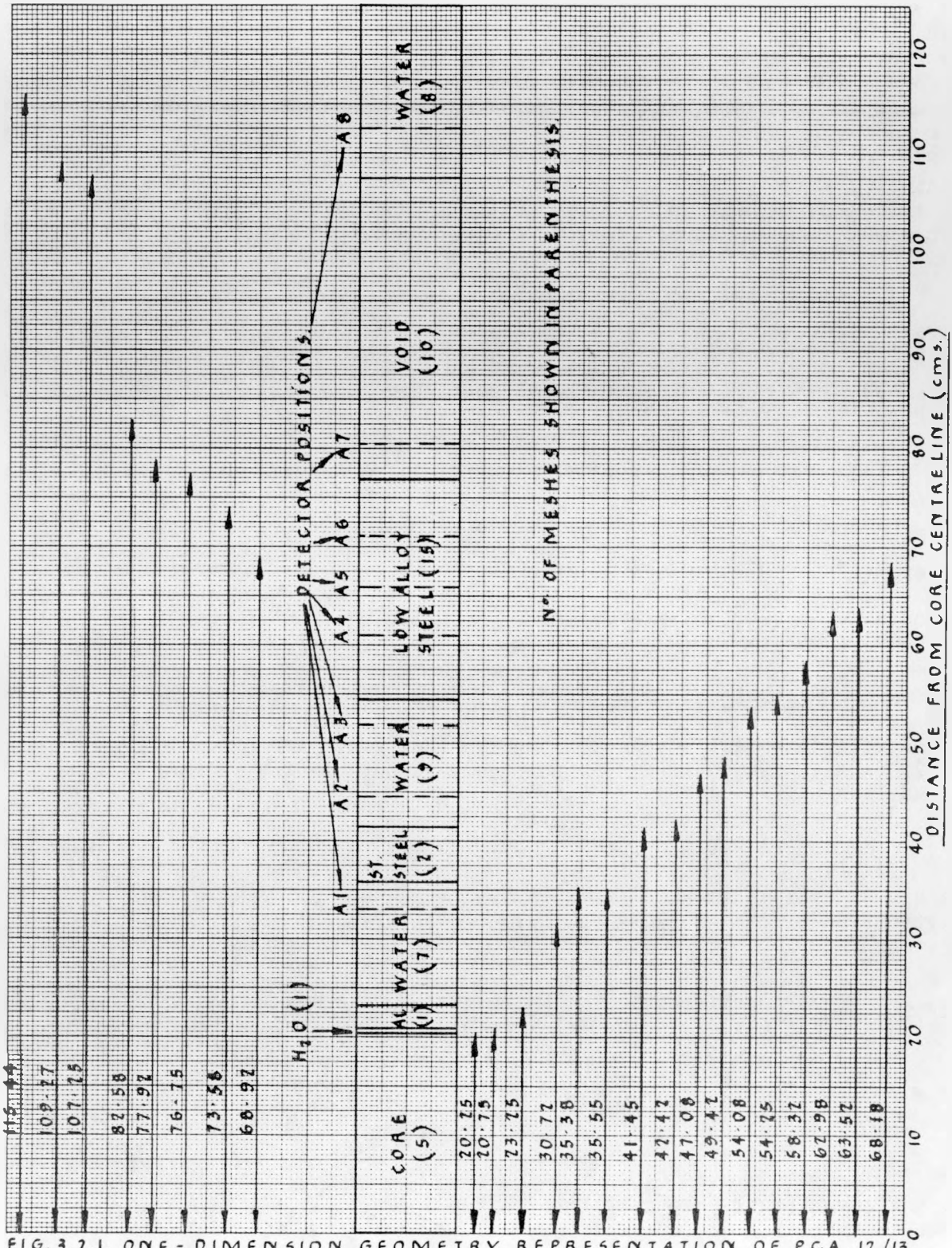

FIG. 3.2.1. ONE-DIMENSION GEOMETRY REPRESENTATION OF PCA. 12/13. USED TO VALIDATE ANISN CALCULATION OF THE PSF. 4/12 CONFIGURATION.

TABLE 3.2.2

MATERIAL ZONE COMPOSITION DATA FOR ANISN PSF CALCULATIONS

Zone	Element	Proportion By Weight	Density gms.cm^{-3}	Number Density Atoms x 10^{24}
Fuel	U^{238}	0.020	19.07	8.45E-5
	U^{238}	0.0014		6.43E-6
	Al	0.631	2.70	2.41E-2
	H	0.038	1.0	4.00E-2
	O	0.310		2.00E-2
Water	H	0.11	1.00	6.69E-2
	O	0.89		3.34E-2
Aluminium	Al	1.00	2.70	6.02E-2
Thermal Shield (and SSC)	Fe	0.74	7.86	6.27E-2
	Ni	0.08	8.90	1.64E-2
	Cr	0.18	7.19	6.66E-3
Pressure Vessel Simulator	Fe	1.00	7.87	8.48E-2
Void Box	Fe	0.0001	7.87×10^{-4}	8.48E-6

TABLE 3.2.3

WATT-CRANBERG 40 NEUTRON ENERGY GROUP FISSION SPECTRUM

Group Number	Group Flux Density	Group Number	Group Flux Density
1	1.870E-4	21	1.148E-1
2	1.026E-3	22	9.051E-2
3	3.857E-3	23	6.735E-2
4	7.055E-3	24	9.742E-2
5	7.929E-3	25	3.402E-2
6	1.847E-2	26	1.332E-2
7	1.758E-2	27	2.115E-3
8	2.231E-2	28	3.006E-4
9	2.711E-2	29	7.329E-5
10	3.191E-2	30	1.032E-5
11	3.630E-2	31	2.511E-6
12	4.033E-2	32	3.534E-7
13	4.321E-2	33	6.856E-8
14	4.555E-2	34	2.790E-8
15	2.335E-2	35	2.666E-9
16	7.137E-2	36	1.260E-9
17	4.745E-2	37	5.950E-10
18	4.665E-2	38	3.122E-10
19	4.535E-2	39	1.016E-10
20	4.311E-2	40	1.189E-10

Source Normalisation

In order to be consistent with the quoted PCA 12/13 experimental reaction rate measurements, the core power was assumed to be equivalent to 1.0 neutron/sec over the whole core. This gave a normalisation factor of 1.067 x 10^{-5} neutrons $\cdot cm^{-3} \cdot s^{-1}$. However, ANISN input requires the total number of source neutrons in the problem to be supplied. This is given by:-

$$P^z \sum V_i \cdot NF \cdot P_i^x$$

where:-

V_i = volume of mesh

NF = normalisation factor

P^z = axial power factor

P_i^x = radial power factor in mesh, i

This gave a total neutron source in the problem of 3.44 x 10^{-4} neutrons/second. [Since PCA experimental measurements were taken at core mid-plane height the axial power factor (P^z) was taken to be 1.3 i.e., the axial power factor at core mid-plane (Mc81)].

Buckling Corrections

Calculations were conducted both without and with buckling correction factors applied. The buckling factor used was the recommended value of 1.42 using lateral core dimensions of 60.0 cms height and 38.5 cms width.

3.2.3.2 Results and Discussion

Neutron Spectra

The method of validation chosen was to compare measured and calculated spectral indices (SI_i^{AB}) at any position, i, for various reaction rates (A,B, etc) across as much as possible of the important damaging region of the neutron spectrum (E>0.1MeV) where:

$$SI_i^{AB} = \frac{RR_i^A}{RR_i^B} = \frac{\int_0^\infty \sigma^A(E)\phi_i(E)dE}{\int_0^\infty \sigma^B(E)\phi_i(E)dE}$$

Since the reactions involved are essentially threshold reactions and have a low energy response, the limits of integration are, in practice, finite, i.e.,

$$SI_i^{AB} \sim \alpha \quad \frac{\int_{E_2}^{E_1} \phi_i(E)\, dE}{\int_{E_4}^{E_3} \phi_i(E)\, dE} \sim \alpha \frac{\text{flux in region } E_1 \to E_2}{\text{flux in region } E_3 \to E_4}$$

The usefulness of this method is:-

(i) that the value of SI^{AB} (measured) does not involve any calculational errors since the flux spectrum $\phi_i(E)$ is implicit in the measured integral quantities.

(ii) that any systematic errors in flux intensity in the calculated values of reaction rate are self-cancelling in SI_i^{AB} (calculated).

For the purposes of validation, therefore, three of the recommended "benchmark referenced" PCA 12/13 measured reaction rates were chosen, with widely varying threshold energies, and a full parametric survey of SI_i^{AB} (calculated) to SI_i^{AB} (measured) carried out at all detector positions for both buckled and unbuckled ANISN calculations. The reaction rates examined were:

$^{27}Al(n,\alpha)^{24}Na$ (~7 MeV threshold)

$^{58}Ni(n,p)^{58}Co$ (~3 MeV threshold)

$^{115}In(n,n)^{115m}In$ (~1 MeV threshold)

and the ratios of calculated (using ENDF/B-IV dosimetry cross sections) to measured SI_i^{AB} are shown in Tables 3.2.4 (a,b,c) and 3.2.5 (a,b,c). It can be seen that there is a significant improvement in calculated spectra where a buckling correction is adopted, although there is still a tendency for the ANISN calculated spectra to over-estimate ($\leq$10%) the high energy (E> 5MeV) contribution. However, this discrepancy is not inconsistent with the experimental error on the measured values of SI_i^{AB} [$\pm$4%(1σ)], the error on ANISN library differential reaction cross sections [$\pm$(2-7)%] compared to value of SI_f for integral measurements), and the errors on transmission cross sections (~$\pm$5%), and is probably as good as can be achieved using a one-dimensional calculational technique. Later analysis using the IRDF82 dosimetry file resulted in even better agreement between calculation and measurement.

TABLE 3.2.4

ANISN VALIDATION CALCULATION:
COMPARISON OF MEASURED AND COMPUTED SPECTRAL
INDICES FOR PCA 12/13 (UNBUCKLED SOLUTION)

Detector Position	(a) SI = $^{27}Al(n,\alpha)/^{115}In(n,n')$ x 10^3		
	M	C	C/M
A_o	-	3.83	-
A_1	5.27	6.55	1.24
A_2	6.06	7.85	1.30
A_3	8.46*	1.10(1.07)	1.30(1.25)
A_4	6.55	7.28	1.12
A_5	5.56	6.18	1.12
A_6	4.95	5.20	1.05
A_7	-	-	-
A_8	-	-	-
SI_f	3.76	4.04	1.07

Detector Position	(b) SI = $^{58}Ni(n,p)/^{115}In(n,n')$ x 10^1		
	M	C	C/M
A_o	-	5.77	-
A_1	6.02	6.78	1.12
A_2	5.86	6.54	1.11
A_3	6.69*	7.59(7.50)	1.13(1.12)
A_4	5.20	5.02	0.97
A_5	4.35	4.16	0.96
A_6	3.66	3.40	0.93
A_7	-	-	-
A_8	-	-	-
SI_f	5.77	6.08	1.05

Contd...

TABLE 3.2.4 (Cont'd)

Detector Position	(c) SI = $^{27}Al(n,\alpha)/^{58}Ni(n,p) \times 10^2$		
	M	C	C/M
A_0	-	0.66	-
A_1	0.88	0.97	1.11
A_2	1.07	1.20	1.17
A_3	1.26*	1.45(1.42)	1.15(1.13)
A_4	1.26	1.40	1.15
A_5	1.28	1.48	1.16
A_6	1.35	1.52	1.12
A_7	-	-	-
A_8	-	-	-
SI_f	0.651	0.663	1.02

*A3 measurements were 0.8cm nearer the core than the original geometry specification.
Actual values are shown in parentheses.

TABLE 3.2.5

ANISN VALIDATION CALCULATION:
COMPARISON OF MEASURED AND COMPUTED SPECTRAL
INDICES FOR PCA 12/13 (BUCKLED SOLUTION)

Detector Position	(a) SI = $^{27}Al(n,\alpha)/^{115}In(n,n')$ x 10^3		
	M	C	C/M
A_o	-	3.69	-
A_1	5.27	5.85	1.11
A_2	6.06	6.99	1.15
A_3	8.46*	9.72(9.40)	1.15(1.11)
A_4	6.55	6.88	1.05
A_5	5.56	5.99	1.08
A_6	4.95	5.24	1.06
A_7	-	-	-
A_8	-	-	-
SI_f	3.76	4.04	1.07

Detector Position	(b) SI = $^{58}Ni(n,p)/^{115}In(n,n')$ x 10^1		
	M	C	C/M
A_o	-	5.72	-
A_1	6.02	6.56	1.08
A_2	5.86	6.34	1.08
A_3	6.69*	7.32(7.26)	1.09(1.08)
A_4	5.20	5.11	0.98
A_5	4.35	4.35	1.00
A_6	3.66	3.65	1.00
A_7	-	-	-
A_8	-	-	-
SI_f	5.71	6.08	1.06

TABLE 3.2.5 (Cont'd)

Detector Position	(c) SI=^{27}Al(n,α)/^{58}Ni(n,p) x 10^2		
	M	C	C/M
A_o	-	0.65	-
A_1	0.88	0.89	1.01
A_2	1.07	1.10	1.03
A_3	1.26*	1.33(1.29)	1.06(1.02)
A_4	1.26	1.35	1.07
A_5	1.28	1.37	1.07
A_6	1.35	1.44	1.07
A_7	-	-	-
A_8	-	-	-
SI_f	0.657	0.663	1.01

*A3 measurements were 0.8cm nearer the core than the original geometry specification.
Actual values are given in parentheses.

Reaction Rates

It was also of interest to compare the ratio of calculated to measured absolute reaction rates (neutron flux) with and without a buckling correction. This comparison is shown in Table 3.2.6 (a,b,c) for the same three reactions as discussed above. As expected it can be seen that the unbuckled calculations produce large and systematically increasing overprediction of reaction rate with attenuation. The buckled calculation on the other hand tends to underpredict but by a systematically much smaller amount. This is due to the fact that the recommended value of BF(=1.42) is not specifically tailored to the PCA 12/13 calculation and in fact results in an unbuckling of the lateral power shape for this particular problem.

Conclusions

As a result of the validation exercise described above it was considered that a suitable ANISN methodology had been determined for the calculation of the PSF 4/12 array, using the recommended buckling factor of 1.42. Using this technique not only would neutron spectra of the required accuracy be achievable but also predictions of absolute fluxes and reaction rates to within -30%. The results of these calculations are described below.

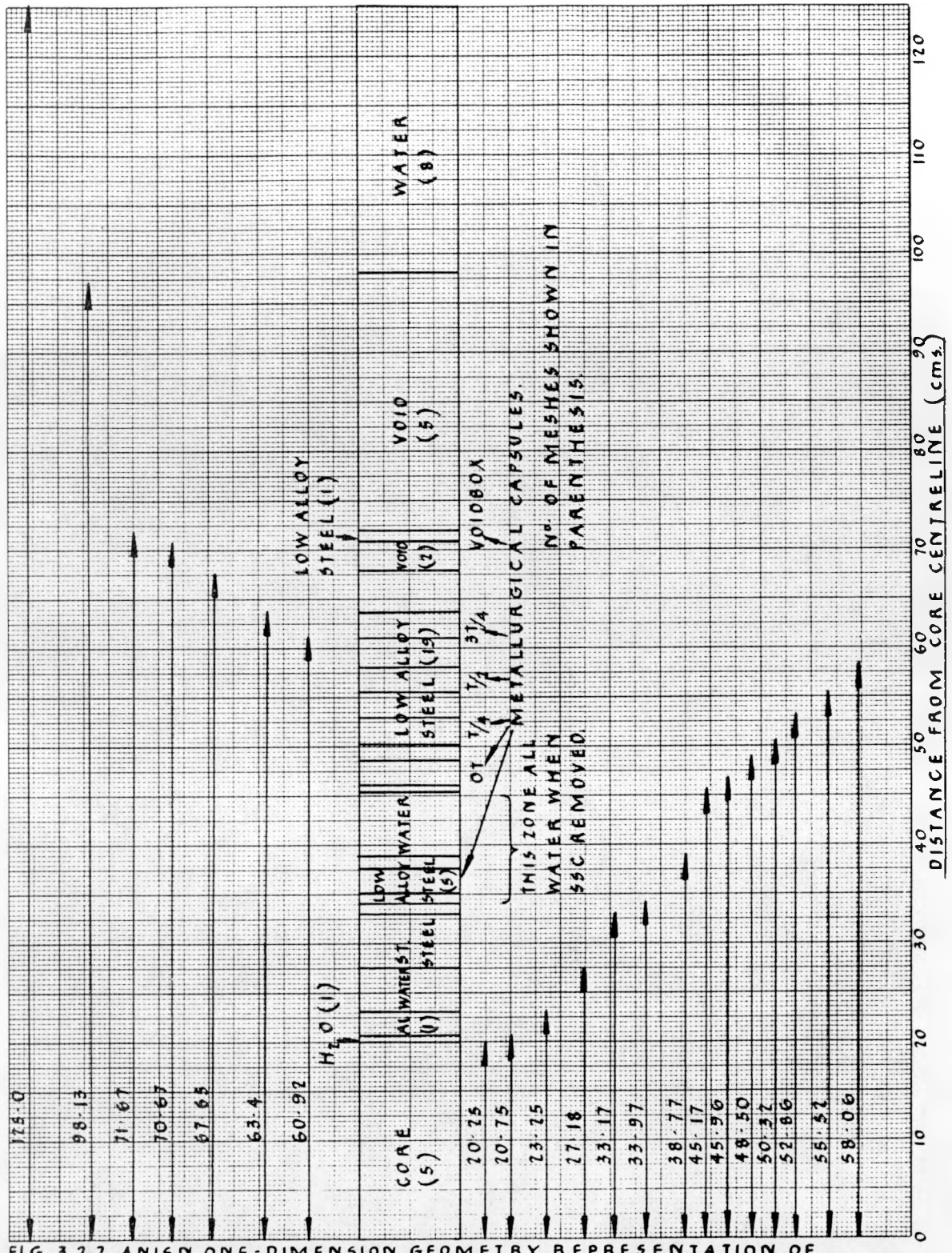

FIG. 3.2.2. ANISN ONE-DIMENSION GEOMETRY REPRESENTATION OF PSF.4/12 CONFIGURATION.

TABLE 3.2.6

ANISN VALIDATION CALCULATION: COMPUTED REACTION RATES FOR PCA 12/13 (UNBUCKLED AND BUCKLED SOLUTIONS)

Detector Position	$^{27}Al(n,\alpha)^{24}Na(\sigma f=0.69mb)$ Measured	BF=0.0	BF=1.42	BF=0.0 / M	BF=1.42 / M	BF=1.42 / BF=0.0
A_0	1.52E-7	1.625E-7	1.38E-7	1.08	0.92	0.85
A_1	5.59E-9	8.39E-9	4.96E-9	1.50	0.89	0.59
A_2	7.27E-10	1.31E-9	6.55E-9	1.80	0.90	0.50
A_3	3.18E-10*	5.76E-10	2.51E-10	1.81	0.79	0.44
A_4	7.27E-11	1.29E-10	5.07E-11	1.80	0.70	0.39
A_5	2.91E-11	5.79E-11	2.17E-11	1.99	0.75	0.38
A_6	1.09E-11	2.21E-11	7.84E-11	2.03	0.72	0.35
A_7	-	8.10E-12	2.56E-12	-	-	0.32
A_8	-	4.30E-12	9.68E-11	-	-	0.23

Detector Position	$^{58}Ni(n,p)^{58}Co(\sigma_f=1.04$ mb) Measured	BF=0.0	BF=1.42	BF=0.0 / M	BF=1.42 / M	BF=1.42 / BF=0.0
A_0	2.50E-5	2.45E-5	2.14E-5	0.98	0.86	0.87
A_1	6.35E-7	8.68E-7	5.57E-7	1.37	0.88	0.64
A_2	6.74E-8	8.49E-8	5.94E-8	1.26	0.88	0.70
A_3	2.52E-8*	3.96E-8	1.89E-8	1.57	0.75	0.48
A_4	5.78E-9	8.90E-9	3.79E-9	1.54	0.66	0.43
A_5	2.28E-9	9.91E-9	1.58E-9	1.72	0.70	0.41
A_6	8.10E-10	1.44E-9	5.47E-10	1.78	0.68	0.38
A_7	-	4.78E-10	1.54E-10	-	-	0.32
A_8	-	1.93E-10	4.60E-11	-	-	0.23

TABLE 3.2.6 (Cont'd)

$^{115}In(n,n')^{115m}In(\sigma_f = 171\ mb)$

Detector Position	Measured	BF=0.0	BF=1.42	BF=0.0 / M	BF=1.42 / M	BF=1.42 / BF=0.0
A_0	-	4.24E-5	3.74E-5	-	-	0.88
A_1	1.06E-6	1.28E-6	8.48E-7	1.21	0.80	0.66
A_2	1.15E-7	1.66E-7	9.36E-8	1.44	0.81	0.56
A_3	3.76E-8*	5.24E-8	2.58E-8	1.40	0.69	0.49
A_4	1.11E-8	1.77E-8	7.42E-8	1.59	0.69	0.43
A_5	5.22E-9	9.38E-9	3.63E-9	1.80	0.70	0.39
A_6	2.21E-9	4.25E-9	1.50E-9	1.92	0.68	0.35
A_7	-	1.55E-9	4.54E-10	-	-	0.29
A_8	-	3.42E-10	8.35E-11	-	-	0.24

*A3 measurements were 0.8cm nearer the core than the original geometry specifications.

3.2.4 ANISN PSF 4/12 Calculations

3.2.4.1 Methodology

For the purposes of a full analysis two ANISN calculations were carried out on the PSF 4/12, ie. with and without the simulated surveillance capsule (SSC) in place. The data used is briefly detailed below.

Geometry

The geometry mesh structure for the PSF 4/12 calculations are shown in Figure 3.2.3 and once again the size of each mesh was kept to a minimum. The critical dimensions were based on those given in Section 1.1. In order to be able to analyse the dosimetry at the 3/4T position in the PSF start-up experiment, a pseudo-metallurgical capsule was modelled although none existed in the PSF metallurgy irradiation.

Materials

The materials compositions used were the same as those for the PCA 12/13 calculation (Table 3.2.2).

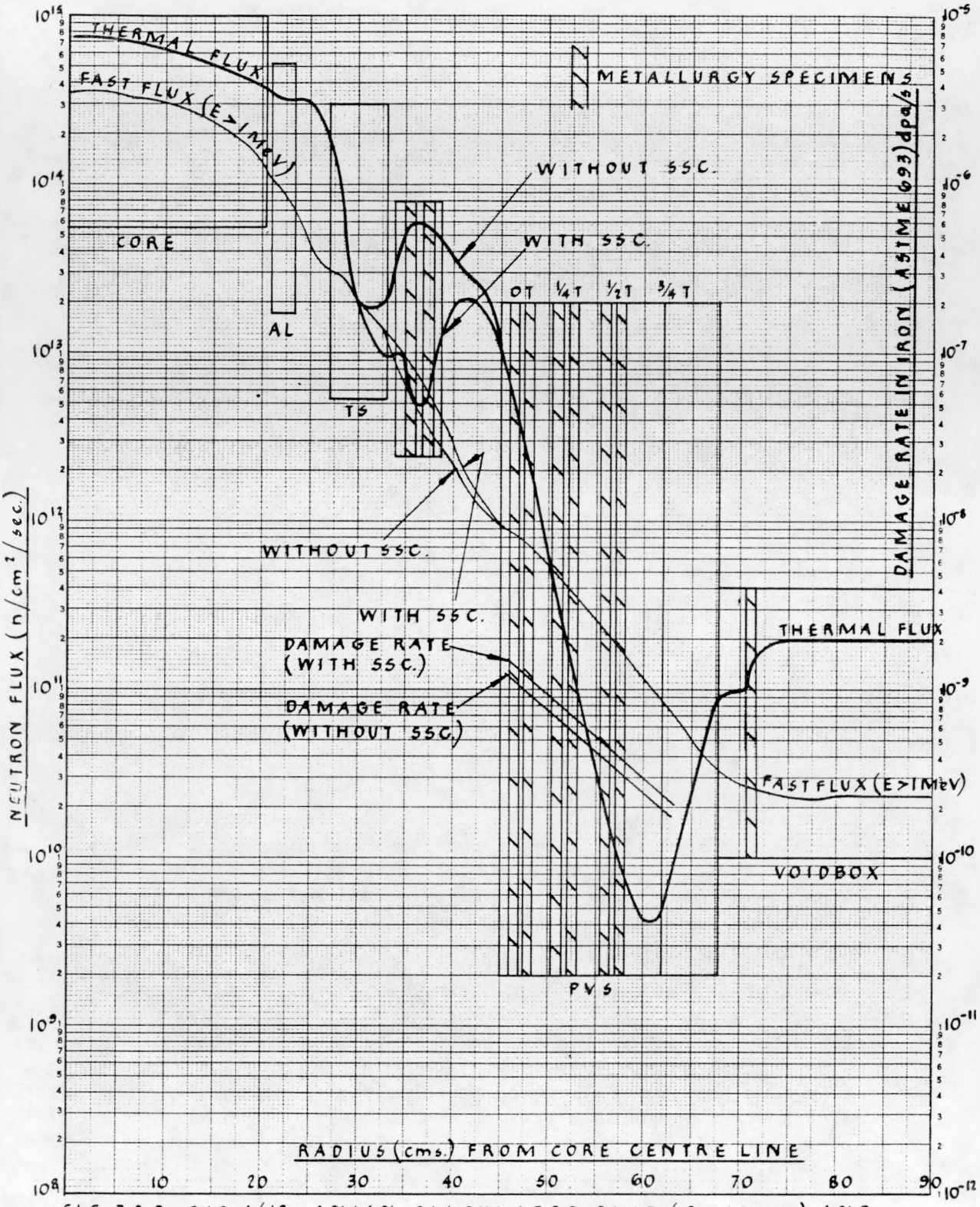

FIG. 3.2.3. PSF 4/12 ANISN CALCULATED FAST (E>1MeV) AND THERMAL NEUTRON FLUXES.

Source Representation

The source distribution was the same as that used for the PCA 12/13 calculation, since at the time these calculations were performed they were the most representative data available and served to meet the objective of the calculations.

Source Normalisation

For the PSF calculation the relevant power level is 30MW. At this power the normalisation factor was calculated to be 2.434×10^{13} neutrons $cm^{-3} \cdot s^{-1}$. Using the same method as in Section 3.2.3 to calculate the required ANISN source data, the total neutron source at mid-plane was found to be 7.8487×10^{13} neutrons/second.

Source Fission Spectrum

The Watt fission neutron spectrum used in the PCA 12/13 calculations was again employed.

Buckling Factor

The recommended buckling factor ($B^F = 1.42$) was used throughout together with the PSF lateral core dimensions (60.01 cm x 38.5 cm).

3.2.4.2 Results

The results of the ANISN calculations of the PSF 4/12 and PSF 4/12 + SSC calculations in terms of attenuation of fast neutron flux (E>1MeV), thermal neutron flux and atom displacement rate are shown in Figure 3.2.3. The variation in effective neutron cross sections, using IRDF 82 dosimetry cross sections data for some important dosimetry reactions through the facility are shown in Figures 3.2.4 and 3.2.5. The effective reaction cross sections of particular relevance to the analysis of the RR&A/AERE dosimeters in the PSF irradiations are given in Table 3.2.7 and damage cross sections are given in Table 3.2.8.

3.2.4.3 Discussion

Several observations from Figures 3.2.4 and 3.2.5 although confirming well known phenomona are worth restating because of the technological significance they hold for the analysis of surveillance experiments generally.

Fast Neutron Spectra

(i) The attenuation of thermal neutron flux in steel is very much greater than that in water whilst the attenuation of fast neutron flux (E> 1MeV) in steel is somewhat less than in water. This causes a large depression in the thermal neutron flux (but a small enhancement in fast neutron flux (E>1MeV) in the region where the SSC is inserted. In neither case, however, does this perturbation propagate into the PVS.

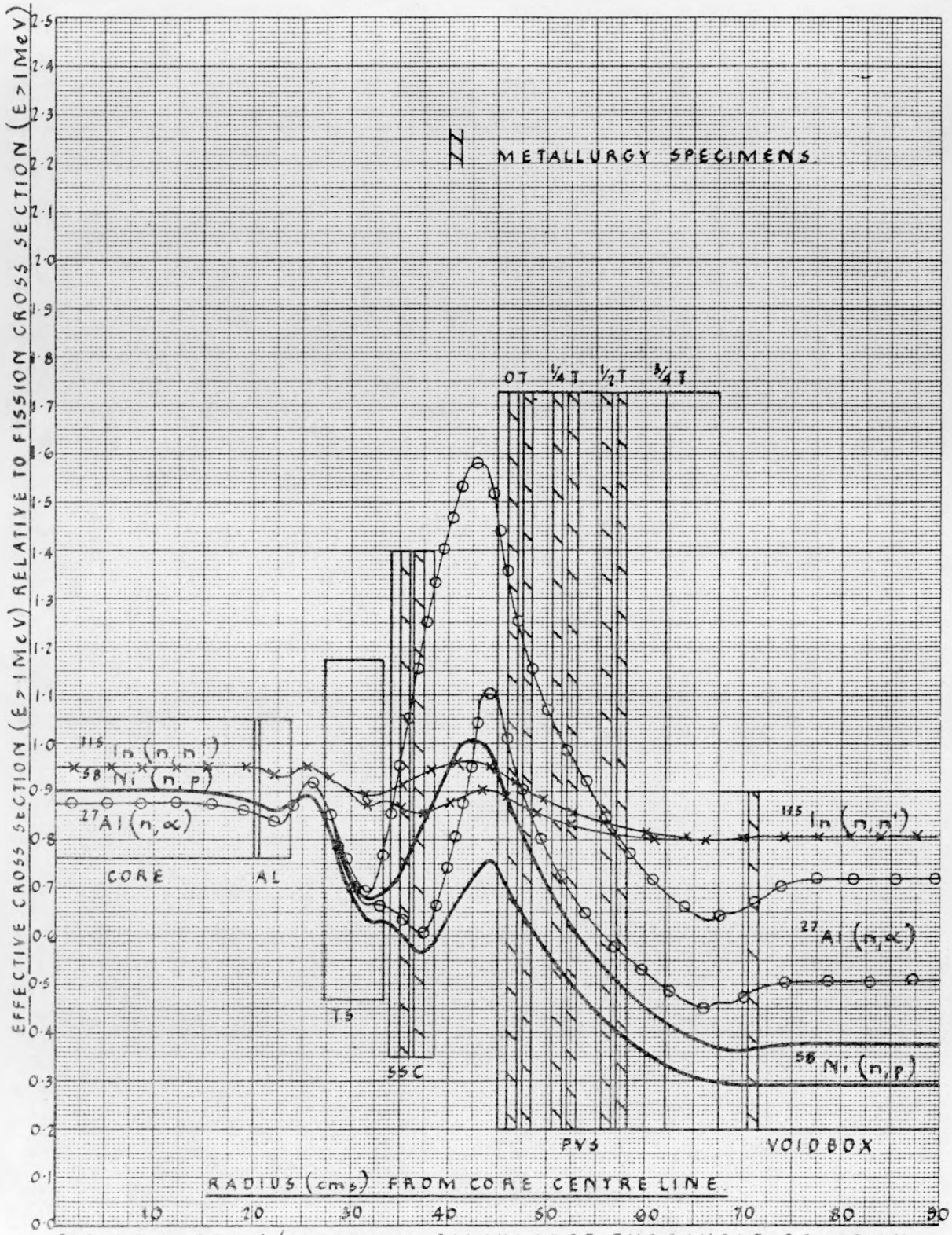

FIG. 3.2.4. P5F 4/12 ANISN CALCULATED THRESHOLD REACTION CROSS SECTIONS.

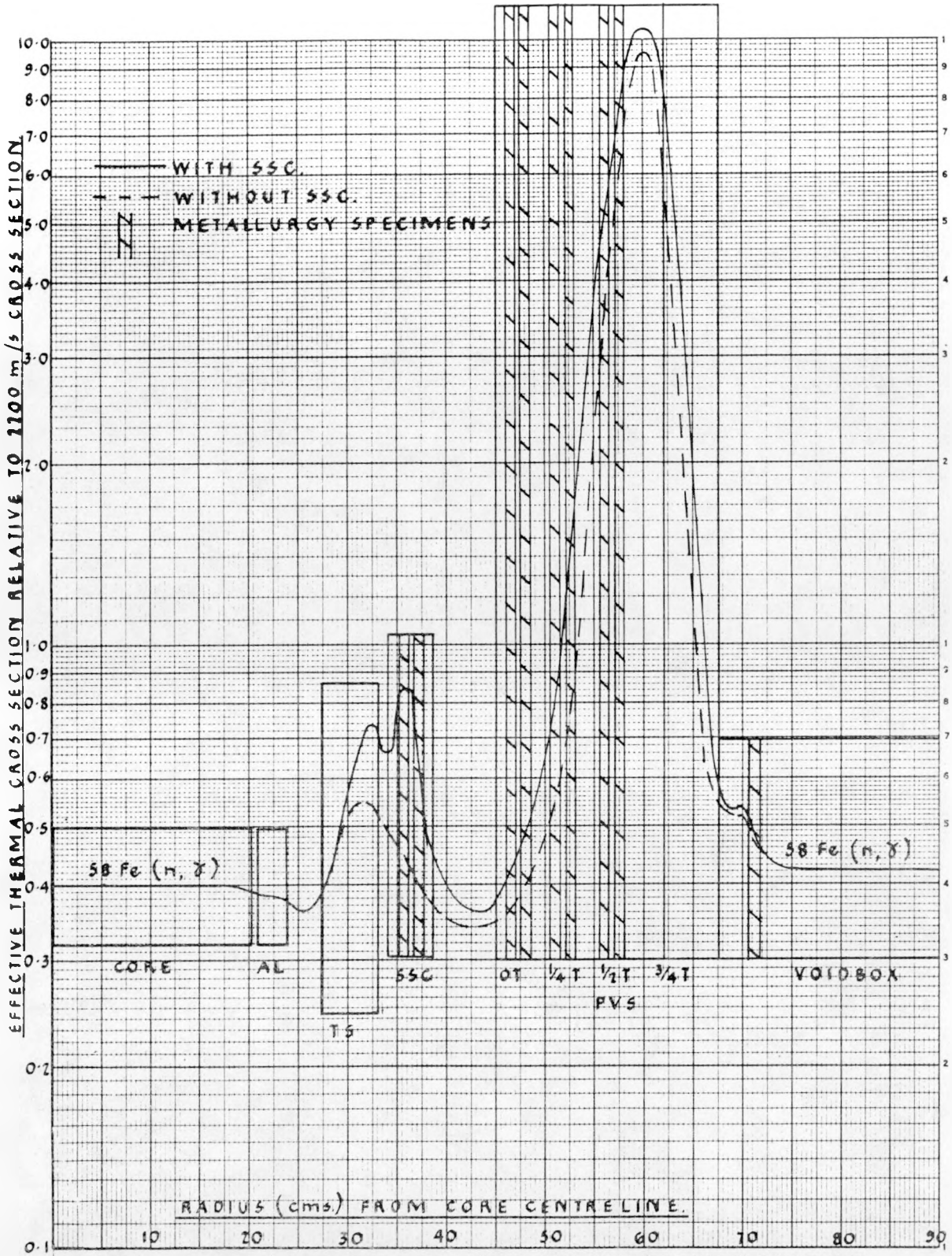

FIG. 3.2.5. PSF. 4/12 ANISN CALCULATED THERMAL REACTION CROSS SECTIONS.

TABLE 3.2.7

ANISN PSF 4/12 + SSC CALCULATION:
EFFECTIVE CROSS SECTIONS FOR RRA/AERE DOSIMETERS (IRDF82 CROSS SECTION PILE)

Reaction	SSC	PVS(0T)	PVS($\frac{1}{4}$T)	PVS($\frac{1}{2}$T)	PVS($\frac{3}{4}$T)***
$^{58}Ni(n,p)$*	85.5	94.7	75.9	60.6	49.2
$^{54}Fe(n,p)$*	63.3	70.6	55.5	43.4	34.3
$^{46}Ti(n,p)$*	8.11	10.1	7.77	5.95	4.63
$^{63}Cu(n,\alpha)$*	0.44	0.61	0.48	0.38	0.31
$^{93}Nb(n,n')$*	222.5	225.6	228.4	238.9	255.0
$^{58}Fe(n,\gamma)$**	1.4	1.06	1.87	7.99	7.74
$^{59}Co(n,\gamma)$**	64.6	38.8	94.1	501.2	473.0

* Cross sections in units of millibarns per unit of neutron flux (E>1MeV) $n.cm^{-2}.s^{-1}$.
** Cross sections in units of barns per unit of neutron flux (E<0.414 eV) $n.cm^{-2}.s^{-1}$.
*** This location relates only to the PSF "Start-Up" irradiation experiment.

TABLE 3.2.8

ANISN PSF 4/12 + SSC CALCULATION:
DISPLACEMENT CROSS SECTIONS AT SPECIMEN LOCATIONS

Reaction	SSC	PVS(0T)	PVS($\frac{1}{4}$T)	PVS($\frac{1}{2}$T)	PVS($\frac{3}{4}$T)**
Iron (ASTM E693)	1589	1630	1839	2228	2746
Aluminium in AL_2O3*	976	956	1242	1669	2267

Values quoted are dpa/second/neutron flux (E>1MeV) in units of barns.

* Sapphire damage monitor.
** This location relates only to the PSF 'Start-Up' irradiation experiment.

(ii) The rate of attenuation of atom displacement rate (dpa/second) through the PVS is significantly less than that of neutron flux (E>1MeV) ($\lambda dpa = 0.135 cm^{-1}$; $\lambda \phi = 0.2 cm^{-1}$). In addition, atom displacement damage rate in the PVS is actually enhanced in the presence of the SSC, by about 25%, although the level of neutron flux (E>1MeV) remains sensibly unaffected.

Since the displaced atom damage function has a significant response for neutrons (E<1MeV), it is clear that not only are there a large number of damaging neutrons (E<1MeV) in the PVS but also that the presence of the SSC propagates a step increase in the ratio of neutrons (E<1MeV) to neutrons (E>1MeV) in the PVS whilst the level of neutron flux (E>1MeV) reaching the PVS is unperturbed.

(iii) The attenuation of fast neutrons in water results in a hardening of the spectrum above 1 MeV, and attenuation in iron results in a softening of the spectrum above 1MeV. The effect of these phenomena on the effective cross sections of threshold detectors irradiated in the PSF is directly proportional to the effective threshold energy of the reaction considered and the depth of penetration. Thus the insertion of the SSC results in a large perturbation to a high threshold reaction cross section, e.g., $^{27}Al(n,\alpha)$, and a small perturbation to a low threshold detector cross section, e.g., $In^{115}(n,n')$.

The technological implications of these effects are:

a) that the insertion of steel shields (such as surveillance capsules and neutron pads) between the thermal shield and the pressure vessel in a given plant can result in an increased damage rate to the vessel wall, even though there may be no significant increase in neutron flux (E>1MeV).

b) the use of neutron fluence (E>1MeV) to characterise the attenuation of dose through a vessel wall results in a significant and systematic underestimation of damage with penetration when compared to atom displacement density.

c) the analysis of high threshold integrating detectors, e.g., $^{63}Cu(n,\alpha)$ used in surveillance capsules, needs to be carried out with great care since assumptions about geometry and materials when doing calculational modelling may introduce large errors in dose estimates.

Thermal Neutron Spectra

It can be seen from Figure 3.2.5 that the effective capture cross sections of thermal neutron reactions such as $^{58}Fe(n,\gamma)^{59}Fe$, throughout the PSF array, can be very sensitive to position particularly in the thermal shield, SSC and PVS. This is due to the rapid reduction in the ratio of thermal to epithermal neutron flux with penetration in iron, which may additionally be enhanced by large epithermal (n,γ) captive resonances in the detector atoms.

Thus the reaction rates of detectors such as $^{58}Fe(n,\gamma)$ and $^{59}Co(n,\gamma)$, which have resonance absorbances, will remain high despite the high attenuation rate of thermal neutrons in iron.

This will only be of technological significance if thermal neutron contribution to damage rates in materials is high (i.e., >5%).

3.2.5 Calculational Methodology - MCBEND

A Monte Carlo transport calculation using the Atomic Energy Establishment, Winfrith (AEEW) code MCBEND (Be82) version 4A was carried out on similar lines to that for the PCA (Mc83) and for the PCA replica (Au85).

Forward and adjoint diffusion theory calculations to provide importance biassing of the MCBEND calculation and to give additional information on the spatial flux variation were carried out using the 3-D code SNAP (Mc75d).

Fluxes were scored at particular regions of interest in the MCBEND calculation and converted to detector reaction rates using 620 group cross-sections derived from IRDF82 (Cu82).

Due to shortage of time and resources the calculations were only carried out using a source averaged over the SSC1 irradiation period. Two MCBEND calculations were carried out, one biased to the SSC1 location and the other biassed to the VEPCO capsule, biassing being necessary to achieve low stochastic errors at locations of interest in an economic way.

3.2.6 MCBEND PSF 4/12 Calculations

3.2.6.1 Source Data

The source distribution used originated in the VENTURE sources supplied by ORNL (the authors of Ma84b) on a tape X19802. Cycles 153B, 153C, 153D and 153F covering the SSC1 irradiation were condensed in space to the mesh used in the SNAP and MCBEND calculating; see Fig. 3.2.8. On inspection the source variation from cycle to cycle seemed to be modest, and so the 4 cycles were simply combined using the same expression as employed by ORNL for their DOT/ANISN calculations (Ma84b), the weighting factors applied being 0.142, 0.194, 0.287 and 0.202, respectively. The Watt-Cranberg fission spectrum (Table 3.2.3) was assumed for these sources. Note that the method used to weight each cycle source includes shutdown periods, and hence the results of the calculations needed to be divided by ~.82 for comparison with 30MW fluxes. In addition, the VENTURE source densities are calculated on a 3-inch (76.2mm) fuel element pitch, which corresponds to the actual fuel element size. However, the reactor pitch is 77.1 by 81.0mm, and the source densities have been carried over directly. Hence the total source in the calculation is too large by a factor of 1.076, and hence the resultant factor by which the fluxes have been multiplied to produce 30MW fluxes is 1.13.

The total source used was summed from the MCBEND output and found to be 2.01×10^{18} neutrons/sec. This factored up by 1.13 and assuming $.316 \times 10^{-10}$ Joules per fission and 2.4 neutrons per fission is equivalent to 30MW.

3.2.6.2 Materials Data

The compositions of the materials used are given in Table 3.2.9 and are based on the recommendations of ORNL (private communication) for the core regions and are largely the same as used in the ANISN calculations for the ex-core regions.

Note that the void box is assumed to be full of water based on post-irradiation examination observation. The cross-section library used in MCBEND was the AEEW 8000 group point energy library (Be82) derived from ENDF/B data.

3.2.6.3 Geometrical Representation

The geometric representation used in both MCBEND and SNAP is shown in Figs. 3.2.6 and 3.2.7, the distances given in Table 3.2.10 being taken from (Mc83d). The mesh structure is more detailed in regions of interest such as the core and experiment centre lines and the sources nearest to the experiment. The cartesian SNAP representation was used in MCBEND to save effort, geometric representation in MCBEND being in principle unrestricted. Some of the representation of components away from the axis of the experiment was approximate again to save effort. There are some small differences between this geometry and that used for the ANISN calculations.

3.2.6.4 Results

The results from MCBEND consist of fluxes scored in the top 27 groups of the 40 energy group scheme (Table 3.2.1) and the reaction rates are given in Table 3.2.11 at the locations shown in Fig. 3.2.6. The fluxes with their stochastic uncertainties are given in Table 3.2.12 where they are compared to the ANISN values, no significant trends being observed. (It should be noted that in order to reduce stochastic uncertainties the MCBEND fluxes quoted in Table 3.2.12, these are the mean of 5 scoring regions in the same XZ plane). The reaction rates given in Table 3.2.11 are also compared with the ANISN values and some HEDL experimental values and the ORNL calculated values both given in Mc83d. The fast flux (E>1MeV) calculated values are also plotted in Figs. 3.2.8 and 3.2.9.

The MCBEND results have been factored up by 1.13 as explained in Section 3.2.6.1. However, for comparison with the DOT/ANISN (ORNL) and ANISN (RRA) point values, the 'buckling' of the flux in the X and Z directions and the exponential attenuation of the flux in the Y direction over the MCBEND scoring volume need to be taken into account. Using the formula given in (St84d) the MCBEND fluxes at the SSC location need to be increased by less than 1%, and so no correction has been made. This is much smaller than the correction necessary in the original MCBEND PCA 'Blind Test' calculation (Mc81), since the scoring regions used in MCBEND for the PSF calculations were much smaller.

The measured (HEDL) values have been corrected to the centre of the MCBEND scoring regions using the same formula as used to size the MCBEND buckling correction although measurements were chosen such that this correction was usually less than 3%.

TABLE 3.2.9

MATERIAL COMPOSITION DATA FOR MCBEND PSF CALCULATION

Description	Material No.	Density g/cc	Element	Proportion By Weight
Fuel	1	1.72	Al	0.625
			O	0.296
			^{235}U	0.39E-1
			H	0.37E-1
			^{238}U	0.30E-2
Fuel 170g ^{235}U (Initially 240g)	12	1.70	Al	0.633
			O	0.300
			H	0.38E-1
			^{235}U	0.26E-1
			^{238}U	0.30E-2
Fuel 70g ^{235}U (Initially 137g)	13	1.67	Al	0.644
			O	0.305
			H	0.38E-1
			^{235}U	0.11E-1
			^{238}U	0.20E-2
In-Core Experiment	14	0.99	O	0.88
			H	0.11
			Al	0.90E-2
			^{235}U	0.10E-2

Cont....

TABLE 3.2.9 (Cont'd)

Description	Material No.	Density g/cc	Element	Proportion By Weight
Void Box (Filled with Water)	2	1.217	O	0.6993
			Fe	0.1578
			H	0.874E-1
			Cr	0.384E-1
			Ni	0.171E-1
RPV Simulator	4	7.87	Fe	1.0
Thermal Shield	3	7.93	Fe	0.74
			Cr	0.18
			Ni	0.08
Be Reflector	7	1.85	Be	1.0
Al Window + Water Gap	6	2.54	Al	0.9638
			O	0.323E-1
			H	0.39E-2
Water	5	0.99	O	0.89
			H	0.11
SSC	8	7.87	Fe	1.0
Unfueled Core Regions	9	1.741	Al	0.66583
			O	0.2967
			H	0.375E-1
Base	10	As Thermal Shield		
VEPCO Capsule	11	7.8	Fe	1.0

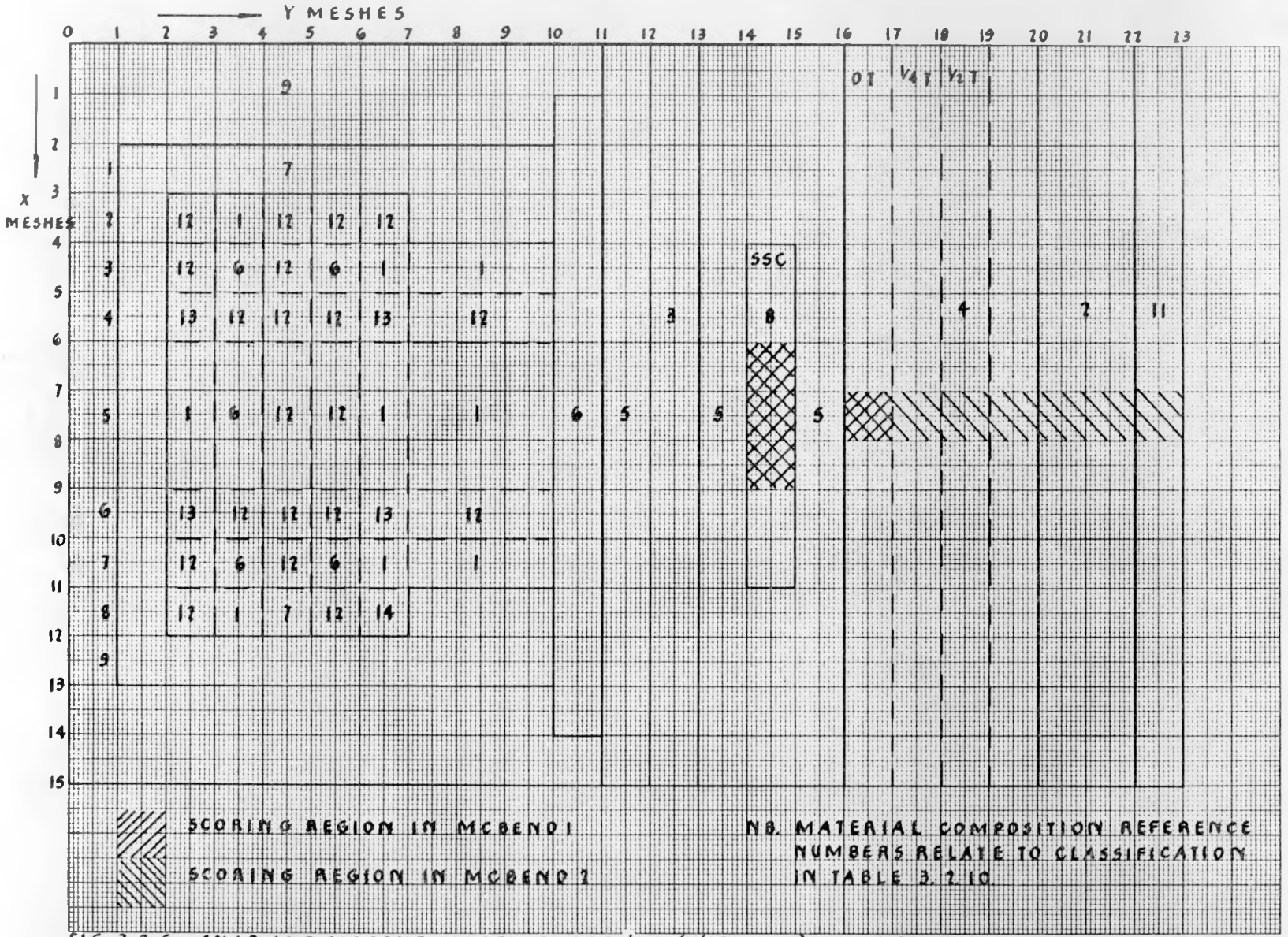

FIG. 3.2.6 SNAP AND MCBEND MODEL OF ORR/PSF(4/12+SSC) IN XY PLANE.

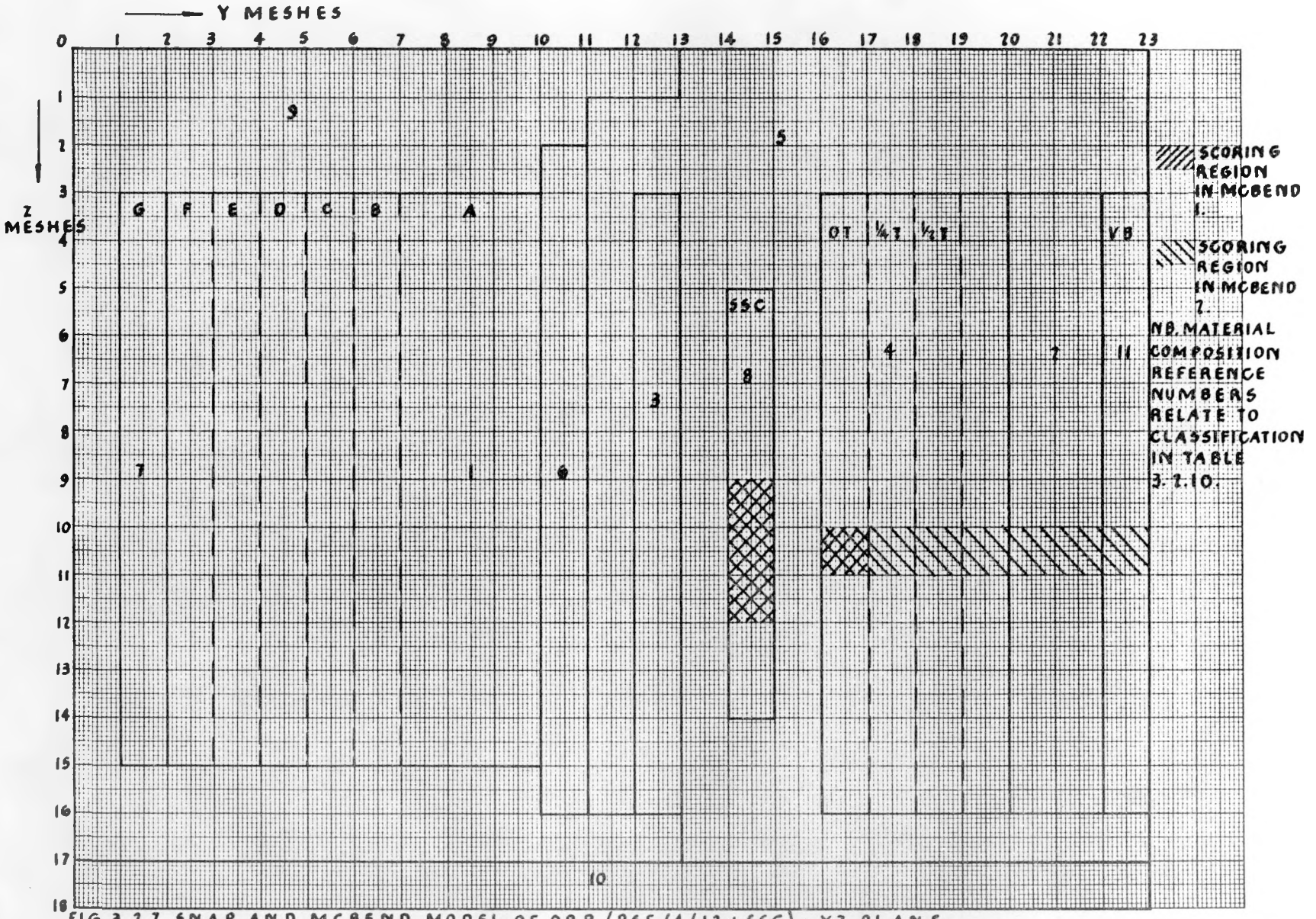

FIG. 3.2.7 SNAP AND MCBEND MODEL OF ORR/PSF (4/12+SSC) - YZ PLANE.

TABLE 3.2.10a)

PSF (4/12 + SSC) MCBEND AND SNAP MODEL DIMENSIONS ALONG 'X' AXIS

MESH INTERSECTION	MESH INTERVAL	DESCRIPTION	MESH SIZE (cm)	DISTANCE FROM ORIGIN (cm)	COMMENTS
0				0.0	
	1		11.0		Arbitrary reflector region
1				11.0	
	2		11.025		
2		Edge of core		22.025	
	3	Reflector block (column 1)	7.71		
3				29.735	
	4	Fuel (column 2)	7.71		
4				37.445	36.4 is edge of SSC
	5	Fuel (column 3)	7.71		
5				45.155	
	6	Fuel (column 4)	7.71		
6				52.865	
	7	Fuel (column 5)	2.57		
7				55.435	
	8	Fuel (column 5)	2.57		Mid-core 56.72
8		Fuel (column 5)		58.005	
	9	Fuel (column 5)	2.57		
9				60.575	
	10	Fuel (column 6)	7.71		
10				68.285	
	11	Fuel (column 7)	7.71		
11				75.995	77.04 is edge of SSC
	12	Fuel (column 8)	7.71		
12				83.705	
	13	Reflector (column 9)	7.71		
13		Edge of core		91.415	
	14		11.025		
14				102.44	
	15		11.0		
15				113.44	

TABLE 3.2.10b)

PSF (4/12 + SSC) MCBEND AND SNAP MODEL DIMENSIONS ALONG 'Y' AXIS

MESH INTERSECTION	MESH INTERNAL	DESCRIPTION	MESH SIZE (cm)	DISTANCE FROM ORIGIN (cm)	COMMENTS
0		Picture edge		0.0	
	1	Arbitrary structure	8.1		
1				8.1	
	2	Be reflector (Row G)	8.1		
2				16.2	
	3	Fuel elements (Row F)	8.1		
3				24.3	
	4	Fuel elements (Row E)	8.1		
4				32.4	
	5	Fuel elements (Row D)	8.1		
5				40.5	
	6	Fuel elements (Row C)	8.1		
6				48.6	
	7	Fuel elements (Row B)	8.1		
7				56.7	
	8	Fuel elements (Row A)	2.7		Row A subdivided
8				59.4	
	9	Fuel elements (Row A)	2.7		
9				62.1	
	10	Fuel elements (Row A)	2.7		
10				64.8	
	11	Al window + water gap	2.8		Water is between core + Al window
11				67.6	
	12	Water gap	4.0		
12				71.6	
	13	Thermal shield	6.0		
13				77.6	
	14	Water gap	0.8		
14				78.4	
	15	Surveillance capsule	5.0		
15				83.4	

Contd...

TABLE 3.2.10b) (Cont'd)

MESH INTERSECTION	MESH INTERVAL	DESCRIPTION	MESH SIZE (cm)	DISTANCE FROM ORIGIN (cm)	COMMENTS
	16	Water gap	6.2		
16		Edge of PVS		89.6	
	17	O/T specimens	4.26		
17				93.86	
	18	1/4 T specimens	4.76		
18				98.62	
	19	1/2 T specimens	5.52		
19				104.14	
	20		7.94		
20		Edge of PVS		112.08	
	21	Void box	15.28		
21		Centre void box		127.36	
	22	Void box	15.28		Water gap between void box & capsule
22		Edge of VEPCO capsule		142.64	incorporated into void box
	23	VEPCO capsule	3.59		
23		Edge of VEPCO capsule		146.23	

TABLE 3.2.10c)

PSF (4/12 + SSC) MCBEND AND SNAP MODEL DIMENSIONS ALONG 'Z' AXIS

MESH INTERSECTION	MESH INTERVAL	DESCRIPTION	MESH SIZE (cm)	DISTANCE FROM ORIGIN (cm)	COMMENTS
0				0	
	1	Region above core	10.0		Arbitrary but based
1				10.00	on VENTURE mesh
	2		9.05		
2				19.05	
	3		3.81		
3		Top of fuel, PVS, VB,TS		22.86	VENTURE
	4		7.62		
4				30.48	VENTURE
	5		11.11		
5		Top of surveill-		41.59	
	6	ance capsule	4.13		
6				45.72	VENTURE
	7		7.62		

Contd...

TABLE 3.2.10c) (Cont'd)

MESH INTERSECTION	MESH INTERVAL	DESCRIPTION	MESH SIZE (cm)	DISTANCE FROM ORIGIN (cm)	COMMENTS
7				53.34	VENTURE mesh 18
	8		2.54		
8				55.88	VENTURE mesh 19
	9		2.54		Core C/L 57.15 cm
9				58.42	VENTURE mesh 20
	10		2.54		
10				60.96	VENTURE mesh 21
	11		2.54		Experiment C/L 62.23 cm
11				63.50	VENTURE mesh 22
	12		5.08		
12				68.58	VENTURE mesh 24
	13		5.08		
13				73.66	VENTURE mesh 26
	14		7.30		
14		Bottom of surveill-		80.96	
	15	ance capsule	2.86		
15		Bottom of fuel (normal)		83.82	VENTURE mesh 30
	16		7.62		
16		Bottom of PVS, VB, TS		91.44	VENTURE mesh 33
	17		2.54		
17		Bottom of fuel (abnormal)		93.98	VENTURE mesh 34
	18		12.7		
18				106.68	VENTURE mesh 36

TABLE 3.2.11

PSF (4/12 + SSC) MCBEND CALCULATED VALUES OF REACTION RATES AND FLUXES (AT 30 MW)

DATA SOURCE	LOCATION	$^{63}Cu(n,\alpha)$	$^{46}Ti(n,p)$	$^{54}Fe(n,p)$	$^{58}Ni(n,p)$	$^{238}U(n,f)$	$^{237}Np(n,f)$	$^{93}Nb(n,n')$	DPA(ASTM)	Flux E>1.0MeV	Flux E>0.1MeV
MCBEND1(RRA)		-	3.82E-14	3.24E-13	4.45E-13	2.01E-12	1.49E-11	1.26E-12	8.77E-9	5.62E+12	1.76E+13
1σ Error		-	±24.2%	±10.3%	±9.5%	±5.6%	±3.5%	±4.4%	±3.5%	±4.6%	±2.7%
MCBEND2(RRA)		2.75E-15	4.97E-14	4.00E-13	5.39E-13	2.33E-12	1.70E-11	1.42E-12	9.56E-9	6.32E+12	2.04E+13
1σ Error	SSC1	±16.5%	±10.1%	±6.6%	±6.3%	±6.7%	±6.1%	±5.7%	±6.8%	±6.7%	±13.2%
ANISN(RRA)		3.08E-15	5.68E-14	4.43E-13	6.17E-13	2.43E-12	1.87E-11	1.18E-12	1.11E-8	6.95E+12	2.10E+13
DOT(ORNL)		2.66E-15	4.93E-14	3.89E-13	5.24E-13	2.11E-12	1.68E-11	-	9.37E-9	6.11E+12	1.90E+13
EXPTL(HEDL)		2.95E-15	5.83E-14	4.33E-13	6.23E-13	2.65E-12	1.94E-11	-	-	-	-
MCBEND2 EXPTL		.93	.85	.92	.87	.88	.88	-	-	-	-
MCBEND2(RRA)		5.54E-16	7.21E-15	4.98E-14	6.74E-14	2.88E-13	1.91E-12	1.70E-13	1.21E-9	7.47E+11	2.04E+12
1σ Error	PVS	±26.1%	±16.1%	±9.3%	±8.8%	±7.8%	±6.5%	±6.9%	±8.3%	±7.6%	±8.3%
DOT(ORNL)	(OT)	4.77E-16	7.97E-15	5.47E-14	7.32E-14	2.70E-13	1.94E-12	-	1.16E-9	7.44E+11	2.32E+12
MCBEND2(RRA)		1.13E-16	2.72E-15	2.11E-14	2.91E-14	1.37E-13	1.18E-12	8.99E-14	6.87E-10	3.79E+11	1.58E+12
1σ Error	PVS	±25.0%	±15.4%	±8.4%	±7.8%	±6.9%	±5.2%	±5.5%	±5.3%	±6.5%	±7.2%
ANISN(RRA)	(¼T)	2.14E-16	3.47E-15	2.48E-14	3.49E-14	-	-	8.28E-14	8.04E-10	4.37E+11	-
DOT(ORNL)		2.02E-16	3.28E-15	2.31E-14	3.14E-14	1.30E-13	1.21E-12	-	7.12E-10	4.01E+11	1.67E+12
MCBEND2(RRA)		6.97E-17	1.15E-15	9.07E-15	1.27E-14	6.31E-14	6.71E-13	4.02E-14	4.03E-10	1.91E+11	1.02E+12
1σ Error	PVS	±24.7%	±14.6%	±8.2%	±7.5%	±5.8%	±5.9%	±4.7%	±5.0%	±6.0%	±6.5%
ANISN(RRA)	(¼T)	7.66E-17	1.20E-15	8.75E-15	1.27E-14	-	-	4.41E-14	4.43E-10	1.99E+11	-

TABLE 3.2.12

CALCULATED SPECTRUM AT THE SSC-1 LOCATION IN THE PSF 4/12 ARRAY

ENERGY GROUP	ANISN	MCBEND1 (±1σ)	ANISN/ MCBEND1	MCBEND2 (± 1σ)	ANISN/ MCBEND2
1	5.00E-5	-	-	-	-
2	2.70E-4	-	-	-	-
3	9.40E-4	2.40E-4 (38%)	3.9	9.00E-4(32%)	1.04
4	1.55E-3	1.54E-3 (36%)	1.01	1.20E-3(24%)	1.29
5	1.68E-3	1.72E-3 (64%)	0.98	1.40E-3(26%)	1.20
6	3.71E-3	2.10E-3 (47%)	1.77	3.30E-3(19%)	1.12
7	3.25E-3	3.02E-3 (31%)	1.08	3.70E-3(16%)	0.88
8	4.18E-3	5.30E-3 (30%)	0.79	5.40E-3(12%)	0.77
9	4.89E-3	5.21E-3 (15%)	0.94	3.70E-3(14%)	1.32
10	5.23E-3	4.15E-3 (18%)	1.26	5.50E-3(12%)	0.95
11	6.32E-3	5.18E-3 (34%)	1.22	5.30E-3(25%)	1.19
12	8.58E-3	8.36E-3 (23%)	1.03	8.90E-3(29%)	0.96
13	1.11E-2	1.19E-2 (9%)	0.93	1.05E-2(16%)	1.06
14	1.29E-2	1.39E-2 (21%)	0.93	1.20E-2(29%)	1.08
15	8.58E-3	9.54E-3 (29%)	0.90	7.90E-3(22%)	1.09
16	2.48E-2	2.56E-2 (10%)	0.97	2.65E-2(9%)	0.94
17	1.76E-2	1.71E-2 (14%)	1.03	2.14E-2(11%)	0.82
18	2.15E-2	2.17E-2 (16%)	0.99	2.77E-2(13%)	0.78
19	1.98E-2	2.46E-2 (10%)	0.80	2.66E-2(15%)	0.74
20	2.38E-2	2.13E-2 (8%)	1.12	3.21E-2(12%)	0.74
21	8.09E-2	6.51E-2 (8%)	1.24	6.97E-2(11%)	1.16
22	8.20E-2	7.86E-2 (5%)	1.04	8.10E-2(7%)	1.01
23	1.13E-1	1.09E-1 (3%)	1.04	1.30E-1(19%)	0.87
24	1.96E-1	2.09E-1 (3%)	0.94	1.75E-1(20%)	1.12
25	1.26E-1	1.32E-1 (4%)	0.95	1.22E-1(40%)	1.03
26	1.16E-1	1.26E-1 (4%)	0.92	-	-
27	1.06E-1	9.78E-2 (4%)	1.08	-	-

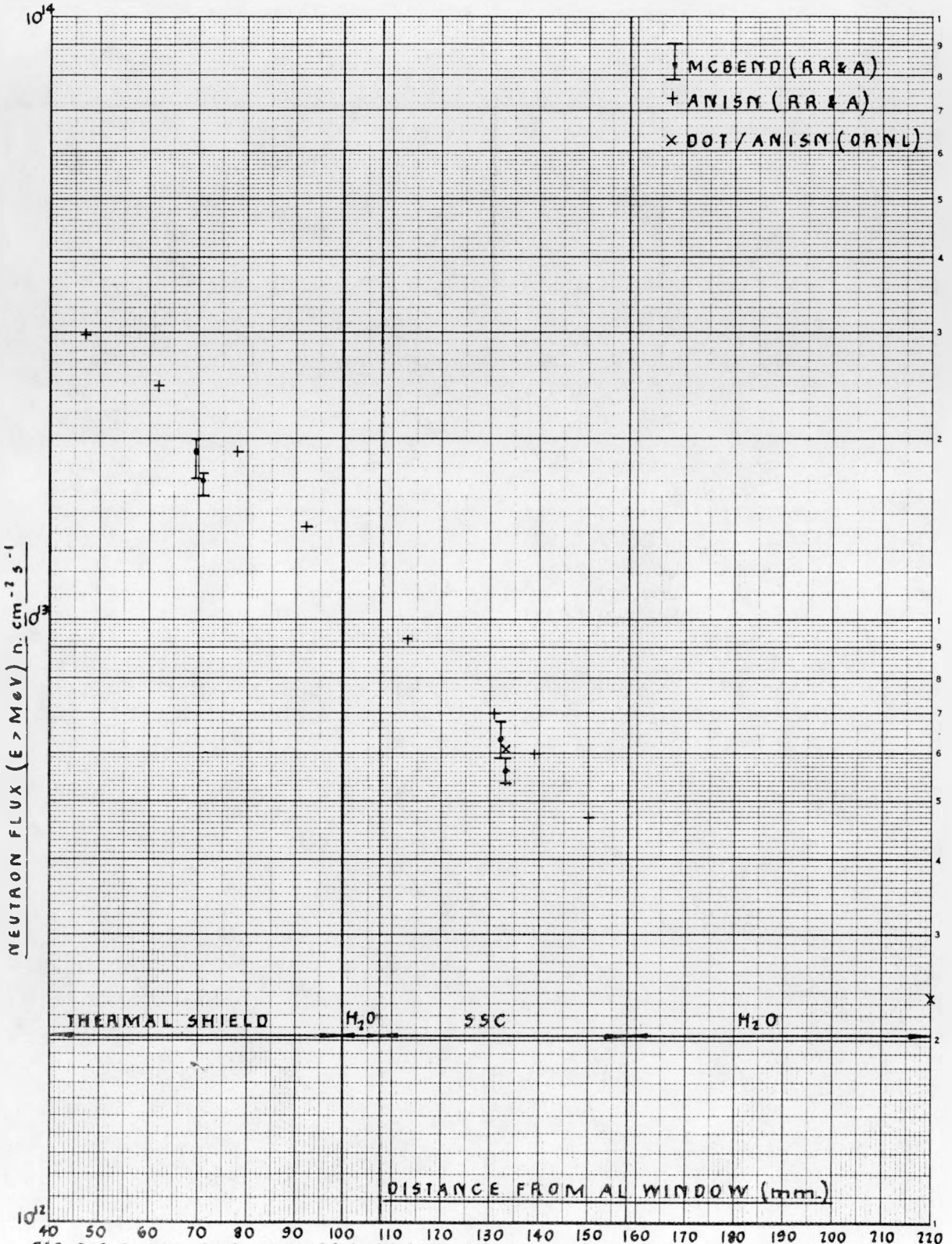

FIG. 3.7.8. COMPARISON OF MCBEND CALCULATED FLUXES (E > 1 MeV) IN THE SSC OF THE PSF 4/12 + SSC ARRAY WITH OTHER CALCULATED VALUES.

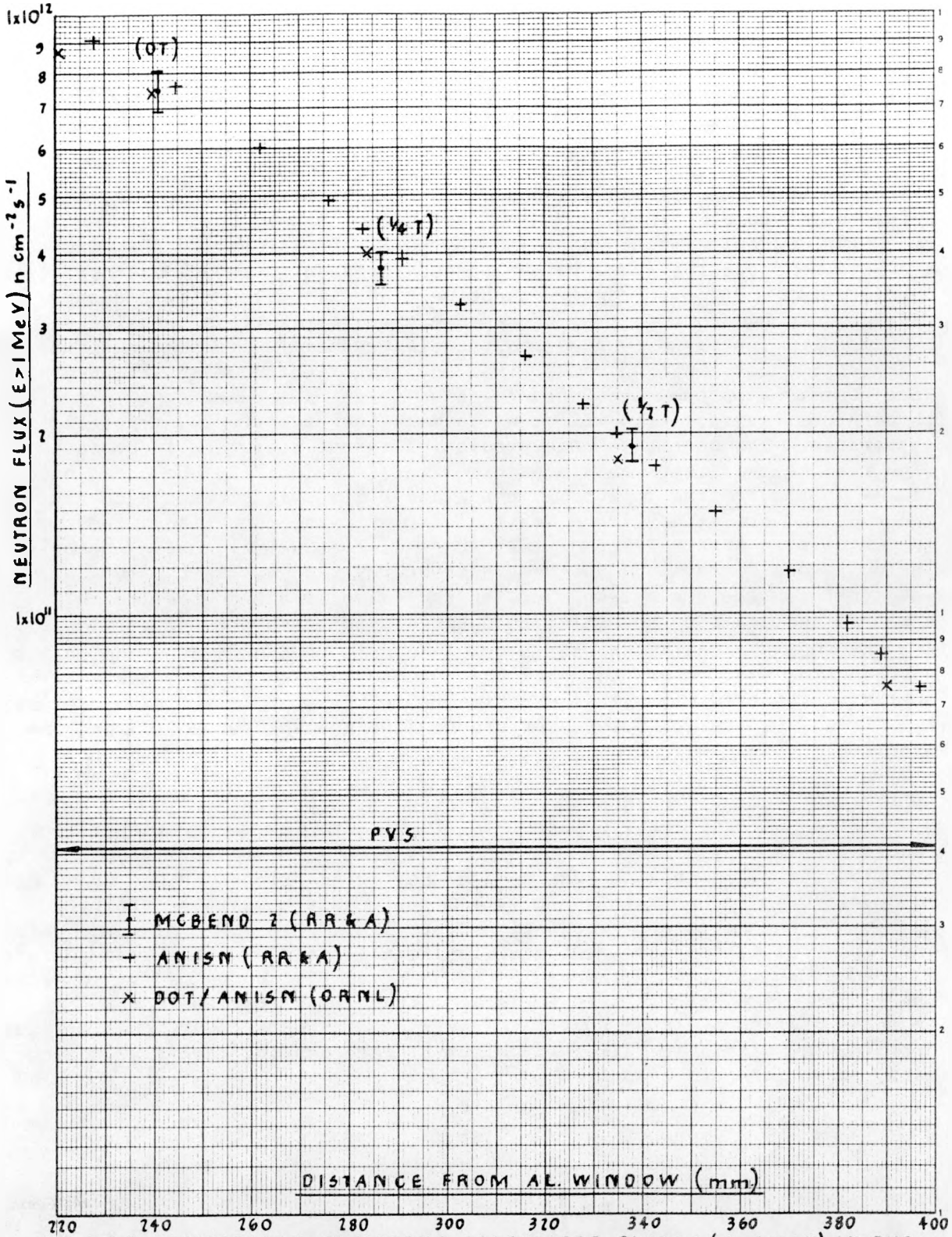

FIG. 3.2.9. COMPARISON OF MCBEND CALCULATED FLUXES (E>1MeV) IN THE PV5. OF THE PSF.4/12+55C ARRAY WITH OTHER CALCULATED VALUES.

The spectral indices for a variety of reaction rates are tabulated in Table 3.2.13 using the same formula as that described in Section 3.2.3.2 and these are shown for both the MCBEND and ANISN calculations of the PSF 4/12 SSC1 irradiation as well as HEDL experimental data.

3.2.6.5 Discussion

Overall MCBEND calculated values agree well with other SSC1 calculated data, but systematically underpredict the SSC1 measurements. However the two MCBEND calculations (one biased to the SSC positions and the other to the void box position) show rather modest agreement with one another at the SSC location. Since the agreement between the two calculations changed from good to bad to better as the stochastic errors were successively reduced with increased running time, the discrepancy is attributed to the stochastic uncertainties, rather than any trend introduced by the biassing. Note that most of the calculated reaction rates will be strongly correlated through the fluxes, which will tend to make any under (or over) predictions systematic. The degree of underprediction is not, therefore, inconsistent with the achieved level of stochastic error (7%-15%). On the other hand, fluxes in the scoring regions in the X and Z directions (though not in the Y direction) are likely to be weakly correlated; and comparisons made over larger volumes (Table 3.2.13) indicate that the SSC1 fluxes in the calculation biased to the SSC, in the higher energy groups, are too low. Nevertheless, the consistency between the calculated and experimental spectral indices for the SSC1 irradiation is remarkably good, particularly for the MCBEND calculation, so it is reasonable to assume that the calculated neutron flux spectra are suitably accurate to be used for the dosimetry analysis of the metallurgical experiments in terms of damage exposure units [i.e., fluence (E>1MeV, E>0.1MeV)] or atomic displacement rates (i.e., dpa in iron).

Further analysis of the MCBEND calculations at other points in the PSF array (i.e., SSC2 and the PVS locations) is hindered by the fact that time and resources only allowed a MCBEND calculation with the core source distribution that obtained during the SSC1 irradiations. Since the ORNL calculations used explicitly the actual source distributions obtaining during all the different irradiation histories and the HEDL measured data obviously relate to those histories implicitly, only an approximate assessment of the MCBEND calculated values in the SSC2 and PVS can be made. Nevertheless, the evidence from the data in Table 3.2.11 suggests that the MCBEND estimates in these regions are good to within their associated stochastic error and certainly to within the likely total error (stochastic, geometry, nuclear data, modelling, etc. errors).

TABLE 3.2.13

ANISN AND MCBEND PSF 4/12 + SSC CALCULATIONS:
COMPARISON OF MEASURED AND CALCULATED SPECTRAL INDICES AT SSC-1

Calculation Method	Spectral Index	Measured (HEDL Data)	Calculated	C/M
ANISN	$^{46}Ti(n,p)/^{237}Np(n,f)$	3.01E-3	3.04E-3	1.01
MCBEND2	"	"	2.92E-3	0.97
ANISN	$^{58}Ni(n,p)/^{237}Np(n,f)$	3.21E-2	3.30E-2	1.03
MCBEND2	"	"	3.17E-2	0.99
ANISN	$^{46}Ti(n,p)/^{58}Ni(n,p)$	9.37E-2	9.21E-2	0.99
MCBEND2	"	"	9.22E-2	0.99
ANISN	$^{238}U(n,f)/^{237}Np(n,f)$	1.36E-1	1.30E-1	0.96
MCBEND2	"	"	1.37E-1	1.01
ANISN	$^{58}Ni(n,p)/^{238}U(n,f)$	2.35E-1	2.54E-1	1.08
MCBEND2	"	"	2.32E-1	0.99
ANISN	$^{46}Ti(n,p)/^{238}U(n,f)$	2.20E-2	2.36E-2	1.07
MCBEND2	"	"	2.13E-2	0.97

3.2.7 Overall Discussion and Conclusions

Overall the results obtained by both the ANISN and MCBEND calculations achieved two of their three main objectives: to provide (a) accurate neutron spectra for the analysis of dosimetry measurements made on the metallurgical PSF 4/12 irradiations and (b) scoping values of reaction rates and neutron fluxes throughout the experimental array. The underprediction by ~10% of reaction rates using the MCBEND technique was, however, something of a disappointment, given the success of the recent reanalysis of the PCA 12/13 'Blind Test' using the same technique (Au85). Nevertheless, these results were not inconsistent with the level of stochastic uncertainty achieved, which was necessarily limited by economic considerations. In that sense the MCBEND technique does provide more realistic and reliable estimates of reaction rates and fluxes than can be achieved by purely deterministic (i.e., ANISN and DOT) transport calculations whose uncertainty is entirely unquantified and where good agreement can often only be achieved after a judicious amount of 'a priori' benchmarking and 'ad hoc' synthesis. However, it is finally worth pointing out that recent experience in running Monte Carlo physics codes on dedicated micro-computers at RR&A has shown that such calculations can be made much more cheaply and hence more competitively with deterministic calculations than the work reported here.

4.0 COMPARISON AND EVALUATION OF EXPERIMENTAL DOSIMETRY MEASUREMENTS AND DERIVED EXPOSURE PARAMETER RESULTS

W. N. McElroy (HEDL)

The comparison and evaluation of experimental dosimetry measurements and derived exposure parameter values by HEDL, ORNL, RR&A, CEN/SCK, and KFA are considered in Sections 4.1 through 4.5.

HEDL-ORNL recommended-consensus physics-dosimetry data and data bases for the metallurgical specimens for the SSC and SPVC experiments have been established and are discussed in Sections 4.1 and 4.2 and in Appendices A through D. In addition to these HEDL-ORNL results, other LWR-PV-SDIP participants have established their own evaluated data bases related to their use of data and/or analyses for Parts I, II, and III of the PSF Blind Test. The reader is referred to Section S.0 and Appendix A of NUREG/CR-3320, Volume 1 for more detailed information. Appendix B of the present report also provides information on the HEDL analysis and derivation of exposure parameter values for the SVBC experiment.

4.1 CONSISTENCY OF EXPERIMENTAL DATA AND DERIVED EXPOSURE PARAMETERS - HEDL

W. N. McElroy, E. P. Lippincott,* R. L. Simons, and L. S. Kellogg (HEDL)

The reader is referred to Appendices A through C for complete documentation and HEDL comments on 1) the consistency of the PSF experimental dosimetry data, 2) a discussion of the FERRET-SAND II least-squares adjustment code procedures and 3) the HEDL derived exposure parameter values and their uncertainties for the PSF-SSC, -SPVC, and -SVBC experiments. The results, detailed comparisons, and evaluations of the HEDL and ORNL derived exposure parameter values are provided in Section 4.2 and Appendix C.

*Westinghouse Nuclear Energy Systems.

4.2 CONSISTENCY OF EXPERIMENTAL DATA AND DERIVED EXPOSURE PARAMETERS - HEDL-ORNL

F. W. Stallmann (ORNL), E. P. Lippincott, R. L. Simons, and W. N. McElroy (HEDL)

Extensive analyses of the PSF physics-dosimetry followed by neutron spectrum adjustment procedures have been performed at HEDL and ORNL. Details of the ORNL analysis are published in (St84). A preliminary HEDL analysis is published in (Gu84d) was distributed as a private HEDL communication to the Blind Test Participants on May 21, 1984 (see Appendix C: HEDL Recommended Exposure Parameter Values for the PSF Blind Test).

The preliminary ORNL data, which were also used in (St84b), have been revised slightly in the final version (St84) (see Appendix D: ORNL Recommended Exposure Parameter Values for the PSF Blind Test). The main difference to the older version was the addition of 18 energy groups below 0.1 MeV taken from a one-dimensional ANISN calculation [see (St84) and Section 2.1 of NUREG/CR-3320, Vol. 1]. The main differences between the HEDL and ORNL evaluations are the following (listed roughly in order of importance):

1. $^{238}U(n,f)$ results corrected for ^{239}Pu production were used in the HEDL analysis but were discarded in the ORNL analysis.

2. The input spectrum used by HEDL was the calculation for the PSF Startup Experiment (Ma84a) whereas ORNL used the two-year PSF calculation augmented by a one-dimensional ANISN calculation for energies between 0.1 MeV and 0.4 eV (see Section 2.1 of NUREG/CR-3320, Vol. 1).

3. The ORNL fluence covariances were obtained from calculation by R. E. Maerker using the LEPRICON methodology (Ma85a). The HEDL fluence covariances are part of the FERRET code.

4. The LSL-M2 code (St84a) used by ORNL simultaneously adjusts the spectra at several positions. In the HEDL evaluation, dosimetry measurements at different locations were transferred to the center of the capsules using gradient corrections.

A comparison between HEDL and ORNL results at the capsule centers is given in Table 4.2.1. There is a consistent difference of about 5% between the HEDL and ORNL calculations for fluence (E > 1.0 MeV), which is due to the added $^{238}U(n,f)$ data in the HEDL calculation. This difference is not inconsistent with the stated uncertainties and is of little consequence for the damage correlation between fluence and steel embrittlement. There is no significant difference between HEDL and ORNL in the fluence (E > 1.0 MeV). The differences are only slightly larger for dpa. These differences in dpa may come from differences in the adjusted spectra for energies below 0.1 MeV. The thermal

TABLE 4.2.1

DAMAGE EXPOSURE PARAMETER VALUES AT CAPSULE CENTERS.
HEDL AND ORNL EVALUATIONS

Location	HEDL	Percent Standard Deviation	ORNL	Percent Standard Deviation	HEDL / ORNL
		$\phi t > 1.0$ MeV (10^{19} n/cm^2)			
SSC-1	2.62	6	2.50	5	1.048
SSC-2	5.59	7	5.34	5	1.047
0-T	4.21	7	3.92	5	1.074
1/4-T	2.25	7	2.14	5	1.051
1/2-T	1.08	7	1.02	5	1.059
		$\phi t > 0.1$ MeV (10^{19} n/cm^2)			
SSC-1	7.59	12	7.60	6	0.999
SSC-2	16.50	12	16.50	6	1.000
0-T	12.50	12	12.10	6	1.033
1/4-T	8.90	12	8.82	6	1.009
1/2-T	5.76	12	5.73	6	1.005
		dpa			
SSC-1	0.0391	7	0.0400	5	0.978
SSC-2	0.0842	7	0.0858	5	0.981
0-T	0.0651	7	0.0645	5	1.009
1/4-T	0.0393	8	0.0404	5	0.973
1/2-T	0.0223	9	0.0233	5	0.957
		ϕt - thermal (10^{19} n/cm^2)			
SSC-1	1.22	16	1.26	7	0.968
SSC-2	2.46	16	2.79	7	0.882
0-T	7.06	16	6.29	8	1.122
1/4-T	0.566	16	0.84	8	0.674
1/2-T	0.114	16	0.27	8	0.422

fluences show the largest differences, which is not surprising since many perturbations in this energy range complicate the evaluation and the neutron transport calculations do not go below 0.4 eV. The quoted uncertainties do not take into account all of these possible sources of error and are, obviously, inconsistent with the large differences in Table 4.2.1.

The extension of damage fluences from the capsule center to the location of the metallurgical specimen is documented for the ORNL evaluation in (St84). The HEDL evaluation used similar procedures with hand-drawn curves instead of computer fits for the determination of gradients. Data for direct comparison between HEDL and ORNL gradients are not available, but differences appear to be insignificant.

Tables 4.2.2 through 4.2.4 list the damage exposure parameter values of the ORNL evaluations at the specimen locations. These data are identical to those published in (St84), suitably rearranged. HEDL data can be obtained by multiplying the ORNL data with the respective conversion factors from Table 4.2.1 (disregarding possible differences in gradients between HEDL and ORNL). An average can be obtained by taking the square root of the conversion factors. It did not seem worthwhile to calculate and tabulate these values explicitly since the differences are small and well within the stated uncertainties.

Assuming that the gradients obtained from the cosine-exponential fit to the spatial data represent the actual spatial distribution to ±5%, the total uncertainties in percent standard deviation of the data in Tables 4.2.2 through 4.2.4 is estimated as follows:

Fluence (E > 1.0 MeV) - 7.4%
Fluence (E > 0.1 MeV) - 7.8%
dpa - 7.4%

The HEDL analysis, however, indicates that these uncertainty estimates may not all be conservative (see Appendix C for further discussion).

TABLE 4.2.2

ORNL DAMAGE EXPOSURE PARAMETER VALUES AT CHARPY LOCATIONS

ID No.	$\phi t > 1.0$ MeV (10^{19} n/cm^2)	$\phi t > 0.1$ MeV (10^{19} n/cm^2)	dpa (10^{-2})
	A302-B Plate		
SSC-1 Capsule			
F23-1	2.548	7.354	3.974
F23-8	2.579	7.463	4.028
F23-25	2.588	7.493	4.042
F23-45	2.591	7.508	4.049
F23-77	2.584	7.488	4.037
F23-84	2.572	7.454	4.019
F23-91	2.535	7.337	3.959
F23-138	2.509	7.255	3.917
F23-11	2.608	7.515	4.062
F32-18	2.640	7.627	4.117
F23-50	2.649	7.658	4.132
F23-70	2.652	7.673	4.138
F32-102	2.644	7.653	4.127
F23-116	2.595	7.499	4.046
F23-163	2.568	7.415	4.003
F23-170	2.537	7.315	3.952
Maximum	2.65	7.67	4.14
Average	2.59	7.48	4.04
Minimum	2.51	7.26	3.92
SSC-2 Capsule			
F23-22	5.607	16.380	8.777
F23-42	5.638	16.490	8.829
F23-74	5.658	16.560	8.862
F23-81	5.661	16.570	8.869
F23-88	5.645	16.520	8.843
F23-142	5.527	16.140	8.647
F23-76	5.464	15.940	8.544
F23-15	5.181	15.130	8.114
F23-47	5.274	15.440	8.267
F23-67	5.303	15.540	8.316
F23-99	5.322	15.600	8.347
F23-106	5.325	15.620	8.353
F23-113	5.310	15.570	8.328
F23-120	5.247	15.360	8.224
F23-167	5.199	15.210	8.144
F23-101	5.140	15.020	8.047
Maximum	5.66	16.57	8.87
Average	5.41	15.82	8.47
Minimum	5.14	15.02	8.05

TABLE 4.2.2 (Cont'd)

ID No.	$\phi t > 1.0$ MeV (10^{19} n/cm^2)	$\phi t > 0.1$ MeV (10^{19} n/cm^2)	dpa (10^{-2})
Wall No. 1, 0-T			
F23-2	3.800	10.890	6.054
F23-9	3.842	11.030	6.127
F23-39	3.853	11.070	6.148
F23-71	3.859	11.090	6.158
F23-78	3.853	11.070	6.147
F23-85	3.841	11.030	6.126
F23-139	3.768	10.780	5.999
F23-7	3.732	10.660	5.936
F23-12	3.642	10.460	5.810
F23-19	3.682	10.600	5.881
F23-64	3.693	10.640	5.901
F23-96	3.699	10.660	5.911
F23-103	3.693	10.630	5.900
F23-110	3.681	10.590	5.880
F23-117	3.640	10.450	5.808
F23-164	3.612	10.360	5.758
F23-17	3.577	10.240	5.697
Maximum	3.86	11.09	6.16
Average	3.73	10.72	5.96
Minimum	3.58	10.24	5.70
Wall No. 2, 1/4-T			
F23-3	2.203	8.385	3.970
F23-10	2.221	8.479	4.009
F23-40	2.226	8.502	4.019
F23-72	2.227	8.511	4.022
F23-79	2.220	8.482	4.009
F23-86	2.212	8.444	3.992
F23-93	2.186	8.323	3.939
F23-140	2.168	8.240	3.902
F23-24	2.147	8.141	3.859
F23-13	2.096	8.007	3.785
F23-20	2.114	8.096	3.823
F32-65	2.118	8.119	3.832
F23-97	2.119	8.127	3.835
F23-104	2.112	8.099	3.822
F23-118	2.080	7.948	3.755
F23-165	2.063	7.868	3.720
F23-49	2.043	7.774	3.679
Maximum	2.23	8.51	4.02
Average	2.15	8.21	3.88
Minimum	2.04	7.77	3.68
Wall No. 3, 1/2-T			
F23-4	1.079	5.650	2.354
F23-21	1.085	5.703	2.374
F23-41	1.086	5.715	2.378
F23-73	1.086	5.717	2.378
F23-80	1.081	5.692	2.368
F23-94	1.065	5.581	2.324
F23-141	1.056	5.525	2.303
F23-44	1.047	5.460	2.277
F23-14	1.036	5.449	2.267
F23-46	1.042	5.500	2.286
F23-66	1.043	5.512	2.290
F23-98	1.043	5.514	2.290
F23-105	1.038	5.489	2.280
F23-112	1.034	5.463	2.270
F23-119	1.022	5.383	2.238
F23-166	1.014	5.329	2.218
F23-69	1.005	5.266	2.193
Maximum	1.09	5.72	2.38
Average	1.05	5.53	2.30
Minimum	1.00	5.27	2.19

TABLE 4.2.2 (Cont'd)

ID No.	$\phi t > 1.0$ MeV (10^{19} n/cm^2)	$\phi t > 0.1$ MeV (10^{19} n/cm^2)	dpa (10^{-2})
	A533-B Plate		
SSC-1 Capsule			
3PU-1	2.443	7.045	3.808
3PU-2	2.403	6.916	3.743
3PU-3	2.310	6.615	3.589
3PU-4	2.256	6.443	3.501
3PU-5	2.199	6.257	3.406
3PU-17	2.501	7.200	3.893
3PU-18	2.460	7.069	3.826
3PU-19	2.364	6.761	3.668
3PU-20	2.309	6.585	3.579
PU-21	2.250	6.395	3.482
Maximum	2.50	7.20	3.89
Average	2.35	6.73	3.65
Minimum	2.20	6.26	3.41
SSC-2 Capsule			
3PT-6	5.390	15.690	8.421
3PT-7	5.305	15.420	8.280
3PT-8	5.101	14.750	7.943
3PT-9	4.983	14.370	7.748
3PT-10	4.854	13.950	7.536
3PT-22	5.070	14.790	7.931
3PT-23	4.990	14.530	7.798
3PT-24	4.798	13.900	7.481
3PT-25	4.687	13.540	7.297
3PT-26	4.566	13.150	7.097
Maximum	5.39	15.69	8.42
Average	4.97	14.41	7.75
Minimum	4.57	13.15	7.10

TABLE 4.2.2 (Cont'd)

ID No.	$\phi t > 1.0$ MeV (10^{19} n/cm^2)	$\phi t > 0.1$ MeV (10^{19} n/cm^2)	dpa (10^{-2})
Wall No. 1, 0-T			
3PU-6	3.690	10.510	5.863
3PU-7	3.642	10.350	5.779
3PU-8	3.530	9.966	5.583
3PU-9	3.466	9.746	5.471
3PU-10	3.396	9.508	5.349
3PU-22	3.537	10.100	5.627
3PU-23	3.491	9.942	5.547
3PU-24	3.384	9.573	5.359
3PU-25	3.322	9.362	5.251
3PU-26	3.255	9.133	5.134
Maximum	3.69	10.51	5.86
Average	3.47	9.82	5.50
Minimum	3.25	9.13	5.13
Wall No. 2, 1/4-T			
3PU-11	2.123	8.029	3.810
3PU-12	2.096	7.901	3.754
3PU-13	2.033	7.604	3.624
3PU-14	1.997	7.434	3.550
3PU-15	1.959	7.251	3.470
3PU-27	2.020	7.667	3.632
3PU-28	1.994	7.545	3.579
3PU-29	1.935	7.261	3.455
3PU-30	1.901	7.099	3.384
3PU-31	1.864	6.925	3.308
Maximum	2.12	8.03	3.81
Average	1.99	7.47	3.56
Minimum	1.86	6.93	3.31
Wall No. 3, 1/2-T			
3PT-1	1.036	5.385	2.248
3PT-2	1.024	5.301	2.216
3PT-3	0.996	5.106	2.141
3PT-4	0.980	4.995	2.098
3PT-5	0.963	4.876	2.052
EPT-17	0.995	5.193	2.165
EPT-18	0.983	5.112	2.134
3PT-19	0.956	4.924	2.062
3PT-20	0.941	4.817	2.021
3PT-21	0.925	4.703	1.976
Maximum	1.04	5.38	2.25
Average	0.98	5.04	2.11
Minimum	0.92	4.70	1.98

TABLE 4.2.2 (Cont'd)

ID No.	$\phi t > 1.0$ MeV (10^{19} n/cm^2)	$\phi t > 0.1$ MeV (10^{19} n/cm^2)	dpa (10^{-2})
	22NIMOCR37 Forging		
SSC-1 Capsule			
K-512	1.722	5.448	2.806
K-513	1.701	5.375	2.770
K-514	1.677	5.290	2.728
K-99	1.619	5.086	2.629
K-62	1.585	4.967	2.571
K-63	1.549	4.838	2.508
K-64	1.509	4.698	2.440
K-65	1.763	5.568	2.868
K-67	1.717	5.406	2.789
K-515	1.689	5.308	2.741
K-610	1.657	5.198	2.687
K-611	1.623	5.077	2.628
K-612	1.585	4.945	2.564
K-613	1.545	4.802	2.494
Maximum	1.76	5.57	2.87
Average	1.64	5.14	2.66
Minimum	1.51	4.70	2.44
SSC-2 Capsule			
K-614	3.794	12.120	6.195
K-72	3.700	11.780	6.033
K-74	3.501	11.080	5.690
K-75	3.420	10.790	5.550
K-76	3.332	10.480	5.398
K-77	3.568	11.420	5.835
K-710	3.528	11.280	5.765
K-711	3.480	11.100	5.682
K-73	3.425	10.910	5.587
K-712	3.363	10.690	5.479
K-713	3.293	10.440	5.359
K-714	3.217	10.170	5.228
K-715	3.134	9.871	5.084
Maximum	3.79	12.12	6.19
Average	3.44	10.93	5.61
Minimum	3.13	9.87	5.08

TABLE 4.2.2 (Cont'd)

ID No.	$\phi t > 1.0$ MeV (10^{19} n/cm^2)	$\phi t > 0.1$ MeV (10^{19} n/cm^2)	dpa (10^{-2})
Wall No. 1, 0-T			
K-410	2.998	9.854	5.067
K-411	2.969	9.741	5.013
K-412	2.936	9.610	4.951
K-414	2.808	9.110	4.715
K-415	2.757	8.909	4.620
K-52	2.701	8.691	4.517
K-53	2.873	9.466	4.863
K-54	2.846	9.357	4.812
K-55	2.814	9.231	4.753
K-413	2.777	9.088	4.685
K-56	2.737	8.928	4.609
K-57	2.692	8.751	4.526
K-510	2.642	8.558	4.435
K-511	2.589	8.349	4.336
Maximum	3.00	9.85	5.07
Average	2.80	9.12	4.71
Minimum	2.59	8.35	4.34
Wall No. 2, 1/4-T			
K-36	1.628	7.094	3.171
K-37	1.612	7.010	3.136
K-312	1.527	6.547	2.945
K-313	1.500	6.401	2.885
K-314	1.471	6.244	2.820
K-315	1.549	6.774	3.023
K-42	1.534	6.694	2.990
K-43	1.517	6.601	2.952
K-311	1.498	6.496	2.909
K-44	1.476	6.380	2.861
K-45	1.453	6.252	2.808
K-46	1.427	6.112	2.750
K-47	1.399	5.962	2.688
Maximum	1.63	7.09	3.17
Average	1.51	6.51	2.92
Minimum	1.40	5.96	2.69
Wall No. 3, 1/2-T			
K-24	0.773	4.568	1.832
K-25	0.766	4.514	1.812
K-26	0.758	4.452	1.789
K-210	0.729	4.221	1.703
K-211	0.718	4.129	1.669
K-212	0.705	4.031	1.633
K-213	0.742	4.405	1.764
K-214	0.736	4.353	1.745
K-215	0.728	4.294	1.723
K-27	0.719	4.227	1.698
K-32	0.710	4.152	1.670
K-33	0.700	4.071	1.640
K-34	0.689	3.983	1.607
K-35	0.677	3.888	1.572
Maximum	0.77	4.57	1.83
Average	0.73	4.23	1.70
Minimum	0.68	3.89	

TABLE 4.2.2 (Cont'd)

ID No.	$\phi t > 1.0$ MeV (10^{19} n/cm^2)	$\phi t > 0.1$ MeV (10^{19} n/cm^2)	dpa (10^{-2})
	A508-3 Forging		
SSC-1 Capsule			
MO-01	1.778	5.636	2.899
MO-02	1.773	5.623	2.892
MO-03	1.766	5.597	2.879
MO-04	1.755	5.559	2.861
MO-05	1.740	5.510	2.836
MO-06	1.812	5.727	2.949
MO-07	1.818	5.751	2.960
MO-08	1.821	5.762	2.965
MO-09	1.820	5.760	2.963
MO-10	1.815	5.746	2.956
MO-11	1.807	5.720	2.943
MO-12	1.796	5.682	2.924
MO-13	1.781	5.631	2.899
Maximum	1.82	5.76	2.97
Average	1.79	5.67	2.92
Minimum	1.74	5.51	2.84
SSC-2 Capsule			
MO-53	3.889	12.450	6.358
MO-54	3.886	12.440	6.353
MO-55	3.875	12.410	6.335
MO-57	3.829	12.240	6.255
MO-58	3.620	11.590	5.922
MO-59	3.640	11.670	5.958
MO-60	3.653	11.710	5.980
MO-62	3.655	11.730	5.984
MO-63	3.645	11.690	5.966
MO-64	3.627	11.630	5.936
MO-65	3.601	11.540	5.892
Maximum	3.89	12.45	6.36
Average	3.72	11.92	6.09
Minimum	3.60	11.54	5.89

TABLE 4.2.2 (Cont'd)

ID No.	$\phi t > 1.0$ MeV (10^{19} n/cm^2)	$\phi t > 0.1$ MeV (10^{19} n/cm^2)	dpa (10^{-2})
Wall No. 1, 0-T			
MO-14	3.070	10.140	5.201
MO-16	3.055	10.080	5.174
MO-17	3.041	10.020	5.147
MO-18	3.022	9.949	5.111
MO-19	2.929	9.686	4.967
MO-20	2.938	9.722	4.984
MO-21	2.943	9.740	4.992
MO-22	2.942	9.740	4.992
MO-23	2.938	9.721	4.983
MO-25	2.914	9.630	4.940
MO-26	2.896	9.557	4.906
Maximum	3.07	10.14	5.20
Average	2.97	9.82	5.04
Minimum	2.90	9.56	4.91
Wall No. 2, 1/4-T			
MO-28	1.667	7.303	3.258
MO-29	1.661	7.270	3.244
MO-30	1.652	7.225	3.225
MO-31	1.641	7.166	3.201
MO-32	1.587	6.971	3.107
MO-33	1.590	6.991	3.114
MO-34	1.591	6.997	3.117
MO-35	1.590	6.992	3.114
MO-36	1.586	6.973	3.106
MO-37	1.580	6.942	3.093
MO-39	1.562	6.843	3.052
Maximum	1.67	7.30	3.26
Average	1.61	7.06	3.15
Minimum	1.56	6.84	3.05
Wall No. 3, 1/2-T			
MO-40	0.794	4.720	1.889
MO-41	0.791	4.705	1.884
MO-43	0.784	4.652	1.863
MO-44	0.779	4.614	1.849
MO-45	0.763	4.547	1.818
MO-46	0.763	4.557	1.822
MO-47	0.763	4.558	1.822
MO-48	0.762	4.552	1.819
MO-49	0.760	4.538	1.814
MO-51	0.753	4.487	1.795
MO-52	0.748	4.450	1.781
Maximum	0.79	4.72	1.89
Average	0.77	4.58	1.83
Minimum	0.75	4.45	1.78

TABLE 4.2.2 (Cont'd)

ID No.	$\phi t > 1.0$ MeV (10^{19} n/cm^2)	$\phi t > 0.1$ MeV (10^{19} n/cm^2)	dpa (10^{-2})
	Submerged Arc Weld (EC)		
SSC-1 Capsule			
EC-1	1.637	5.111	2.652
EC-2	1.666	5.216	2.702
EC-3	1.714	5.392	2.786
EC-4	1.733	5.463	2.819
EC-5	1.749	5.522	2.847
EC-6	1.761	5.569	2.869
EC-7	1.675	5.223	2.710
EC-8	1.705	5.331	2.762
EC-9	1.754	5.511	2.847
EC-10	1.774	5.583	2.882
EC-11	1.790	5.643	2.910
EC-12	1.803	5.691	2.933
Maximum	1.80	5.69	2.93
Average	1.73	5.44	2.81
Minimum	1.64	5.11	2.65
SSC-2 Capsule			
EC-49	3.477	10.960	5.645
EC-50	3.553	11.230	5.776
EC-51	3.682	11.700	6.000
EC-52	3.736	11.890	6.093
EC-53	3.781	12.060	6.171
EC-54	3.819	12.200	6.237
EC-55	3.270	10.330	5.317
EC-56	3.342	10.590	5.440
EC-57	3.464	11.030	5.651
EC-58	3.514	11.210	5.738
EC-59	3.557	11.360	5.813
EC-60	3.592	11.490	5.874
Maximum	3.82	12.20	6.24
Average	3.57	11.34	5.81
Minimum	3.27	10.33	5.32

TABLE 4.2.2 (Cont'd)

ID No.	$\phi t > 1.0$ MeV (10^{19} n/cm^2)	$\phi t > 0.1$ MeV (10^{19} n/cm^2)	dpa (10^{-2})
Wall No. 1, 0-T			
EC-13	2.858	9.302	4.806
EC-14	2.900	9.468	4.884
EC-15	2.971	9.747	5.016
EC-16	2.999	9.859	5.069
EC-17	3.023	9.952	5.113
EC-18	3.042	10.030	5.148
EC-19	2.739	8.935	4.613
EC-20	2.780	9.095	4.688
EC-21	2.847	9.363	4.814
EC-22	2.875	9.470	4.865
EC-23	2.897	9.560	4.907
EC-24	2.916	9.632	4.941
Maximum	3.04	10.03	5.15
Average	2.90	9.53	4.91
Minimum	2.74	8.93	4.61
Wall No. 2, 1/4-T			
EC-25	1.579	6.792	3.053
EC-26	1.598	6.903	3.098
EC-27	1.631	7.087	3.173
EC-28	1.644	7.160	3.202
EC-29	1.654	7.220	3.226
EC-30	1.662	7.266	3.245
EC-31	1.502	6.485	2.911
EC-32	1.521	6.591	2.954
EC-33	1.552	6.767	3.025
EC-34	1.564	6.837	3.053
EC-35	1.574	6.894	3.076
EC-36	1.582	6.939	3.094
Maximum	1.66	7.27	3.25
Average	1.59	6.91	3.09
Minimum	1.50	6.49	2.91
Wall No. 3, 1/2-T			
EC-37	0.762	4.424	1.784
EC-38	0.770	4.489	1.807
EC-39	0.782	4.596	1.846
EC-40	0.786	4.637	1.861
EC-41	0.790	4.671	1.873
EC-42	0.793	4.697	1.882
EC-43	0.732	4.266	1.718
EC-44	0.739	4.329	1.740
EC-45	0.751	4.432	1.778
EC-46	0.755	4.473	1.792
EC-47	0.758	4.505	1.804
EC-48	0.761	4.530	1.812
Maximum	0.79	4.70	1.88
Average	0.76	4.50	1.81
Minimum	0.73	4.27	1.72

TABLE 4.2.2 (Cont'd)

ID No.	$\phi t > 1.0$ MeV (10^{19} n/cm^2)	$\phi t > 0.1$ MeV (10^{19} n/cm^2)	dpa (10^{-2})
	Submerged Arc Weld (R)		
SSC-1 Capsule			
R-1	2.338	6.652	3.624
R-2	2.384	6.806	3.702
R-3	2.426	6.946	3.772
R-4	2.464	7.071	3.834
R-6	2.497	7.181	3.889
R-7	2.524	7.275	3.935
R-8	2.393	6.798	3.704
R-9	2.441	6.956	3.783
R-11	2.484	7.099	3.855
R-12	2.522	7.227	3.919
R-13	2.555	7.339	3.975
R-14	2.584	7.435	4.022
Maximum	2.58	7.44	4.02
Average	2.47	7.07	3.83
Minimum	2.34	6.65	3.62
SSC-2 Capsule			
R-31	4.944	14.200	7.679
R-32	5.065	14.600	7.879
R-33	5.176	14.960	8.063
R-34	5.276	15.290	8.228
R-36	5.365	15.580	8.376
R-37	5.442	15.840	8.505
R-38	4.650	13.380	7.232
R-39	4.764	13.760	7.421
R-41	4.868	14.100	7.594
R-42	4.962	14.410	7.750
R-43	5.046	14.680	7.889
R-44	5.119	14.930	8.010
Maximum	5.44	15.84	8.50
Average	5.06	14.64	7.89
Minimum	4.65	13.38	7.23

TABLE 4.2.2 (Cont'd)

ID No.	$\phi t > 1.0$ MeV (10^{19} n/cm^2)	$\phi t > 0.1$ MeV (10^{19} n/cm^2)	dpa (10^{-2})
Wall No. 1, 0-T			
R-46	3.534	9.975	5.588
R-47	3.593	10.180	5.690
R-48	3.646	10.360	5.783
R-49	3.693	10.520	5.866
R-51	3.734	10.660	5.939
R-52	3.770	10.780	6.001
R-53	3.387	9.582	5.363
R-54	3.443	9.775	5.462
R-56	3.494	9.949	5.551
R-57	3.540	10.110	5.630
R-58	3.579	10.240	5.700
R-59	3.614	10.360	5.760
Maximum	3.77	10.78	6.00
Average	3.59	10.21	5.69
Minimum	3.39	9.58	5.36
Wall No. 2, 1/4-T			
R-16	2.073	7.745	3.695
R-17	2.102	7.888	3.756
R-18	2.129	8.017	3.812
R-19	2.152	8.131	3.861
R-21	2.172	8.231	3.904
R-22	2.189	8.315	3.940
R-23	1.973	7.396	3.522
R-24	2.000	7.533	3.581
R-26	2.025	7.655	3.634
R-27	2.048	7.765	3.681
R-28	2.067	7.860	3.722
R-29	2.083	7.940	3.756
Maximum	2.19	8.32	3.94
Average	2.08	7.87	3.74
Minimum	1.97	7.40	3.52
Wall No. 3, 1/2-T			
R-68	1.030	5.263	2.209
R-69	1.042	5.351	2.242
R-71	1.052	5.429	2.272
R-72	1.061	5.499	2.298
R-74	1.074	5.609	2.339
R-76	0.989	5.076	2.127
R-77	0.989	5.076	2.127
R-78	1.010	5.237	2.188
R-79	1.018	5.303	2.213
R-81	1.025	5.361	2.235
R-82	1.031	5.410	2.253
Maximum	1.07	5.61	2.34
Average	1.03	5.33	2.23
Minimum	0.99	5.08	2.13

TABLE 4.2.3

ORNL DAMAGE PARAMETER VALUES AT THE LOCATION OF THE 1/2 CT SPECIMENS

Front				Rear			
ID No.	$\phi t > 1.0$ MeV (10^{19} n/cm^2)	$\phi t > 0.1$ MeV (10^{19} n/cm^2)	dpa (10^{-2})	ID No.	$\phi t > 1.0$ MeV (10^{19} n/cm^2)	$\phi t > 0.1$ MeV (10^{19} n/cm^2)	dpa (10^{-2})
			Capsule SSC-1				
F23-10R	2.511	7.301	3.930	F23-40R	2.008	6.158	3.224
F23-15R	2.657	7.796	4.174	F23-42R	2.125	6.576	3.424
F23-20R	2.762	8.161	4.353	F23-52R	2.209	6.884	3.571
F23-25R	2.793	8.271	4.406	F23-63R	2.233	6.977	3.614
F23-30R	2.774	8.218	4.376	F23-66R	2.218	6.932	3.590
3PU-1	2.716	8.034	4.282	3PU-21	2.172	6.776	3.512
3PU-9	2.574	7.567	4.046	3PU-29	2.058	6.383	3.319
3PU-13	2.399	6.991	3.755	3PU-33	1.918	5.897	3.080
			Capsule SSC-2				
F23-7R	5.179	15.258	8.143	F23-38R	4.141	12.871	6.679
F23-17R	5.552	16.518	8.769	F23-46R	4.440	13.933	7.193
F23-19R	5.842	17.499	9.255	F23-54R	4.672	14.761	7.592
F23-27R	5.944	17.849	9.427	F23-58R	4.753	15.056	7.732
F23-29R	5.943	17.852	9.425	F23-62R	4.752	15.058	7.731
3PU-8	5.839	17.507	9.251	3PU-30	4.669	14.767	7.588
3PU-16	5.546	16.531	8.762	3PU-32	4.435	13.944	7.187
3PU-17	5.171	15.276	8.134	3PU-37	4.135	12.886	6.672
			SPV-Capsule 0-T				
F23-1R	3.830	11.158	6.128	F23-39R	3.343	10.578	5.543
F23-5R	4.015	11.812	6.455	F23-43R	3.504	11.198	5.839
F23-11R	4.151	12.296	6.697	F23-51R	3.624	11.657	6.058
F23-21R	4.193	12.446	6.772	F23-59R	3.660	11.799	6.126
F23-31R	4.175	12.384	6.741	F23-67R	3.645	11.741	6.098
3PU-2	4.109	12.149	6.624	3PU-18	3.587	11.518	5.991
3PU-10	3.938	11.546	6.322	3PU-14	3.438	10.946	5.719
3PU-26	3.726	10.797	5.947	3PU-34	3.253	10.236	5.379

TABLE 4.2.3 (Cont'd)

Front				Rear			
ID No.	$\phi t > 1.0$ MeV (10^{19} n/cm^2)	$\phi t > 0.1$ MeV (10^{19} n/cm^2)	dpa (10^{-2})	ID No.	$\phi t > 1.0$ MeV (10^{19} n/cm^2)	$\phi t > 0.1$ MeV (10^{19} n/cm^2)	dpa (10^{-2})
			SPV-Capsule 1/4-T				
F23-3R	2.163	8.355	3.926	F23-45R	1.825	7.644	3.471
F23-8R	2.252	8.802	4.116	F23-47R	1.899	8.054	3.639
F23-13R	2.314	9.123	4.251	F23-53R	1.952	8.347	3.759
F23-18R	2.330	9.212	4.288	F23-55R	1.966	8.428	3.791
F23-23R	2.314	9.141	4.256	F23-61R	1.952	8.363	3.763
3PU-3	2.275	8.954	4.175	3PU-27	1.919	8.192	3.691
3PU-11	2.182	8.497	3.978	3PU-15	1.840	7.774	3.516
3PU-19	2.068	7.939	3.737	3PU-35	1.744	7.264	3.304
			SPV-Capsule 1/2-T				
F23-4R	1.054	5.556	2.311	F23-37R	0.875	4.962	2.017
F23-9R	1.087	5.823	2.410	F23-41R	0.903	5.201	2.104
F23-14R	1.109	6.010	2.479	F23-49R	0.922	5.367	2.164
F23-24R	1.114	6.055	2.495	F23-57R	0.925	5.408	2.178
F23-28R	1.104	5.998	2.472	F23-65R	0.917	5.357	2.158
3PU-4	1.086	5.873	2.424	3PU-24	0.902	5.246	2.116
3PU-12	1.044	5.577	2.310	3PU-31	0.868	4.981	2.017
3PU-20	0.995	5.220	2.174	3PU-36	0.827	4.662	1.898

TABLE 4.2.4

ORNL DAMAGE PARAMETER VALUES AT THE LOCATION OF THE 1 CT SPECIMEN

Left				Right			
ID No.	$\phi t > 1.0$ MeV (10^{19} n/cm^2)	$\phi t > 0.1$ MeV (10^{19} n/cm^2)	dpa (10^{-2})	ID No.	$\phi t > 1.0$ MeV (10^{19} n/cm^2)	$\phi t > 0.1$ MeV (10^{19} n/cm^2)	dpa (10^{-2})
			Capsule SSC-1				
F23-5R	2.236	6.701	3.550	F23-17R	2.257	6.761	3.582
F23-9R	2.406	7.303	3.842	F23-21R	2.429	7.368	3.876
F23-13R	2.373	7.210	3.790	3PS-12	2.396	7.274	3.824
3PS-11	2.149	6.455	3.414	3PS-14	2.169	6.513	3.444
			Capsule SSC-2				
F23-2R	4.704	14.274	7.499	F23-24R	4.589	13.938	7.321
F23-6R	5.170	15.894	8.292	F23-28R	5.044	15.519	8.094
F23-20R	5.168	15.899	8.289	3PS-7	5.042	15.524	8.091
3PS-6	4.697	14.289	7.492	3PS-8	4.583	13.952	7.313
			SPV Capsule 0-T				
F23-15R	3.587	10.931	5.855	F23-27R	3.526	10.755	5.759
F23-19R	3.819	11.786	6.273	F23-1R	3.754	11.596	6.170
F23-23R	3.787	11.670	6.217	3PS-10	3.722	11.482	6.114
3PS-9	3.503	10.625	5.705	3PS-15	3.443	10.453	5.611
			SPV-Capsule 1/4-T				
F23-4R	1.997	8.065	3.720	F23-16R	1.956	7.914	3.648
F23-8R	2.102	8.629	3.954	F23-30R	2.060	8.467	3.878
F23-12R	2.074	8.497	3.896	3PS-16	2.032	8.338	3.820
3PS-13	1.920	7.717	3.565	3PT-1	1.881	7.572	3.495
			SPV-Capsule 1/2-T				
F23-3R	0.963	5.294	2.173	F23-25R	0.947	5.215	2.139
F23-7R	1.001	5.620	2.292	F23-29R	0.984	5.536	2.257
F23-11R	0.984	5.515	2.250	3PT-3	0.967	5.433	2.215
3PT-2	0.916	5.016	2.061	3PT-4	0.901	4.941	2.029

4.3 CONSISTENCY OF EXPERIMENTAL DATA AND DERIVED EXPOSURE PARAMETERS - CEN/SCK

H. Tourwé and J. Lacroix (CEN/SCK)

The results of the CEN/SCK analysis and comparison of the Mol and HEDL dosimetry measurements and the derivation of exposure parameter values of neutron fluence (E > 1 MeV) and dpa in iron are documented in Appendix A.5 of Reference (Mc86b). The reader is referred to Appendix A.5 for more detailed information and a tabulation of the Mol results for the six PV steels.

4.4 CONSISTENCY OF EXPERIMENTAL DATA AND DERIVED EXPOSURE PARAMETERS - RR&A

A. F. Thomas (Rolls-Royce and Associates)

4.4.1 Consistency Analysis of UK Dosimetry Measurements in ORR/PSF Pressure Vessel Simulator (PVS Capsules)

The consistency analysis of the measured reaction rates in the UK dosimetry in the ORR/PSF (4/12) SSC-1 and SSC-2 and PVS capsules at the OT, 1/4T, and 1/2T positions was conducted using both deterministic and statistical methods.

4.4.2 Deterministic Analysis

The methods used for the deterministic analysis for the PVS OT, 1/4T, and 1/2T positions were identical to those reported for the consistency analysis of the SSC-1 and SSC-2 capsules (NUREG/CR-3320, Vol. 2). This involved the conversion of the measured reaction rates given in Tables 2.3.3.2 and 2.3.3.5 into appropriate exposure parameters using the ANISN-calculated flux-weighted cross sections reported in Table 4.4.1 (NUREG/CR-3310, Vol. 2, Table 6.4.1). These exposure parameters are given in Table 4.4.2. As observed in the SSC-1, SSC-2, OT, 1/4T, and 1/2T analysis, there is generally good agreement in the exposure parameters within the various types of dosimetry reaction. However, the tendency for the ^{93}Nb(n,n′) reaction to predict a value of neutron flux (E > 1 MeV) about 25% lower than the other threshold monitors is seen in both the SSC and PVS results.

4.4.3 Statistical Analysis

The statistical approach to the consistency analysis of the UK dosimetry in the PVS capsules was again identical to that reported for the SSC-1 and SSC-2 capsules using the UK least-squares adjustment code SENSAK (NUREG/CR-3320, Vol. 2, Section 6.4).

The results of the SENSAK analyses for the SSC and PVS capsules are given in Table 4.4.3. The source scale factors are all close to unity, indicating good prior estimates of the calculated flux intensities. The values of variance scale factor (VSF), which is the value of χ^2 per degree of freedom, are all less than 1.0, indicating that the consistency betwen the reaction rates was better than might be inferred from the input data uncertainties. However, taken in conjunction with the values of VSF from the SSC-1 and SSC-2 irradiations, the degree of consistency becomes less the further away from the radiation source the measurements were made. This result is to be expected since the uncertainties on the calculated input spectra were not determined explicitly and are likely to increase with increasing attenuation.

No suspect measurements were noted in any of the sets of reaction rates analyzed; none of the calculated (adjusted)-to-measured reaction rate ratios deviated by more than 1% from unity. However, the reconciliation between the ^{93}Nb(n,n′) reaction rates and the other threshold detectors for the PVS locations were achieved by a gradual reduction of the ^{93}Nb(n,n′) cross section in the threshold region (0.1 to 2 MeV) by up to 25%. This result

TABLE 4.4.1

EFFECTIVE NEUTRON CROSS SECTIONS FOR ACTIVATION DETECTORS
USED IN ORR/PSF (4/12) CONFIGURATIONS

Reaction	Effective Cross Section (millibarns)				
	SSC	OT	$\frac{1}{4}$T	$\frac{1}{2}$T	$\frac{3}{4}$T
FAST NEUTRON FLUX*					
$^{63}Cu(n,\alpha)^{60}Co$	0.44	0.61	0.48	0.38	0.31
$^{46}Ti(n,p)^{46}Sc$	8.11	10.1	7.77	5.95	4.63
$^{54}Fe(n,p)^{54}Mn$	63.3	70.6	55.5	43.4	34.3
$^{58}Ni(n,p)^{58}Co$	85.5	94.7	75.9	60.6	49.2
$^{93}Nb(n,n')^{93m}Nb$	222.5	225.6	228.4	238.9	255.0
EPITHERMAL NEUTRON FLUX*					
$^{58}Fe(n,\gamma)^{59}Fe$(Gd)	570	170	990	7,060	6,810
$^{59}Co(n,\gamma)^{60}Co$(Gd)	38,400	12,000	67,800	470,800	443,100
THERMAL NEUTRON FLUX*					
$^{58}Fe(n,\gamma)^{59}Fe$(Bare)	1,400	1,060	1,870	7,990	7,740
$^{59}Co(n,\gamma)^{60}Co$(Bare)	64,600	38,800	94,100	501,200	473,000

*N.B. Fast neutron flux = $n/cm^2/s$ ($E > 1MeV$)
Epithermal neutron flux = $n/cm^2/s$ ($0.4eV < E < 0.1$ MeV)
Thermal neutron flux = $n/cm^2/s$ ($E < 0.4eV$)

supported the conclusion of the SSC-1 and SSC-2 analysis that greater accuracy of the $^{93}Nb(n,n')$ cross section is required in the threshold region.

The uncertainties on the exposure parameters estimated by the SENSAK analysis for the SSC-1 and SSC-2 locations are all within ±6% to ±10% (1σ). If the variances are not scaled, however, the range of uncertainties lies in the band from ±13% to ±22%. The uncertainties on the exposure parameters for the OT, 1/4T, and 1/2T locations are larger than those for the SSC-1 and SSC-2 capsules, falling within the band ±10% to ±18%. If the variances are not scaled, the range of uncertainties lies in the band from ±15% to ±22%, which is very similar to that of the SSC-1 and SSC-2 analysis.

TABLE 4.4.2

COMPARISON OF EXPOSURE PARAMETERS ESTIMATED FROM DETECTORS IRRADIATED IN THE SSC AND PVS CAPSULES

	Exposure Parameter Value				
REACTION	SSC-1	SSC-2	PVS(OT)	PVS(1/4T)	PVS(1/2T)
	(34-A)	(34-A)	(34-A)	(34-A)	(34-A)
FAST NEUTRON FLUX*					
$^{63}Cu(n,\alpha)^{60}Co$	7.12E12	6.66E12	7.90E11	4.27E11	2.08E11
$^{46}Ti(n,p)^{46}Sc$	8.24E12	8.07E12	8.50E11	4.94E11	2.52E11
$^{54}Fe(n,p)^{54}Mn$	7.51E12	7.52E12	8.27E11	4.73E11	2.39E11
$^{58}Ni(n,p)^{58}Co$	7.82E12	7.64E12	7.78E11	4.71E11	2.32E11
$^{93}Nb(n,n')^{93m}Nb$	5.88E12	6.38E12	6.69E11	3.80E11	1.65E11
EPITHERMAL NEUTRON FLUX*					
$^{58}Fe(n,\gamma)^{59}Fe(Gd)$	-	2.65E12	1.09E12	8.35E10	5.97E9
$^{59}Co(n,\gamma)^{60}Co(Gd)$	2.64E12	2.52E12	1.17E12	1.05E10	7.36E9
THERMAL NEUTRON FLUX*					
$^{58}Fe(n,\gamma)^{59}Fe(Bare)$	-	2.65E12**	7.54E11	6.28E10	6.02E9
$^{59}Co(n,\gamma)^{60}Co(Bare)$	-	2.38E12**	8.98E11	8.61E10	6.98E9

*N.B. Thermal neutron flux = n/cm/s (E > 1 MeV)
Fast neutron flux = $n/cm^2/s$ (E_2 > 1 MeV)
Epithermal neutron flux = $n/cm^2/s$ (0.4eV < E < 0.1MeV)

** 34-B Locations

TABLE 4.4.3

SUMMARY OF RESULTS OF SENSAK CONSISTENCY ANALYSIS OF
ORR/PSF (4/12) SSC AND PVS CAPSULES

LOCATION	SOURCE SCALE FACTOR	VARIANCE SCALE FACTOR	FLUX* (E>1MeV)	FLUX* (E>0.1MeV	DPA RATE* IRON	DPA RATE* SAPPHIRE
SSC-1	0.95	0.23	7.05E12 ±8.1%	2.13E13 ±9.1%	1.13E-8 ±7.1%	6.84E-9 ±8.3%
SSC-2	0.91	0.22	6.89E12 ±7.7%	2.07E13 ±8.3%	1.10E-8 ±6.5%	6.64E-9 ±7.6%
PVS (OT)	0.78	0.44	7.32E11 ±11.0%	2.20E12 ±12.4%	1.22E-9 ±10.4%	7.08E-10 ±11.5%
PVS (1/4T)	0.81	0.58	4.18E11 ±13.5%	1.64E12 ±14.9%	7.73E-10 ±11.9%	4.92E-10 ±13.9
PVS (1/2T)	0.87	0.70	2.00E11 ±16.8%	1.08E12 ±18.0%	4.49E-10 ±15.1%	3.06E-10 ±17.3%

All errors quoted are to one standard deviation (1σ)
* FLUX = neutrons/cm^2/s (30MW)
DPA RATE = dpa/s (30MW)

4.4.4 Recommended Exposure Parameter Estimates

The RR&A recommended exposure parameter estimates integrated over the appropriate exposure times for the ORR/PSF (4/12) simulated surveillance capsules (SSC-1 and SSC-2) and the pressure vessel simulator OT, 1/4T, and 1/2T capsules are shown in Table 4.4.4. The uncertainty values associated with these estimates are based on the unscales variances. While it is probable that the input errors on the neutron flux spectra have been overestimated, until such time that these have been evaluated explicitly, it is more justifiable and more conservative to recommend the unscaled exposure parameter errors.

As in the case of the SSC-1 and SSC-2 capsules (see Table 4.4.4), it should be emphasized that the OT, 1/4T, and 1/2T exposure parameter values are the exposure values at the locations of the UK dosimetry capsules that were defined in Section 2.1.3. In order to define the radiation exposures to the metallurgical specimens and the Sapphire Damage Monitors in the SSC and PVS capsules, extrapolation must be made. These extrapolations are based on the same analysis of the HEDL measurements of the relative activity of ^{54}Mn in the HEDL gradient wires discussed in NUREG/CR-3320, Vol. 2 for the SSC-1 and SSC-2 capsules; these are shown in Tables 4.4.5a and 4.4.5b for the SSC capsules and Tables 4.4.6a and 4.4.6b for the PVS capsules.

It should be noted that the precision of the relative values of exposure parameters on the metallurgy specimens is on the order of a few percent. However, the uncertainty over the location of the Sapphire Damage Monitors within the OT, 1/4T, and 1/2T capsules was similar to that obtained in the SSC-1 and SSC-2 capsules.

TABLE 4.4.4

RR&A RECOMMENDED EXPOSURE PARAMETER ESTIMATES
IN ORR/PSF SSC AND PVS CAPSULES

LOCATION (DOSIMETER HOLE)	IRRADIATION TIME(S)	FLUENCE* (E>1MeV)	FLUENCE* (E>0.1MeV)	DPA (IRON)	DPA (SAPPHIRE)
SSC-1 (34-A)	3.866E6	2.73E19 ±17%	8.23E19 ±19%	4.37E-2 ±15%	2.64E-2 ±17%
SSC-2 (34-A)	7.746E6	5.34E19 ±16%	1.60E20 ±17%	8.52E-2 ±14%	5.14E-2 ±16%
PVS/OT (34-A)	5.141E7	3.76E19 ±17%	1.13E20 ±19%	6.27E-2 ±16%	3.65E-2 ±17%
PVS/1/4T (34-A)	5.141E7	2.15E19 ±18%	8.43E19 ±20%	3.97E-2 ±16%	2.53E-2 ±18%
PVS/1/2T (34-A)	5.141E7	1.03E19 ±20%	5.55E19 ±22%	2.31E-2 ±18%	1.57E-2 ±21%

* FLUENCE = neutrons/cm^2
All errors quoted are to one standard deviation (1σ).

TABLE 4.4.5a

RELATIVE VALUES OF EXPOSURE PARAMETERS FOR RR&A METALLURGY SPECIMENS IN SSC-1 AND SSC-2 WITH RESPECT TO UK DOSIMETRY

SPECIMEN NUMBER		EXPOSURE RELATIVE TO UK DOSIMETRY		
SSC1	SSC2	FLUENCE (E > 1 MEV)	FLUENCE (E > 0.1 MEV)	DPA (IRON)
R88T	R64T	0.88	0.82	0.85
R1	R31	0.89	0.83	0.86
R2	R32	0.91	0.84	0.88
R3	R33	0.93	0.86	0.90
R4	R34	0.95	0.88	0.92
R6	R36	0.97	0.90	0.94
R7	R37	0.99	0.92	0.96
R89T	R65T	0.88	0.82	0.85
R8	R38	0.89	0.83	0.86
R9	R39	0.91	0.84	0.88
R11	R41	0.93	0.86	0.90
R12	R42	0.95	0.88	0.92
R13	R43	0.97	0.90	0.92
R14	R44	0.99	0.92	0.96

TABLE 4.4.5b

RELATIVE VALUES OF EXPOSURE PARAMETERS FOR UK SAPPHIRE DAMAGE MONITORS IN SSC-1 AND SSC-2 WITH RESPECT TO UK DOSIMETRY

SAPPHIRE NUMBER (HOLE)		EXPOSURE RELATIVE TO UK DOSIMETRY		
SSC1	SSC2	FLUENCE (E > 1 MEV)	FLUENCE (E > 0.1 MEV)	DPA (IRON)
1(2V17)	3(4V17)	0.9(±0.1)	0.9(±0.1)	0.9(±0.1)
2(2V18)	4(4V18)	0.9(±0.1)	0.9(±0.1)	0.9(±0.1)

TABLE 4.4.6a

RELATIVE VALUES OF EXPOSURE PARAMETERS FOR RR&A METALLURGY SPECIMENS IN THE PVS CAPSULES WITH RESPECT TO UK DOSIMETRY

SPECIMEN NUMBERS			EXPOSURE RELATIVE TO UK DOSIMETRY
PVS(OT)	PVS($\frac{1}{4}$T)	PVS ($\frac{1}{2}$T)	
R62T	R86T	R84T	0.84
R46	R16	R68	0.85
R47	R17	R69	0.86
R48	R18	R71	0.88
R49	R19	R72	0.89
R51	R21	R73	0.90
R52	R22	R74	0.91
R63T	R87T	R85T	0.84
R53	R23	R76	0.85
R54	R24	R77	0.86
R56	R25	R78	0.88
R57	R26	R79	0.89
R58	R27	R81	0.90
R59	R28	R82	0.91

TABLE 4.4.6b

RELATIVE VALUES OF EXPOSURE PARAMETERS FOR UK SAPPHIRE DAMAGE MONITORS IN THE PVS CAPSULES WITH RESPECT TO UK DOSIMETRY

SAPPHIRE NUMBERS (HOLE)			EXPOSURE RELATIVE TO UK DOSIMETRY
PVS (OT)	PVS ($\frac{1}{4}$T)	PVS ($\frac{1}{2}$T)	
5(E17)	9(4T17)	7(2T17)	0.9 - 0.7
6(E18)	10(4T18)	8(2T18)	0.9 - 0.7

4.5 CONSISTENCY OF EXPERIMENTAL DATA AND DERIVED EXPOSURE PARAMETERS - KFA W. Schneider (KFA)

4.5.1 Introduction

The results of the (exclusively radiometric) KFA measurements from the SSC-1 and SSC-2 irradiations in the ORR-PSF Physics-Dosimetry-Metallurgy Experiments (within the LWR Pressure Vessel Surveillance Dosimetry Improvement Program) have been reported in Section 2.3.4 of this NUREG report.

In the following, the results will be given of some further evaluation carried out for checking the consistency of those measurement results. These further results will finally be discussed.

4.5.2 Search for Consistency of the Data

In Lists 3a,b in Section 2.3.4, the measured neutron reactions and the evaluated reaction rates were presented. In List 2 ibid., the corrections applied to the single dosimeters were reported. In particular, for the ^{237}Np dosimeters, other corrections [as mentioned in Ref. (As83b) for ^{238}Pu or even ^{239}Pu fission] proved to be negligible.

The reaction rate R_i to the reaction i has been obtained using the common definitions:

- for activation reactions:

$$R_i = A_{oi} \cdot H(\lambda_i)/N_{io} \qquad (1a)$$

where:

A_{oi} = Measuring activity resulting from reaction i, taken at the end of the irradiation

$H(\lambda_i)$ = Irradiation history correction factor, defined here as usual (cf., e.g., the equivalent presentations in Refs. (As83c,Ne83), depending upon the decay constant λ_i of the measuring nuclide

N_{io} = Number of atoms of the original nuclide of the measuring reaction i in the dosimeter, determined as usual (cf., Lists 1a,b in Section 2.3.4), taken at the beginning (t = 0) of the irradiation

- for fission reactions:

$$R_i = A_{oip} \cdot H(\lambda_p)/N_{io}\, Y_{ip} \qquad (1b)$$

where:

p = Subscript for considered fission product
Y_{ip} = Fission yield for the production of the fission product nuclide p by the measuring reaction i

The other quantities correspond to Eq. (1a).

For checking the consistency of the presented reaction rates, three further quantities have been evaluated:

- The variation of the reaction rates from the SSC-2 to that from the SSC-1 irradiation, respectively (see Table 4.5.1)
- The "neutron spectrum index" of the fast neutron reaction rates for each irradiation and each dosimeter irradiation position (see Tables 4.5.1a,b and Figure 4.5.1)
- The absolute neutron fluence, using an available neutron spectrum conversion factor (see Tables 4.5.2a,b)

The definitions of the mentioned quantities are given in Section 4.5.3; the discussion of the consistency check is reported in Section 4.5.4.

4.5.3 Presentation of the Check Results

The variation of the reaction rates, as given in Table 4.5.1, has the following definition:

$$R(Ri) \equiv \left[\frac{Ri(SSC\text{-}2)}{Ri(SCC\text{-}1)} - 1\right] \cdot 100\% \qquad (2)$$

with R_i according to Eq. (1). The R_i values in the numerator and denominator, respectively, refer to the same dosimeter type. The (1σ) relative uncertainty in Table 4.5.1 results from the error propagation of the relative part of the reaction rate uncertainties.

The neutron spectrum index reported in Tables 4.5.1a,b has been defined as follows:

$$I\left({}_{f}\varphi_{j}\right) \equiv \left[\frac{f\varphi_{j}\ (X,P)}{f\varphi_{Mn}\ (X,P)} - 1\right] \cdot 100\% \qquad (3)$$

where:

j = Those out of the reactions i that respond to fast neutrons
Mn = Reference reaction $^{54}Fe(n,p)^{54}Mn$, fission neutron spectrum equivalent neutron flux density as follows:

TABLE 4.5.1

Date: Jan.1984

Dosimeter description and measurement results from KFA Jülich to LWR-PV-SDIP PSF Specimen Set: SSC-2 to SSC-1

Measured Reaction	Variation of Reaction Rates %	±(1σ) Rel. Uncert. %	Dosimeter	Irradiation Position
Ti (n,x)Sc46	- 5.5	± 2.8	Ti	
Fe54 (n,p)Mn54	+ .2	± 2.7	Fe	
Fe58 (n,γ)Fe59	- .9	± 3.0		Cube "32"
Ni58 (n,p)Co58	- 3.6	± 2.4	Ni	
Sc45 (n,γ)Sc46	+51.2	± 2.8		(Dosimeters without Gd cover)
Sc45 (n,γ)Sc46	+ 5.7	± 3.1	Sc_2O_3 Sc/MgO	
Co59 (n,γ)Co60	- 1.6	± 3.6	Co	
Ag109 (n,γ)Ag110m	- 1.6	± 2.4	Ag	
Cu63 (n,α)Co60	- 2.2	± 2.9	Cu	
Ti (n,x)Sc46	+ .5	± 2.4	Ti	
Fe54 (n,p)Mn54	+ .8	± 2.3	Fe	
Fe58 (n,γ)Fe59	- 4.0	± 2.5		KFA Charpy (Dosimeters with Gd cover)
Ni58 (n,p)Co58	- 5.7	± 2.4	Ni	
U 238(n,f)F.P.	+ 4.4	± 2.6	U-238	
Th232(n,f)F.P.	+ 1.6	± 5.7	Th	
Np237(n,f)F.P.	- 7.1	± 3.7	Np	
Sc45 (n,γ)Sc46	-22.7	± 2.9	Sc	
Co59 (n,γ)Co60	-		Co	
Ag109(n,γ)Ag110m	- 1.6	± 1.6	Ag	
U 235(n,f)F.P.	- 5.0	± 3.1	U-235	

TABLE 4.5.1a

Date: Jan.1984

Dosimeter description and measurement results from KFA Jülich to LWR-PV-SDIP PSF Specimen Set: SSC-1

Measured Reaction	Spectrum Index /A/ %	±(1σ) Uncert. %	Dosimeter	Irradiation Position
Ti (n,x)Sc46	- 11,6	± 9.7	Ti	
Fe54 (n,p)Mn54	/B/6.304 E+12	± 6.7	Fe	
Fe58 (n,γ)Fe59	-			Cube "32"
Ni58 (n,p)Co58	+ 1,3	± 8.8	Ni	
Sc45 (n,γ)Sc46	-			(Dosi-
Sc45 (n,γ)Sc46	-		Sc_2O_3 Sc/MgO	meters without Gd cover)
Co59 (n,γ)Co60	-		Co	
Ag109 (n,γ)Ag110m	-		Ag	
Cu63 (n,α)Co60	+ 5.4	± 13.3	Cu	
Ti (n,x)Sc46	- 9.5	± 9.6	Ti	
Fe54 (n,p)Mn54	/B/5.540 E+12	± 6.8	Fe	
Fe58 (n,γ)Fe59	-			KFA
Ni58 (n,p)Co58	+ 2.0	± 8.8	Ni	Charpy
U 238(n,f)F.P.	+ 32.7	± 8.1	U-238	(Dosi-
Th232(n,f)F.P.	+ 33.0	± 10.7	Th	meters with Gd
Np237(n,f)F.P.	+ 134.0	± 8.6	Np	cover)
Sc45 (n,γ)Sc46	-		Sc	
Co59 (n,γ)Co60	-		Co	
Ag109(n,γ)Ag110m	-		Ag	
U 235(n,f)F.P.	-		U-235	

/A/ according to eq. (3)

/B/ Equivalent Flux Density in $cm^{-2}s^{-1}$, according to eq. (4)

TABLE 4.5.1b

Date: Jan.1984

Dosimeter description and measurement results from KFA Jülich to LWR-PV-SDIP PSF Specimen Set: SSC-2

Measured Reaction	Spectrum Index /A/ %	±(1σ) Uncert. %	Dosimeter	Irradiation Position
Ti (n,x)Sc46	- 16.6	± 9.7	Ti	
Fe54 (n,p)Mn54	/B/6.314 E+12	± 6.8	Fe	
Fe58 (n,γ)Fe59	-			Cube "32"
Ni58 (n,p)Co58	- 2.5	± 8.9	Ni	
Sc45 (n,γ)Sc46	-			(Dosi-
Sc45 (n,γ)Sc46	-		Sc_2O_3 Sc/MgO	meters without Gd cover)
Co59 (n,γ)Co60	-		Co	
Ag109 (n,γ)Ag110m	-		Ag	
Cu63 (n,α)Co60	+ 2.3	± 13.2	Cu	
Ti (n,x)Sc46	- 9.7	± 9.6	Ti	
Fe54 (n,p)Mn54	/B/5.583 E+12	± 6.6	Fe	
Fe58 (n,γ)Fe59	-			KFA
Ni58 (n,p)Co58	- 4.6	± 8.7	Ni	Charpy
U 238(n,f)F.P.	+ 37.5	± 8.0	U-238	(Dosi-
Th232(n,f)F.P.	+ 34.1	± 10.9	Th	meters with Gd
Np237(n,f)F.P.	+ 115.6	± 8.2	Np	cover)
Sc45 (n,γ)Sc46	-		Sc	
Co59 (n,γ)Co60	-		Co	
Ag109(n,γ)Ag110m	-		Ag	
U 235(n,f)F.P.	-		U-235	

/A/ according to eq. (3)

/B/ Equivalent Flux Density in $cm^{-2}s^{-1}$, according to eq. (4)

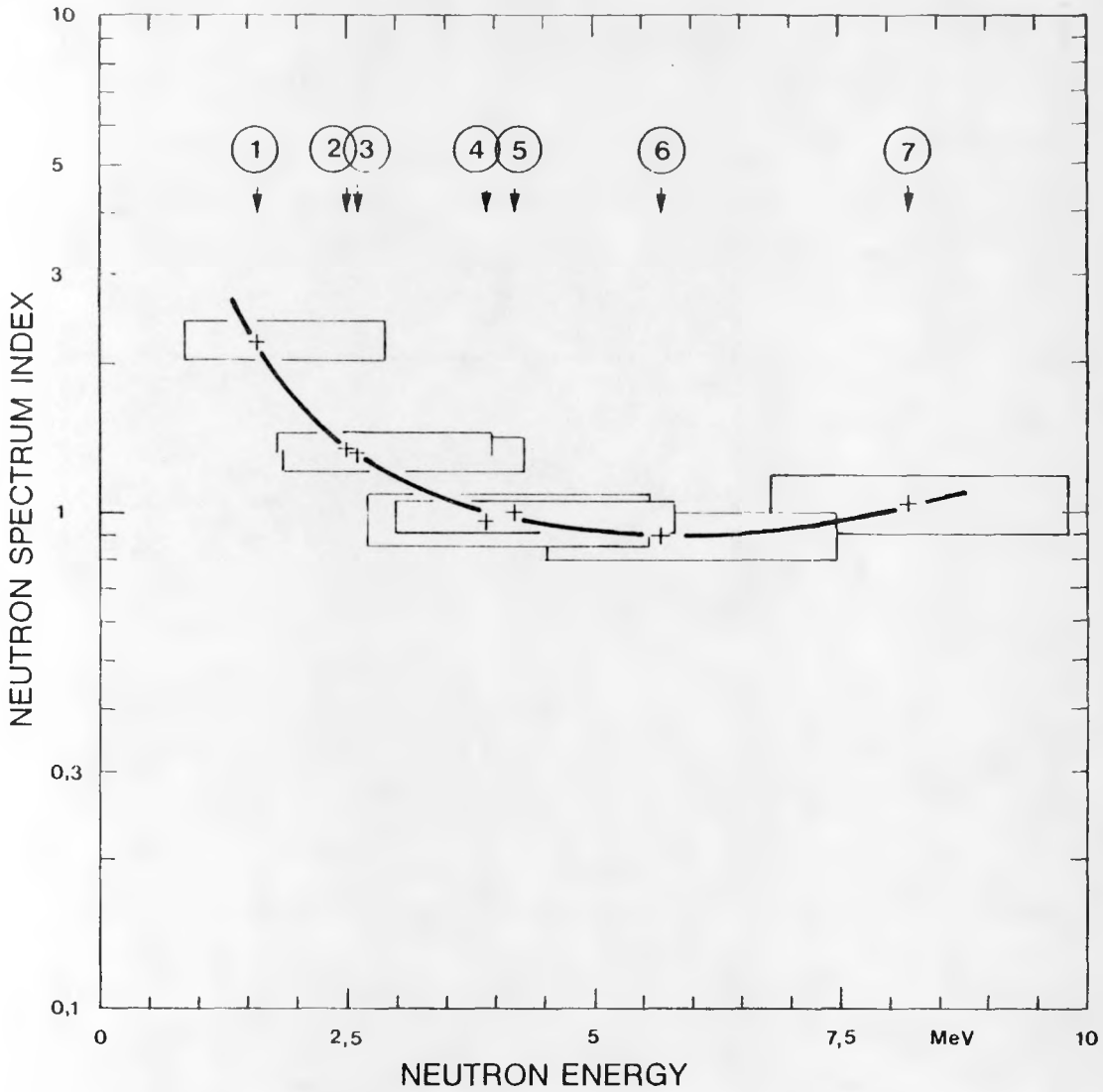

Neutron Spectrum Index

in the "KFA Charpy" Position,
Averaged Over SSC-1 and SSC-2,
for the Following Reactions:

1	Np 237	(n,f)
2	U 238	(n,f)
3	Th 232	(n,f)
4	Ni 58	(n,p)
5	Fe 54	(n,p)
6	Ti	(n,x)
7	Cu 63	(n,α)

FIGURE 4.5.1. Neutron Spectrum Index.

TABLE 4.5.2a

Date: Jan.1984

Dosimeter description and measurement results from KFA Jülich to LWR-PV-SDIP PSF Specimen Set: SSC-1

Measured Reaction	Fluence >1MeV corrected /C/ cm^{-2}	±(1σ)Uncert./D/ %	Dosimeter	Irradiation Position
Ti (n,x)Sc46			Ti	
Fe54 (n,p)Mn54			Fe	
Fe58 (n,γ)Fe59				Cube "32"
Ni58 (n,p)Co58	2.921 E+19	± 2.6	Ni	
Sc45 (n,γ)Sc46				(Dosimeters without Gd cover)
Sc45 (n,γ)Sc46			Sc_2O_3 Sc/MgO	
Co59 (n,γ)Co60			Co	
Ag109 (n,γ)Ag110m			Ag	
Cu63 (n,α)Co60			Cu	
Ti (n,x)Sc46			Ti	
Fe54 (n,p)Mn54			Fe	
Fe58 (n,γ)Fe59				KFA Charpy (Dosimeters with Gd cover)
Ni58 (n,p)Co58	2.583 E+19	± 2.7	Ni	
U 238(n,f)F.P.	2.458 E+19	± 3.1	U-238	
Th232(n,f)F.P.			Th	
Np237(n,f)F.P.	2.443 E+19	± 3.8	Np	
Sc45 (n,γ)Sc46	A v e r a g e /E/:		Sc	
Co59 (n,γ)Co60			Co	
Ag109(n,γ)Ag110m	2.509 E+19	± 2.3	Ag	
U 235(n,f)F.P.			U-235	

/C/ With flux conversion factors by C.A.BALDWIN, cf. eq. (5)

/D/ Solely reaction rate uncertainty considered

/E/ Weighted regarding the /D/ uncertainties

TABLE 4.5.2b

Date: Jan.1984

Dosimeter description and measurement results from KFA Jülich to LWR-PV-SDIP PSF Specimen Set: SSC-2

Measured Reaction	Fluence >1MeV corrected /C/ cm^{-2}	±(1σ) Uncert./D/ %	Dosimeter	Irradiation Position
Ti (n,x)Sc46			Ti	
Fe54 (n,p)Mn54			Fe	
Fe58 (n,γ)Fe59				Cube "32"
Ni58 (n,p)Co58	5.783 E+19	± 2.8	Ni	
Sc45 (N,γ)Sc46				(Dosimeters without Gd cover)
Sc45 (n,γ)Sc46			Sc_2O_3 Sc/MgO	
Co59 (n,γ)Co60			Co	
Ag109 (n,γ)Ag110m			Ag	
Cu63 (n,α)Co60			Cu	
Ti (n,x)Sc46			Ti	
Fe54 (n,p)Mn54			Fe	
Fe58 (n,γ)Fe59				KFA Charpy (Dosimeters with Gd cover)
Ni58 (n,p)Co58	5.006 E+19	± 2.7	Ni	
U 238(n,f)F.P.	5.274 E+19	± 3.1	U-238	
Th232(n,f)F.P.			Th	
Np237(n,f)F.P.	4.663 E+19	± 3.1	Np	
Sc45 (n,γ)Sc46	Average /E/:		Sc	
Co59 (n,γ)Co60			Co	
Ag109(n,γ)Ag110m	4.981 E+19	± 3.4	Ag	
U 235(n,f)F.P.			U-235	

/C/ With flux conversion factors by C.A.BALDWIN, cf. eq (5)

/D/ Solely reaction rate uncertainty considered

/E/ Weighted regarding the /D/ uncertainties

$$ {}_f\varphi_i \equiv R_j / \sigma_j^f \qquad (4) $$

σ_j^f = Cross section for reaction j, averaged over the fission neutron spectrum according to integral measurements by Fabry et al. (compiled in Ref. (Zi79, Part I, Table 4).

The numerator and the denominator in Eq. (3) are by definition related to the same parameters X,P, i.e., to the same irradiation (X = SSC-1 or X = SSC-2) and to the same dosimeter irradiation position (P = Cube 32 or P = KFA Charpy). The (1σ) uncertainties reported in Tables 4.5.1a,b result from the (absolute) reaction rate uncertainties and from the uncertainties reported by Fabry et al. (Zi79).

In Figure 4.5.1 a curve is presented for showing the slope of the neutron spectrum index $I({}_f\varphi_j)$ as a function of the neutron energy E. For a graphical presentation we could not but restrict ourselves to averages (in the KFA Charpy position) over the SSC-1 and SSC-2 results since the difference between these results was too small. The arrows at reactions j = 1 to 7 point to the median energies E_j for a MTR neutron spectrum (Zi79); the rectangles in Figure 4.5.1 show the uncertainty windows for reactions j = 1 to 7, opened by the measurement uncertainty (as in Tables 4.5.1a,b and by the 60% energy response range [correspondingly from (Zi79)].

In Tables 4.5.2a,b are given neutron fluence values evaluated for those (k) out of the measured reactions i for which neutron spectrum "conversion factors" have been made available, as follows:

$$ {}_c\Phi_k \ (>1 \text{ MeV}) = {}_f\Phi_k \cdot C_k \qquad (5a) $$

where:

${}_c\Phi_k$ = Neutron fluence corrected for the spectrum for reaction k
${}_f\Phi_k$ = Fission spectrum equivalent neutron fluence for reaction k
C_k = Conversion factor for reaction k

For the conversion factor, we made use of

$$ C_k = [\varphi^C \ (>1 \text{ MeV}) / \varphi_f^C \ ]_k \qquad (5b) $$

according to C. A. Baldwin's calculation [in (Mc80a), Appendix 3-D, Table 3]. We assumed this same C_k for both SSC irradiations and for both dosimeter positions. The fission spectrum equivalent neutron fluences, as applied in Eq. (5a,b), have been determined as usual:

$$f\varphi_k = f\varphi_k \cdot t_I \qquad (6)$$

with the cumulative irradiation time t_I and accordingly to Eq. (4) but for the sake of comparison using here the fission spectrum averaged cross sections from (Mc80a, Appendix 3-D, Table 4) for the σ_k^f.

4.5.4 Discussion

Looking through the obtained reaction rate variations from the SSC-1 to the SSC-2 irradiation in Table 4.5.1. With two exceptions they are in satisfying agreement with the relative uncertainties reported to them. So at first one may conclude that the neutron flux density level was (at least approximately) the same for both the SSC irradiations. Furthermore, it can be seen that no different systematic errors appeared between both measurement series.

For two dosimeter types, however, there were found larger variations in the reaction rates than expected from the uncertainties, i.e., for:

- The Sc_2O_3 dosimeters (in the Cube 32 position)
- The (metallic) Sc dosimeters (in the KFA Charpy position)

Causes for the large variations that were found apparently can neither be seen in problems with the $^{45}Sc(n,\gamma)$ reaction nor in the radiometric measurement. Presumably both the variations resulted from a damage or corrosion of (in any case two out of) the dosimeters before, during, or after the irradiation. Bearing in mind that surely the dosimeter preparation as well as the irradiation procedure were carried out with the highest possible care, we must wonder whether both these dosimeter types should in the future be considered as satisfyingly suitable ones for irradiations such as we are dealing with here. Assuming that the flux density level as well as the neutron spectrum in both SSC irradiations were identical, we compared neutron flux densities estimated from all the obtained reaction rates of the "slow neutron" dosimeters. In consequence of statistically significant deviations, we found that the following reaction rates reported in Section 2.3.4 should be deleted:

- in List 3a (for SSC-1): R_i - 5.147 E-11 1/s for the Sc_2O_3 dosimeter
- in List 3b (for SSC-2): R_i = 1.281 E-11 1/s for the (metallic) Sc dosimeter

The differences in the neutron spectrum indices between the measurements from both SSC irradiations turned out to be small and in concordance with the reported uncertainties (cf. Tables 4.5.1a,b). The consistency of the

spectrum indices (and so of the reaction rates belonging to them) can be seen as proved by its behavior as a steady function $I(E_j)$ (see Figure 4.5.1). This function has a curved downwards trend, which means that the neutron spectrum has been weakened in comparison with the fission neutron spectrum (i.e., with I = const = 1). The grade of this weakening is governed by the mass of material (in our case: iron), which causes inelastic neutron scattering processes between the fission neutron source (the ORR) and the measuring position.

The neutron fluence values given in Tables 4.5.2a,b fit together from the statistical point of view concerning each irradiation and each dosimeter position. If we assume equal flux densities over both SSC irradiations, as we may infer from the reaction rate ratios and from the neutron spectrum index comparison, the variations of the fluence ratios will amount to:

- 3.7% in Cube 32 position compared with
- 3.4% for the average in KFA Charpy position

where:

$$t_I(2)/t_I(1) = 7.955_5/3.871_0 \qquad (7)$$

= Ratio of cumulative irradiation times (in 10^6 s) of SSC-2 to SSC-1 irradiation, respectively (Gu84d)

5.0 BIBLIOGRAPHY

(Al79a) A. A. Alberman, J. P. Jenthon, L. Lariviere, P. Leger, M. Salon and M. Phierry, "Miniaturised Tungsten Damage Monitor," Proc. of CEA Conference, France, DCEN/FPF/EAR/79/099, p. 4734, 1979.

(As83a) ASTM E910-82, "Standard Method for Application and Analysis of Helium Accumulation Fluence Monitors for Reactor Vessel Surveillance," 1983 Annual Book of ASTM Standards, American Society for Testing and Materials, Philadelphia, PA, Section 12, Volume 12.02, pp. 761-774, 1983.

(As83b) ASTM E844, "Standard Guide for Sensor Set Design and Irradiation for Reactor Surveillance," Annual Book of ASTM Standards, American Society for Testing and Materials, Philadelphia, PA, Volume 12.02, current edition.

(As83c) ASTM E263-82, "Standard Method for Determining Fast-Neutron Flux Density by Radioactivation of Iron," 1983 Annual Book of ASTM Standards, American Society for Testing and Materials, Philadelphia, PA, Volume 12.02, 1983.

(As85b) ASTM E944, "Standard Guide for Application of Neutron Spectrum Adjustment Methods," Annual Book of ASTM Standards, American Society for Testing and Materials, Philadelphia, PA, current edition.

(As85f) ASTM E1035, "Standard Practice for Determining Radiation Exposure for Nuclear Reactor Support Structures, "Annual Book of ASTM Standards, American Society for Testing and Materials, Philadelphia, PA, current edition.

(Au85) M. Austin, A. Dolan and A. F. Thomas, "A Comparative Analysis of the Oak Ridge PCA and NESDIP PCA Replica Experiments Using the LONDON Adjustment Technique," Proc. of the 5th ASTM-EURATOM Symposium on Reactor Dosimetry, Geesthacht, Federal Republic of Germany, September 24-28, 1984, EUR 9869, Commission of the European Communities, 1985.

(Ba83a) C. A. Baldwin and F. B. K. Kam, ORR-Surveillance Dosimetry Measurement Facility (ORR-SDMF) Simulated Surveillance Capsule Perturbation Test, NUREG/CR-3341, Vol 2, HEDL-TME 83-22, NRC, Washington, DC, pp. ORNL-4 - ORNL-10, April 1984.

(Ba84a) C. A. Baldwin and F. B. K. Kam, "ORR-Surveillance Dosimetry Measurement Facility (ORR-SDMF) Simulated Surveillance Capsule Perturbation Experiment," LWR-PV-SDIP: Quarterly Progress Report, April 1983 - June 1983, NUREG/CR-3391, Vol. 2, HEDL-TME 83-22, pp. ORNL-9 - ORNL-25, April 1984.

(Be82) D. E. Bendall and R. J. Brissenden, "McBend Program User Guide WRS Modular Code," Trans. Am. Nucl. Soc. 41, pp. 332-333, 1982.

(Bu84) J. Butler, M. D. Carter, I. J. Curl, M. R. March, A. K. McCracken, M. F. Murphy and A. Packwood, The PCA Replica Experiment Part I: Winfrith Measurements and Calibrations, NUREG/CR-3324, AEEW-R 1736, Part I, NRC, Washington, DC, January 1984.

(Co83) L. E. Collins, Analysis of the Behavior of Advanced Reactor Pressure Vessel Steels Under Neutron Irradiation: The UK Programme, L. M. Davies, Ed., UKAEA, UK, p. 98, 1983.

(Cu78) J. G. Cuninghame, "Status of Fission Product Yield Data," Fission Product Nuclear Data - 1977, IAEA-213, Vol. I, International Atomic Energy Agency, Vienna, Austria, pp. 351-419, 1978.

(Cu82) D. E. Cullen et al., "The IAEA International Reactor Dosimetry File (IRDF-82)," Proc. of the 4th ASTM-EURATOM Symposium on Reactor Dosimetry, Gaithersburg, MD, March 22-26, 1982, NUREG/CP-0029, Vol. 2, NRC, Washington, DC, pp. 917-927, July 1982.

(En67) W. W. Engle Jr, A User's Manual for ANISN, A One-Dimensional Discrete Ordinates Transport Code with Anisotropic Scattering, K-1693, Union Carbide Corp., Oak Ridge, TN, 1967.

(Fa76) A. Fabry et al., "Review of Microscopic Integral Cross Section Data in Fundamental Dosimetry Benchmark Neutron Fields," Neutron Cross Sections for Reactor Dosimetry, IAEA-208, Vol. 1, International Atomic Energy Agency, Vienna, Austria, p. 233, November 1976.

(Fa86) Harry Farrar IV and B. M. Oliver, "A Mass Spectrometer System to Determine Very Low Levels of Helium in Small Solid and Liquid Samples," J. Vac. Sci. Technol. A 4, p. 1740, 1986.

(Ga76) T. A. Gabriel, J. D. Gurney and N. M. Greene, Radiation-Damage Calculations: Primary Recoil Spectra, Displacement Rates, and Gas-Production Rates, ORNL/TM-5160, Oak Ridge National Laboratory, Oak Ridge, TN, March 1976.

(Gi85) D. M. Gilliam, J. A. Grundl, G. P. Lamaze, E. D. McGarry and A. Fabry, "Cross-Section Measurements in the ^{235}U Fission Spectrum Neutron Field," Proc. of the 5th ASTM-EURATOM Symposium on Reactor Dosimetry, Geesthacht, Federal Republic of Germany, September 24-28, 1984, EUR 9869, Commission of the European Communities, 1985.

(Go86) R. Gold and W. N. McElroy, "Current Limitations of Trend Curve Analysis for the Prediction of Reactor Pressure Vessel Embrittlement," HEDL-SA-3390, Proc. of the 13th International Symposium on Effects of Radiation on Materials, June 23-25, 1986, Seattle, WA, Hanford Engineering Development Laboratory, Richland, WA, September 1986.

(Go87b) R. Gold, L. S. Kellogg, W. N. McElroy and A. Fabry, "State-of-the-Art of Radiometric Neutron Dosimetry for LWR-PV Surveillance," LWR-PV-SDIP: 1986 Annual Progress Report, NUREG/CR-4307, Vol. 3, HEDL-TME 86-2, NRC, Washington, DC, February 1987.

(Go87c) R. Gold and W. N. McElroy, "Light Water Reactor Pressure Vessel Surveillance Dosimetry Improvement Program (LWR-PV-SDIP): Past Accomplishments, Recent Developments, and Future Directions," Proc. of the 6th ASTM-EURATOM Symposium on Reactor Dosimetry, Jackson Hole, WY, May 31 - June 5 1987.

(Gr79) L. B. Gross, Fabrication Data Package: LWR-PVSIP Dosimeter Capsules, LR:79:2875-01:1, Babcock & Wilcox Company, Lynchburg, VA, p. 1.2-10, June 1979.

(Gu82c) G. L. Guthrie, "Development of Trend Curve Formulas Using Surveillance Data - II," LWR-PV-SDIP: Quarterly Progress Report, April 1982 - June 1982, NUREG/CR-2805, Vol. 2, HEDL-TME 82-19, NRC, Washington, DC, pp. HEDL-3 - HEDL-13, December 1982.

(Gu84d) G. L. Guthrie, E. P. Lippincott and E. D. McGarry, LWR-PV-SDIP: PSF Blind Test Workshop Minutes, HEDL-7467, Hanford Engineering Development Laboratory, Richland, WA, April 9-10, 1984.

(Ha84) J. R. Hawthorne, B. H. Menke and A. L. Hiser, LWR-PV-SDIP: Notch Ductility and Fracture Toughness Degradation of A302-B and A533-B Reference Plates from PSF Simulated Surveillance and Through-Wall Irradiation Capsules, NUREG/CR-3295, MEA-2017, Vol. 1, NRC, Washington, DC, April 1984.

(Ha84a) J. R. Hawthorne and B. H. Menke, LWR-PV-SDIP: Postirradiation Notch Ductility and Tensile Strength Determinations for PSF Simulated Surveillance and Through-Wall Specimen Capsules, NUREG/CR-3295, MEA-2017, Vol. 2, NRC, Washington, DC, April 1984.

(He71) B. Henderson and D. H. Bowen, J. Phys. C. 4, p. 1487, 1971.

(Ho79) N. E. Holden, "Atomic Weights of the Elements, 1977," Pure & Appl. Chem. 51, pp. 405-433, 1979.

(Ka82) F. B. K. Kam, Ed., Proc. of the 4th ASTM-EURATOM Symposium on Reactor Dosimetry, Gaithersburg, MD, March 22-26, 1982, NUREG/CP-0029, Vols. 1 and 2, NRC, Washington, DC, July 1982.

(Ke82) L. S. Kellogg and E. P. Lippincott, "PSF Interlaboratory Comparison," Proc. of the 4th ASTM-EURATOM Symposium on Reactor Dosimetry, Gaithersburg, MD, March 22-26, 1982, NUREG/CP-0029, Vol. 2, CONF-820321/V2, NRC, Washington, DC, pp. 929-945, July 1982.

(Ke85) L. S. Kellogg, W. N. McElroy, W. Y. Matsumoto, R. Gold, C. C. Preston, R. L. Simons, J. H. Roberts, B. M. Oliver and H. Farrar IV, Evaluation of Reactor Cavity and Surveillance Capsules S and T Dosimetry from Turkey Point Unit 3, HEDL-7576, Westinghouse Hanford Co., Richland, WA, December 1985.

(Li81) E. P. Lippincott, W. M. McElroy, L. S. Kellogg et al., Fabrication Data Package for HEDL Dosimetry in the ORNL Poolside Facility LWR-PV Mockup Irradiation, HEDL-TC-2065, Cleared 2/23/82, Hanford Engineering Development Laboratory, Richland, WA, September 1981.

(Li86) E. P. Lippincott and R. L. Simons, "HEDL-Recommended Exposure Parameter Values for the PSF Blind Test," Appendix B, LWR-PV-SDIP: PSF Experiments Summary and Blind Test Results, NUREG/CR-3320, Vol. 1, HEDL-TME 86-8, NRC, Washington, DC, July 1986.

(Li87) E. P. Lippincott et al., Evaluation of Surveillance Capsule and Reactor Cavity Dosimetry from H. B. Robinson Unit 2, Cycle 9, WCAP-11104, NUREG/CR-4576, Westinghouse-Nuclear Technology Division, Pittsburgh, PA, February 1987.

(Ma82) N. Maene, R. Menil, G. Minsart and L. Ghoos, "Gamma Dosimetry and Calculations," Proc. of the 4th ASTM-EURATOM Symposium on Reactor Dosimetry, Gaithersburg, MD, March 22-26, 1982, NUREG/CP-0029, Vol. 1, NRC, Washington, DC, pp. 355-363, July 1982.

(Ma82b) P. Mas and R. Perdreau, "Caracterisation d' Emplacements d'Irradiation en Spectres Neutroniques et en Dommages," Proc. of the 4th ASTM-EURATOM Symposium on Reactor Dosimetry, Gaithersburg, MD, March 22-26, 1982, NUREG/CP-0029, Vol. 2, NRC, Washington, DC, pp. 847-854, July 1982.

(Ma84a) R. E. Maerker and B. A. Worley, Activity and Fluence Calculations for the Startup and Two-Year Irradiation Experiments Performed at the Poolside Facility, NUREG/CR-3886, ORNL/TM-9265, NRC, Washington, DC, October 1984.

(Ma84b) R. E. Maerker and B. A. Worley, "Calculated Spectral Fluences and Dosimeter Activities for the Metallurgical Blind Test Irradiations at the ORR-PSF," Proc. of the 5th ASTM-EURATOM Symposium on Reactor Dosimetry, Geesthacht, Federal Republic of Germany, September 24-28, 1984, EUR 9869, Commission of the European Communities, 1985.

(Ma85a) R. E. Maerker et al., Revision and Expansion of the Data Base in the LEPRICON Dosimetry Methodology, EPRI NP-3841, RP1399-01, Electric Power Research Institute, Palo Alto, CA, January 1985.

(Ma86) R. E. Maerker et al., Application of the LEPRICON Methodology to the Arkansas Nuclear One-Unit Reactor, EPRI NP-4469, Electric Power Research Institute, Palo Alto, CA, February 1986.

(Mc67) W. N. McElroy, S. Berg and T. Crocket, A Computer-Automated Iterative Method of Neutron Flux Spectra Determined by Foil Activation, AFWL-TR-67-41, Vol. I-IV, Air Force Weapons Laboratory, Kirkland AFB, NM, July 1967.

(Mc75d) C. W. J. McCallien, Snap-3D, UKAEA-Risley TRG Report 2677(R), H. M. Stationery Office, UK, October 1975.

(Mc80) W. N. McElroy et al., LWR-PV-SDIP: 1979 Annual Report, NUREG/CR-1291, HEDL-SA-1949, NRC, Washington, DC, February 1980.

(Mc80a) W. N. McElroy et al., "NRC Metallurgy and Materials Research Branch LWR-PV-SDIP Review Graphics," HEDL-SA-2225, and Proc. of the 8th WRSR Information Meeting, Gaithersburg, MD, October 27-31, 1980.

(Mc81) W. N. McElroy, Ed., LWR-PV-SDIP: PCA Experiments and Blind Test, NUREG/CR-1861, HEDL-TME 80-87, NRC, Washington, DC, July 1981.

(Mc83) J. P. McNeece, R. Gold, D. D. Preston and J. H. Roberts, "Automated Scanning of Solid-State Track Recorders: Computer-Controlled Microscope," Nucl. Tracks 7, pp. 137-140, 1983.

(Mc83d) W. N. McElroy and F. B. K. Kam, PSF Blind Test Instructions and Data Packages, HEDL-7448, Hanford Engineering Development Laboratory, Richland, WA, April 1983.

(Mc83g) A. K. McCracken and A. Packwood, The Spectral Unfolding Program SENSAK, DPT/SC/P(83)13, UKAEA, Winfrith, UK, 1983.

(Mc84b) W. N. McElroy and F. B. K. Kam, Eds., PSF Blind Test SSC, SPVC, and SVBC Physics-Dosimetry-Metallurgy Data Packages, HEDL-7449, Hanford Engineering Development Laboratory, Richland, WA, February 1984.

(Mc84c) W. M. McElroy et al., LWR-PV-SDIP: Semiannual Progress Report, October 1983 - March 1984, NUREG/CR-3746, Vol. 1, HEDL-TME 84-20, NRC, Washington, DC, November 1984.

(Mc84i) W. N. McElroy, LWR-PV-SDIP: PCA Experiments, Blind Test, and Physics-Dosimetry Support for the PSF Experiments, NUREG/CR-3318, HEDL-TME 84-1, NRC, Washington, DC, September 1984.

(Mc86) W. N. McElroy et al., Trend Curve Data Development and Testing, MC2-TR-86-10, HEDL-7591, Metrology Control Corporation and Hanford Engineering Development Laboratory, Richland, WA, March 1986 and HEDL-SA-3400, Proc. of the 13th International Symposium on the Effects of Radiation on Materials, June 23-25, 1986, Seattle, WA, Metrology Control Corporation and Hanford Engineering Development Laboratory, Richland, WA, September 1986.

(Mc86b) W. N. McElroy, Ed., LWR-PV-SDIP: PSF Experiments Summary and Blind Test Results, NUREG/CR-3320, Vol. 1, HEDL-TME 86-8, NRC, Washington, DC, July 1986.

(Mc87) W. N. McElroy, LWR-PV-SDIP: 1986 Annual Progress Report, NUREG/CR-4307, Vol. 3, HEDL-TME 86-2, NRC, Washington, DC, February 1987.

(Mc87e) W. N. McElroy, Ed., LWR-PV-SDIP: LWR Power Reactor Surveillance Physics-Dosimetry Data Base Compendium, NUREG/CR-3319, HEDL-TME 85-3, Hanford Engineering Development Laboratory, Richland, WA, March 1987 Update.

(Mi81) L. F. Miller, Analysis of the Temperature Data from the ORR-PSF Irradiation Experiment: Methodology and Computer Software, NUREG/CR-2273, ORNL/TM-7766, NRC, Washington, DC, November 1981.

(Mo78) W. C. Morgan, Ed., Proc. of the 2nd ASTM-EURATOM Symposium on Reactor Dosimetry, Palo Alto, CA, October 3-7, 1977, NUREG/CP-0004, Vols. 1-3, NRC, Washington, DC, 1978.

(Mu76) S. F. Mughabghab and D. I. Garber, Neutron Cross Sections, BNL-325, 3rd ed., Brookhaven National Laboratory, Upton, NY, Vol. I, 1973, Vol. II, 1976.

(Ne83) Neutronenfluenzmessung, Teil 1: "Bestimmung der Fluenz schneller Neutronen mit Aktivierungs- und Spaltungsdetektoren," DIN 25456, Beuth Verlag GmbH, Berlin, Federal Republic of Germany, May 1983.

(Ni72) V. A. Nikolaenko, V. I. Karpukhin and S. I. Alekseev, Use of Diamond as a Reference Standard for Irradiation Conditions, IAE-1650, Kurchatov Institute of Atomic Energy, Moscow, USSR, English translation in HaP41972y, Harwell, UK.

(Oli83) B. M. Oliver, Helium Analysis of Samples from Maine Yankee and HFBR, Informal Report 83ESG-5544, Rockwell International, Energy Systems Group, Canoga Park, CA, September 22, 1983.

(Oli84) B. M. Oliver and H. Farrar, "Application of Helium Accumulation Fluence Monitors (HAFM) to LWR Surveillance," LWR-PV-SDIP: Quarterly Progress Report, April 1983 - June 1983, NUREG/CR-3391, Vol. 2, HEDL-TME 83-22, NRC, Washington, DC, pp. RI-3 - RI-5, April 1984.

(Oli84a) B. M. Oliver, J. G. Bradley and Harry Farrar IV, "Helium Concentration in the Earth's Lower Atmosphere," Geochim. Cosmochim. Acta 48, p. 1759, 1984.

(Pe82) G. P. Pells, A. J. Fudge, M. J. Murphy and M. Wilkins, "An Investigation into the Use of Sapphire as a Fast Neutron Damage Monitor," Proc. of the 4th ASTM-EURATOM Symposium on Reactor Dosimetry, Gaithersburg, MD, March 22-26, 1982, NUREG/CP-0029, Vol. 1, NRC, Washington, DC, pp. 331-344, July 1982.

(Pe86) J. S. Perrin, Simulated Void Box Capsule (SVBC) Charpy Impact Test Results, EPRI NP-4630, NUREG/CR-3320, Vol. 5, Electric Power Research Institute, Palo Alto, CA, August 1986.

(Pe87) G. P. Pells, A. J. Fudge and M. J. Murphy, "The Use of Sapphire as a Neutron Damage Monitor for Pressure Vessel Steels," Proc. of the 6th ASTM-EURATOM Symposium on Reactor Dosimetry, Jackson Hole, WY, May 31 - June 5, 1987.

(Ro80) H. Röttger, Ed., Dosimetry Methods for Fuels, Cladding, and Structural Materials: Proc. of the 3rd ASTM-EURATOM Symposium on Reactor Dosimetry, Ispra, Italy, October 1-5, 1979, EUR 6813, Vols. I and II, Commission of the European Communities, 1980.

(Sa72) L. Salmon and D. V. Booker, FATAL - A General Purpose Computer Program for Fitting Experimental Data to Any Required Function, AERE-R-7129, Atomic Energy Research Establishment, Harwell, UK, 1972.

(Sc79) F. A. Schmittroth, FERRET Data Analysis Code, HEDL-TME 79-40, Hanford Engineering Development Laboratory, Richland, WA, September 1979.

(Sc86a) W. Schneider et al., Report on the Nuclear Radiation Measurements in KFA Jülich in the Frame of the Pressure Vessel Survillance Dosimetry Improvement Program (PVSDIP), KFA-ZBB-1B-14/86, Kernforschungsanlage Jülich GmbH, Federal Repulic of Germany, September 1986.

(Se81) W. Seelmann-Eggebert, G. Pfennig et al., Karlsruher Nuklidkarte, 5th ed., Kernforschungszentrum Karlsruhe, Federal Republic of Germany, 1981.

(Si82a) R. L. Simons et al., "Re-evaluation of the Dosimetry for Reactor Pressure Vessel Surveillance Capsules," Proc. of the 4th ASTM-EURATOM Symposium on Reactor Dosimetry, Gaithersburg, MD, March 22-26, 1982, NUREG/CP-0029, Vol. 2, NRC, Washington, DC, pp. 903-916, July 1982.

(St82) F. W. Stallmann, "Workshop on Adjustment Codes and Uncertainties," Proc. of the 4th ASTM-EURATOM Symposium on Reactor Dosimetry, Gaithersburg, MD, March 22-26, 1982, NUREG/CP-0029, Vol. 2, NRC, Washington, DC, pp. 1219-1220, July 1982.

(St84) F. W. Stallmann, Determination of Damage Exposure Parameter Values in the PSF Metallurgical Irradiation Experiment, NUREG/CR-3814, ORNL/TM-9166, Oak Ridge National Laboratory, Oak Ridge, TN, 1984.

(St84a) F. W. Stallmann, "LSL-M1 and LSL-M2: Two Extensions of the LSL Adjustment Procedure for Including Multiple Spectrum Locations," Proc. of the 5th ASTM-EURATOM Symposium on Reactor Dosimetry, Geesthacht, Federal Republic of Germany, September 24-28, 1984, EUR 9869, Commission of the European Communities, 1985.

(St84b) F. W. Stallmann, Statistical Evaluation of the Metallurgical Test Data in the ORR-PSF-PVS Irradiation Experiment, NUREG/CR-3815, ORNL/TM-9207, NRC, Washington, DC, August 1984.

(St84d) F. W. Stallmann, "Determination of Damage Exposure Parameter Values in the PSF Metallurgical Irradiation Experiment," LWR-PV-SDIP: PSF Blind Test Workshop Minutes, HEDL-7467, Appendix D, Hanford Engineering Development Laboratory, Richland, WA, 1984.

(To80) H. Tourwé and N. Maene, "Fast Neutron Fluence Measurement with the ^{93m}Nb(N,n')^{93m}Nb Reaction," Proc. of the 3rd ASTM-EURATOM Symposium on Reactor Dosimetry, Ispra, Italy, October 1-5, 1979, EUR 6813, Commission of the European Communities, 1980.

(To82a) H. Tourwé et al., "Interlaboratory Comparison of Fluence Neutron Dosimeters in the Frame of the PSF Start-Up Measurement Programme," Proc. of the 4th ASTM-EURATOM Symposium on Reactor Dosimetry, Gaithersburg, MD, March 22-26, 1982, NUREG/CP-0029, Vol. 1, NRC, Washington, DC, pp. 159-168, July 1982.

(Ve80) V. V. Verbinski, C. G. Cassapakis, W. K. Hagen and G. L. Simmons, "Photointerference Corrections in Neutron Dosimetry for Reactor Pressure Vessel Lifetime Studies," Nucl. Sci. & Eng. 75, p. 159, 1980.

(We83) L. Weise, Neutron Spectra Unfolding from Measured Detector Activations, Jul-1837, in German, Kernforschungsanlage Jülich, Federal Republic of Germany, 1983.

(Wi68) R. S. Wilks, "Neutron-Induced Damage in BeO, Al_2O_3 and MgO - A Review," J. Nucl. Mater. 26, p. 137, 1968.

(Zi79) W. L. Zijp and J. H. Baard, Nuclear Data Guide for Reactor Neutron Metrology, EUR 7167, Parts I and II, Energieonderzoek Centrum Nederland (Energy Research Center Netherlands), Petten, The Netherlands, August 1979.

(Zi83) W. L. Zijp et al., Final Report on REAL-80 Exercise, ECN-128, Energieonderzoek Centrum Nederland (Energy Research Center Netherlands), Petten, The Netherlands, February 1983.

A P P E N D I X A

HEDL RADIOMETRIC MEASUREMENTS IN THE PSF EXPERIMENTS

APPENDIX A

HEDL RADIOMETRIC MEASUREMENTS IN THE PSF EXPERIMENTS

L. S. Kellogg, W. Y. Matsumoto, J. M. Ruggles, W. N. McElroy, R. Gold

A1 INTRODUCTION

A1.1 PSF Tests and Radiometric Measurements

This appendix provides the necessary references and/or documentation for all HEDL radiometric (RM) measurements associated with the PSF experiments.

Not including the first 18-day Simulated Dosimetry Measurement Facility (SDMF-1) and other startup tests, six test irradiations have been performed in the ORNL ORR-PSF Benchmark Facility in support of the NRC LWR-PV-SDIP Program. These consisted of:

1) SDMF-2 Westinghouse Surveillance Capsule Perturbation Test

2) Simulated Surveillance Capsule Metallurgical Test 1 (SSC-1)

3) Simulated Surveillance Capsule Metallurgical Test 2 (SSC-2)

4) Simulated Pressure Vessel Capsule (SPVC) [zero thickness (OT), quarter thickness (QT) and half thickness (HT) positions] and Simulated Void Box Capsule (SVBC) Metallurgical Test

5) SDMF-3 Babcock and Wilcox Surveillance Capsule Perturbation Test

6) SDMF-4 SPVC-SVBC RM, SSTR, HAFM, and DM Dosimetry Test

All HEDL-RM measurements have been completed and reported to ORNL and other LWR-PV-SDIP participants, with the exception of the SVBC-RM results reported herein.

A1.2 State-of-the-Art of Radiometric Neutron Dosimetry for LWR-PV Surveillance

In Reference (Go87b), Gold et al. studied the current state-of-the-art of radiometric neutron dosimetry for LWR-PV surveillance. It was concluded that: "While the agreement among the majority of the laboratories participating in the RM-I* and RM-II* interlaboratory comparisons is generally satisfactory, with nonfissile dosimeter results generally falling within ±5% and the fissionable dosimeter results falling within ±10%, improvement is still required in order to routinely meet accuracy goals of LWR-PV surveillance dosimetry. Improved agreement was attained in the RM-III* experiment,

* RM-I and RM-II are the Section A1.1 SDMF-2 and SSC-1 tests, respectively, while RM-III is the PSF 18-day High-Power Startup Test, SDMF-1.

wherein nonfissile RM monitors generally agreed to better than 2% and fission monitors generally agreed to better than 5%. The results obtained from these tests along with the subsequent corrections indicate that a critical review of both analytical and calculational techniques must be conducted on a periodic basis by all of the laboratories. In addition, it is recommended that each laboratory review and utilize, where possible, the appropriate ASTM Standard Methods and Guides, maintain system calibration and/or control documentation, and continue in this or similar programs using existing benchmark facilities for verifications and direct correlations.

In the RM-I and RM-II experiments, intercomparisons of dosimetry results from six service laboratories have provided experimental estimates of measured reaction rates accuracies. Preliminary results were distributed over a range of relative values as large as 60%. Had results from a single laboratory been used to derive surveillance capsule fluence values (often based on only one or two reactions), a bias of 40% or more could easily have been introduced. Following discussions of the preliminary analysis results and identification of existing problems, these biases were generally reduced to below 15%.

In the RM-III experiment, systematic problems were uncovered with Cu and Nb dosimeters. Any Co impurity in the Cu dosimeters can seriously comprise results. As stressed in earlier dosimetry work with Nb (To80), more accurate cross-section data are needed for the $^{93}Nb(n,n')$ reaction.

An important distinction between the RM-I and RM-II intercomparisons and the RM-III intercomparison must be stressed. The use of HEDL-determined normalization factors reduces the RM-I and RM-II tests to essentially an interlaboratory comparison of absolute gamma-ray counting measurements. However in RM-III, factors that arise in the use of dosimetry materials from different suppliers, such as mass and impurities, were included along with absolute gamma-ray counting measurements. Both types of tests are clearly needed. In fact, interlaboratory RM dosimetry results from the long-term PSF one- and two-year metallurgical irradiations will be used to obtain an additional intercomparison of the type treated here in the RM-III test. Finally, these tests and intercomparisons establish a clear and significant difference in accuracy between fissile and nonfissile RM dosimeters. The important contribution of fast neutrons to PV embrittlement, especially in the region from roughly 0.1 up to 1.0 MeV, makes the use of the threshold fission monitors ^{238}U and ^{237}Np crucial in LWR-PVS dosimetry. The higher uncertainties of fissile RM dosimeters relative to nonfissile RM dosimeters (by about a factor of two) are just barely acceptable, given the goal accuracies of LWR-PVS work. Indeed, there is no fundamental reason that fissile RM dosimeters must possess such considerably higher uncertainties. If anything, these two threshold RM fissile dosimeters generally possess as accurate or more accurate integral cross sections in standard neutron fields than do the fast neutron nonfissile RM dosimeters (Fa76,Gi85,Ma82,Ma82b). Consequently, additional work is clearly needed to resolve systematic effects that are adversely impacting the accuracy of RM dosimetry with fissile monitors."

A2 DOCUMENTATION OF HEDL DOSIMETRY MEASUREMENT RESULTS

A2.1 SDMF-1

All LWR-PV-SDIP RM, SSTR, HAFM, and DM dosimeter measurements results are expected to be documented and/or referenced in NUREG/CR-3320, Volume 2.

A2.2 SDMF-2

All HEDL dosimetry measurement results have been reported to S. Anderson of Westinghouse, W-NTD. A partial tabulation of the results may be found in Reference (Ke82). The remaining HEDL results are expected to be referenced and/or documented in the LWR-PV-SDIP 1987 Annual Report.

A2.3 SSC-1

A tabulation of all HEDL dosimetry measurement results is provided in Table A1; see Appendix B for the FERRET-SAND II analysis results for the mid-point data and Reference (Li86) for a tabulation of the HEDL exposure parameter values for individual Charpy specimens. Also included in Table A1 are the RM results reported by participants in the LWR-PV-SDIP vendor-service laboratory intercomparison.

A2.4 SSC-2

A tabulation of all HEDL dosimetry measurement results is provided in Table A2; see Appendix B for the FERRET-SAND II analysis results for the midpoint data and Reference (Li86) for a tabulation of the HEDL exposure parameter values for individual Charpy specimens.

A2.5 SPVC-SVBC

A tabulation of all HEDL dosimetry measurement results is provided in Table A3; see Appendix B for the FERRET-SAND II analysis results for the SPVC midpoint data and Reference (Li86) for a tabulation of the HEDL exposure parameter values for individual Charpy specimens. A more detailed discussion of the SVBC dosimetry measurement results is provided in Section A3. Appendix B provides the FERRET-SAND II analysis results for the SVBC midpoint data. Also reported in Table A3 are the GE laboratory RM results of their own dosimeters.

A2.6 SDMF-3

All HEDL dosimetry measurement results have been reported to F. Walters of B&W. The HEDL results are expected to be referenced and/or documented in the LWR-PV-SDIP 1987 Annual Report.

A2.7 SDMF-4

All LWR-PV-SDIP RM, SSTR, HAFM, and DM dosimetry measurements results are expected to be documented and/or referenced in NUREG/CR-3321.

A3 SVBC DOSIMETRY MEASUREMENT RESULTS

Because of the inadvertant flooding of the void box (VB) of the SVBC and the perturbation and reduction in magnitude of the SVBC fluence-spectra, a final analysis of the void box dosimetry data was never completed. The recent publication by Perrin (Pe86) of the SVBC Charpy shift metallurgical results increased interest in completing the HEDL analysis and documentation of the physics-dosimetry for this experiment. As stated above, a tabulation of the HEDL-SVBC dosimetry measurement results is provided in Table A3 and Appendix B provides the FERRET-SAND II analysis results for the SVBC data (HB-12 location).

A3.1 SVBC Assembly

A mistake in the as-built documentation (Mc84b,Mc86b) of the relative core orientation for the SVBC was found. Figures A1 and A2 are copies of the ORR-SVBC drawings showing the VB assembly and the individual Charpy specimen placement. Notes have been added to each drawing showing assembly characteristics that indicate the initial core orientation depiction was reversed. This had been noted previously and the corrected x,y,z coordinates were given to LWR-PV-SDIP participants.

A3.2 Radiometric Analysis of the SVBC Dosimeters

The extremely low dosimeter sensor activities observed at HEDL, due to the low neutron exposure and long decay of sensor activities, resulted in a limited analysis of the individual SVBC dosimeter sensors. This analysis included the HB-12 dosimetry capsule sensors, some of the bare axial gradient samples, and the four iron gradient wires. (However, the total number of samples and their low activity precluded high-precision counting of the ^{54}Mn gradient wire samples). The gradient Id's listed as R-4, R-3, L-2, L-1 in the as-built are listed in Table A-3 as S-4, S-3, N-2 and N-1 respectively due to: 1) Reversal of orientation of assembly and, 2) Change of designation to North and South rather than Right and Left to eliminate ambiguity.

Comparative plots of the bare vertical axial gradient wire dosimetry for four SVBC sensor reactions are presented in Figures A3 through A6. A review of these data make it apparent that the vertical axial flux profile in the SVBC was completely different from that observed in the SPVC. Though some vertical asymmetry from a cosine distribution was observed in the SSC and SPVC axial profiles, the SVBC profile possesses no symmetry and rises with increasing axial location.

The cosine fitting of the vertical midplane SSC and SPVC data, Figures A3-A6*, was made with the least-squares computer code FATAL (Sa72) using only those data points from midplane and below. Points above midplane were not used because of the possible contribution from streaming through the upper portion of the SPVC assembly and incomplete VB flooding. Because of decay and low activity, ^{59}Fe data were not available from SVBC for curve fitting.

* The HEDL cosine fit shown here for the SSC and SPVC locations are for illustration only and were not used for gradient corrections (see Appendix C).

The fitting parameters and the statistical parameter values that show the deviations from a cosine fit for the SSC and SPVC data points are given in Table A4. The deviation from a cosine fit for the data points above mid-plane becomes more pronounced in going from the SSC to the SPVC-1/2T to the SVBC position; see Figures A3-A6.

A3.3 Discussion of the SVBC Dosimetry Measurements

Knowledge of the water flooding conditions of the void box was needed to establish the flux time-history for correcting dosimetry sensor-measured time-of-removal activities to saturated activities (reaction rates). Another concern was whether the VB was completely filled with water and, if not, to what degree did this contribute to the above-midplane reaction rate asymmetry indicated in Figures A3-A6. The ratios of short and long-lived reaction products given in Table A5 would suggest the possibility of an incomplete fill of the void box.

ORNL personnel were consulted concerning the VB water fill and were of the general opinion that the flooding commenced within the first month of irradiation, was rapid (possibly within one week), and was complete, though the latter is uncertain. It was only after the completion of the ~2 years of irradiation, that a large and significant amount of water was detected in the void box. Considerable time (estimated as several hours) was required to pressurize all of this water out of the VB assembly. Unfortunately, no measurement was made of the total volume of removed water. The effect of the void space immediately above the SPVC assembly (within the steel filler plates) to allow access for heating and cooling tubes, thermocouples, and electrical heater wires was also discussed with ORNL staff members. An estimate of this void volume was made at one time, but no one could remember the exact estimate of the volume fraction, which might have been as high as 25%. This voidage would be a source for neutron streaming since the SVBC assembly, steel specimens, and dosimetry extend up into this area. Such streaming could contribute to the observed SVBC and SPVC above midplane reaction rate asymmetry. An experiment was performed by ORNL to determine perturbation effects of the SSC on the 1/4T position and possible streaming effects on the SSC (Ba83a); no results have been reported.

To attempt an assessment of the uniformity of the SVBC axial reaction rate profiles during the irradiation, plots of the ^{54}Mn from the gradient wires and axial gradient dosimeters are presented in Figure A7. Prolonged counting times precluded the counting of the iron gradient wire samples to the same precision as the axial iron gradient dosimeters; consequently, the scatter in the gradient wire results is much greater. The N-2 data appear anomalous, but assuming a mix up in the determination of the relative wire orientation, these data appear to be consistent with the other results. It would appear that, at least for the higher energy threshold reactions, an overall data consistancy did exist during the entire irradiation. Because of an approximate factor of 4 difference in the ^{58}Co and ^{54}Mn half-lifes, the ratio of Fe and Ni gradient wire and other data, as given in Table A5, suggests that the rate of water fill was (in all probability) quite rapid; but these data do not eliminate the possibility of an incomplete water fill.

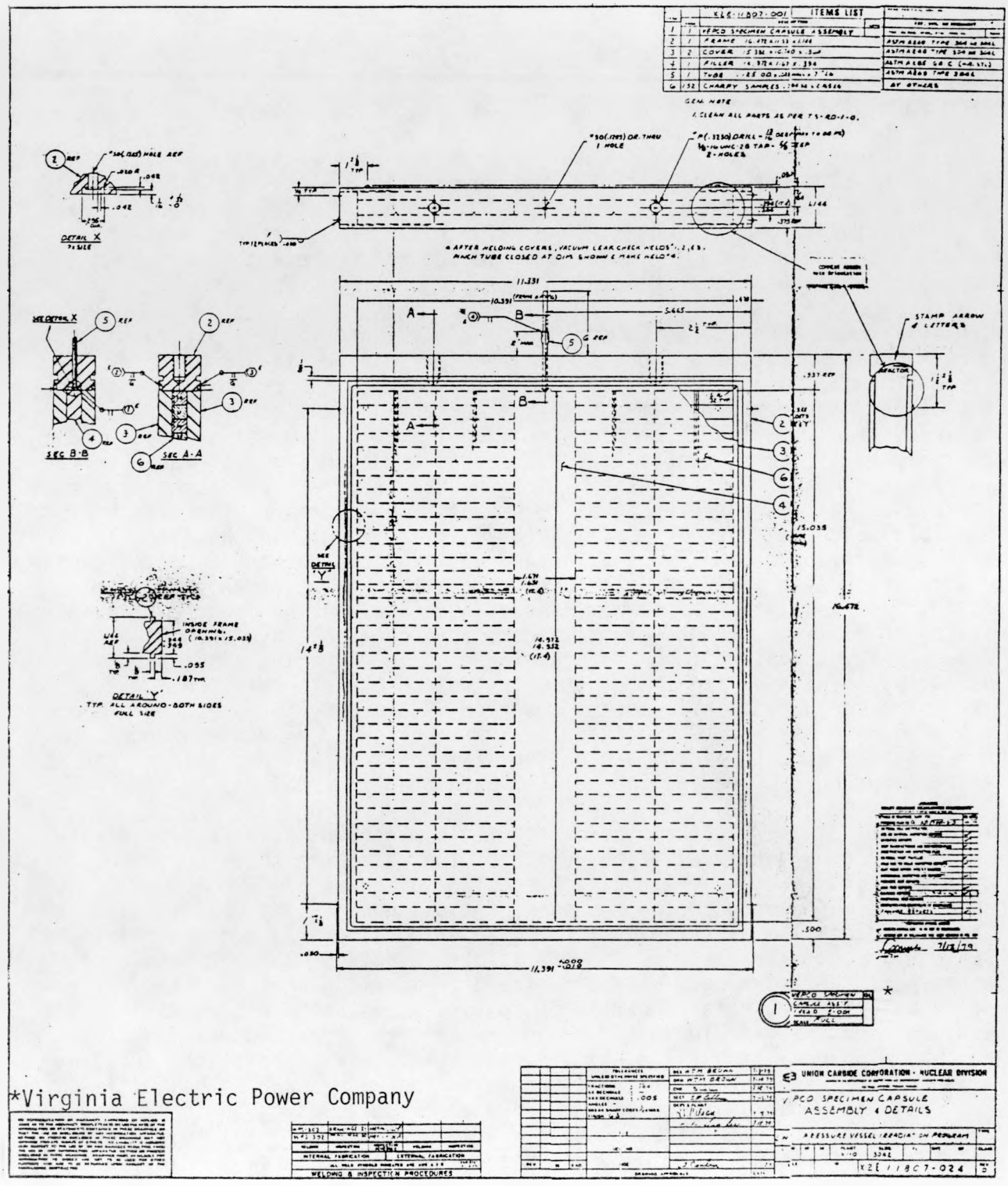

FIGURE A1. Specimen Capsule Assembly and Details.

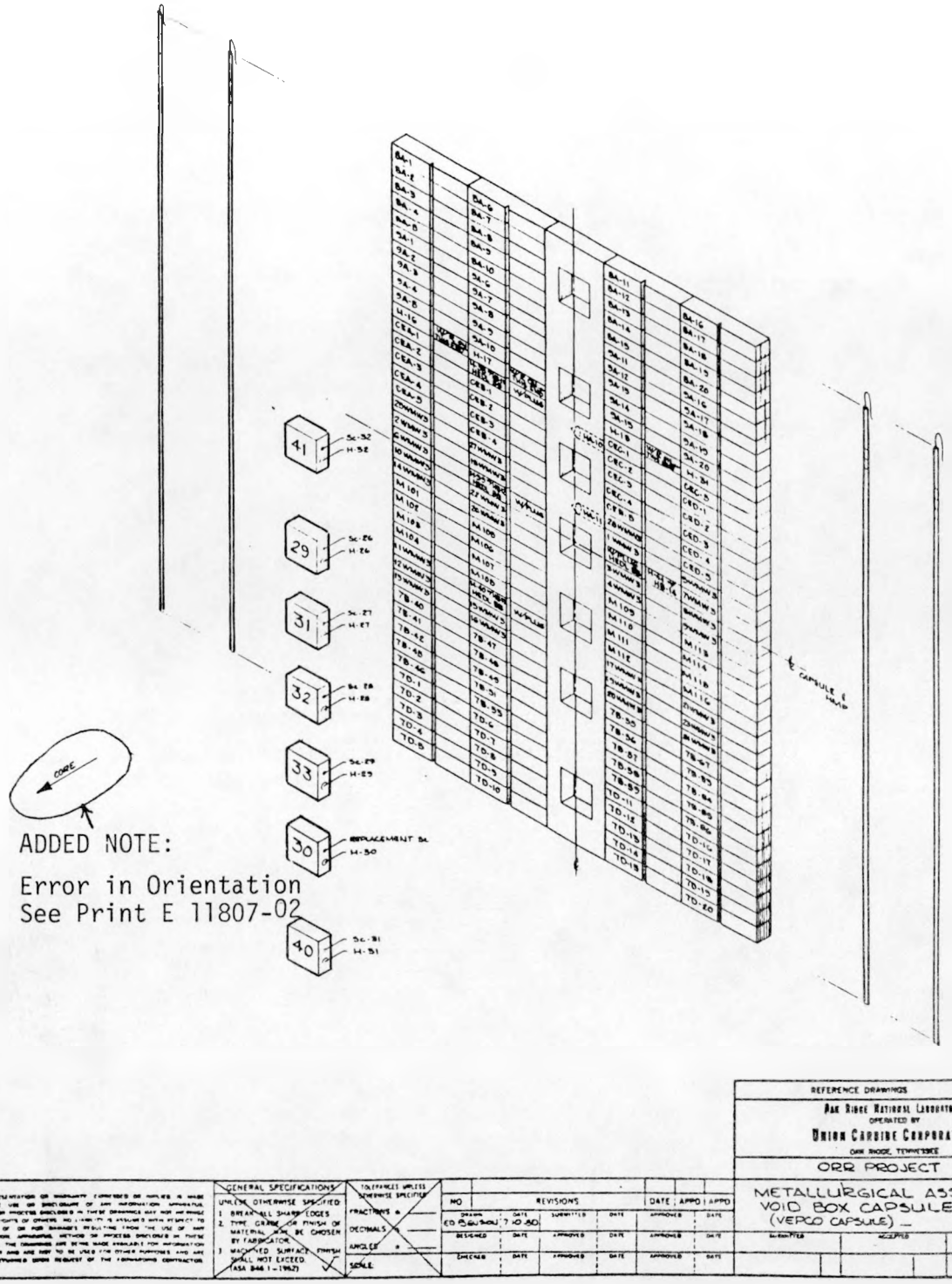

FIGURE A2. Identification of the Metallurgical Test Specimens and Dosimeter Location in the SVBC.

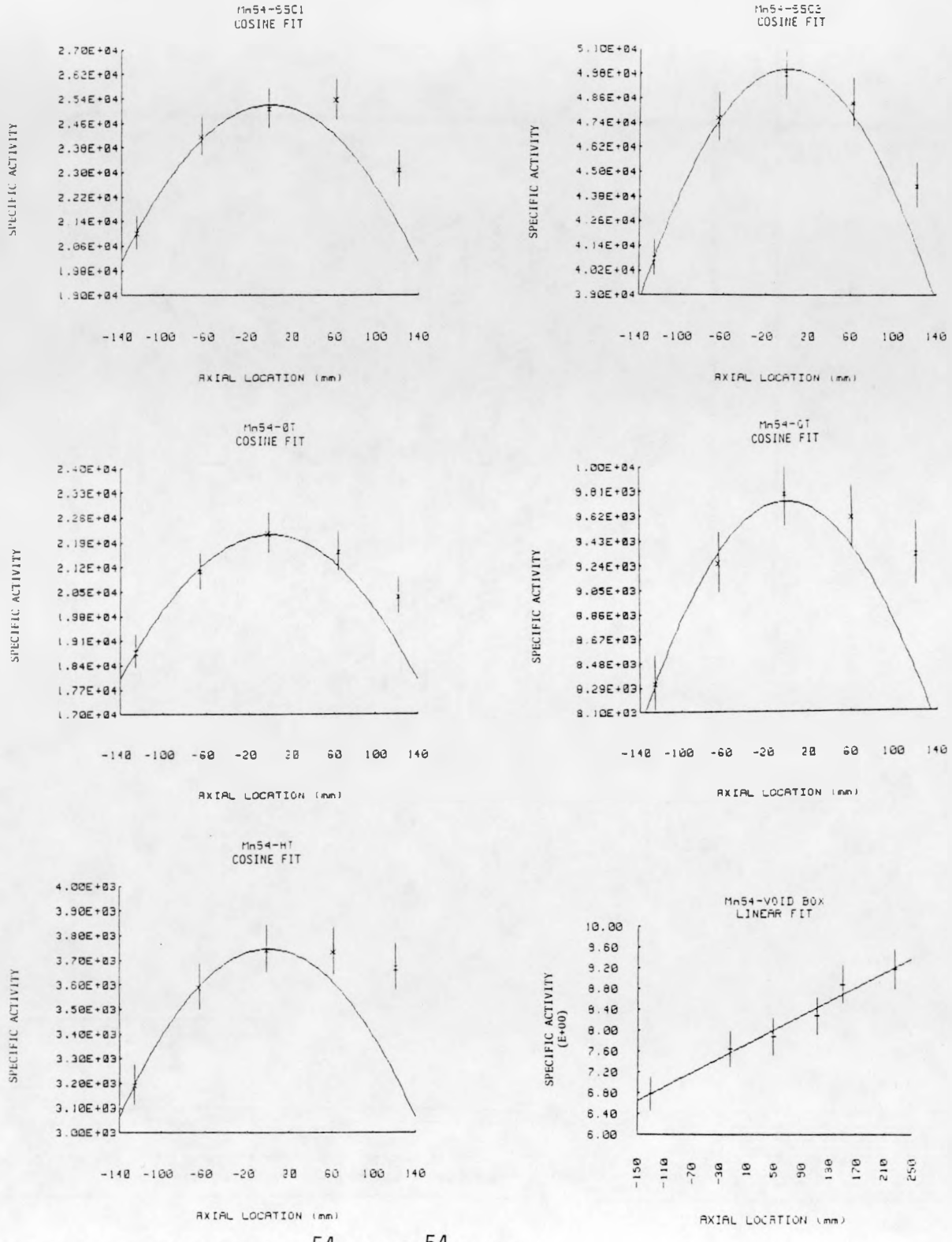

FIGURE A3. Fit of Axial $^{54}Fe(n,p)^{54}Mn$ Data.

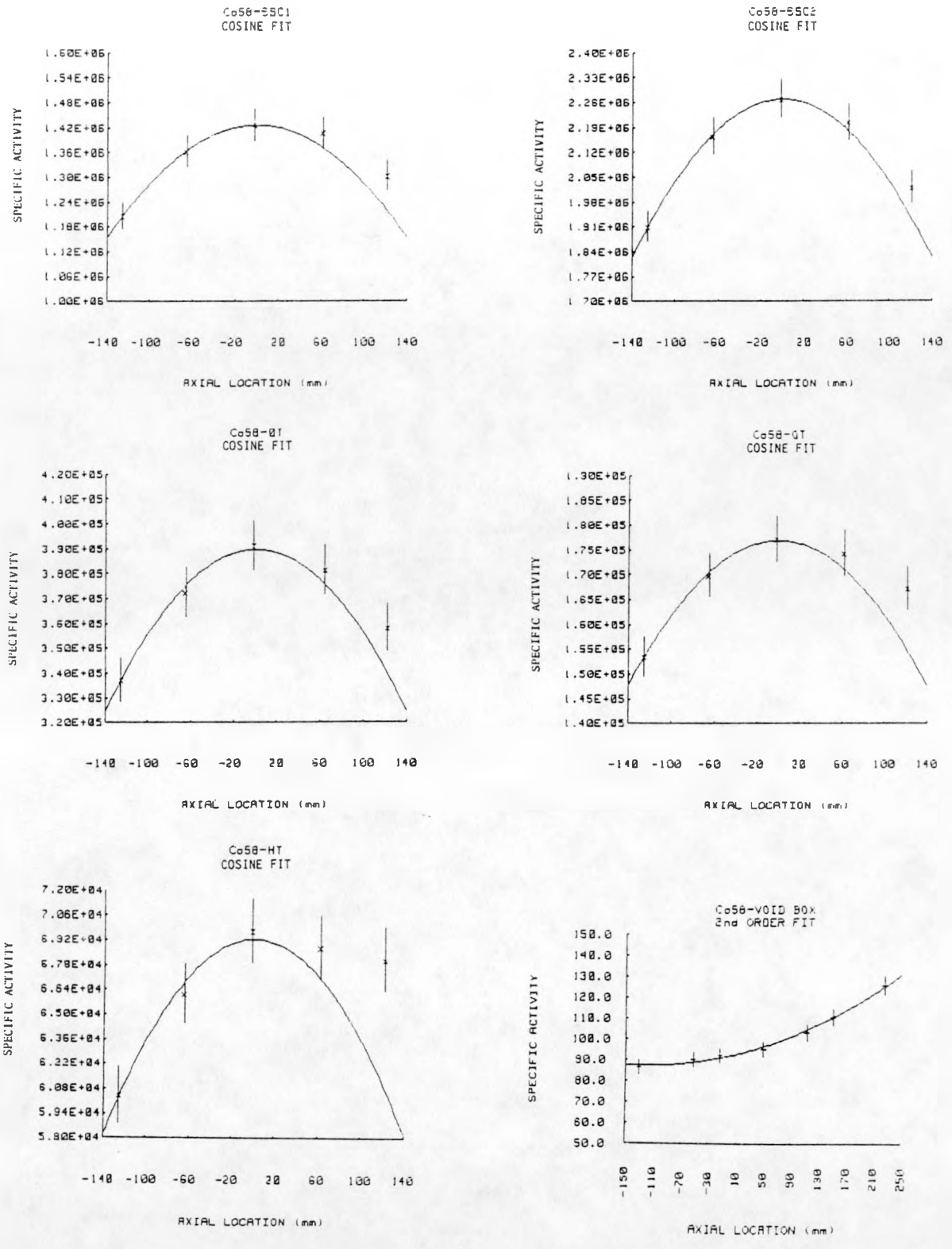

FIGURE A4. Fit of Axial $^{58}Ni(n,p)^{58}Co$ Data.

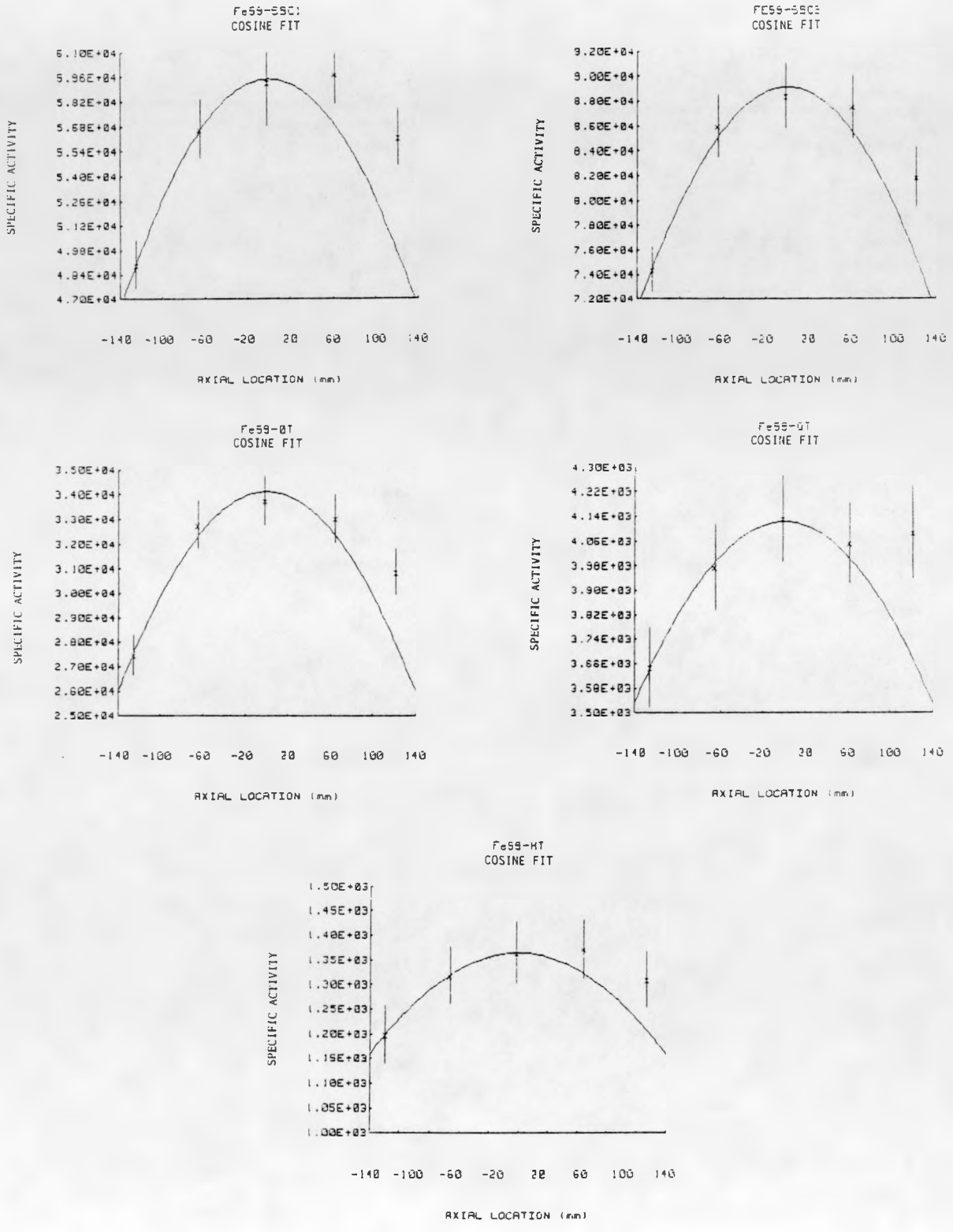

FIGURE A5. Fit of Axial $^{58}Fe(n,\gamma)^{59}Fe$ Data.

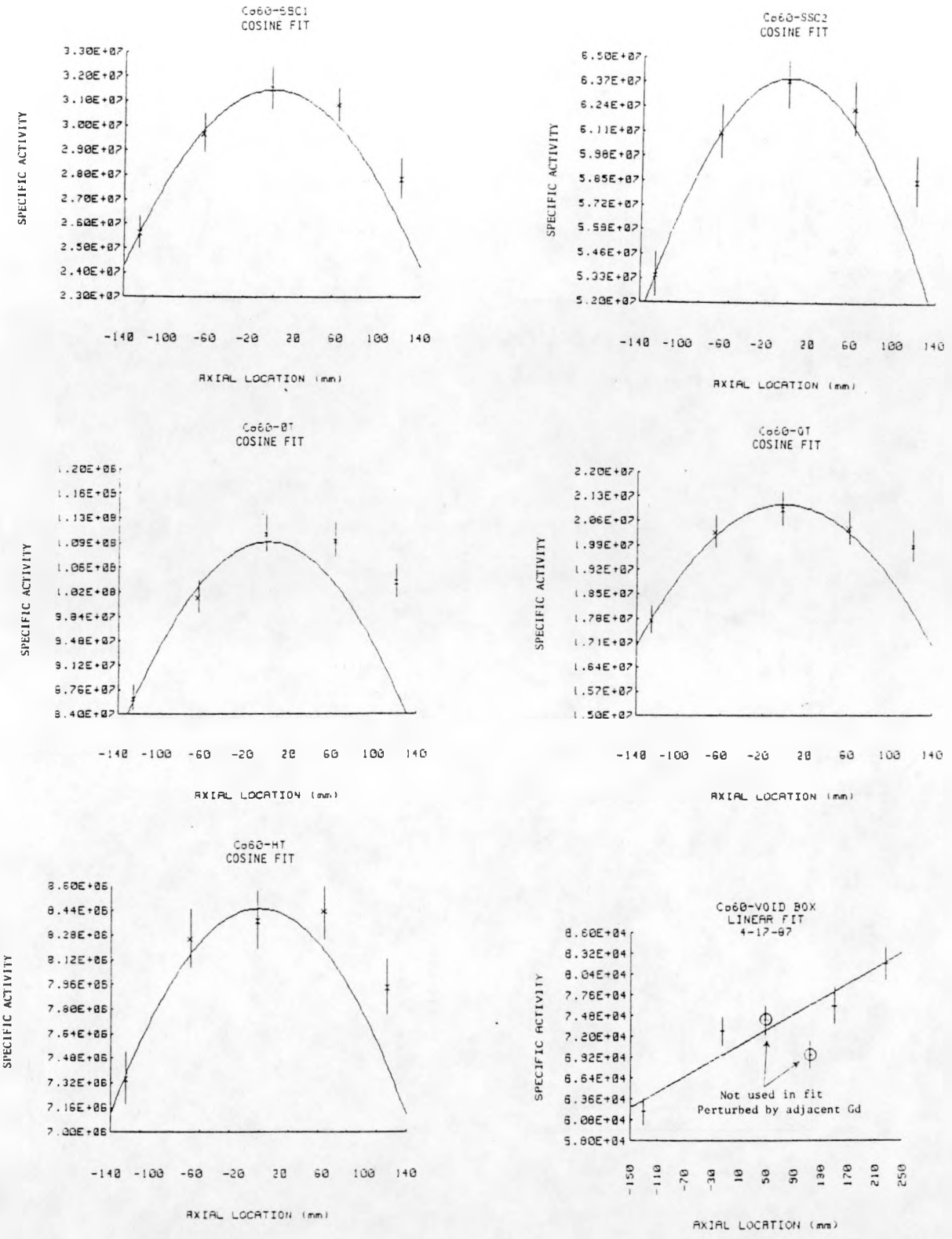

FIGURE A6. Fit of Axial $^{59}Co(n,\gamma)^{60}Co$ Data.

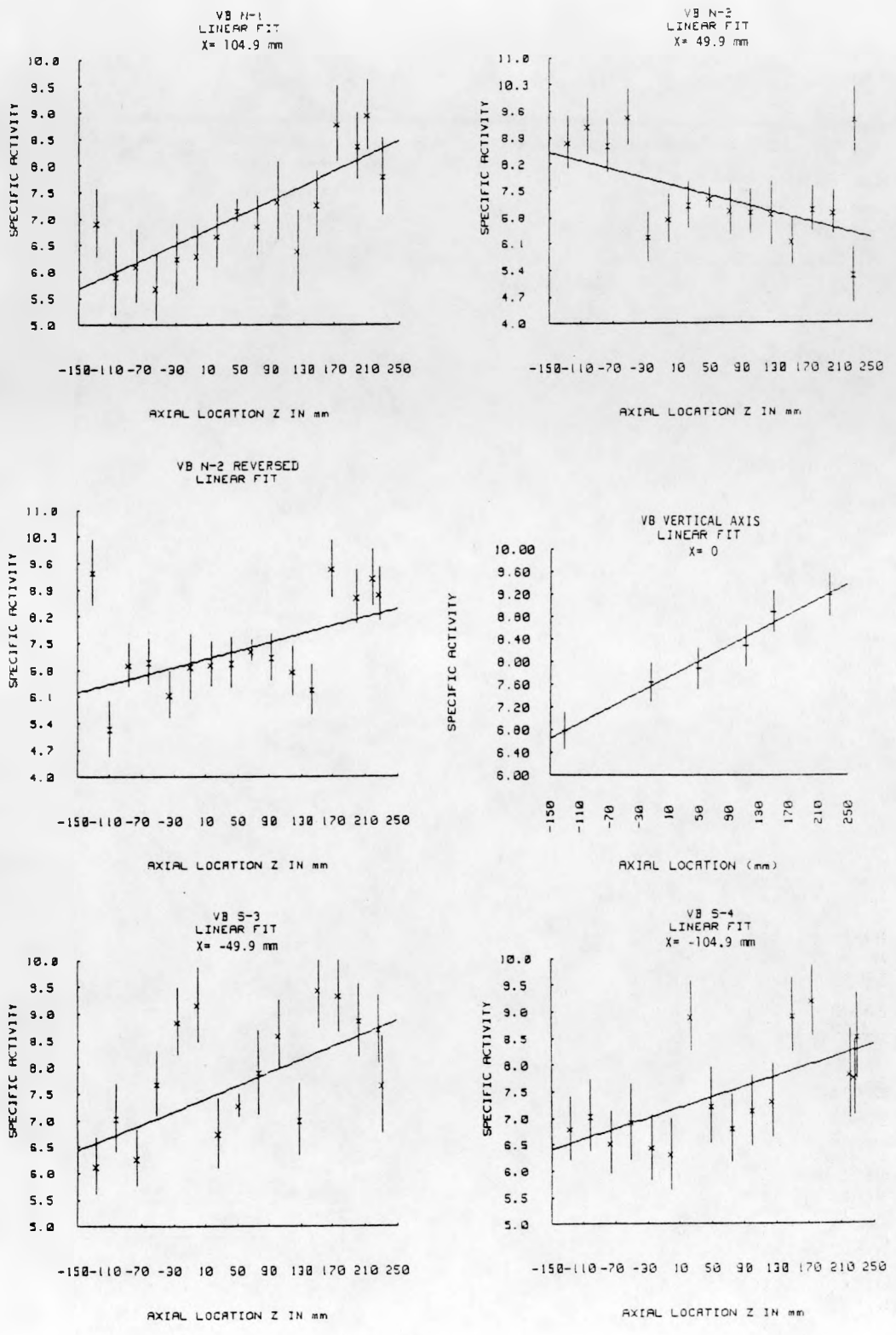

FIGURE A7. SVBC Vertical Profile ^{54}Mn.

TABLE A1

ORR-PSF SSC-1 INPUT DATA AND CALCULATED REACTION RATES

DATE AND TIME IN -	4/30/80 AT 13:34	EXPOSURE-	MW SEC.	MW HOURS	MW DAYS
DATE AND TIME OUT-	6/23/80 AT 12:55		1.0678+008	2.9661+004	1.2359+003

TOTAL TIME IN REACTOR = 1295.3300 HRS
NORMALIZED TO POWER OF 30.00 MW

POWER (MW) WAS-

28.0000	.0000	27.8300	.0000	27.9800
.0000	27.8300	.0000	26.6600	

TIME (HRS) WAS-

184.4200	10.7300	140.7600	44.4700	112.3300
32.5300	370.6300	132.3100	267.1500	

54FE(N,P)54MN
LAMBDA =2.5672-008, K =1.5989-019, YIELD =1.0000+000

ID	MONITOR LOCATION X	Y	Z	ACTIVITY (DPS/MG)	ACTIVITY (DPS/NUCLEUS)	REACTION RATE (RPS/NUCLEUS)
KFA TS1	73.2	125.5	1.9	2.5830+004	4.12996-015	4.80632-014
GE D SVQ 19	-52.5	126.2	12.7	2.6900+004	4.30104-015	5.00542-014
GE C SVQ 19	-52.5	130.3	12.7	2.2800+004	3.64549-015	4.24251-014
GE SVQ 19	-52.5	132.6	12.7	2.4100+004	3.85335-015	4.48441-014
GE B SVQ 19	-52.5	134.5	12.7	2.2800+004	3.64549-015	4.24251-014
GE A SVQ 19	-52.5	138.9	12.7	2.0800+004	3.32571-015	3.87036-014
H-1 29	.0	131.5	96.9	2.3123+004	3.69714-015	4.30261-014
H-3 31	.0	131.5	62.0	2.5400+004	4.06121-015	4.72630-014
H-4 32	.0	131.5	-1.5	2.5103+004	4.01372-015	4.67104-014
H-5 33	.0	131.5	-65.0	2.4203+004	3.86982-015	4.50357-014
H-2 30	.0	131.5	-100.0	2.1040+004	3.36409-015	3.91502-014
HA-4 16 39G	53.4	133.0	-.6	2.4462+004	3.91123-015	4.55176-014
HA-4 15 39G	46.3	133.0	-.6	2.4630+004	3.93809-015	4.58303-014
HA-4 14 39G	43.0	133.0	-.6	2.4945+004	3.98846-015	4.64164-014
HA-4 13 39G	41.5	133.0	-.6	2.5040+004	4.00365-015	4.65932-014
HB-4 39E	37.7	133.0	-8.5	2.3280+004	3.72224-015	4.33182-014
HB-3 38E	-37.7	133.0	-8.4	2.4417+004	3.90403-015	4.54339-014
HA-3 9 38G	-41.5	133.0	-.6	2.4412+004	3.90323-015	4.54246-014
HA-3 10 38G	-43.0	133.0	-.6	2.4606+004	3.93425-015	4.57856-014
HA-3 11 38G	-46.3	133.0	-.6	2.4677+004	3.94561-015	4.59177-014
HA-3 12 38G	-53.4	133.0	-.6	2.4423+004	3.90499-015	4.54451-014
FHSNF-1 37D	40.3	139.9	-67.5	2.0026+004	3.20196-015	3.72634-014
F	.0	.0	.0	1.9800+004	3.16582-015	3.68428-014
EHSNF-2 37D	39.8	139.9	-67.5	2.0105+004	3.21459-015	3.74104-014
DHSNF-3 37D	39.3	139.9	-67.5	1.9954+004	3.19045-015	3.71294-014
D	.0	.0	.0	2.0100+004	3.21379-015	3.74011-014
CHSNF-4 37D	38.8	139.9	-67.5	2.0194+004	3.22882-015	3.75760-014
C-1	.0	.0	.0	1.8900+004	3.02192-015	3.51682-014
C-2	.0	.0	.0	1.9500+004	3.11785-015	3.62846-014
BHSNF-5 37D	38.3	139.9	-67.5	2.0157+004	3.22290-015	3.75071-014
AHSNF-6 37D	37.7	139.9	-67.5	2.0198+004	3.22946-015	3.75834-014
A	.0	.0	.0	2.0600+004	3.29373-015	3.83314-014
W1RE1 11 SF	-103.7	121.4	123.0	2.3541+004	3.76397-015	4.38039-014
W1RE1 10 SF	-103.7	121.4	105.4	2.5104+004	4.01388-015	4.67122-014
W1RE1 9 SF	-103.7	121.4	80.0	2.5826+004	4.12932-015	4.80557-014
W1RE1 8 SF	-103.7	121.4	54.6	2.6651+004	4.26123-015	4.95908-014
W1RE1 7 SF	-103.7	121.4	29.2	2.7171+004	4.34437-015	5.05584-014
W1RE1 6 SF	-103.7	121.4	3.8	2.7223+004	4.35269-015	5.06552-014
W1RE1 5 SF	-103.7	121.4	-21.5	2.7007+004	4.31815-015	5.02533-014
W1RE1 4 SF	-103.7	121.4	-46.9	2.6362+004	4.21502-015	4.90531-014
W1RE1 3 SF	-103.7	121.4	-72.4	2.5717+004	4.11189-015	4.78529-014
W1RE1 2 SF	-103.7	121.4	-97.7	2.4770+004	3.96048-015	4.60908-014

TABLE A1 (CONT'D)

54FE(N,P)54MN (CONTINUED)

ID	MONITOR LOCATION X	Y	Z	ACTIVITY (DPS/MG)	ACTIVITY (DPS/NUCLEUS)	REACTION RATE (RPS/NUCLEUS)
W1RE1 1 SF	-103.7	121.4	-120.1	2.3547+004	3.76493-015	4.38151-014
W1RE2 10 NF	103.7	121.4	105.4	2.5631+004	4.09814-015	4.76929-014
W1RE2 9 NF	103.7	121.4	80.0	2.6463+004	4.23117-015	4.92410-014
W1RE2 8 NF	103.7	121.4	54.6	2.7197+004	4.34853-015	5.06068-014
W1RE2 7 NF	103.7	121.4	29.2	2.7656+004	4.42192-015	5.14609-014
W1RE2 6 NF	103.7	121.4	3.8	2.7647+004	4.42048-015	5.14441-014
W1RE2 5 NF	103.7	121.4	-21.5	2.7415+004	4.38338-015	5.10124-014
W1RE2 4 NF	103.7	121.4	-46.9	2.7024+004	4.32087-015	5.02849-014
W1RE2 3 NF	103.7	121.4	-72.4	2.6078+004	4.16961-015	4.85246-014
W1RE2 2 NF	103.7	121.4	-97.7	2.4803+004	3.96575-015	4.61522-014
W1RE2 1 NF	103.7	121.4	-119.8	2.3334+004	3.73087-015	4.34187-014
W1RE3 2 SR	-103.7	144.6	119.7	1.5331+004	2.45127-015	2.85271-014
W1RE3 1 SR	-103.7	144.6	112.5	1.5469+004	2.47334-015	2.87839-014
W1RE3 3 SR	-103.7	144.6	94.3	1.5749+004	2.51811-015	2.93049-014
W1RE3 4 SR	-103.7	144.6	68.9	1.6340+004	2.61260-015	3.04046-014
W1RE3 5 SR	-103.7	144.6	46.0	1.6781+004	2.68311-015	3.12252-014
W1RE3 6 SR	-103.7	144.6	18.1	1.6776+004	2.68231-015	3.12159-014
W1RE3 7 SR	-103.7	144.6	-7.3	1.6624+004	2.65801-015	3.09331-014
W1RE3 8 SR	-103.7	144.6	-32.7	1.6653+004	2.66265-015	3.09871-014
W1RE3 9 SR	-103.7	144.6	-58.1	1.6027+004	2.56256-015	2.98222-014
W1RE3 10 SR	-103.7	144.6	-83.5	1.5477+004	2.47462-015	2.87988-014
W1RE3 11 SR	-103.7	144.6	-108.9	1.4683+004	2.34766-015	2.73214-014
W1RE3 12 SR	-103.7	144.6	-119.2	1.4095+004	2.25365-015	2.62273-014
W1RE4 11 NR	103.7	144.6	123.6	1.4956+004	2.39131-015	2.78294-014
W1RE4 12 NR	103.7	144.6	113.5	1.5135+004	2.41994-015	2.81624-014
W1RE4 10 NR	103.7	144.6	105.4	1.5835+004	2.53186-015	2.94650-014
W1RE4 9 NR	103.7	144.6	80.0	1.6447+004	2.62971-015	3.06037-014
W1RE4 8 NR	103.7	144.6	54.6	1.6759+004	2.67960-015	3.11843-014
W1RE4 7 NR	103.7	144.6	29.2	1.6921+004	2.70550-015	3.14857-014
W1RE4 6 NR	103.7	144.6	3.8	1.7234+004	2.75554-015	3.20682-014
W1RE4 5 NR	103.7	144.6	-21.5	1.6926+004	2.70630-015	3.14950-014
W1RE4 4 NR	103.7	144.6	-46.9	1.6535+004	2.64378-015	3.07675-014
W1RE4 3 NR	103.7	144.6	-72.4	1.5823+004	2.52994-015	2.94426-014
W1RE4 2 NR	103.7	144.6	-97.7	1.5278+004	2.44280-015	2.84285-014
W1RE4 1 NR	103.7	144.6	-119.9	1.4213+004	2.27252-015	2.64468-014

58FE(N,G)59FE

LAMBDA =1.7988-007, K =2.8102-017, YIELD =1.0000+000

ID	MONITOR LOCATION X	Y	Z	ACTIVITY (DPS/MG)	ACTIVITY (DPS/NUCLEUS)	REACTION RATE (RPS/NUCLEUS)
H-1 29	.0	131.5	96.9	5.6177+004	1.57869-012	3.69279-012
H-3 31	.0	131.5	62.0	5.9772+004	1.67971-012	3.92911-012
H-4 32	.0	131.5	-1.5	5.9315+004	1.66687-012	3.89907-012
H-5 33	.0	131.5	-65.0	5.6704+004	1.59350-012	3.72743-012
H-2 30	.0	131.5	-100.0	4.8980+004	1.37644-012	3.21970-012
GE SVQ 19	-52.5	132.6	12.7	2.2000+004	6.18244-013	1.44617-012
HA-4 16 39G	53.4	133.0	-.6	2.0660+004	5.80587-013	1.35808-012
HA-4 15 39G	46.3	133.0	-.6	2.0513+004	5.76456-013	1.34842-012
HA-4 14 39G	43.0	133.0	-.6	2.1646+004	6.08296-013	1.42290-012
HA-4 13 39G	41.5	133.0	-.6	2.1809+004	6.12877-013	1.43361-012
HB-4 39E	37.7	133.0	-8.5	2.0308+004	5.70695-013	1.33495-012
HB-3 38E	-37.7	133.0	-8.5	2.1536+004	6.05205-013	1.41567-012
HA-3 9 38G	-41.5	133.0	-.6	2.1176+004	5.95088-013	1.39200-012
HA-3 10 38G	-43.0	133.0	-.6	2.1359+004	6.00231-013	1.40403-012
HA-3 11 38G	-46.3	133.0	-.6	2.1398+004	6.01327-013	1.40660-012
HA-3 12 38G	-53.4	133.0	-.6	2.0246+004	5.68953-013	1.33087-012
FHSNF-6 37D	40.3	139.9	-67.5	1.8364+004	5.16065-013	1.20716-012
EHSNF-5 37D	39.8	139.9	-67.5	1.8275+004	5.13564-013	1.20131-012
DHSNF-4 37D	39.3	139.9	-67.5	1.8010+004	5.06117-013	1.18389-012
D	.0	.0	.0	1.8400+004	5.17077-013	1.20952-012
CHSNF-3 37D	38.8	139.9	-67.5	1.8359+004	5.15925-013	1.20683-012

TABLE A1 (CONT'D)

58FE(N,G)59FE (CONTINUED)

ID	MONITOR LOCATION X	Y	Z	ACTIVITY (DPS/MG)	ACTIVITY (DPS/NUCLEUS)	REACTION RATE (RPS/NUCLEUS)
C-1	.0	.0	.0	1.7900+004	5.03026-013	1.17666-012
C-2	.0	.0	.0	1.8400+004	5.17077-013	1.20952-012
BHSNF-2 37D	38.3	139.9	-67.5	1.8252+004	5.12918-013	1.19979-012
AHSNF-1 37D	37.7	139.9	-67.5	1.8181+004	5.10922-013	1.19513-012
A	.0	.0	.0	1.8200+004	5.11456-013	1.19638-012
W1RE1 11 SF	-103.7	121.4	123.0	5.4051+004	1.51894-012	3.55304-012
W1RE1 10 SF	-103.7	121.4	105.4	5.7379+004	1.61246-012	3.77181-012
W1RE1 9 SF	-103.7	121.4	80.0	6.0725+004	1.70649-012	3.99175-012
W1RE1 8 SF	-103.7	121.4	54.9	6.3330+004	1.77970-012	4.16299-012
W1RE1 7 SF	-103.7	121.4	29.2	6.5468+004	1.83978-012	4.30354-012
W1RE1 6 SF	-103.7	121.4	3.8	6.5176+004	1.83158-012	4.28434-012
W1RE1 5 SF	-103.7	121.4	-21.5	6.4090+004	1.80106-012	4.21295-012
W1RE1 4 SF	-103.7	121.4	-46.9	6.3210+004	1.77633-012	4.15511-012
W1RE1 3 SF	-103.7	121.4	-72.3	6.2202+004	1.74800-012	4.08884-012
W1RE1 2 SF	-103.7	121.4	-97.7	5.9334+004	1.66740-012	3.90032-012
W1RE1 1 SF	-103.7	121.4	-120.1	5.6657+004	1.59218-012	3.72434-012
W1RE2 10 NF	103.7	121.4	105.4	5.8203+004	1.63562-012	3.82597-012
W1RE2 9 NF	103.7	121.4	80.0	6.1521+004	1.72886-012	4.04408-012
W1RE2 8 NF	103.7	121.4	54.6	6.3487+004	1.78411-012	4.17331-012
W1RE2 7 NF	103.7	121.4	29.2	6.2113+004	1.74550-012	4.08299-012
W1RE2 6 NF	103.7	121.4	3.8	5.4616+004	1.53482-012	3.59018-012
W1RE2 5 NF	103.7	121.4	-21.5	6.1812+004	1.73704-012	4.06321-012
W1RE2 4 NF	103.7	121.4	-46.9	6.0414+004	1.69775-012	3.97131-012
W1RE2 3 NF	103.7	121.4	-72.3	5.8561+004	1.64568-012	3.84950-012
W1RE2 2 NF	103.7	121.4	-97.7	5.5153+004	1.54991-012	3.62548-012
W1RE2 1 NF	103.7	121.4	-119.8	5.1863+004	1.45745-012	3.40921-012
W1RE3 2 SR	-103.7	144.6	119.7	5.7726+004	1.62222-012	3.79462-012
W1RE3 1 SR	-103.7	144.6	112.5	5.6813+004	1.59656-012	3.73460-012
W1RE3 3 SR	-103.7	144.6	94.3	5.9887+004	1.68294-012	3.93667-012
W1RE3 4 SR	-103.7	144.6	68.9	6.1929+004	1.74033-012	4.07090-012
W1RE3 5 SR	-103.7	144.6	46.0	6.2461+004	1.75528-012	4.10587-012
W1RE3 6 SR	-103.7	144.6	18.1	6.3196+004	1.77593-012	4.15419-012
W1RE3 7 SR	-103.7	144.6	-7.3	6.2457+004	1.75517-012	4.10561-012
W1RE3 8 SR	-103.7	144.6	-32.7	6.1913+004	1.73988-012	4.06985-012
W1RE3 9 SR	-103.7	144.6	-58.1	5.9899+004	1.68328-012	3.93746-012
W1RE3 10 SR	-103.7	144.6	-83.5	5.7477+004	1.61522-012	3.77825-012
W1RE3 11 SR	-103.7	144.6	-108.9	5.3918+004	1.51520-012	3.54430-012
W1RE3 12 SR	-103.7	144.6	-119.2	5.2585+004	1.47774-012	3.45667-012
W1RE4 11 NR	103.7	144.6	123.6	5.8472+004	1.64318-012	3.84365-012
W1RE4 10 NR	103.7	144.6	105.4	5.9146+004	1.66212-012	3.88796-012
W1RE4 9 NR	103.7	144.6	80.0	6.1572+004	1.73030-012	4.04743-012
W1RE4 8 NR	103.7	144.6	54.6	6.2913+004	1.76798-012	4.13558-012
W1RE4 7 NR	103.7	144.6	29.2	6.2900+004	1.76762-012	4.13473-012
W1RE4 6 NR	103.7	144.6	3.8	6.1292+004	1.72243-012	4.02903-012
W1RE4 5 NR	103.7	144.6	-21.5	6.1957+004	1.74112-012	4.07274-012
W1RE4 4 NR	103.7	144.6	-46.9	6.1175+004	1.71914-012	4.02133-012
W1RE4 3 NR	103.7	144.6	-72.4	5.9026+004	1.65875-012	3.88007-012
W1RE4 2 NR	103.7	144.6	-97.8	5.5901+004	1.57093-012	3.67465-012
W1RE4 1 NR	103.7	144.6	-119.0	5.2968+004	1.48851-012	3.48185-012

58NI(N,P)58CO

LAMBDA =1.1323-007, K =1.4278-019, YIELD =1.0000+000

ID	MONITOR LOCATION X	Y	Z	ACTIVITY (DPS/MG)	ACTIVITY (DPS/NUCLEUS)	REACTION RATE (RPS/NUCLEUS)
KFA-1 32	.0	125.9	-1.5	1.6440+006	2.34730-013	7.56515-013
KFA TS1	73.2	125.5	1.9	1.4550+006	2.07745-013	6.69543-013
H-1 29	.0	131.5	96.9	1.3050+006	1.86328-013	6.00518-013
H-3 31	.0	131.5	62.0	1.4086+006	2.01120-013	6.48192-013
H-4 32	.0	131.5	-1.5	1.4269+006	2.03733-013	6.56613-013
H-5 33	.0	131.5	-65.0	1.3641+006	1.94766-013	6.27714-013
H-2 30	.0	131.5	-100.0	1.2084+006	1.72535-013	5.56066-013

TABLE A1 (CONT'D)

58NI(N,P)58CO (CONTINUED)

ID	MONITOR LOCATION X	Y	Z	ACTIVITY (DPS/MG)	ACTIVITY (DPS/NUCLEUS)	REACTION RATE (RPS/NUCLEUS)
HA-4 39G	49.1	133.0	-.6	1.4050+006	2.00606-013	6.46535-013
HB-4 39E	38.3	133.0	-8.5	1.3833+006	1.97508-013	6.36549-013
HB-3 38E	-38.3	133.0	-8.5	1.3742+006	1.96208-013	6.32362-013
HA-3 38G	-49.1	133.0	-.6	1.3902+006	1.98493-013	6.39725-013
FHSNF-6 37D	49.7	139.9	-67.5	1.1316+006	1.61570-013	5.20725-013
F	.0	.0	.0	1.1700+006	1.67053-013	5.38396-013
EHSNF-5 37D	49.2	139.9	-67.5	1.1411+006	1.62926-013	5.25097-013
DHSNF-4 37D	48.7	139.9	-67.5	1.1406+006	1.62855-013	5.24867-013
D	.0	.0	.0	1.1300+006	1.61341-013	5.19989-013
CHSNF-3 37D	48.1	139.9	-67.5	1.1377+006	1.62441-013	5.23532-013
C-1	.0	.0	.0	1.0300+006	1.47063-013	4.73972-013
C-2	.0	.0	.0	1.0600+006	1.51347-013	4.87777-013
BHSNF-2 37D	47.6	139.9	-67.5	1.1372+006	1.62369-013	5.23302-013
AHSNF-1 37D	47.1	139.9	-67.5	1.1444+006	1.63397-013	5.26615-013
A	.0	.0	.0	1.1600+006	1.65625-013	5.33794-013
GE B SVQ 19	-52.5	123.9	12.7	1.6200+006	2.31304-013	7.45471-013
GE BA SVQ 19	.0	123.9	12.7	1.6000+006	2.28448-013	7.36268-013
GE BB SVQ 19	.0	123.9	12.7	1.6400+006	2.34159-013	7.54674-013
GE BC SVQ 19	.0	123.9	12.7	1.6100+006	2.29876-013	7.40869-013
GE BD SVQ 19	.0	123.9	12.7	1.6300+006	2.32731-013	7.50073-013
GE T SVQ 19	-52.5	141.3	12.7	1.1500+006	1.64197-013	5.29192-013

63CU(N,A)60CO

LAMBDA =4.1671-009, K =1.5255-019, YIELD =1.0000+000

ID	MONITOR LOCATION X	Y	Z	ACTIVITY (DPS/MG)	ACTIVITY (DPS/NUCLEUS)	REACTION RATE (RPS/NUCLEUS)
KFA TS1	125.5	73.2	1.9	3.0930+002	4.71837-017	3.21338-015
CU-2 39H	53.7	130.7	-4.0	2.9483+002	4.49763-017	3.06305-015
GE B SVQ 19	-52.5	128.6	12.7	3.0400+002	4.63752-017	3.15832-015
GE SVQ 19	-52.5	132.6	12.7	2.8000+002	4.27140-017	2.90898-015
GE A SVQ 19	-52.5	137.1	12.7	2.5900+002	3.95104-017	2.69081-015
CU-1 38H	-37.7	130.7	-4.0	3.0178+002	4.60365-017	3.13526-015
HA-4F 39G	49.4	133.0	-.6	2.9401+002	4.48512-017	3.05453-015
HA-4W 39G	49.3	133.0	-.6	2.9382+002	4.48222-017	3.05256-015
HB-4 39E	39.3	133.0	-8.5	2.9109+002	4.44058-017	3.02420-015
HB-3 38E	-39.3	133.0	-8.5	2.8838+002	4.39924-017	2.99604-015
HA-3W 38G	-49.3	133.0	-.6	2.9216+002	4.45690-017	3.03531-015
HA-3F 38G	-49.4	133.0	-.6	2.9292+002	4.46849-017	3.04321-015
FHSNF-6 37D	43.5	139.9	-67.5	2.3841+002	3.63694-017	2.47689-015
F	.0	.0	.0	2.4300+002	3.70696-017	2.52458-015
EHSNF-5 37D	42.9	139.9	-67.5	2.4004+002	3.66181-017	2.49383-015
DHSNF-4 37D	42.4	139.9	-67.5	2.3857+002	3.63939-017	2.47855-015
D	.0	.0	.0	2.4300+002	3.70696-017	2.52458-015
CHSNF-3 37D	41.9	139.9	-67.5	2.3986+002	3.65906-017	2.49196-015
C-1	.0	.0	.0	2.3100+002	3.52390-017	2.39991-015
C-2	.0	.0	.0	2.3500+002	3.58492-017	2.44146-015
BHSNF-2 37D	41.4	139.9	-67.5	2.3772+002	3.62642-017	2.46972-015
AHSNF-1 37D	40.9	139.9	-67.5	2.3893+002	3.64488-017	2.48229-015
A	.0	.0	.0	2.4100+002	3.67645-017	2.50380-015

TABLE A1 (CONT'D)

46TI(N,P)46SC

LAMBDA =9.5677-008, K =9.8198-019, YIELD =1.0000+000

ID	MONITOR LOCATION X	Y	Z	ACTIVITY (DPS/MG)	ACTIVITY (DPS/NUCLEUS)	REACTION RATE (RPS/NUCLEUS)
KFA-1 32	.0	125.9	-1.5	1.9930+004	1.95709-014	7.17976-014
KFA TS1	73.2	125.5	1.9	1.7940+004	1.76167-014	6.46287-014
H-1 29	.0	131.5	96.9	1.5393+004	1.51156-014	5.54531-014
H-3 31	.0	131.5	62.0	1.6599+004	1.62999-014	5.97977-014
H-4 32	.0	131.5	-1.5	1.7060+004	1.67526-014	6.14585-014
H-5 33	.0	131.5	-65.0	1.6084+004	1.57942-014	5.79424-014
H-2 30	.0	131.5	-100.0	1.3708+004	1.34610-014	4.93829-014
HB-4 39E	38.8	133.0	-8.5	1.7086+004	1.67781-014	6.15521-014
HB-3 38E	-38.8	133.0	-8.5	1.7057+004	1.67496-014	6.14477-014
GE SVQ 19	-52.5	139.2	12.7	1.4700+004	1.44351-014	5.29566-014

59CO(N,G)60CO

LAMBDA =4.1671-009, K =9.7862-020, YIELD =1.0000+000

ID	MONITOR LOCATION X	Y	Z	ACTIVITY (DPS/MG)	ACTIVITY (DPS/NUCLEUS)	REACTION RATE (RPS/NUCLEUS)
H-1 29	.0	131.5	96.9	2.7862+007	2.72663-012	1.85694-010
H-3 31	.0	131.5	62.0	3.0884+007	3.02237-012	2.05834-010
H-4 32	.0	131.5	-1.5	3.1543+007	3.08686-012	2.10227-010
H-5 33	.0	131.5	-65.0	2.9730+007	2.90944-012	1.98143-010
H-2 30	.0	131.5	-100.0	2.5657+007	2.51085-012	1.70998-010
HA-3 38G	-43.0	133.0	-.6	1.3955+007	1.36566-012	9.30067-011
HB-3 38E	-39.8	133.0	-8.5	1.6049+007	1.57059-012	1.06963-010
HB-4 39E	39.8	133.0	-8.5	1.6102+007	1.57577-012	1.07316-010
HA-4 39G	43.0	133.0	-.6	1.4050+007	1.37496-012	9.36399-011
GE SVQ 19	-52.5	139.2	12.7	1.5300+007	1.49729-012	1.01971-010
FHSNF-6 37D	46.6	139.9	-67.5	1.3844+007	1.35480-012	9.22669-011
F	.0	.0	.0	1.3270+007	1.29863-012	8.84414-011
EHSNF-5 37D	46.1	139.9	-67.5	1.3826+007	1.35304-012	9.21470-011
DHSNF-4 37D	45.5	139.9	-67.5	1.3874+007	1.35774-012	9.24669-011
D	.0	.0	.0	1.4200+007	1.38964-012	9.46396-011
CHSNF-3 37D	45.0	139.9	-67.5	1.3901+007	1.36038-012	9.26468-011
C-1	.0	.0	.0	1.3300+007	1.30156-012	8.86413-011
C-2	.0	.0	.0	1.3700+007	1.34071-012	9.13072-011
BHSNF-2 37D	44.5	139.9	-67.5	1.3806+007	1.35108-012	9.20137-011
AHSNF-1 37D	44.0	139.9	-67.5	1.3818+007	1.35226-012	9.20936-011
A	.0	.0	.0	1.4000+007	1.37007-012	9.33066-011

109AG(N,G)110AGM

LAMBDA =3.2118-008, K =3.7185-019, YIELD =1.0000+000

ID	MONITOR LOCATION X	Y	Z	ACTIVITY (DPS/MG)	ACTIVITY (DPS/NUCLEUS)	REACTION RATE (RPS/NUCLEUS)
H-1 29	.0	131.5	96.9	2.9733+007	1.10562-011	1.04424-010
H-3 31	.0	131.5	62.0	3.3758+007	1.25529-011	1.18560-010
H-4 32	.0	131.5	-1.5	3.3650+007	1.25128-011	1.18181-010
H-5 33	.0	131.5	-65.0	3.2458+007	1.20695-011	1.13994-010
H-2 30	.0	131.5	-100.0	2.7552+007	1.02452-011	9.67641-011
HA-4 39G	42.9	133.0	-.6	2.7951+007	1.03936-011	9.81654-011
HB-4 39E	40.9	133.0	-8.5	2.7953+007	1.03943-011	9.81724-011
HB-3 38E	-40.9	133.0	-8.5	2.7719+007	1.03073-011	9.73506-011
HA-3 38G	-42.9	133.0	-.6	2.7913+007	1.03794-011	9.80320-011
GE SVQ 19	-52.5	139.2	12.7	2.5000+007	9.29625-012	8.78013-011

TABLE A1 (CONT'D)

45SC(N,G)46SC

LAMBDA =9.5677-008, K =7.4652-020, YIELD =1.0000+000

ID	MONITOR LOCATION X	Y	Z	ACTIVITY (DPS/MG)	ACTIVITY (DPS/NUCLEUS)	REACTION RATE (RPS/NUCLEUS)
H-1 29	-14.0	131.5	100.0	2.6732+008	1.99560-011	7.32104-011
MGO H-1 29	12.4	131.5	100.0	2.6609+008	1.98642-011	7.28736-011
H-3 31	-14.0	131.5	65.0	2.7461+008	2.05002-011	7.52069-011
MGO H-3 31	12.4	131.5	65.0	2.7003+008	2.01583-011	7.39526-011
H-4 32	-14.0	131.5	1.5	2.7376+008	2.04367-011	7.49742-011
MGO H-4 32	12.4	131.5	1.5	2.7075+008	2.02120-011	7.41498-011
H-5 33	-14.0	131.5	-62.0	2.6114+008	1.94946-011	7.15179-011
MGO H-5 33	12.4	131.5	-62.0	2.6675+008	1.99134-011	7.30543-011
H-2 30	-14.0	131.5	-96.9	2.2957+008	1.71379-011	6.28719-011
MGO H-2 30	12.4	131.5	-96.9	2.3266+008	1.73685-011	6.37182-011
HA-4 39G	49.8	133.0	-.6	6.0448+007	4.51256-012	1.65548-011
HB-4 39E	39.7	133.0	-8.5	6.0190+007	4.49330-012	1.64841-011
HB-3 38E	-39.7	133.0	-8.5	6.1856+007	4.61767-012	1.69404-011
HA-3 38G	-49.8	133.0	-.6	5.8768+007	4.38715-012	1.60947-011

235U(N,F)140BA

LAMBDA =6.2730-007, K =3.9030-019, YIELD =6.1050-002

ID	MONITOR LOCATION X	Y	Z	ACTIVITY (DPS/MG)	ACTIVITY (DPS/NUCLEUS)	REACTION RATE (RPS/NUCLEUS)
HB-4 39E	44.2	133.0	-8.5	4.3807+007	1.70979-011	3.97320-010
HB-3 38E	-44.2	133.0	-8.5	4.3365+007	1.69254-011	3.93311-010

235U(N,F)137CS

LAMBDA =7.2793-010, K =3.9030-019, YIELD =6.1510-002

ID	MONITOR LOCATION X	Y	Z	ACTIVITY (DPS/MG)	ACTIVITY (DPS/NUCLEUS)	REACTION RATE (RPS/NUCLEUS)
HB-4 39E	44.2	133.0	-8.5	1.5679+005	6.11951-014	3.84662-010
HB-3 38E	-44.2	133.0	-8.5	1.6098+005	6.28305-014	3.94942-010

235U(N,F)103RU

LAMBDA =2.0346-007, K =3.9030-019, YIELD =3.2760-002

ID	MONITOR LOCATION X	Y	Z	ACTIVITY (DPS/MG)	ACTIVITY (DPS/NUCLEUS)	REACTION RATE (RPS/NUCLEUS)
HB-4 39E	44.2	133.0	-8.5	1.4750+007	5.75692-012	3.81418-010
HB-3 38E	-44.2	133.0	-8.5	1.4813+007	5.78151-012	3.83047-010

235U(N,F)95ZR

LAMBDA =1.2516-007, K =3.9030-019, YIELD =6.3630-002

ID	MONITOR LOCATION X	Y	Z	ACTIVITY (DPS/MG)	ACTIVITY (DPS/NUCLEUS)	REACTION RATE (RPS/NUCLEUS)
HB-4 39E	44.2	133.0	-8.5	2.1363+007	8.33798-012	3.92178-010
HB-3 38E	-44.2	133.0	-8.5	2.1672+007	8.45858-012	3.97851-010

TABLE A1 (CONT'D)

238U(N,F)140BA

LAMBDA =6.2730-007, K =3.9530-019, YIELD =5.9480-002

ID	MONITOR LOCATION X	Y	Z	ACTIVITY (DPS/MG)	ACTIVITY (DPS/NUCLEUS)	REACTION RATE (RPS/NUCLEUS)
HB-4 39E	44.8	133.0	-8.5	3.5835+005	1.41656-013	3.37868-012
HB-4A 39E	44.8	133.0	-8.5	2.6197+005	1.03557-013	2.46997-012
HB-3 38E	-44.8	133.0	-8.5	3.6613+005	1.44731-013	3.45203-012
HB-3A 38E	-44.8	133.0	-8.5	2.7073+005	1.07020-013	2.55256-012
HSF-A 38B	-43.1	133.0	7.4	3.0640+005	1.21120-013	2.88887-012
HSF-B 38B	-43.1	133.0	7.4	3.1527+005	1.24626-013	2.97250-012
HSF-C 38B	-43.1	133.0	7.4	2.8631+005	1.13178-013	2.69946-012
HSF-D 38B	-43.1	133.0	7.4	3.0927+005	1.22254-013	2.91593-012
HSF-E 38B	-43.1	133.0	7.4	3.0888+005	1.22100-013	2.91226-012
HSF-F 38B	-43.1	133.0	7.4	2.9888+005	1.18147-013	2.81797-012

238U(N,F)137CS

LAMBDA =7.2793-010, K =3.9530-019, YIELD =6.0000-002

ID	MONITOR LOCATION X	Y	Z	ACTIVITY (DPS/MG)	ACTIVITY (DPS/NUCLEUS)	REACTION RATE (RPS/NUCLEUS)
GE SVQ 19	-52.5	132.6	12.7	1.1200+003	4.42736-016	2.85300-012
HB-4 39E	44.8	133.0	-8.5	1.3565+003	5.36224-016	3.45544-012
HB-4A*39E	44.8	133.0	-8.5	1.0116+003	3.99885-016	2.57687-012
HSF-A 38B	-43.1	133.0	7.4	1.0950+003	4.32853-016	2.78932-012
A	.0	.0	.0	1.0800+003	4.26924-016	2.75111-012
HSF-B 38B	-43.1	133.0	7.4	1.0920+003	4.31668-016	2.78168-012
HSF-C 38B	-43.1	133.0	7.4	1.1298+003	4.46610-016	2.87797-012
C-1	.0	.0	.0	9.4000+002	3.71582-016	2.39448-012
C-2	.0	.0	.0	1.0400+003	4.11112-016	2.64922-012
HSF-D 38B	-43.1	133.0	7.4	1.0158+003	4.01546-016	2.58757-012
D	.0	.0	.0	1.0300+003	4.07159-016	2.62374-012
HSF-E 38B	-43.1	133.0	7.4	1.0962+003	4.33328-016	2.79238-012
HSF-F 38B	-43.1	133.0	7.4	1.0498+003	4.14986-016	2.67418-012
HB-3 38E	-44.8	133.0	-8.5	1.3854+003	5.47649-016	3.52906-012
HB-3A*38E	-44.8	133.0	-8.5	1.0312+003	4.07633-016	2.62680-012

238U(N,F)103RU

LAMBDA =2.0346-007, K =3.9530-019, YIELD =6.2290-002

ID	MONITOR LOCATION X	Y	Z	ACTIVITY (DPS/MG)	ACTIVITY (DPS/NUCLEUS)	REACTION RATE (RPS/NUCLEUS)
GE SVQ 19	-52.5	132.6	12.7	2.0900+005	8.26177-014	2.87878-012
HB-4 39E	44.8	133.0	-8.5	2.2508+005	8.89741-014	3.10027-012
HB-4A*39E	44.8	133.0	-8.5	1.9263+005	7.61466-014	2.65330-012
HSF-A 38B	-43.1	133.0	7.4	2.0076+005	7.93604-014	2.76528-012
A	.0	.0	.0	2.0500+005	8.10365-014	2.82369-012
HSF-B 38B	-43.1	133.0	7.4	2.0532+005	8.11630-014	2.82809-012
HSF-C 38B	-43.1	133.0	7.4	1.9746+005	7.80559-014	2.71983-012
C-1	.0	.0	.0	1.7400+005	6.87822-014	2.39669-012
C-2	.0	.0	.0	1.8000+005	7.11540-014	2.47933-012
HSF-D 38B	-43.1	133.0	7.4	1.9977+005	7.89691-014	2.75165-012
HSF-E 38B	-43.1	133.0	7.4	2.0340+005	8.04040-014	2.80165-012
HSF-F 38B	-43.1	133.0	7.4	2.0222+005	7.99376-014	2.78539-012
HB-3 38E	-44.8	133.0	-8.5	2.2972+005	9.08083-014	3.16418-012
HB-3A*38E	-44.8	133.0	-8.5	1.9713+005	7.79255-014	2.71528-012

TABLE A1 (CONT'D)

238U(N,F)95ZR

LAMBDA =1.2516-007, K =3.9530-019, YIELD =5.1050-002

ID	MONITOR LOCATION X	Y	Z	ACTIVITY (DPS/MG)	ACTIVITY (DPS/NUCLEUS)	REACTION RATE (RPS/NUCLEUS)
GE SVQ 19	-52.5	132.6	12.7	1.1700+005	4.62501-014	2.71145-012
HB-4 39E	44.8	133.0	-8.5	1.5579+005	6.15838-014	3.61040-012
HB-4A*39E	44.8	133.0	-8.5	1.0879+005	4.30047-014	2.52118-012
HSF-A 38B	-43.1	133.0	7.4	1.1593+005	4.58271-014	2.68665-012
A	.0	.0	.0	1.1500+005	4.54595-014	2.66510-012
HSF-B 38B	-43.1	133.0	7.4	1.2071+005	4.77167-014	2.79743-012
HSF-C 38B	-43.1	133.0	7.4	1.1419+005	4.51393-014	2.64633-012
C-1	.0	.0	.0	1.0100+005	3.99253-014	2.34065-012
C-2	.0	.0	.0	1.1600+005	4.58548-014	2.68827-012
HSF-D 38B	-43.1	133.0	7.4	1.1626+005	4.59576-014	2.69430-012
HSF-E 38B	-43.1	133.0	7.4	1.1834+005	4.67798-014	2.74250-012
HSF-F 38B	-43.1	133.0	7.4	1.1736+005	4.63924-014	2.71979-012
HB-3 38E	-44.8	133.0	-8.5	1.5907+005	6.28804-014	3.68641-012
HB-3A*38E	-44.8	133.0	-8.5	1.1139+005	4.40325-014	2.58144-012

237NP(N,F)140BA

LAMBDA =6.2730-007, K =3.9363-019, YIELD =5.4890-002

ID	MONITOR LOCATION X	Y	Z	ACTIVITY (DPS/MG)	ACTIVITY (DPS/NUCLEUS)	REACTION RATE (RPS/NUCLEUS)
HB-4 39E	40.5	133.0	-8.5	1.9425+006	7.64626-013	1.97624-011
HB-3 38E	-40.5	133.0	-8.5	1.8946+006	7.45771-013	1.92751-011
HSF-A 38B	-42.7	133.0	7.4	2.0173+006	7.94070-013	2.05234-011
HSF-B 38B	-42.7	133.0	7.4	1.9557+006	7.69822-013	1.98967-011
HSF-C 38B	-42.7	133.0	7.4	2.0973+006	8.25560-013	2.13373-011
HSF-D 38B	-42.7	133.0	7.4	2.0047+006	7.89110-013	2.03952-011
HSF-E 38B	-42.7	133.0	7.4	2.0843+006	8.20443-013	2.12050-011
HSF-F 38B	-42.7	133.0	7.4	2.0884+006	8.22057-013	2.12468-011

237NP(N,F)137CS

LAMBDA =7.2793-010, K =3.9363-019, YIELD =6.2670-002

ID	MONITOR LOCATION X	Y	Z	ACTIVITY (DPS/MG)	ACTIVITY (DPS/NUCLEUS)	REACTION RATE (RPS/NUCLEUS)
GE SVQ 19	-52.5	132.6	12.7	8.0100+003	3.15298-015	1.94522-011
HB-4 39E	40.5	133.0	-8.5	8.4057+003	3.30874-015	2.04132-011
HB-3 38E	-40.5	133.0	-8.5	8.0688+003	3.17612-015	1.95950-011
HSF-A 38B	-42.7	133.0	7.4	8.3680+003	3.29390-015	2.03216-011
A	.0	.0	.0	8.4900+003	3.34192-015	2.06179-011
HSF-B 38B	-42.7	133.0	7.4	8.1560+003	3.21045-015	1.98068-011
HSF-C 38B	-42.7	133.0	7.4	8.4840+003	3.33956-015	2.06033-011
C-1	.0	.0	.0	7.8200+003	3.07819-015	1.89908-011
C-2	.0	.0	.0	8.3700+003	3.29468-015	2.03265-011
HSF-D 38B	-42.7	133.0	7.4	8.1690+003	3.21556-015	1.98384-011
D	.0	.0	.0	8.3100+000	3.27107-018	6.72693-021
HSF-E 38B	-42.7	133.0	7.4	8.5910+003	3.38168-015	2.08632-011
HSF-F 38B	-42.7	133.0	7.4	9.3081+003	3.66395-015	2.26047-011

TABLE A1 (CONT'D)

237NP(N,F)103RU

LAMBDA =2.0346-007, K =3.9363-019, YIELD =5.5840-002

ID	MONITOR LOCATION X	Y	Z	ACTIVITY (DPS/MG)	ACTIVITY (DPS/NUCLEUS)	REACTION RATE (RPS/NUCLEUS)
GE SVQ 19	-52.5	132.6	12.7	1.2800+006	5.03846-013	1.95842-011
HB-4 39E	40.5	133.0	-8.5	1.3377+006	5.26559-013	2.04671-011
HB-3 38E	-40.5	133.0	-8.5	1.2868+006	5.06523-013	1.96883-011
HSF-A 38B	-42.7	133.0	7.4	1.3147+006	5.17505-013	2.01152-011
A	.0	.0	.0	1.3600+006	5.35337-013	2.08083-011
HSF-B 38B	-42.7	133.0	7.4	1.2870+006	5.06602-013	1.96913-011
HSF-C 38B	-42.7	133.0	7.4	1.3509+006	5.31755-013	2.06690-011
C-1	.0	.0	.0	1.2200+006	4.80229-013	1.86662-011
C-2	.0	.0	.0	1.2100+006	4.76292-013	1.85132-011
HSF-D 38B	-42.7	133.0	7.4	1.3020+006	5.12506-013	1.99208-011
HSF-E 38B	-42.7	133.0	7.4	1.3104+006	5.15813-013	2.00494-011
HSF-F 38B	-42.7	133.0	7.4	1.3322+006	5.24394-013	2.03829-011

237NP(N,F)95ZR

LAMBDA =1.2516-007, K =3.9363-019, YIELD =5.6990-002

ID	MONITOR LOCATION X	Y	Z	ACTIVITY (DPS/MG)	ACTIVITY (DPS/NUCLEUS)	REACTION RATE (RPS/NUCLEUS)
GE SVQ 19	-52.5	132.6	12.7	8.9300+005	3.51512-013	1.84597-011
HB-4 39E	40.5	133.0	-8.5	9.6287+005	3.79015-013	1.99041-011
HB-3 38E	-40.5	133.0	-8.5	9.3105+005	3.66489-013	1.92463-011
HSF-A 38B	-42.7	133.0	7.4	9.5714+005	3.76759-013	1.97856-011
A	.0	.0	.0	9.4200+005	3.70799-013	1.94726-011
HSF-B 38B	-42.7	133.0	7.4	9.3745+005	3.69008-013	1.93786-011
HSF-C 38B	-42.7	133.0	7.4	9.7930+005	3.85482-013	2.02437-011
C-1	.0	.0	.0	8.7200+005	3.43245-013	1.80256-011
C-2	.0	.0	.0	9.2400+005	3.63714-013	1.91006-011
HSF-D 38B	-42.7	133.0	7.4	9.4307+005	3.71221-013	1.94948-011
HSF-E 38B	-42.7	133.0	7.4	9.4564+005	3.72232-013	1.95479-011
HSF-F 38B	-42.7	133.0	7.4	9.6023+005	3.77975-013	1.98495-011

TABLE A2

ORR-PSF SSC-2 INPUT DATA AND CALCULATED REACTION RATES

DATE AND TIME IN - 5/29/81 AT 11:29

DATE AND TIME OUT- 9/25/81 AT 2: 0

TOTAL TIME IN REACTOR = 2846.3499 HRS
NORMALIZED TO POWER OF 30.00 MW

EXPOSURE-	MW SEC.	MW HOURS	MW DAYS
	2.5260+008	7.0168+004	2.9237+003

POWER (MW) WAS-

32.4500	.0000	32.5600	.0000	32.7800
.0000	32.4500	.0000	32.1100	.0000
32.0000	.0000	30.5000	.0000	30.3300
.0000	30.4100			

TIME (HRS) WAS-

9.1000	63.0700	187.4100	25.0200	308.1300
55.9500	359.6700	289.7800	352.5700	36.7300
296.9300	35.2700	224.7200	67.0200	141.6300
63.6400	329.7100			

54FE(N,P)54MN

LAMBDA =2.5672-008, K =1.5989-018, YIELD =1.0000+000

ID	MONITOR LOCATION X	Y	Z	ACTIVITY (DPS/MG)	ACTIVITY (DPS/NUCLEUS)	REACTION RATE (RPS/NUCLEUS)
HE-14 34 25	25.3	122.6	-12.7	5.8070+004	9.28481-014	4.87713-013
HE-13 53 24	-25.3	122.6	-12.7	6.0040+004	9.59980-014	5.04259-013
GE D SVH 19	-52.5	126.3	12.7	5.1400+004	8.21835-014	4.31694-013
GE C SVH 19	-52.5	130.7	12.7	4.7800+004	7.64274-014	4.01459-013
GE SVH 19	-52.5	132.6	12.7	4.7100+004	7.53082-014	3.95579-013
GE B SVH 19	-52.5	134.9	12.7	4.3800+004	7.00318-014	3.67864-013
GE A SVH 19	-52.5	139.1	12.7	4.0000+004	6.39560-014	3.35949-013
H-6 29	.0	131.5	96.9	4.4362+004	7.09304-014	3.72584-013
H-8 31	.0	131.5	62.0	4.8417+004	7.74139-014	4.06641-013
H-9 32	.0	131.5	-1.5	4.9862+004	7.97244-014	4.18777-013
H-10 33	.0	131.5	-65.0	4.7718+004	7.62963-014	4.00770-013
H-7 30	.0	131.5	-100.0	4.0831+004	6.52847-014	3.42928-013
HA-2 8 39G	53.4	133.0	-.6	4.7290+004	7.56120-014	3.97175-013
HA-2 7 39G	46.3	133.0	-.6	4.7650+004	7.61876-014	4.00199-013
HA-2 6 39G	43.0	133.0	-.6	4.7350+004	7.57079-014	3.97679-013
HA-2 5 39G	41.5	133.0	-.6	4.7150+004	7.53881-014	3.95999-013
HB-6 39E	37.7	133.0	-8.5	4.6914+004	7.50108-014	3.94017-013
HB-5 38E	-37.7	133.0	-8.5	4.7462+004	7.58870-014	3.98620-013
HA-1 1 38G	-41.5	133.0	-.6	4.9140+004	7.85699-014	4.12713-013
HA-1 2 38G	-43.0	133.0	-.6	4.9610+004	7.93214-014	4.16660-013
HA-1 3 38G	-46.3	133.0	-.6	4.9320+004	7.88577-014	4.14225-013
HA-1 4 38G	-53.4	133.0	-.6	4.8570+004	7.76586-014	4.07926-013
HE-14 18 25	25.3	135.1	-12.7	4.5550+004	7.28299-014	3.82561-013
HE-13 5 24	-25.3	135.1	-12.7	4.7010+004	7.51643-014	3.94824-013

TABLE A2 (CONT'D)

58FE(N,G)59FE

LAMBDA =1.7988-007, K =2.8102-017, YIELD =1.0000+000

ID	MONITOR LOCATION X	Y	Z	ACTIVITY (DPS/MG)	ACTIVITY (DPS/NUCLEUS)	REACTION RATE (RPS/NUCLEUS)
HE-14 53 25	25.3	122.6	-12.7	3.7290+004	1.04792-012	1.49101-012
HE-13 34 24	-25.3	122.6	-12.7	3.9980+004	1.12352-012	1.59857-012
H-6 29	.0	131.5	96.9	8.1871+004	2.30074-012	3.27355-012
H-8 31	.0	131.5	62.0	8.7528+004	2.45971-012	3.49974-012
H-9 32	.0	131.5	-1.5	8.8417+004	2.48469-012	3.53528-012
H-10 33	.0	131.5	-65.0	8.6021+004	2.41736-012	3.43948-012
H-7 30	.0	131.5	-100.0	7.4437+004	2.09183-012	2.97630-012
GE SVH 19	-52.5	132.6	12.7	3.2200+004	9.04884-013	1.28749-012
HA-2 8 39G	53.4	133.0	-.6	2.8970+004	8.14115-013	1.15834-012
HA-2 7 39G	46.3	133.0	-.6	3.0860+004	8.67228-013	1.23391-012
HA-2 6 39G	43.0	133.0	-.6	3.0880+004	8.67790-013	1.23471-012
HA-2 5 39G	41.5	133.0	-.6	3.0920+004	8.68914-013	1.23631-012
HB-6 39E	37.7	133.0	-8.5	3.0236+004	8.49692-013	1.20896-012
HB-5 38E	-37.7	133.0	-8.5	3.0828+004	8.66328-013	1.23263-012
HA-1 1 38G	-41.5	133.0	-.6	3.1980+004	8.98702-013	1.27870-012
HA-1 2 38G	-43.0	133.0	-.6	3.3180+004	9.32424-013	1.32668-012
HA-1 3 38G	-46.3	133.0	-.6	3.2160+004	9.03760-013	1.28589-012
HA-1 4 38G	-53.4	133.0	-.6	3.2040+004	9.00388-013	1.28109-012
HE-14 18 25	25.3	135.1	-12.7	2.8020+004	7.87418-013	1.12036-012
HE-13 5 24	-25.3	135.1	-12.7	2.8590+004	8.03436-013	1.14315-012

58NI(N,P)58CO

LAMBDA =1.1323-007, K =1.4278-019, YIELD =1.0000+000

ID	MONITOR LOCATION X	Y	Z	ACTIVITY (DPS/MG)	ACTIVITY (DPS/NUCLEUS)	REACTION RATE (RPS/NUCLEUS)
GE B SVH 19	-52.5	123.9	12.7	2.5900+006	3.69800-013	6.49608-013
GE BA SVH 19	0	123.9	12.7	2.6000+006	3.71228-013	6.52116-013
GE BB SVH 19	0	123.9	12.7	2.6000+006	3.71228-013	6.52116-013
GE BC SVH 19	.0	123.9	12.7	2.6100+006	3.72656-013	6.54624-013
GE T SVH 19	-52.5	141.3	12.7	1.8400+006	2.62715-013	4.61497-013
H-6 29	.0	131.5	96.9	2.0223+006	2.88744-013	5.07221-013
H-8 31	.0	131.5	62.0	2.2056+006	3.14916-013	5.53195-013
H-9 32	.0	131.5	-1.5	2.2719+006	3.24382-013	5.69824-013
H-10 33	.0	131.5	-65.0	2.1672+006	3.09433-013	5.43564-013
H-7 30	.0	131.5	-100.0	1.9124+006	2.73052-013	4.79656-013
HA-2 39G	43.2	133.0	-.6	2.1640+006	3.08976-013	5.42761-013
HB-6 39E	38.3	133.0	-8.5	2.1981+006	3.13845-013	5.51314-013
HB-5 38E	-38.3	133.0	-8.5	2.2473+006	3.20869-013	5.63654-013
HA-1 38G	-43.2	133.0	-.6	2.2390+006	3.19684-013	5.61572-013
CE F23-6R 20	-25.3	.0	12.7	2.1800+006	3.11260-013	5.46774-013

63CU(N,A)60CO

LAMBDA =4.1671-009, K =1.5255-019, YIELD =1.0000+000

ID	MONITOR LOCATION X	Y	Z	ACTIVITY (DPS/MG)	ACTIVITY (DPS/NUCLEUS)	REACTION RATE (RPS/NUCLEUS)
GE SVH 19	-52.5	128.5	12.7	6.2800+002	9.58014-017	2.78837-015
GE SVH 19	-52.5	137.0	12.7	5.3200+002	8.11566-017	2.36213-015
CU-4 39H	53.7	130.7	-4.9	6.1460+002	9.37572-017	2.72888-015
CU-3 38H	-37.7	130.7	-4.9	6.1280+002	9.34826-017	2.72088-015
HA-2 F 39G	43.5	133.0	-.6	5.8280+002	8.89061-017	2.58768-015
HA-2 W 39G	43.4	133.0	-.6	5.8570+002	8.93485-017	2.60056-015
HB-6 39E	39.3	133.0	-8.5	5.7730+002	8.80671-017	2.56326-015
HB-5 38E	-39.3	133.0	-8.5	5.9210+002	9.03249-017	2.62898-015
HA-1 W 38G	-43.4	133.0	-.6	5.9960+002	9.14690-017	2.66228-015
HA-1 F 38G	-43.5	133.0	-.6	6.0290+002	9.19724-017	2.67693-015
CE F23-6R 20	-25.3	.0	12.7	5.9500+002	9.07672-017	2.64185-015

TABLE A2 (CONT'D)

46TI(N,P)46SC

LAMBDA =9.5677-008, K =9.8198-019, YIELD =1.0000+000

ID		MONITOR LOCATION X	Y	Z	ACTIVITY (DPS/MG)	ACTIVITY (DPS/NUCLEUS)	REACTION RATE (RPS/NUCLEUS)
H-6	29	.0	131.5	96.9	2.4175+004	2.37394-014	4.59004-014
H-8	31	.0	131.5	62.0	2.8489+004	2.79756-014	5.40912-014
H-9	32	.0	131.5	-1.5	2.8587+004	2.80719-014	5.42773-014
H-10	33	.0	131.5	-65.0	2.7627+004	2.71292-014	5.24546-014
H-7	30	.0	131.5	-100.0	2.4189+004	2.37531-014	4.59269-014
HB- 5	38E	-38.8	133.0	-8.5	2.8541+004	2.80267-014	5.41900-014
HB- 6	39E	38.8	133.0	-8.5	2.7769+004	2.72686-014	5.27242-014
GE SVH	19	-52.5	139.2	12.7	2.5100+004	2.46477-014	4.76566-014

59CO(N,G)60CO

LAMBDA =4.1671-009, K =9.7862-020, YIELD =1.0000+000

ID		MONITOR LOCATION X	Y	Z	ACTIVITY (DPS/MG)	ACTIVITY (DPS/NUCLEUS)	REACTION RATE (RPS/NUCLEUS)
H-6	29	.0	131.5	96.9	5.8551+007	5.72992-012	1.66774-010
H-8	31	.0	131.5	62.0	6.2370+007	6.10365-012	1.77652-010
H-9	32	.0	131 5	-1.5	6.3868+007	6.25025-012	1.81918-010
H-10	33	.0	131 5	-65.0	6.1121+007	5.98142-012	1.74094-010
H-7	30	.0	131.5	-100.0	5.3515+007	5.23708-012	1.52429-010
HA-2	39G	43.0	133.0	-.6	3.0941+007	3.02795-012	8.81308-011
HB-6	39E	39.8	133.0	-8.5	3.1659+007	3.09821-012	9.01759-011
HB-5	38E	-39.8	133.0	-8.5	3.2826+007	3.21242-012	9.34999-011
HA-1	38G	-43.0	133.0	-.6	3.2360+007	3.16681-012	9.21726-011
CE F23-6R	20	-25.3	.0	12.7	3.6000+005	3.52303-014	1.02541-012
GE SVH	19	-52.5	139.2	12.7	3.1900+007	3.12180-012	9.08624-011

109AG(N,G)110AGM

LAMBDA =3.2118-008, K =3.7185-019, YIELD =1.0000+000

ID		MONITOR LOCATION X	Y	Z	ACTIVITY (DPS/MG)	ACTIVITY (DPS/NUCLEUS)	REACTION RATE (RPS/NUCLEUS)
H-6	29	.0	131.5	96.9	5.5022+007	2.04599-011	8.86032-011
H-8	31	.0	131.5	62.0	6.1114+007	2.27252-011	9.84133-011
H-9	32	.0	131.5	-1.5	6.2398+007	2.32027-011	1.00481-010
H-10	33	.0	131.5	-65.0	5.8933+007	2.19142-011	9.49012-011
H-7	30	.0	131.5	-100.0	5.1179+007	1.90309-011	8.24148-011
HA-2	39G	42.9	133.0	-.6	4.9880+007	1.85479-011	8.03229-011
HB-6	39E	40.9	133.0	-8.5	4.9991+007	1.85892-011	8.05017-011
HB-5	38E	-40.9	133.0	-8.5	5.2509+007	1.95255-011	8.45565-011
HA-1	38E	-42.9	133.0	-.6	5.2590+007	1.95556-011	8.46869-011

45SC(N,G)46SC

LAMBDA =9.5677-008, K =7.4652-020, YIELD =1.0000+000

ID		MONITOR LOCATION X	Y	Z	ACTIVITY (DPS/MG)	ACTIVITY (DPS/NUCLEUS)	REACTION RATE (RPS/NUCLEUS)
H-6 MGO	29	12.4	131.5	100.0	4.3769+008	3.26744-011	6.31764-011
H-6	29	-14.0	131.5	100.0	4.4317+008	3.30835-011	6.39674-011
H-8 MGO	31	12.4	131.5	65.0	3.9739+008	2.96660-011	5.73595-011
H-8	31	-14.0	131.5	65.0	4.0000+008	2.98608-011	5.77362-011
H-9 MGO	32	12.4	131.5	1.5	4.6908+008	3.50178-011	6.77073-011
H-9	32	-14.0	131.5	1.5	4.6563+008	3.47602-011	6.72093-011
H-10 MGO	33	12.4	131.5	-62.0	4.5357+008	3.38599-011	6.54685-011
H-10	33	-14.0	131.5	-62.0	4.5258+008	3.37860-011	6.53257-011

TABLE A2 (CONT'D)

45SC(N,G)46SC (CONTINUED)

ID	MONITOR LOCATION X	Y	Z	ACTIVITY (DPS/MG)	ACTIVITY (DPS/NUCLEUS)	REACTION RATE (RPS/NUCLEUS)
H-7 MGO 30	12.4	131 5	-96.9	4.4975+008	3.35747-011	6.49172-011
H-7 30	-14.0	131 5	-96.9	4.6062+008	3.43862-011	6.64861-011
HA-2 39G	43.8	133 0	-.6	9.5420+007	7.12329-012	1.37730-011
HB-6 39E	39.7	133.0	-8.5	9.6883+007	7.23251-012	1.39841-011
HB-5 38E	-39.7	133.0	-8.5	1.0275+008	7.67049-012	1.48310-011
HA-1 38G	-43.8	133.0	-.6	8.6840+007	6.48278-012	1.25345-011

235U(N,F)137CS

LAMBDA =7.2793-010, K =3.9030-019, YIELD =6.2210-002

ID	MONITOR LOCATION X	Y	Z	ACTIVITY (DPS/MG)	ACTIVITY (DPS/NUCLEUS)	REACTION RATE (RPS/NUCLEUS)
HB-6 39E	44.2	133.0	-8.5	3.5490+005	1.38517-013	3.64616-010
HB-6A* 39E	44.2	133.0	-8.5	3.5470+005	1.38439-013	3.64410-010
CE F23-6R 20	-25.3	.0	12.7	4.5400+003	1.77196-015	4.66428-012
HB-5 38E	-44.2	133.0	-8.5	3.6400+005	1.42069-013	3.73965-010
HB-5A* 38E	-44.2	133.0	-8.5	3.6380+005	1.41991-013	3.73759-010

235U(N,F)103RU

LAMBDA =2.0346-007, K =3.9030-019, YIELD =3.0420-002

ID	MONITOR LOCATION X	Y	Z	ACTIVITY (DPS/MG)	ACTIVITY (DPS/NUCLEUS)	REACTION RATE (RPS/NUCLEUS)
HB-6 39E	44.2	133.0	-8.5	2.2320+007	8.71150-012	3.90586-010
HB-6A* 39E	44.2	133.0	-8.5	2.2298+007	8.70291-012	3.90201-010
HB-5 38E	-44.2	133.0	-8.5	2.3010+007	8.98080-012	4.02661-010
HB-5A* 38E	-44.2	133.0	-8.5	2.2985+007	8.97105-012	4.02223-010

235U(N,F)95ZR

LAMBDA =1.2516-007, K =3.9030-019, YIELD =6.4950-002

ID	MONITOR LOCATION X	Y	Z	ACTIVITY (DPS/MG)	ACTIVITY (DPS/NUCLEUS)	REACTION RATE (RPS/NUCLEUS)
HB-6 39E	44.2	133.0	-8.5	3.6590+007	1 42811-011	3.66536-010
HB6A* 39E	44.2	133.0	-8.5	3.6590+007	1.42811-011	3.66536-010
CE F23-6R 20	-25.3	.0	12.7	3.8500+005	1.50265-013	3.85669-012
HB-5 38E	-44.2	133.0	-8.5	3.7870+007	1.47807-011	3.79358-010
HB5A* 38E	-44.2	133.0	-8.5	3.7860+007	1.47768-011	3.79258-010

238U(N,F)137CS

LAMBDA =7.2793-010, K =3.9530-019, YIELD =6.0000-002

ID	MONITOR LOCATION X	Y	Z	ACTIVITY (DPS/MG)	ACTIVITY (DPS/NUCLEUS)	REACTION RATE (RPS/NUCLEUS)
GE SVH 19	-52.5	132.6	12.7	2.6000+003	1.02778-015	2.80504-012
HB-6 39E	44.8	133.0	-8.5	3.4810+003	1.37604-015	3.75552-012
HB6A* 39E	44.8	133.0	-8.5	2.7010+003	1.06771-015	2.91401-012
CE F23-6R 20	-25.3	.0	12.7	2.4200+003	9.56626-016	2.61085-012
HB-5 38E	-44.8	133.0	-8.5	3.7020+003	1.46340-015	3.99395-012
HB5A* 38E	-44.8	133.0	-8.5	2.9020+003	1.14716-015	3.13086-012

TABLE A2 (CONT'D)

238U(N,F)103RU

LAMBDA =2.0345-007, K =3.9530-019, YIELD =6.2290-002

ID	MONITOR LOCATION X	Y	Z	ACTIVITY (DPS/MG)	ACTIVITY (DPS/NUCLEUS)	REACTION RATE (RPS/NUCLEUS)
GE SVH 19	-52.5	132.6	12.7	3.5200+005	1.39146-013	3.04678-012
HB-6 39E	44.8	133.0	-8.5	4.0480+005	1.60017-013	3.50380-012
HB6A* 39E	44.8	133.0	-8.5	3.5575+005	1.40628-013	3.07924-012
HB-5 38E	-44.8	133.0	-8.5	4.4370+005	1.75395-013	3.84050-012
HB5A* 38E	-44.8	133.0	-8.5	3.9310+005	1.55392-013	3.40253-012

238U(N,F)95ZR

LAMBDA =1.2516-007, K =3.9530-019, YIELD =5.1050-002

ID	MONITOR LOCATION X	Y	Z	ACTIVITY (DPS/MG)	ACTIVITY (DPS/NUCLEUS)	REACTION RATE (RPS/NUCLEUS)
GE SVH 19	-52.5	132.6	12.7	2.0900+005	8.26177-014	2.69781-012
HB-6 39E	44.8	133.0	-8.5	3.0080+005	1.18906-013	3.88279-012
HB6A* 39E	44.8	133.0	-8.5	2.2030+005	8.70846-014	2.84368-012
CE F23-6R 20	-25.3	.0	12.7	2.0000+005	7.90600-014	2.58164-012
HB-5 38E	-44.8	133.0	-8.5	3.2060+005	1.26733-013	4.13837-012
HB5A* 38E	-44.8	133.0	-8.5	2.3730+005	9.38047-014	3.06311-012

237NP(N,F)137CS

LAMBDA =7.2793-010, K =3.9363-019, YIELD =6.2670-002

ID	MONITOR LOCATION X	Y	Z	ACTIVITY (DPS/MG)	ACTIVITY (DPS/NUCLEUS)	REACTION RATE (RPS/NUCLEUS)
GE SVH 19	-52.5	132.6	12.7	1.6100+004	6.33744-015	1.65594-011
HB-6 39E	40.5	133.0	-8.5	1.7036+004	6.70588-015	1.75221-011
HB-5 38E	-40.5	133.0	-8.5	1.7542+004	6.90506-015	1.80426-011

237NP(N,F)103RU

LAMBDA =2.0346-007, K =3.9363-019, YIELD =5.5840-002

ID	MONITOR LOCATION X	Y	Z	ACTIVITY (DPS/MG)	ACTIVITY (DPS/NUCLEUS)	REACTION RATE (RPS/NUCLEUS)
GE SVH 19	-52.5	132.6	12.7	1.7300+006	6.80980-013	1.66331-011
HB-6 39E	40.5	133.0	-8.5	1.8287+006	7.19831-013	1.75820-011
HB-5 38E	-40.5	133.0	-8.5	1.8524+006	7.29160-013	1.78099-011

237NP(N,F)95ZR

LAMBDA =1.2516-007, K =3.9363-019, YIELD =5.6990-002

ID	MONITOR LOCATION X	Y	Z	ACTIVITY (DPS/MG)	ACTIVITY (DPS/NUCLEUS)	REACTION RATE (RPS/NUCLEUS)
GE SVH 19	-52.5	132.6	12.7	1.3700+006	5.39273-013	1.57741-011
HB-6 39E	40.5	133.0	-8.5	1.4905+006	5.86706-013	1.71615-011
HB-5 38E	-40.5	133.0	-8.5	1.5136+006	5.95798-013	1.74275-011

TABLE A3

ORR-PSF SPVC-SVBC INPUT DATA AND CALCULATED REACTION RATES

DATE AND TIME IN - 4/30/80 AT 13:34

DATE AND TIME OUT- 6/22/82 AT 24:00

TOTAL TIME IN REACTOR = 18800.3887 HRS
NORMALIZED TO POWER OF 30.00 MW

EXPOSURE-	MW SEC.	MW HOURS	MW DAYS
	1.5291+009	4.2476+005	1.7698+004

POWER (MW) WAS-

28.0000	.0000	27.8300	.0000	27.9800	.0000
.0000	27.8300	.0000	26.6600	.0000	28.6700
28.2600	.0000	28.1800	.0000	28.6700	.0000
.0000	9.4200	.0000	27.8700	.0000	28.9400
28.9200	.0000	29.1900	.0000	28.9400	.0000
.0000	26.5400	.0000	27.3300	.0000	27.4700
27.6500	.0000	27.1800	.0000	27.4700	.0000
.0000	27.4200	.0000	27.1900	.0000	31.7200
26.8300	.0000	32.5500	.0000	31.7200	.0000
.0000	31.3200	.0000	30.1700	.0000	33.3100
30.4900	.0000	32.8900	.0000	33.3100	.0000
.0000	33.1900	.0000	30.0100	.0000	32.2100
29.8600	.0000	29.9200	.0000	32.2100	.0000
.0000	32.1700	.0000	32.0500	.0000	32.4500
32.1700	.0000	32.0900	.0000	32.4500	.0000
.0000	32.5600	.0000	32.7800	.0000	32.0000
32.4500	.0000	32.1100	.0000	32.0000	.0000
.0000	30.5000	.0000	30.3300	.0000	29.7400
30.4100	.0000	29.6800	.0000	29.7400	.0000
.0000	29.7300	.0000	29.8200	.0000	30.9100
29.8100	.0000	30.8300	.0000	30.9100	.0000
.0000	30.5000	.0000	30.8400	.0000	28.3200
28.5600	.0000	28.4400	.0000	28.3200	.0000
.0000	28.4900	.0000	28.5400	.0000	25.7400
26.4000	.0000	26.1000	.0000		
.0000	24.7300	.0000			

TIME (HRS) WAS-

184.4200	10.7300	140.7600	44.4700	112.3300	
32.5300	370.6300	132.3100	267.1500	101.5800	
173.6800	61.7400	19.5700	5.8100	111.6900	
129.9900	.5000	5.3300	52.3400	30.9100	
199.5300	24.7200	288.3700	68.1000	1.2700	
138.6800	124.6900	22.8900	108.9500	54.4300	
141.5500	27.8900	302.9000	11.6000	295.2300	
40.6700	244.0400	91.0000	183.1300	13.8500	
228.9300	607.1400	128.6800	37.3700	184.3500	
12.5170	278.2300	8.1830	183.5300	14.4100	
173.8600	31.9000	80.4700	36.8800	21.3400	
9.9200	255.0900	174.1900	351.5000	9.9200	
398.8800	2.9000	65.6100	79.8200	276.4300	
12.9000	39.3700	13.2500	399.8400	194.1900	
325.5000	16.7000	370.6000	55.6500	9.1000	
63.0670	187.4100	25.0200	308.1300	55.9500	
359.6700	289.7830	352.5700	36.7300	296.9300	
35.2700	224.7200	67.0170	141.6300	63.6400	
329.7100	21.1670	412.0500	17.2900	221.9300	
11.0400	78.6300	14.5900	185.8900	12.6000	
255.7400	222.2900	423.7900	147.7900	243.1200	
80.4500	130.5400	6.4100	180.3300	180.9700	
251.3600	13.9800	135.0500	129.5700	135.3800	
10.0500	421.2100	31.3600	370.0100	41.3600	
223.7400	16.0100	259.7300	314.3100	584.9200	
91.8500	623.8000	1.7300			

TABLE A3 (CONT'D)

54FE(N,P)54MN

LAMBDA =2.5672-008, K =1.5989-018, YIELD =1.0000+000

ID	MONITOR LOCATION X	Y	Z	ACTIVITY (DPS/MG)	ACTIVITY (DPS/NUCLEUS)	REACTION RATE (RPS/NUCLEUS)
OTLF FE10	-103.7	229.7	114.1	2.1964+004	3.51182-014	5.63773-014
OTLF FE09	-103.7	229.7	90.7	2.2476+004	3.59369-014	5.76916-014
OTLF FE08	-103.7	229.7	65.5	2.3075+004	3.68946-014	5.92291-014
OTLF FE07	-103.7	229.7	40.0	2.3546+004	3.76477-014	6.04380-014
OTLF FE06	-103.7	229.7	14.4	2.3418+004	3.74430-014	6.01095-014
OTLF FE05	-103.7	229.7	-10.0	2.3506+004	3.75837-014	6.03354-014
OTLF FE04	-103.7	229.7	-37.9	2.3091+004	3.69202-014	5.92701-014
OTLF FE03	-103.7	229.7	-63.4	2.2392+004	3.58026-014	5.74759-014
OTLF FE02	-103.7	229.7	-88.8	2.2575+004	3.60952-014	5.79457-014
OTLF FE01	-103.7	229.7	-112.3	2.0577+004	3.29006-014	5.28172-014
OTRF FE11	103.7	229.7	117.3	2.0963+004	3.35177-014	5.38080-014
OTRF FE10	103.7	229.7	112.9	2.1022+004	3.36121-014	5.39594-014
OTRF FE09	103.7	229.7	90.5	2.1592+004	3.45234-014	5.54225-014
OTRF FE08	103.7	229.7	65.2	2.1973+004	3.51326-014	5.64004-014
OTRF FE07	103.7	229.7	40.0	2.2417+004	3.58425-014	5.75401-014
OTRF FE06	103.7	229.7	14.0	2.2507+004	3.59864-014	5.77711-014
OTRF FE05	103.7	229.7	12.4	2.2447+004	3.58905-014	5.76171-014
OTRF FE04	103.7	229.7	-38.4	2.2265+004	3.55995-014	5.71500-014
OTRF FE03	103.7	229.7	-63.6	2.1659+004	3.46306-014	5.55945-014
OTRF FE02	103.7	229.7	-88.8	2.0792+004	3.32443-014	5.33690-014
OTRF FE01	103.7	229.7	-112.3	1.9771+004	3.16119-014	5.07483-014
HE-16 39 25	25.3	231.0	-12.7	2.4750+004	3.95728-014	6.35285-014
HE-15 26 24	-25.3	231.0	-12.7	2.5070+004	4.00844-014	6.43498-014
H-11 29	.0	239.8	122.2	2.0396+004	3.26112-014	5.23526-014
H-13 31	.0	239.8	62.0	2.1666+004	3.46418-014	5.56124-014
H-14 32	.0	239.8	-1.5	2.2177+004	3.54588-014	5.69241-014
H-15 33	.0	239.8	-65.0	2.1130+004	3.37848-014	5.42366-014
H-12 30	.0	239.8	-125.5	1.8807+004	3.00705-014	4.82739-014
HB-2 39G	37.7	241.3	-.3	2.1158+004	3.38295-014	5.43085-014
HB-1 38E	-37.7	241.3	-8.5	2.1428+004	3.42612-014	5.50015-014
HA- 6 17 38G	-41.5	242.3	-.6	2.1230+004	3.39446-014	5.44933-014
HA- 6 19 38G	-43.0	242.3	-.6	2.1150+004	3.38167-014	5.42880-014
HA- 6 20 38G	-46.3	242.3	-.6	2.1120+004	3.37688-014	5.42110-014
HA- 6 21 38G	-53.4	242.3	-.6	2.1070+004	3.36888-014	5.40826-014
HA- 7 25 39E	53.4	242.3	-.6	2.0540+004	3.28414-014	5.27222-014
HA- 7 24 39E	46.3	242.3	-.6	2.0760+004	3.31932-014	5.32869-014
HA- 7 23 39E	43.0	242.3	-.6	2.0860+004	3.33531-014	5.35436-014
HA- 7 22 39E	41.5	242.3	-.6	2.0870+004	3.33690-014	5.35693-014
GE D F2319R	-50.7	234.7	12.7	2.3700+004	3.78939-014	6.08333-014
GE C F2319R	-50.7	239.2	12.7	2.2300+004	3.56555-014	5.72398-014
GE19SFF2319R	-50.7	240.8	12.7	2.1300+004	3.40566-014	5.46730-014
GE B F2319R	-50.7	243.5	12.7	2.0600+004	3.29373-014	5.28762-014
HE-16 41 25	25.3	243.4	-12.7	2.0510+004	3.27934-014	5.26452-014
HE-15 59 24	-25.3	243.4	-12.7	2.0730+004	3.31452-014	5.32099-014
GE A F2319R	-50.7	247.5	12.7	1.9200+004	3.06989-014	4.92827-014
OTLR FE11	-103.7	252.9	119.0	1.4736+004	2.35614-014	3.78245-014
OTLR FE10	-103.7	252.9	109.9	1.4891+004	2.38092-014	3.82223-014
OTLR FE09	-103.7	252.9	86.2	1.5110+004	2.41594-014	3.87845-014
OTLR FE08	-103.7	252.9	61.1	1.5474+004	2.47414-014	3.97188-014
OTLR FE07	-103.7	252.9	35.2	1.5659+004	2.50372-014	4.01936-014
OTLR FE06	-103.7	252.9	9.8	1.5818+004	2.52914-014	4.06018-014
OTLR FE05	-103.7	252.9	-13.5	1.5775+004	2.52226-014	4.04914-014
OTLR FE04	-103.7	252.9	-38.2	1.5369+004	2.45735-014	3.94493-014
OTLR FE03	-103.7	252.9	-62.9	1.4945+004	2.38956-014	3.83609-014
OTLR FE02	-103.7	252.9	-88.2	1.4544+004	2.32544-014	3.73316-014
OTLR FE01	-103.7	252.9	-112.1	1.3771+004	2.20185-014	3.53475-014
OTRR FE11	103.7	252.9	114.5	1.4219+004	2.27348-014	3.64974-014
OTRR FE10	103.7	252.9	112.7	1.4115+004	2.25685-014	3.62305-014
OTRR FE09	103.7	252.9	88.7	1.4461+004	2.31217-014	3.71186-014
OTRR FE08	103.7	252.9	63.4	1.4699+004	2.35022-014	3.77295-014
OTRR FE07	103.7	252.9	38.1	1.4972+004	2.39387-014	3.84302-014
OTRR FE06	103.7	252.9	12.8	1.5087+004	2.41226-014	3.87254-014
OTRR FE05	103.7	252.9	-12.8	1.5055+004	2.40714-014	3.86433-014
OTRR FE04	103.7	252.9	-38.3	1.4742+004	2.35710-014	3.78399-014
OTRR FE03	103.7	252.9	-63.6	1.4367+004	2.29714-014	3.68773-014

TABLE A3 (CONT'D)

54FE(N,P)54MN (CONTINUED)

ID	MONITOR LOCATION X	Y	Z	ACTIVITY (DPS/MG)	ACTIVITY (DPS/NUCLEUS)	REACTION RATE (RPS/NUCLEUS)
OTRR FE02	103.7	252.9	-89.2	1.3930+004	2.22727-014	3.57556-014
OTRR FE01	103.7	252.9	-112.6	1.3208+004	2.11183-014	3.39024-014
QTLF FE10	-103.7	274.8	122.3	1.0158+004	1.62416-014	2.60736-014
QTLF FE09	-103.7	274.8	94.8	1.0338+004	1.65294-014	2.65356-014
QTLF FE08	-103.7	274.8	69.2	1.0546+004	1.68620-014	2.70695-014
QTLF FE07	-103.7	274.8	43.4	1.0654+004	1.70347-014	2.73468-014
QTLF FE06	-103.7	274.8	17.7	1.0659+004	1.70427-014	2.73596-014
QTLF FE05	-103.7	274.8	-2.2	1.0660+004	1.70443-014	2.73622-014
QTLF FE04	-103.7	274.8	-33.1	1.0405+004	1.66366-014	2.67076-014
QTLF FE03	-103.7	274.8	-58.9	1.0213+004	1.63296-014	2.62148-014
QTLF FE02	-103.7	274.8	-84.4	9.8805+003	1.57979-014	2.53613-014
QTLF FE01	-103.7	274.8	-110.1	9.3316+003	1.49203-014	2.39524-014
QTRF FE10	103.7	274.8	115.3	9.7266+003	1.55519-014	2.49663-014
QTRF FE09	103.7	274.8	91.1	9.4152+003	1.50540-014	2.41670-014
QTRF FE08	103.7	274.8	66.2	9.2455+003	1.47826-014	2.37314-014
QTRF FE07	103.7	274.8	41.3	1.0028+004	1.60338-014	2.57399-014
QTRF FE06	103.7	274.8	15.8	1.0217+004	1.63360-014	2.62251-014
QTRF FE05	103.7	274.8	-3.8	1.0244+004	1.63791-014	2.62944-014
QTRF FE04	103.7	274.8	-35.3	1.0181+004	1.62784-014	2.61327-014
QTRF FE03	103.7	274.8	-61.2	9.9815+003	1.59594-014	2.56206-014
QTRF FE02	103.7	274.8	-86.3	9.8144+003	1.56922-014	2.51917-014
QTRF FE01	103.7	274.8	-111.0	9.6107+003	1.53665-014	2.46688-014
H-16 29	.0	284.9	122.2	9.3233+003	1.49070-014	2.39311-014
H-18 31	.0	284.9	62.0	9.6101+003	1.53656-014	2.46673-014
H-19 32	.0	284.9	-1.5	9.7923+003	1.56569-014	2.51349-014
H-20 33	.0	284.9	-65.0	9.2663+003	1.48159-014	2.37848-014
H-17 30	.0	284.9	-125.5	8.3312+003	1.33208-014	2.13846-014
GE D F23-8R	-66.2	279.8	12.7	1.0500+004	1.67884-014	2.69515-014
GE C F23-8R	-66.2	284.3	12.7	9.9600+003	1.59250-014	2.55654-014
GE19QTF23-8R	-66.2	285.9	12.7	9.4000+003	1.50297-014	2.41280-014
GE B F23-8R	-66.2	288.6	12.7	9.2100+003	1.47259-014	2.36403-014
GE A F23-8R	-66.2	292.6	12.7	8.4400+005	1.34947-012	2.16638-012
HB-3 39E	37.7	286.4	-8.5	9.4056+003	1.50386-014	2.41424-014
HB-7 38E	-37.7	286.4	-8.5	9.5199+003	1.52214-014	2.44357-014
HA- 8 27 38G	-41.5	286.4	-.6	8.9090+003	1.42446-014	2.28677-014
HA- 8 28 38G	-43.0	286.4	-.6	9.4010+003	1.50313-014	2.41306-014
HA- 8 29 38G	-46.3	286.4	-.6	9.4340+003	1.50840-014	2.42153-014
HA- 8 30 38G	-53.4	286.4	-.6	9.7450+003	1.55813-014	2.50135-014
QTLR FE10	-103.7	298.0	115.3	6.7296+003	1.07600-014	1.72736-014
QTLR FE09	-103.7	298.0	91.0	6.7247+003	1.07521-014	1.72610-014
QTLR FE08	-103.7	298.0	66.0	6.8728+003	1.09889-014	1.76411-014
QTLR FE07	-103.7	298.0	40.8	6.9369+003	1.10914-014	1.78057-014
QTLR FE06	-103.7	298.0	14.9	7.0054+003	1.12009-014	1.79815-014
QTLR FE05	-103.7	298.0	-8.6	6.9237+003	1.10703-014	1.77718-014
QTLR FE04	-103.7	298.0	-38.2	6.7800+003	1.08405-014	1.74030-014
QTLR FE03	-103.7	298.0	-64.0	6.6207+003	1.05858-014	1.69941-014
QTLR FE02	-103.7	298.0	-89.3	6.4204+003	1.02656-014	1.64799-014
QTLR FE01	-103.7	298.0	-112.5	6.0656+003	9.69829-015	1.55692-014
QTRF FE11	103.7	274.8	118.6	9.9552+003	1.59174-014	2.55531-014
QTRR FE11	103.7	298.0	122.3	6.4297+003	1.02804-014	1.65038-014
QTRR FE10	103.7	298.0	109.0	6.3817+003	1.02037-014	1.63806-014
QTRR FE09	103.7	298.0	85.7	6.4529+003	1.03175-014	1.65633-014
QTRR FE08	103.7	298.0	61.1	6.5789+003	1.05190-014	1.68868-014
QTRR FE07	103.7	298.0	36.4	6.6088+003	1.05668-014	1.69635-014
QTRR FE06	103.7	298.0	9.5	6.6890+003	1.06950-014	1.71694-014
QTRR FE05	103.7	298.0	-14.2	6.6079+003	1.05654-014	1.69612-014
QTRR FE04	103.7	298.0	-39.6	6.4689+003	1.03431-014	1.66044-014
QTRR FE03	103.7	298.0	-64.7	6.3357+003	1.01302-014	1.62625-014
QTRR FE02	103.7	298.0	-89.4	6.1229+003	9.78990-015	1.57163-014
QTRR FE01	103.7	298.0	-112.4	5.8432+003	9.34269-015	1.49984-014
HTLF FE11	-103.7	326.2	120.4	4.0663+003	6.50161-015	1.04374-014
HTLF FE10	-103.7	326.2	115.6	4.1065+003	6.56588-015	1.05406-014
HTLF FE09	-103.7	326.2	91.5	4.1242+003	6.59418-015	1.05860-014
HTLF FE08	-103.7	326.2	66.2	4.1704+003	6.66805-015	1.07046-014
HTLF FE07	-103.7	326.2	40.8	4.1622+003	6.65494-015	1.06836-014
HTLF FE06	-103.7	326.2	14.9	4.2002+003	6.71570-015	1.07811-014
HTLF FE05	-103.7	326.2	-9.2	4.1387+003	6.61737-015	1.06232-014

TABLE A3 (CONT'D)

54FE(N,P)54MN (CONTINUED)

ID	MONITOR LOCATION X	Y	Z	ACTIVITY (DPS/MG)	ACTIVITY (DPS/NUCLEUS)	REACTION RATE (RPS/NUCLEUS)
HTLF FE04	-103.7	326.2	-37.5	4.0417+003	6.46227-015	1.03743-014
HTLF FE03	-103.7	326.2	-62.9	3.9796+003	6.36298-015	1.02149-014
HTLF FE02	-103.7	326.2	-88.3	3.8346+003	6.13114-015	9.84268-015
HTLF FE01	-103.7	326.2	-112.2	3.6725+003	5.87196-015	9.42660-015
HTRF FE10	103.7	326.2	112.1	3.8553+003	6.16424-015	9.89581-015
HTRF FE09	103.7	326.2	88.8	3.9085+003	6.24930-015	1.00324-014
HTRF FE08	103.7	326.2	64.9	3.9522+003	6.31917-015	1.01445-014
HTRF FE07	103.7	326.2	39.9	3.9948+003	6.38729-015	1.02539-014
HTRF FE06	103.7	326.2	13.5	3.9723+003	6.35131-015	1.01961-014
HTRF FE05	103.7	326.2	-11.8	3.9592+003	6.33036-015	1.01625-014
HTRF FE04	103.7	326.2	-38.5	3.9154+003	6.26033-015	1.00501-014
HTRF FE03	103.7	326.2	-63.5	3.7941+003	6.06639-015	9.73872-015
HTRF FE02	103.7	326.2	-88.6	3.7012+003	5.91785-015	9.50027-015
HTRF FE01	103.7	326.2	-112.2	3.5480+003	5.67290-015	9.10703-015
GE D F23-7R	-66.2	331.2	12.7	4.0700+003	6.50752-015	1.04469-014
GE C F23-7R	-66.2	335.7	12.7	3.8000+003	6.07582-015	9.75387-015
GE19HTF23-7R	-66.2	337.3	12.7	3.6400+003	5.82000-015	9.34318-015
GE B F23-7R	-66.2	340.0	12.7	3.5200+003	5.62813-015	9.03516-015
GE A F23-7R	-66.2	343.9	12.7	3.3600+003	5.37230-015	8.62447-015
H-21 29	.0	336.3	122.3	3.6726+003	5.87212-015	9.42685-015
H-23 31	.0	336.3	62.0	3.7388+003	5.97797-015	9.59678-015
H-24 32	.0	336.3	-1.5	3.7469+003	5.99092-015	9.61757-015
H-25 33	.0	336.3	-65.0	3.5941+003	5.74661-015	9.22536-015
H-22 30	.0	336.3	-125.5	3.1961+003	5.11024-015	8.20377-015
HB-10 39E	37.7	337.8	-8.5	3.6616+003	5.85453-015	9.39862-015
HB-9 38E	-37.7	337.8	-8.5	3.6804+003	5.88459-015	9.44688-015
HA- 9 31 38G	-41.5	337.8	-.6	3.5780+003	5.72086-015	9.18403-015
HA- 9 32 38G	-43.0	337.8	-.6	3.6170+003	5.78322-015	9.28414-015
HA- 9 33 38G	-46.3	337.8	-.6	3.5870+003	5.73525-015	9.20714-015
HA- 9 35 38G	-53.4	337.8	-.6	3.6490+003	5.83439-015	9.36628-015
HTLR FE11	-103.7	349.4	121.6	2.6304+003	4.20575-015	6.75173-015
HTLR FE10	-103.7	349.4	110.2	2.6883+003	4.29832-015	6.90035-015
HTLR FE09	-103.7	349.4	86.8	2.6817+003	4.28777-015	6.88341-015
HTLR FE08	-103.7	349.4	62.8	2.7051+003	4.32518-015	6.94347-015
HTLR FE07	-103.7	349.4	38.5	2.7141+003	4.33957-015	6.96657-015
HTLR FE06	-103.7	349.4	12.5	2.6986+003	4.31479-015	6.92678-015
HTLR FE05	-103.7	349.4	-13.2	2.6809+003	4.28649-015	6.88135-015
HTLR FE04	-103.7	349.4	-38.8	2.6330+003	4.20990-015	6.75840-015
HTLR FE03	-103.7	349.4	-63.9	2.5365+003	4.05561-015	6.51071-015
HTLR FE02	-103.7	349.4	-88.9	2.4854+003	3.97391-015	6.37954-015
HTLR FE01	-103.7	349.4	-112.3	2.3805+003	3.80618-015	6.11028-015
HTRR FE08	103.7	349.4	56.9	2.6062+003	4.16705-015	6.68961-015
HTRR FE07	103.7	349.4	39.0	2.5435+003	4.06680-015	6.52867-015
HTRR FE06	103.7	349.4	13.2	2.5691+003	4.10773-015	6.59438-015
HTRR FE05	103.7	349.4	-12.4	2.5942+003	4.14787-015	6.65881-015
HTRR FE04	103.7	349.4	-38.2	2.6051+003	4.16529-015	6.68679-015
HTRR FE03	103.7	349.4	-63.2	2.6175+003	4.18512-015	6.71862-015
HTRR FE02	103.7	349.4	-88.1	2.5731+003	4.11413-015	6.60465-015
HTRR FE01	103.7	349.4	-111.9	2.5421+003	4.06456-015	6.52508-015
HB-12 2-19L	-73.7	765.0	55.8	7.8550+000	1.25594-017	2.01623-017
VBN1 FE16	-103.8	768.9	230.4	7.7986+000	1.24692-017	2.00175-017
VBN1 FE15	-103.8	768.9	211.3	8.9616+000	1.43287-017	2.30027-017
VBN1 FE14	-103.8	768.9	198.7	8.3789+000	1.33970-017	2.15070-017
VBN1 FE13	-103.8	768.9	173.6	8.8023+000	1.40740-017	2.25938-017
VBN1 FE12	-103.8	768.9	147.4	7.2874+000	1.16518-017	1.87053-017
VBN1 FE11	-103.8	768.9	122.4	6.4098+000	1.02486-017	1.64527-017
VBN1 FE10	-103.8	768.9	97.6	7.3388+000	1.17340-017	1.88373-017
VBN1 FE9	-103.8	768.9	71.8	6.8736+000	1.09902-017	1.76432-017
VBN1 FE8	-103.8	768.9	46.4	7.1650+000	1.14561-017	1.83912-017
VBN1 FE7	-103.8	768.9	21.2	6.6809+000	1.06821-017	1.71486-017
VBN1 FE6	-103.8	768.9	-4.0	6.3148+000	1.00967-017	1.62089-017
VBN1 FE5	-103.8	768.9	-29.2	6.2525+000	9.99712-018	1.60490-017
VBN1 FE4	-103.8	768.9	-44.6	5.7008+000	9.11501-018	1.46329-017
VBN1 FE3	-103.8	768.9	-79.3	6.1129+000	9.77392-018	1.56906-017
VBN1 FE2	-103.8	768.9	-104.4	5.9245+000	9.47268-018	1.52070-017
VBN1 FE1	-103.8	768.9	-128.2	6.9235+000	1.10700-017	1.77713-017

TABLE A3 (CONT'D)

54FE(N,P)54MN (CONTINUED)

ID		MONITOR LOCATION X	Y	Z	ACTIVITY (DPS/MG)	ACTIVITY (DPS/NUCLEUS)	REACTION RATE (RPS/NUCLEUS)
VBN2	FE16	-48.8	768.9	230.9	9.3721+000	1.49851-017	2.40564-017
VBL2	FE15	-48.8	768.9	229.5	5.2724+000	8.43004-018	1.35332-017
VBN2	FE14	-48.8	768.9	204.2	6.9378+000	1.10928-017	1.78080-017
VBN2	FE13	-48.8	768.9	178.4	7.0240+000	1.12307-017	1.80293-017
VBN2	FE12	-48.8	768.9	152.8	6.1631+000	9.85418-018	1.58195-017
VBN2	FE11	-48.8	768.9	127.2	6.9046+000	1.10398-017	1.77228-017
VBN2	FE10	-48.8	768.9	101.3	6.9509+000	1.11138-017	1.78416-017
VBN2	FE9	-48.8	768.9	75.8	6.9933+000	1.11816-017	1.79505-017
VBN2	FE8	-48.8	768.9	51.2	8.0185+000	1.28208-017	2.05819-017
VBN2	FE7	-48.8	768.9	24.7	7.1354+000	1.14088-017	1.83152-017
VBN2	FE6	-48.8	768.9	-5.4	6.7742+000	1.08313-017	1.73881-017
VBN2	FE5	-48.8	768.9	-26.0	6.3002+000	1.00734-017	1.61714-017
VBN2	FE4	-48.8	768.9	-51.4	9.4545+000	1.51168-017	2.42679-017
VBN2	FE3	-48.8	768.9	-76.8	8.7102+000	1.39267-017	2.23574-017
VBN2	FE2	-48.8	768.9	-102.3	9.2112+000	1.47278-017	2.36434-017
VBN2	FE1	-48.8	768.9	-127.2	8.7816+000	1.40409-017	2.25407-017
H-32	41'	.0	764.9	225.7	9.1880+000	1.46907-017	2.35838-017
H-26	29'	.0	764.9	150.2	8.8870+000	1.42094-017	2.28112-017
H-27	31'	.0	764.9	112.1	8.2850+000	1.32469-017	2.12660-017
HB-12	2-19N	57.0	763.9	55.8	7.8550+000	1.25594-017	2.01623-017
H-28	32'	.0	764.9	48.6	7.8930+000	1.26201-017	2.02598-017
H-29	33'	.0	764.9	-14.6	7.6580+000	1.22444-017	1.96566-017
H-30	30'	.0	764.9	-52.7	7.1770+000	1.14753-017	1.84220-017
H-31	40'	.0	764.9	-130.9	6.7820+000	1.08437-017	1.74081-017
VBS3	FE16	48.8	768.9	231.3	7.6657+000	1.22567-017	1.96764-017
VBS3	FE15	48.8	768.9	227.6	8.7118+000	1.39293-017	2.23615-017
VBS3	FE14	48.8	768.9	203.2	8.8783+000	1.41955-017	2.27889-017
VBS3	FE13	48.8	768.9	178.0	9.3412+000	1.49356-017	2.39771-017
VBS3	FE12	48.8	768.9	152.7	9.4470+000	1.51048-017	2.42486-017
VBS3	FE11	48.8	768.9	127.4	7.0095+000	1.12075-017	1.79920-017
VBS3	FE10	48.8	768.9	102.1	8.6102+000	1.37668-017	2.21007-017
VBS3	FE9	48.8	768.9	76.7	7.9042+000	1.26380-017	2.02886-017
VBS3	FE8	48.8	768.9	51.1	7.2886+000	1.16537-017	1.87084-017
VBS3	FE7	48.8	768.9	25.8	6.7586+000	1.08063-017	1.73480-017
VBS3	FE6	48.8	768.9	.5	9.1748+000	1.46696-017	2.35499-017
VBS3	FE5	48.8	768.8	-25.1	8.8623+000	1.41699-017	2.27478-017
VBS3	FE4	48.8	768.9	-50.6	7.6946+000	1.23029-017	1.97506-017
VBS3	FE3	48.8	768.9	-76.0	6.2915+000	1.00595-017	1.61491-017
VBS3	FE2	48.8	768.9	-101.4	7.0546+000	1.12796-017	1.81078-017
VBS3	FE1	48.8	768.9	-126.7	6.1397+000	9.81677-018	1.57594-017
VBS4	FE16	103.8	768.9	230.6	8.5240+000	1.36290-017	2.18795-017
VBS4	FE15	103.8	768.9	226.6	7.7552+000	1.23998-017	1.99061-017
VBS4	FE14	103.8	768.9	201.8	7.8304+000	1.25200-017	2.00991-017
VBS4	FE13	103.8	768.9	195.5	9.1953+000	1.47024-017	2.36026-017
VBS4	FE12	103.8	768.9	150.6	8.9297+000	1.42777-017	2.29208-017
VBS4	FE11	103.8	768.9	125.3	7.3197+000	1.17035-017	1.87883-017
VBS4	FE10	103.8	768.9	100.0	7.1417+000	1.14189-017	1.83314-017
VBS4	FE9	103.8	768.9	75.5	6.8047+000	1.08800-017	1.74664-017
VBS4	FE8	103.8	768.9	49.0	7.2295+000	1.15592-017	1.85567-017
VBS4	FE7	103.8	768.9	23.8	8.9143+000	1.42531-017	2.28813-017
VBS4	FE6	103.8	768.9	-1.0	6.3163+000	1.00991-017	1.62127-017
VBS4	FE5	103.8	768.9	-25.6	6.4442+000	1.03036-017	1.65410-017
VBS4	FE4	103.8	768.9	-51.0	6.9377+000	1.10927-017	1.78077-017
VBS4	FE3	103.8	768.9	-76.2	6.5397+000	1.04563-017	1.67861-017
VBS4	FE2	103.8	768.9	-101.5	7.0505+000	1.12730-017	1.80973-017
VBS4	FE1	103.8	768.9	-126.7	6.8069+000	1.08836-017	1.74720-017

TABLE A3 (CONT'D)

58FE(N,G)59FE

LAMBDA =1.7988-007, K =2.8102-017, YIELD =1.0000+000

ID	MONITOR LOCATION X	Y	Z	ACTIVITY (DPS/MG)	ACTIVITY (DPS/NUCLEUS)	REACTION RATE (RPS/NUCLEUS)
OTLF FE11	-103.7	229.7	114.5	5.1875+004	1.45779-012	2.01674-012
OTLF FE10	-103.7	229.7	114.1	5.3552+004	1.50492-012	2.08194-012
OTLF FE09	-103.7	229.7	90.7	5.6011+004	1.57402-012	2.17754-012
OTLF FE08	-103.7	229.7	65.5	5.7954+004	1.62862-012	2.25308-012
OTLF FE07	-103.7	229.7	40.0	5.8979+004	1.65743-012	2.29292-012
OTLF FE06	-103.7	229.7	14.4	5.9647+004	1.67620-012	2.31889-012
OTLF FE05	-103.7	229.7	-10.0	5.8694+004	1.64942-012	2.28184-012
OTLF FE04	-103.7	229.7	-37.9	5.8313+004	1.63871-012	2.26703-012
OTLF FE03	-103.7	229.7	-63.4	5.6359+004	1.58380-012	2.19107-012
OTLF FE02	-103.7	229.7	-88.8	5.6421+004	1.58554-012	2.19348-012
OTLF FE01	-103.7	229.7	-112.3	5.1037+004	1.43424-012	1.98416-012
OTRF FE11	103.7	229.7	117.3	5.3404+004	1.50076-012	2.07619-012
OTRF FE10	103.7	229.7	112.9	5.3607+004	1.50646-012	2.08408-012
OTRF FE09	103.7	229.7	90.5	5.5571+004	1.56166-012	2.16043-012
OTRF FE08	103.7	229.7	65.2	5.7550+004	1.61727-012	2.23737-012
OTRF FE07	103.7	229.7	40.0	5.8641+004	1.64793-012	2.27978-012
OTRF FE06	103.7	229.7	14.0	5.5503+004	1.55975-012	2.15779-012
OTRF FE05	103.7	229.7	12.4	5.6971+004	1.60100-012	2.21486-012
OTRF FE04	103.7	229.7	-38.4	5.8158+004	1.63436-012	2.26101-012
OTRF FE03	103.7	229.7	-63.6	5.7597+004	1.61859-012	2.23920-012
OTRF FE02	103.7	229.7	-88.8	5.4558+004	1.53319-012	2.12105-012
OTRF FE01	103.7	229.7	-112.3	5.1492+004	1.44703-012	2.00185-012
HE-16 39 25	25.3	231.0	-12.7	5.5710+003	1.56556-013	2.16584-013
HE-15 26 24	.0	231.0	-25.3	5.7690+003	1.62120-013	2.24281-013
H-11 29	.0	239.8	122.2	3.0880+004	8.67790-013	1.20052-012
H-13 31	.0	239.8	62.0	3.3058+004	9.28996-013	1.28519-012
H-14 32	.0	239.8	-1.5	3.3780+004	9.49286-013	1.31326-012
H-15 33	.0	239.8	-65.0	3.2783+004	9.21268-013	1.27450-012
H-12 30	.0	239.8	-125.5	2.7473+004	7.72046-013	1.06807-012
GE19SFF2319R	-66.2	240.8	12.7	4.9100+003	1.37981-013	1.90886-013
HB-2 39G	37.7	241.3	-.2	4.7294+003	1.32906-013	1.83865-013
HB-1 38E	-37.7	241.3	-8.5	4.6731+003	1.31323-013	1.81676-013
HA- 7 25 39E	53.4	242.3	-8.2	4.4250+003	1.24351-013	1.72031-013
HA- 7 24 39E	46.3	242.3	-8.2	4.5190+003	1.26993-013	1.75685-013
HA- 7 23 39E	43.0	242.3	-8.2	4.6010+003	1.29297-013	1.78873-013
HA- 7 22 39E	41.5	242.3	-8.2	4.7140+003	1.32473-013	1.83266-013
HA- 6 17 38G	-41.5	242.3	-.6	4.6680+003	1.31180-013	1.81478-013
HA- 6 19 38G	-43.0	242.3	-.6	4.6370+003	1.30309-013	1.80272-013
HA- 6 20 38G	-46.3	242.3	-.6	4.6710+003	1.31264-013	1.81594-013
HA- 6 21 38G	-53.4	242.3	-.6	4.3570+003	1.22440-013	1.69387-013
HE-16 41 25	25.3	243.4	-12.7	4.1820+003	1.17523-013	1.62583-013
HE-15 59 24	.0	243.4	-25.3	4.0320+003	1.13307-013	1.56752-013
OTLR FE11	-103.7	252.9	119.0	1.3473+004	3.78618-013	5.23789-013
OTLR FE10	-103.7	252.9	109.9	1.3488+004	3.79040-013	5.24372-013
OTLR FE09	-103.7	252.9	86.2	1.3807+004	3.88004-013	5.36774-013
OTLR FE08	-103.7	252.9	61.1	1.4191+004	3.98795-013	5.51703-013
OTLR FE07	-103.7	252.9	35.2	1.4242+004	4.00229-013	5.53686-013
OTLR FE06	-103.7	252.9	9.8	1.4648+004	4.11638-013	5.69470-013
OTLR FE05	-103.7	252.9	-13.5	1.4645+004	4.11554-013	5.69353-013
OTLR FE04	-103.7	252.9	-38.2	1.4331+004	4.02730-013	5.57146-013
OTLR FE03	-103.7	252.9	-62.9	1.4072+004	3.95451-013	5.47077-013
OTLR FE02	-103.7	252.9	-88.2	1.3773+004	3.87049-013	5.35452-013
OTLR FE01	-103.7	252.9	-112.1	1.2420+004	3.49027-013	4.82852-013
OTRR FE11	103.7	252.9	114.5	1.3944+004	3.91854-013	5.42100-013
OTRR FE10	103.7	252.9	112.7	1.2871+004	3.61701-013	5.00385-013
OTRR FE09	103.7	252.9	88.7	1.3406+004	3.76735-013	5.21185-013
OTRR FE08	103.7	252.9	63.4	1.3783+004	3.87330-013	5.35841-013
OTRR FE07	103.7	252.9	38.1	1.3878+004	3.90000-013	5.39535-013
OTRR FE06	103.7	252.9	12.8	1.3142+004	3.69316-013	5.10921-013
OTRR FE05	103.7	252.9	-12.8	1.3520+004	3.79939-013	5.25617-013
OTRR FE04	103.7	252.9	-38.3	1.4327+004	4.02617-013	5.56990-013
OTRR FE03	103.7	252.9	-63.6	1.4108+004	3.96463-013	5.48476-013
OTRR FE02	103.7	252.9	-89.2	1.3426+004	3.77297-013	5.21962-013
OTRR FE01	103.7	252.9	-112.6	1.2498+004	3.51219-013	4.85884-013
QTLF FE09	-103.7	274.8	64.8	5.4213+003	1.52349-013	2.10764-013

TABLE A3 (CONT'D

58FE(N,G)59FE (CONTINUED)

ID	MONITOR LOCATION X	Y	Z	ACTIVITY (DPS/MG)	ACTIVITY (DPS/NUCLEUS)	REACTION RATE (RPS/NUCLEUS)
QTLF FE08	-103.7	274.8	69.2	5.4472+003	1.53077-013	2.11771-013
QTLF FE07	-103.7	274.8	43.4	5.6809+003	1.59645-013	2.20856-013
QTLF FE06	-103.7	274.8	17.7	5.5063+003	1.54738-013	2.14068-013
QTLF FE05	-103.7	274.8	-2.2	5.7560+003	1.61755-013	2.23776-013
QTLF FE04	-103.7	274.8	-33.1	5.6824+003	1.59687-013	2.20914-013
QTLF FE03	-103.7	274.8	-58.9	5.5918+003	1.57141-013	2.17392-013
QTLF FE02	-103.7	274.8	-84.4	5.2572+003	1.47738-013	2.04384-013
QTLF FE01	-103.7	274.8	-110.1	4.7886+003	1.34569-013	1.86166-013
QTRF FE11	103.7	274.8	118.6	5.2036+003	1.46232-013	2.02300-013
QTRF FE10	103.7	274.8	115.3	5.4073+003	1.51956-013	2.10219-013
QTRF FE09	103.7	274.8	91.1	5.2590+003	1.47788-013	2.04454-013
QTRF FE08	103.7	274.8	66.2	5.0722+003	1.42539-013	1.97192-013
QTRF FE07	103.7	274.8	41.3	5.4648+003	1.53572-013	2.12455-013
QTRF FE06	103.7	274.8	15.8	4.9351+003	1.38686-013	1.91862-013
QTRF FE05	103.7	274.8	-3.8	5.5530+003	1.56050-013	2.15884-013
QTRF FE04	103.7	274.8	-35.2	5.5353+003	1.55553-013	2.15196-013
QTRF FE03	103.7	274.8	-61.2	5.2462+003	1.47429-013	2.03956-013
QTRF FE02	103.7	274.8	-86.3	5.2802+003	1.48384-013	2.05278-013
QTRF FE01	103.7	274.8	-111.0	5.3130+003	1.49306-013	2.06553-013
H-16 29	.0	284.9	122.2	4.0879+003	1.14878-013	1.58925-013
H-18 31	.0	284.9	62.0	4.0546+003	1.13942-013	1.57631-013
H-19 32	.0	284.9	-1.5	4.1347+003	1.16193-013	1.60745-013
H-20 33	.0	284.9	-65.0	3.9766+003	1.11750-013	1.54598-013
H-17 30	.0	284.9	-125.5	3.6493+003	1.02553-013	1.41874-013
GE19QTF23-8R	-66.2	285.9	12.7	2.2600+003	6.35105-014	8.78619-014
HB-8 39E	37.7	286.4	-8.5	2.0276+003	5.69796-014	7.88269-014
HB-7 38E	-37.7	286.4	-8.5	2.2472+003	6.31508-014	8.73643-014
HA- 8 27 38G	-41.5	286.4	-.6	1.9320+003	5.42931-014	7.51103-014
HA- 8 28 38G	-43.0	286.4	-.6	2.1850+003	6.14029-014	8.49462-014
HA- 8 29 38G	-46.3	286.4	-.6	2.0590+003	5.78620-014	8.00477-014
HA- 8 30 38G	-53.4	286.4	-.6	2.2010+003	6.18525-014	8.55682-014
QTLR FE10	-103.7	298.0	115.3	2.5552+003	7.18062-014	9.93384-014
QTLR FE09	-103.7	298.0	91.0	2.6026+003	7.31383-014	1.01181-013
QTLR FE08	-103.7	298.0	66.0	2.5837+003	7.26071-014	1.00446-013
QTLR FE07	-103.7	298.0	40.8	2.6587+003	7.47148-014	1.03362-013
QTLR FE06	-103.7	298.0	14.9	2.7367+003	7.69067-014	1.06395-013
QTLR FE05	-103.7	298.0	-8.6	2.6994+003	7.58585-014	1.04944-013
QTLR FE04	-103.7	298.0	-38.2	2.6233+003	7.37200-014	1.01986-013
QTLR FE03	-103.7	298.0	-64.0	2.6300+003	7.39083-014	1.02246-013
QTLR FE02	-103.7	298.0	-89.3	2.4723+003	6.94766-014	9.61155-014
QTLR FE01	-103.7	298.0	-112.5	2.3901+003	6.71666-014	9.29198-014
QTRR FE11	103.7	298.0	122.3	2.5614+003	7.19805-014	9.95795-014
QTRR FE10	103.7	298.0	109.0	2.5202+003	7.08227-014	9.79777-014
QTRR FE09	103.7	298.0	85.7	2.5740+003	7.23345-014	1.00069-013
QTRR FE08	103.7	298.0	61.1	2.4808+003	6.97154-014	9.64460-014
QTRR FE07	103.7	298.0	36.4	2.4987+003	7.02185-014	9.71419-014
QTRR FE06	103.7	298.0	9.5	2.4872+003	6.98953-014	9.66948-014
QTRR FE05	103.7	298.0	-14.2	2.4970+003	7.01707-014	9.70758-014
QTRR FE04	103.7	298.0	-39.6	2.5262+003	7.09913-014	9.82110-014
QTRR FE03	103.7	298.0	-64.7	2.6502+003	7.44759-014	1.03032-013
QTRR FE02	103.7	298.0	-89.4	2.5956+003	7.29416-014	1.00909-013
QTRR FE01	103.7	298.0	-112.4	2.3192+003	6.51742-014	9.01635-014
HTLF FE11	-103.7	326.2	120.4	1.5000+003	4.21530-014	5.83154-014
HTLF FE10	-103.7	326.2	115.6	1.4987+003	4.21165-014	5.82649-014
HTLF FE09	-103.7	326.2	91.5	1.4586+003	4.09896-014	5.67059-014
HTLF FE08	-103.7	326.2	66.2	1.5674+003	4.40471-014	6.09358-014
HTLF FE07	-103.7	326.2	40.8	1.5972+003	4.48845-014	6.20943-014
HTLF FE06	-103.7	326.2	14.9	1.6194+003	4.55084-014	6.29574-014
HTLF FE05	-103.7	326.2	-9.2	1.5351+003	4.31394-014	5.96800-014
HTLF FE04	-103.7	326.2	-37.5	1.5360+003	4.31647-014	5.97150-014
HTLF FE03	-103.7	326.2	-62.9	1.4908+003	4.18945-014	5.79578-014
HTLF FE02	-103.7	326.2	-88.3	1.5231+003	4.28022-014	5.92135-014
HTLF FE01	-103.7	326.2	-112.2	1.3200+003	3.70946-014	5.13176-014
HTRF FE10	103.7	326.2	112.1	1.3558+003	3.81007-014	5.27094-014
HTRF FE09	103.7	326.2	88.8	1.4318+003	4.02364-014	5.56640-014
HTRF FE08	103.7	326.2	64.9	1.4502+003	4.07535-014	5.63794-014

TABLE A3 (CONT'D)

58FE(N,G)59FE (CONTINUED)

ID	MONITOR LOCATION X	Y	Z	ACTIVITY (DPS/MG)	ACTIVITY (DPS/NUCLEUS)	REACTION RATE (RPS/NUCLEUS)
HTRF FE07	103.7	326.2	39.9	1.5261+003	4.28865-014	5.93301-014
HTRF FE06	103.7	326.2	12.5	1.4333+003	4.02786-014	5.57224-014
HTRF FE05	103.7	326.2	-13.5	1.4856+003	4.17483-014	5.77556-014
HTRF FE04	103.7	326.2	-38.5	1.4927+003	4.19479-014	5.80316-014
HTRF FE03	103.7	326.2	-63.5	1.5144+003	4.25577-014	5.88753-014
HTRF FE02	103.7	326.2	-88.6	1.4369+003	4.03798-014	5.58623-014
HTRF FE01	103.7	326.2	-112.2	1.3808+003	3.88032-014	5.36813-014
H-21 29	.0	336.3	122.2	1.3110+003	3.68417-014	5.09677-014
H-23 31	.0	336.3	62.0	1.3731+003	3.85869-014	5.33820-014
H-24 32	.0	336.3	-1.5	1.3653+003	3.83677-014	5.30787-014
H-25 33	.0	336.3	-65.0	1.3192+003	3.70722-014	5.12865-014
H-22 30	.0	336.3	-125.5	1.1987+003	3.36859-014	4.66018-014
GE19HTF23-7R	-66.2	337.3	12.7	1.1200+003	3.14742-014	4.35422-014
HB-10 39E	37.7	337.8	-8.5	1.1623+003	3.26630-014	4.51867-014
HB-9 38E	-37.7	337.8	-8.5	1.0626+003	2.98612-014	4.13107-014
HA- 9 31 38G	-41.5	337.8	-.6	1.0380+003	2.91699-014	4.03543-014
HA- 9 32 38G	-43.0	337.8	-.6	1.0390+003	2.91980-014	4.03932-014
HA- 9 33 38G	-46.3	337.8	-.6	1.0410+003	2.92542-014	4.04709-014
HA- 9 35 38G	-53.4	337.8	-.6	1.0190+003	2.86359-014	3.96156-014
HTLR FE11	-103.7	349.4	121.6	9.0893+002	2.55428-014	3.53364-014
HTLR FE10	-103.7	349.4	110.2	1.0871+003	3.05497-014	4.22631-014
HTLR FE09	-103.7	349.4	86.8	1.0131+003	2.84701-014	3.93863-014
HTLR FE08	-103.7	349.4	62.8	1.1317+003	3.18030-014	4.39971-014
HTLR FE07	-103.7	349.4	38.5	1.1358+003	3.19183-014	4.41565-014
HTLR FE06	-103.7	349.4	12.5	1.1054+003	3.10640-014	4.29746-014
HTLR FE05	-103.7	349.4	-13.2	1.0389+003	2.91952-014	4.03893-014
HTLR FE04	-103.7	349.4	-38.8	1.0707+003	3.00888-014	4.16256-014
HTLR FE03	-103.7	349.4	-63.9	1.0920+003	3.06874-014	4.24536-014
HTLR FE02	-103.7	349.4	-88.9	1.0872+003	3.05525-014	4.22670-014
HTLR FE01	-103.7	349.4	-112.3	9.8597+002	2.77077-014	3.83315-014
HTRR FE08	103.7	349.4	56.9	1.0258+003	2.88270-014	3.98800-014
HTRR FE07	103.7	349.4	39.0	9.8576+002	2.77018-014	3.83234-014
HTRR FE06	103.7	349.4	13.2	1.0870+003	3.05469-014	4.22593-014
HTRR FE05	103.7	349.4	-12.4	1.0961+003	3.08026-014	4.26130-014
HTRR FE04	103.7	349.4	-38.3	1.0434+003	2.93216-014	4.05642-014
HTRR FE03	103.7	349.4	-63.2	1.1028+003	3.09909-014	4.28735-014
HTRR FE02	103.7	349.4	-88.1	1.0546+003	2.96364-014	4.09996-014
HTRR FE01	103.7	349.4	-111.9	1.0544+003	2.96307-014	4.09919-014

58NI(N,P)58CO

LAMBDA =1.1323-007, K =1.4278-019, YIELD =1.0000+000

ID	MONITOR LOCATION X	Y	Z	ACTIVITY (DPS/MG)	ACTIVITY (DPS/NUCLEUS)	REACTION RATE (RPS/NUCLEUS)
H-11 29	.0	239.8	122.2	3.5817+005	5.11395-014	7.01038-014
H-13 31	.0	239.8	62.0	3.8162+005	5.44877-014	7.46936-014
H-14 32	.0	239.8	-1.5	3.9152+005	5.59012-014	7.66313-014
H-15 33	.0	239.8	-65.0	3.7283+005	5.32327-014	7.29731-014
H-12 30	.0	239.8	-125.5	3.3758+005	4.81997-014	6.60737-014
HB-2 39G	38.3	241.3	-.2	3.7748+005	5.38966-014	7.38833-014
HB-1 38E	-38.3	241.3	-8.5	3.8508+005	5.49817-014	7.53708-014
HA-7 39E	43.2	242.3	-8.2	3.7440+005	5.34568-014	7.32804-014
HA- 6 38G	-43.2	242.3	-.6	3.7780+005	5.39423-014	7.39459-014
GE19SFF2319R	-50.7	249.5	12.7	3.2900+005	4.69746-014	6.43944-014
H-16 29	.0	284.9	96.9	1.6744+005	2.39071-014	3.27726-014
H-18 31	.0	284.9	62.0	1.7446+005	2.49094-014	3.41466-014
H-19 32	.0	284.9	-1.5	1.7730+005	2.53149-014	3.47025-014
H-20 33	.0	284.9	-65.0	1.6999+005	2.42712-014	3.32717-014
H-17 30	.0	284.9	-125.5	1.5359+005	2.19296-014	3.00618-014
HB-8 39E	38.3	286.4	-8.5	1.7149+005	2.44853-014	3.35653-014
HB-7 38E	-38.3	286.4	-8.5	1.7204+005	2.45639-014	3.36730-014

TABLE A3 (CONT'D)

58FE(N,G)59FE (CONTINUED)

ID	MONITOR LOCATION X	Y	Z	ACTIVITY (DPS/MG)	ACTIVITY (DPS/NUCLEUS)	REACTION RATE (RPS/NUCLEUS)
GE19QTF23-8R	-66.2	294.6	12.7	1.4600+005	2.08459-014	2.85762-014
HA- 8 38G	-43.2	286.4	-.6	1.7080+005	2.43868-014	3.34303-014
GE19HTF23-7R	-66.2	328.6	12.7	7.7400+004	1.10512-014	1.51493-014
H-21 29	.0	336.3	96.9	6.8153+004	9.73089-015	1.33394-014
H-23 31	.0	336.3	62.0	6.8852+004	9.83069-015	1.34762-014
H-24 32	.0	336.3	-1.5	6.9781+004	9.96333-015	1.36581-014
H-25 33	.0	336.3	-65.0	6.6222+004	9.45518-015	1.29615-014
H-22 30	.0	336.3	-99.9	6.0456+004	8.63191-015	1.18329-014
HB-10 39E	38.3	337.8	-8.5	6.7246+004	9.60138-015	1.31619-014
HB-9 38E	-38.3	337.8	-8.5	6.7308+004	9.61024-015	1.31740-014
HA- 9 38G	-43.2	337.8	-.6	6.7250+004	9.60195-015	1.31627-014
GE19HTF23-7R	-66.2	346.0	12.7	5.8000+004	8.28124-015	1.13522-014
H-32 41'	.0	764.9	225.8	1.2630+002	1.80331-017	2.47204-017
H-26 29'	.0	764.9	150.2	1.1060+002	1.57915-017	2.16475-017
H-27 31'	.0	764.9	112.1	1.0340+002	1.47635-017	2.02382-017
HB-12 2-19H	73.2	763.9	55.8	9.6800+001	1.38211-017	1.89464-017
H-28 32'	.0	764.9	48.6	9.5140+001	1.35841-017	1.86215-017
H-29 33'	.0	764.9	-14.6	9.2320+001	1.31814-017	1.80696-017
H-30 30'	.0	764.9	-52.7	9.0100+001	1.28645-017	1.76351-017
H-31 40'	.0	764.9	-130.7	8.6740+001	1.23847-017	1.69774-017

63CU(N,A)60CO

LAMBDA =4.1671-009, K =1.5255-019, YIELD =1.0000+000

ID	MONITOR LOCATION X	Y	Z	ACTIVITY (DPS/MG)	ACTIVITY (DPS/NUCLEUS)	REACTION RATE (RPS/NUCLEUS)
CU6 39H	53.7	239.0	-4.3	5.4470+002	8.30940-017	4.48234-016
GE D F2319R	-50.7	234.7	12.7	5.8800+002	8.96994-017	4.83866-016
GE C F2319R	-50.7	239.3	12.7	5.5100+002	8.40550-017	4.53418-016
GE19SFF2319R	-66.2	240.8	12.7	5.4200+002	8.26821-017	4.46012-016
HA-6 CUF 38G	-43.5	241.3	-.3	5.4600+002	8.32923-017	4.49304-016
HA-6 CUW 38G	-43.4	241.3	-.3	5.4750+002	8.35211-017	4.50538-016
HA-7 CUW 39E	43.4	241.3	-8.2	5.3720+002	8.19499-017	4.42062-016
HA-7 CUF 39E	43.5	241.3	-8.2	5.3660+002	8.18583-017	4.41568-016
HB-1 38E	-39.3	241.3	-8.2	5.4390+002	8.29719-017	4.47576-016
HB-2 39G	39.3	241.3	-.3	5.3560+002	8.17058-017	4.40746-016
GE B F2319R	-50.7	243.5	12.7	5.0800+002	7.74954-017	4.18033-016
GE A F2319R	-50.7	247.5	12.7	4.7200+002	7.20036-017	3.88409-016
GE D F23-8R	-50.9	279.8	12.7	2.5900+002	3.95104-017	2.13131-016
GE C F23-8R	-50.9	284.3	12.7	2.4300+002	3.70696-017	1.99965-016
GE19QTF23-8R	-66.2	285.9	12.7	2.4200+002	3.69171-017	1.99142-016
HA-8 CUF 38G	-43.5	286.4	-.3	2.3620+002	3.60323-017	1.94369-016
HA-8 CUW 39G	-43.4	286.4	-.3	2.3880+002	3.64289-017	1.96509-016
HB-7 38E	-39.3	286.4	-8.2	2.4040+002	3.66730-017	1.97825-016
HB-8 39E	39.3	286.4	-8.2	2.3710+002	3.61696-017	1.95110-016
GE B F23-8R	-50.9	288.6	12.7	2.2600+002	3.44763-017	1.85976-016
GE A F23-8R	-50.9	292.6	12.7	2.1000+002	3.20355-017	1.72809-016
GE D F23-7R	-50.9	331.2	12.7	1.0100+002	1.54075-017	8.31130-017
GE C F23-7R	-50.9	335.8	12.7	9.4000+001	1.43397-017	7.73526-017
GE19HTF23-7R	-66.2	337.3	12.7	9.2300+001	1.40804-017	7.59537-017
HA-9 CUF 38G	-43.5	337.8	-.3	9.1900+001	1.40193-017	7.56246-017
HA-9 CUW 38G	-43.4	337.8	-.3	9.1300+001	1.39278-017	7.51308-017
HB-9 38E	-39.3	337.8	-8.2	9.2000+001	1.40346-017	7.57068-017
HB-10 39E	39.3	337.7	-8.2	9.0700+001	1.38363-017	7.46371-017
GE B F23-7R	-50.9	340.0	12.7	8.7500+001	1.33481-017	7.20038-017
GE A F23-7R	-50.9	344.0	12.7	8.0300+001	1.22498-017	6.60789-017
HB-12 2-19N	72.1	764.9	55.8	4.3800-001	6.68169-020	3.60430-019

TABLE A3 (CONT'D)

46TI(N,P)46SC

LAMBDA =9.5677-008, K =9.8198-019, YIELD =1.0000+000

ID	MONITOR LOCATION X	Y	Z	ACTIVITY (DPS/MG)	ACTIVITY (DPS/NUCLEUS)	REACTION RATE (RPS/NUCLEUS)
H-11 29	.0	239.8	122.2	5.6401+003	5.53847-015	7.55451-015
H-13 31	.0	239.8	64.7	6.0068+003	5.89856-015	8.04567-015
H-14 32	.0	239.8	-1.5	6.3451+003	6.23076-015	8.49880-015
H-15 33	.0	239.8	-65.0	5.8801+003	5.77414-015	7.87597-015
HB-2 39G	38.8	241.3	-.2	5.9839+003	5.87607-015	8.01500-015
HB-1 38E	-38.8	241.3	-8.5	6.0350+003	5.92625-015	8.08345-015
H-16 29	.0	284.9	122.2	2.5160+003	2.47066-015	3.37000-015
H-18 31	.0	284.9	62.0	2.6192+003	2.57200-015	3.50823-015
H-19 32	.0	284.9	-1.5	2.6761+003	2.62788-015	3.58444-015
H-20 33	.0	284.9	-65.5	2.5428+003	2.49698-015	3.40590-015
H-17 30	.0	284.9	-125.5	2.2823+003	2.24117-015	3.05698-015
HB-8 39E	38.8	286.4	-8.5	2.6050+003	2.55806-015	3.48921-015
HB-7 38E	-38.8	286.4	-8.5	2.6338+003	2.58634-015	3.52778-015
GE19QTF23-8R	-50.9	292.5	-66.2	3.0500+003	2.99504-015	4.08525-015
H-21 29	.0	336.3	122.2	9.6270+002	9.45352-016	1.28947-015
H-23 31	.0	336.3	62.0	9.8163+002	9.63941-016	1.31482-015
H-24 32	.0	336.3	-1.5	9.8430+002	9.66563-016	1.31840-015
H-25 33	.0	336.3	-65.0	9.2738+002	9.10669-016	1.24216-015
H-22 30	.0	336.3	-125.5	8.7895+002	8.63111-016	1.17729-015
HB-10 39E	38.8	337.8	-8.5	9.5433+002	9.37133-016	1.27826-015
HB-9 38E	-38.8	337.8	-8.5	9.7196+002	9.54445-016	1.30187-015
GE19HTF23-7R	-66.2	343.9	12.7	1.1500+003	1.12928-015	1.54034-015
HB-12 2-19N	72.6	763.9	55.8	2.6260+000	2.57868-018	3.51734-018

45SC(N,G)46SC

LAMBDA =9.5677-008, K =7.4652-020, YIELD =1.0000+000

ID	MONITOR LOCATION X	Y	Z	ACTIVITY (DPS/MG)	ACTIVITY (DPS/NUCLEUS)	REACTION RATE (RPS/NUCLEUS)
H-11 MGO 29	1.9	239.8	125.2	2.7421+008	2.04703-011	2.79217-011
H-11 29	-3.5	239.8	125.2	2.7004+008	2.01590-011	2.74971-011
H-13 MGO 31	1.9	239.8	65.0	2.8472+008	2.12549-011	2.89919-011
H-13 31	-3.5	239.8	65.0	2.7628+008	2.06249-011	2.81324-011
H-14 MGO 32	1.9	239.8	1.5	2.8644+008	2.13833-011	2.91670-011
H-14 32	-3.5	239.8	1.5	2.8787+008	2.14901-011	2.93126-011
H-15 MGO 33	1.9	239.8	-62.0	2.8543+008	2.13079-011	2.90642-011
H-15 33	-3.5	239.8	-62.0	2.8378+008	2.11847-011	2.88961-011
H-12 MGO 30	1.9	239.8	-122.4	2.3890+008	1.78344-011	2.43262-011
H-12 30	-3.5	239.8	-122.4	2.3712+008	1.77015-011	2.41449-011
H-16 MGO 29	1.9	284.9	125.2	2.6492+007	1.97768-012	2.69757-012
H-16 29	-3.5	284.9	125.2	2.6677+007	1.99149-012	2.71641-012
H-18 MGO 31	1.9	284.9	65.0	1.7505+007	1.30678-012	1.78246-012
H-18 31	-3.5	284.9	65.0	2.6675+007	1.99134-012	2.71620-012
H-19 MGO 32	1.9	284.9	1.5	3.3969+007	2.53585-012	3.45892-012
H-20 MGO 33	1.9	284.9	-62.0	2.1827+007	1.62943-012	2.22255-012
H-20 33	-3.5	284.9	-62.0	2.6822+007	2.00232-012	2.73117-012
H-17 MGO 30	1.9	284.9	-122.4	3.1271+007	2.33444-012	3.18420-012
H-22 MGO 30	1.9	336.3	-122.4	5.3883+006	4.02247-013	5.48668-013
H-22 30	-3.5	336.3	-122.4	5.4830+006	4.09317-013	5.58311-013
H-21 MGO 29	1.9	336.3	125.2	6.1254+006	4.57273-013	6.23724-013
H-21 29	-3.5	336.3	125.2	6.2091+006	4.63522-013	6.32247-013
H-23 MGO 31	1.9	336.3	65.0	6.1397+006	4.58341-013	6.25180-013
H-23 31	-3.5	336.3	65.0	6.1909+006	4.62163-013	6.30394-013
H-24 MGO 32	1.9	336.3	1.5	5.8374+006	4.35774-013	5.94398-013
H-24 32	-3.5	336.3	1.5	6.1270+006	4.57393-013	6.23887-013
H-25 MGO 33	1.9	336.3	-62.0	5.9966+006	4.47658-013	6.10609-013
H-25 33	-3.5	336.3	-62.0	6.1273+006	4.57415-013	6.23918-013
HB-12MG2-19N	71.5	763.9	55.8	1.2370+003	9.23445-017	1.25959-016

TABLE A3 (CONT'D)

59CO(N,G)60CO

LAMBDA =4.1671-009, K =9.7862-020, YIELD =1.0000+000

ID		MONITOR LOCATION X	Y	Z	ACTIVITY (DPS/MG)	ACTIVITY (DPS/NUCLEUS)	REACTION RATE (RPS/NUCLEUS)
H-11	29	.0	239.8	122.0	1.0352+008	1.01307-011	5.46479-011
H-13	31	.0	239.8	62.0	1.0948+008	1.07139-011	5.77942-011
H-14	32	.0	239.8	-1.5	1.1059+008	1.08226-011	5.83801-011
H-15	33	.0	239.8	-65.0	1.0133+008	9.91636-012	5.34918-011
H-12	30	.0	239.8	-125.5	8.6319+007	8.44735-012	4.55675-011
HB-2	39E	39.8	241.3	-8.5	2.7045+007	2.64668-012	1.42770-011
HB-1	38E	-39.8	241.3	-8.5	2.8387+007	2.77801-012	1.49854-011
HA- 7	39E	43.0	242.3	-.6	2.7590+007	2.70001-012	1.45647-011
HA- 6	38G	-43.0	242.3	-.6	2.8830+007	2.82136-012	1.52193-011
GE19SFF2319R		-50.9	247.4	12.7	3.4800+007	3.40560-012	1.83708-011
H-16	29	.0	284.9	122.0	1.9865+007	1.94403-012	1.04867-011
H-18	31	.0	284.0	62.0	2.0391+007	1.99550-012	1.07643-011
H-19	32	.0	284.0	-1.5	2.0952+007	2.05040-012	1.10605-011
H-20	33	.0	284.9	-65.0	2.0286+007	1.98523-012	1.07089-011
H-17	30	.0	284.0	-125.5	1.7759+007	1.73793-012	9.37492-012
HB-8	39E	39.8	286.4	-8.5	1.3480+007	1.31918-012	7.11605-012
HB-7	38E	-39.8	286.4	-8.5	1.4134+007	1.38318-012	7.46130-012
HA- 8	38G	-43.0	286.4	-.6	1.4140+007	1.38377-012	7.46446-012
GE19QTF23-8R		-66.2	292.5	12.7	1.7000+007	1.66365-012	8.97425-012
H-21	29	.0	336.3	122.2	7.9472+006	7.77729-013	4.19530-012
H-23	31	.0	336.3	62.0	8.4449+006	8.26435-013	4.45804-012
H-24	32	.0	336.3	-1.5	8.3796+006	8.20044-013	4.42357-012
H-25	33	.0	336.3	-65.0	8.2622+006	8.08555-013	4.36159-012
H-22	30	.0	336.3	-125.5	7.3526+006	7.19540-013	3.88142-012
HB-10	39E	39.8	337.8	-8.5	6.6828+006	6.53992-013	3.52783-012
HB-9	38E	-39.8	337.8	-8.5	6.9981+006	6.84848-013	3.69428-012
HA- 9	38G	-43.0	337.8	-.6	7.0440+006	6.89340-013	3.71851-012
E19HTF23-7R		-50.9	343.9	12.7	8.3100+006	8.13233-013	4.38682-012
H-32	41'	.0	764.9	225.7	8.1840+004	8.00903-015	4.32031-014
H-26	29'	.0	764.9	150.2	7.6190+004	7.45611-015	4.02205-014
H-27	31'	.0	764.9	112.1	6.9750+004	6.82587-015	3.68208-014
H-28	32'	.0	764.9	48.6	7.4410+004	7.28191-015	3.92808-014
HB-12	2-19N	71.6	763.9	55.8	2.1370+004	2.09131-015	1.12812-014
H-29	33'	.0	764.9	-14.6	7.2750+004	7.11946-015	3.84045-014
H-30	30'	.0	764.9	-52.7	.0000	.00000	.00000
H-31	40'	.0	764.9	-130.9	6.1930+004	6.06059-015	3.26927-014

109AG(N,G)110AG

LAMBDA =3.2118-008, K =3.7185-019, YIELD =1.0000+000

ID		MONITOR LOCATION X	Y	Z	ACTIVITY (DPS/MG)	ACTIVITY (DPS/NUCLEUS)	REACTION RATE (RPS/NUCLEUS)
H-11	29	.0	239.8	96.9	3.0687+007	1.14110-011	1.70543-011
H-13	31	.0	239.8	62.0	3.4082+007	1.26734-011	1.89411-011
H-14	32	.0	239.8	-1.5	3.5288+007	1.31218-011	1.96113-011
H-15	33	.0	239.8	-65.0	3.3435+007	1.24328-011	1.85815-011
H-12	30	.0	239.8	-99.9	2.8140+007	1.04639-011	1.56388-011
HB-2	39E	40.9	241.3	-.3	2.4073+007	8.95155-012	1.33786-011
HB-1	38E	-40.9	241.3	-8.5	2.5216+007	9.37657-012	1.40138-011
HA-7	39E	42.9	242.3	-8.6	2.3670+007	8.80169-012	1.31546-011
HA- 6	38G	-42.9	242.3	-.6	2.4220+007	9.00621-012	1.34603-011
GE19SFF2319R		-66.2	247.4	12.7	2.9300+007	1.08952-011	1.62835-011
H-16	29	.0	286.9	96.9	1.2096+007	4.49790-012	6.72236-012
H-18	31	.0	284.9	62.0	1.2525+007	4.65742-012	6.96078-012
H-19	32	.0	284.9	-1.5	1.3273+007	4.93557-012	7.37648-012
H-20	33	.0	284.9	-65.0	1.2763+007	4.74592-012	7.09305-012
H-17	30	.0	284.9	-125.5	1.0944+007	4.06953-012	6.08214-012
HB-8	39E	40.9	286.4	-8.5	1.1158+007	4.14910-012	6.20107-012
HB-7	38E	-40.9	286.4	-8.5	1.1572+007	4.30305-012	6.43115-012
HA- 8	38G	-42.9	286.4	-.6	1.1220+007	4.17216-012	6.23552-012
GE19QTF23-8R		-66.2	292.5	12.7	1.3200+007	4.90842-012	7.33591-012

TABLE A3 (CONT'D)

109AG(N,G)110AG (CONTINUED)

ID		MONITOR LOCATION X	Y	Z	ACTIVITY (DPS/MG)	ACTIVITY (DPS/NUCLEUS)	REACTION RATE (RPS/NUCLEUS)
H-21	29	.0	336.3	122.2	5.6607+006	2.10493-012	3.14594-012
H-23	31	.0	336.3	62.0	5.9969+006	2.22995-012	3.33278-012
H-24	32	.0	336.3	-1.5	5.9389+006	2.20838-012	3.30055-012
H-25	33	.0	336.3	-65.0	5.7500+006	2.13814-012	3.19557-012
GE19HTF23-7R		-66.2	343.9	12.7	6.0900+006	2.26457-012	3.38452-012
H-22	30	.0	336.3	-125.5	5.1440+006	1.91280-012	2.85878-012
HB-10	39E	40.9	337.8	-8.5	5.2124+006	1.93823-012	2.89679-012
HB-9	38E	-40.9	337.8	-8.5	5.4652+006	2.03223-012	3.03729-012
HA- 9	38G	-42.9	337.8	-.6	5.3650+006	1.99498-012	2.98160-012

235U(N,F)137CS

LAMBDA =7.2793-010, K =3.9030-019, YIELD =6.2210-002

ID		MONITOR LOCATION X	Y	Z	ACTIVITY (DPS/MG)	ACTIVITY (DPS/NUCLEUS)	REACTION RATE (RPS/NUCLEUS)
HB- 1	38E	-44.2	241.3	-8.5	3.6640+005	1.43006-013	6.34745-011
HB-2	39G	44.2	241.3	-.3	3.5260+005	1.37620-013	6.10838-011
HB- 7	38E	-44.2	286.4	-8.5	1.6670+005	6.50630-014	2.88788-011
HB- 8	39E	44.2	286.4	-8.5	1.6020+005	6.25261-014	2.77528-011
HB- 9	38E	-44.2	337.8	-8.5	8.0060+004	3.12474-014	1.38695-011
HB-10	39E	44.2	337.8	-8.5	7.5390+004	2.94247-014	1.30604-011
HB-12	2-19N	67.3	763.9	55.8	3.6210+002	1.41328-016	6.27296-014

235U(N,F)103RU

LAMBDA =2.0346-007, K =3.9030-019, YIELD =3.0420-002

ID		MONITOR LOCATION X	Y	Z	ACTIVITY (DPS/MG)	ACTIVITY (DPS/NUCLEUS)	REACTION RATE (RPS/NUCLEUS)
HB- 1	38E	-44.2	241.3	-8.5	3.4760+006	1.35668-012	6.16886-011
HB-2	39G	44.2	241.3	-.3	3.2970+006	1.28682-012	5.85118-011
HB- 7	38E	-44.2	286.4	-8.5	1.5640+006	6.10429-013	2.77563-011
HB- 8	39E	44.2	286.4	-8.5	1.5420+006	6.01843-013	2.73659-011
HB- 9	38E	-44.2	337.8	-8.5	7.7510+005	3.02522-013	1.37557-011
HB-10	39E	44.2	337.8	-8.5	7.1920+005	2.80704-013	1.27636-011
HB-12	2-19N	67.3	763.9	55.8	1.5910+002	6.20967-017	2.82355-015

235U(N,F)95ZR

LAMBDA =1.2516-007, K =3.9030-019, YIELD =6.4950-002

ID		MONITOR LOCATION X	Y	Z	ACTIVITY (DPS/MG)	ACTIVITY (DPS/NUCLEUS)	REACTION RATE (RPS/NUCLEUS)
HB- 1	38E	-44.2	241.3	-8.5	7.1090+006	2.77464-012	5.87323-011
HB-2	39G	44.2	241.3	-.3	6.7540+006	2.63609-012	5.57994-011
HB- 7	38E	-44.2	286.4	-8.5	3.2330+006	1.26184-012	2.67100-011
HB- 8	39E	44.2	286.4	-8.5	3.1650+006	1.23530-012	2.61482-011
HB- 9	38E	-44.2	337.8	-8.5	1.5330+006	5.98330-013	1.26651-011
HB-10	39E	44.2	337.8	-8.5	1.4910+006	5.81937-013	1.23182-011
HB-12	2-19N	67.3	763.9	55.8	3.4600+002	1.35044-016	2.85854-015

TABLE A3 (CONT'D)

238U(N,F)137CS

LAMBDA =7.2793-010, K =3.9530-019, YIELD =6.0000-002

ID	MONITOR LOCATION X	Y	Z	ACTIVITY (DPS/MG)	ACTIVITY (DPS/NUCLEUS)	REACTION RATE (RPS/NUCLEUS)
GE19SFF2319R	-66.2	240.8	12.7	2.4900+003	9.84297-016	4.52981-013
HB- 1 38E	-44.8	241.3	-8.5	3.2510+003	1.28512-015	5.91423-013
HB- 1A				2.3900+003	9.44767-016	4.34789-013
HB-2 39G	44.8	241.3	-.3	3.0660+003	1.21199-015	5.57768-013
HB- 2A				2.2500+003	8.89425-016	4.09321-013
GE19QTF23-8R	-66.2	285.9	12.7	9.3400+002	3.69210-016	1.69914-013
HB- 7 38E	-44.8	286.4	-8.5	1.2630+003	4.99264-016	2.29765-013
HB- 7A				9.6090+002	3.79844-016	1.74807-013
HB- 8 39E	44.8	286.4	-8.5	1.1990+003	4.73965-016	2.18122-013
HB- 8A				8.3950+002	3.31854-016	1.52722-013
GE19HTF23-7R	-66.2	337.3	12.7	3.8400+002	1.51795-016	6.98574-014
HB- 9 38E	-44.8	337.8	-8.5	5.3230+002	2.10418-016	9.68362-014
HB -9A				3.6530+002	1.44403-016	6.64555-014
HB-10 39E	44.8	337.8	-8.5	5.2260+002	2.06584-016	9.50715-014
HB-10A				3.6120+002	1.42782-016	6.57096-014
HB-12 2-19N	67.2	763.9	55.8	2.2460+000	8.87844-019	4.08593-016
HB-12A				2.2200+000	8.77566-019	4.03863-016

238U(N,F)103RU

LAMBDA =2.0346-007, K =3.9530-019, YIELD =6.2290-002

ID	MONITOR LOCATION X	Y	Z	ACTIVITY (DPS/MG)	ACTIVITY (DPS/NUCLEUS)	REACTION RATE (RPS/NUCLEUS)
GE19SFF2319R	-66.2	240.8	12.7	6.1700+004	2.43900-014	5.41601-013
HB- 1 38E	-44.8	241.3	-8.5	6.8600+004	2.71176-014	6.02169-013
HB- 1A				6.0440+004	2.38919-014	5.30540-013
HB-2 39G	44.8	241.3	-.3	6.4210+004	2.53822-014	5.63633-013
HB- 2A				5.6450+004	2.23147-014	4.95516-013
GE19QTF23-8R	-66.2	285.9	12.7	1.9900+004	7.86647-015	1.74682-013
HB- 7 38E	-44.8	286.4	-8.5	2.3510+004	9.29350-015	2.06370-013
HB- 7A				2.0170+004	7.97320-015	1.77052-013
HB- 8 39E	44.8	286.4	-8.5	2.2330+004	8.82705-015	1.96012-013
HB- 8A				1.8860+004	7.45536-015	1.65552-013
GE19HTF23-7R	-66.2	337.3	12.7	7.9800+003	3.15449-015	7.00482-014
HB- 9 38E	-44.8	337.8	-8.5	9.1390+003	3.61265-015	8.02218-014
HB- 9A				7.5230+003	2.97384-015	6.60367-014
HB-10 39E	-44.8	337.8	-8.5	8.9910+003	3.55414-015	7.89227-014
HB-10A				7.4510+003	2.94538-015	6.54046-014
HB-12 2-19N	67.2	763.9	55.8	9.7220+000	3.84311-018	8.53394-017
HB-12A				9.4040+000	3.71740-018	8.25480-017

238U(H,F)95ZR

LAMBDA =1.2516-007, K =3.9530-019, YIELD =5.1050-002

ID	MONITOR LOCATION X	Y	Z	ACTIVITY (DPS/MG)	ACTIVITY (DPS/NUCLEUS)	REACTION RATE (RPS/NUCLEUS)
GE19SFF2319R	-66.2	240.8	12.7	4.4600+004	1.76304-014	4.74804-013
HB- 1 38E	-44.8	241.3	-8.5	6.0140+004	2.37733-014	6.40241-013
HB- 1A				4.3440+004	1.71718-014	4.62455-013
HB-2 39G	44.8	241.3	-.3	5.6740+004	2.24293-014	6.04045-013
HB- 2A			.0	4.1010+004	1.62113-014	4.36586-013
GE19QTF23-8R	-66.2	285.9	12.7	1.5200+004	6.00856-015	1.61817-013
HB- 7 38E	-44.8	286.4	-8.5	2.2070+004	8.72427-015	2.34954-013
HB- 7A				1.5170+004	5.99670-015	1.61497-013
HB- 8 39E	44.8	286.4	-8.5	2.0960+004	8.28549-015	2.23137-013
HB- 8A				1.3850+004	5.47490-015	1.47445-013
GE19HTF23-7R	-66.2	337.3	12.7	6.0800+003	2.40342-015	6.47267-014

TABLE A3 (CONT'D)

238U(N,F)95ZR (CONTINUED)

ID	MONITOR LOCATION X	Y	Z	ACTIVITY (DPS/MG)	ACTIVITY (DPS/NUCLEUS)	REACTION RATE (RPS/NUCLEUS)
HB- 9 38E	-44.8	337.8	-8.5	9.2800+003	3.66838-015	9.87934-014
HB- 9A				6.0810+003	2.40382-015	6.47373-014
HB-10 39E	44.8	337.8	-8.5	8.8450+003	3.49643-015	9.41624-014
HB-10A				5.6530+003	2.23463-015	6.01809-014
HB-12 2-19N	67.2	763.9	55.8	6.6440+000	2.62637-018	7.07309-017
HB-12A				5.9350+000	2.34611-018	6.31830-017

237NP(N,F)137CS

LAMBDA =7.2793-010, K =3.9363-019, YIELD =6.2670-002

ID	MONITOR LOCATION X	Y	Z	ACTIVITY (DPS/MG)	ACTIVITY (DPS/NUCLEUS)	REACTION RATE (RPS/NUCLEUS)
GE19SFF2319R	-66.2	240.8	12.7	1.3000+004	5.11719-015	2.25464-012
HB- 1 38E	-40.5	241.3	-8.5	1.3130+004	5.16836-015	2.27719-012
HB- 2 39E	40.5	241.3	-8.5	1.2790+004	5.03453-015	2.21822-012
GE19QTF23-8R	-66.2	285.9	12.7	7.7300+003	3.04276-015	1.34064-012
HB- 7 38E	-40.5	286.4	-8.5	7.8460+003	3.08842-015	1.36076-012
HB- 8 39E	40.5	286.4	-8.5	7.7080+003	3.03410-015	1.33683-012
GE19HTF23-7R	-66.2	337.3	12.7	4.3800+003	1.72410-015	7.59641-013
HB- 9 38E	-40.5	337.8	-8.5	4.3440+003	1.70993-015	7.53397-013
HB-10 39E	40.5	337.8	-8.5	4.2740+003	1.68237-015	7.41257-013

237NP(N,F)103RU

LAMBDA =2.0346-007, K =3.9363-019, YIELD =5.5840-002

ID	MONITOR LOCATION X	Y	Z	ACTIVITY (DPS/MG)	ACTIVITY (DPS/NUCLEUS)	REACTION RATE (RPS/NUCLEUS)
GE19SFF2319R	-66.2	240.8	12.7	2.2000+005	8.65986-014	2.14512-012
HB- 1 38E	-40.5	241.3	-8.5	2.1980+005	8.65199-014	2.14317-012
HB- 2 39E	40.5	241.3	-.3	2.1430+005	8.43549-014	2.08954-012
GE19QTF23-8R	-66.2	285.9	12.7	1.2800+005	5.03846-014	1.24807-012
HB- 7 38E	-40.5	286.4	-8.5	1.3000+005	5.11719-014	1.26757-012
HB- 8 39E	40.5	286.4	-8.5	1.2890+005	5.07389-014	1.25684-012
GE19HTF23-7R	-66.2	337.3	12.7	7.3500+004	2.89318-014	7.16664-013
HB- 9 38E	-40.5	337.8	-8.5	7.1760+004	2.82469-014	6.99698-013
HB-10 39E	40.5	337.8	-8.5	7.2420+004	2.85067-014	7.06133-013

237NP(N,F)95ZR

LAMBDA =1.2516-007, K =3.9363-019, YIELD =5.6990-002

ID	MONITOR LOCATION X	Y	Z	ACTIVITY (DPS/MG)	ACTIVITY (DPS/NUCLEUS)	REACTION RATE (RPS/NUCLEUS)
GE19SFF2319R	-66.2	240.8	12.7	2.1300+005	8.38432-014	2.02264-012
HB- 1 38E	-40.5	241.3	-8.5	2.2150+005	8.71890-014	2.10335-012
HB- 2 39E	40.5	241.3	-.3	2.1670+005	8.52996-014	2.05777-012
GE19QTF23-8R	-66.2	285.9	12.7	1.2600+005	4.95974-014	1.19649-012
HB- 7 38E	-40.5	286.4	-8.5	1.3050+005	5.13687-014	1.23922-012
HB- 8 39E	40.5	286.4	-8.5	1.3020+005	5.12506-014	1.23637-012
GE19HTF23-7R	-66.2	337.3	12.7	7.1100+004	2.79871-014	6.75162-013
HB- 9 38E	-40.5	337.8	-8.5	7.2410+004	2.85027-014	6.87602-013
HB-10 39E	40.5	337.8	-8.5	7.1830+004	2.82744-014	6.82094-013

TABLE A4

COSINE FITTING INFORMATION FOR SPVC BARE Mp AXIAL DATA[a]

	SSC-1	SSC-2	OT	QT	HT
	$^{54}Fe(n,p)^{54}Mn$				
P1[b]	2.5201E4 (2.1)[b]	5.0038E4 (2.1)	2.2122E4 (2.0)	9.7278E3 (2.0)	3.7459E3 (2.1)
P2	2.1575E2 (9.4)	2.0361E2 (7.1)	2.2578E2 (9.8)	2.2983E2 (10.2)	2.2863E2 (10.2)
Max. Dev[c] from Fit	0.6	0.4	0.3	0.8	0.4
Deviation 1[d]	5.1	1.4	2.1	2.5	3.6
Deviation 2	8.7	7.5	7.6	11.2	14.0
	$^{58}Ni(n,p)^{59}Co$				
P1	1.4257E6 (2.2)	2.2691E6 (1.7)	3.8964E5 (2.1)	1.7690E5 (2.1)	6.9282E4 (2.1)
P2	2.2360E2 (10.1)	2.2006E2 (8.5)	2.3874E2 (11.5)	2.4113E2 (11.8)	2.4387E2 (12.1)
Max. Dev from Fit	0.1	0.2	0.7	0.3	0.9
Deviation 1	2.8	1.2	1.6	2.0	2.7
Deviation 2	7.2	5.3	5.4	8.2	12.2

TABLE A4 (CONT'D)

COSINE FITTING INFORMATION FOR SPVC BARE Mp AXIAL DATA

	SSC-1	SSC-2	OT	QT	HT
			$^{58}Fe(n,\gamma)^{59}Fe$		
P1	5.9481E4 (2.9)	8.9120E4 (2.4)	3.4130E4 (2.4)	4.1233E3 (2.8)	1.3646E3 (3.7)
P2	2.0788E2 (10.5)	2.1621E2 (9.2)	1.9895E2 (8.8)	2.5796E2 (18.0)	2.5196E2 (23.5)
Max. Dev from Fit	0.3	1.1	1.4	0.3	0.4
Deviation 1 (%)	5.1	2.4	2.2	1.5	3.7
Deviation 2 (%)	13.5	8.8	10.7	11.4	8.6
			$^{59}Co(n,\gamma)^{60}Co$		
P1	3.1439E2 (2.2)	6.3917E7 (1.9)	1.0928E8 (1.9)	2.1050E7 (1.9)	8.4539E6 (1.8)
P2	2.0299E2 (8.2)	2.1671E2 (8.1)	1.8879E2 (6.2)	2.2231E2 (8.3)	2.4561E2 (10.5)
Max. Dev from Fit	0.4	0.1	1.5	0.6	1.3
Deviation 1	3.0	1.7	6.4	0.8	3.2
Deviation 2	7.6	8.4	18.7	10.7	7.0

(a) Cosine Fit to y = P1 * Cos(z/P2) where z is axial location in mm, cosine in radians. Points above midplane are plotted but were not used in the cosine fit.
(b) P1 and P2 are the calculated fitting parameters (with estimated errors) derived from only those reported values midplane or below.
(c) Maximum deviation from Fit is the maximum error in % between the derived activity and observed specific activity for those points (generally 3) used for calculation of the fit.
(d) Deviations 1 and 2 are the ranges in % between the derived and observed activities for the two respective locations above midplane.

TABLE A5

RATIO OF MEASURED SPECIFIC ACTIVITIES
(Short and Long Half-Life Reactions)

Axial Location (mm)	$^{58}Co/^{54}Mn$	$^{60}Co/^{58}Co$	$^{60}Co/^{54}Mn$
225.6	13.746	64.798	8907
150.2	12.431	86.971	8564
112.1	12.480	67.456	8419
48.6	12.054	78.211	9427
-14.6	12.055	78.802	9500
-52.7	------	------	----
-130.9	12.790	71.397	9132

A P P E N D I X B

FERRET-SAND II ANALYSIS OF DOSIMETRY IN THE PSF EXPERIMENTS

APPENDIX B

FERRET-SAND II ANALYSIS OF DOSIMETRY IN THE PSF EXPERIMENTS

R. L. Simons, W. N. McElroy, L. S. Kellogg, R. Gold (HEDL)

B1 INTRODUCTION

HEDL and ORNL derived values of the PSF Experiment's neutron exposure parameter values for the Simulated Surveillance Capsule (SSC-1 and SSC-2), the Simulated Pressure Vessel Capsule (SPVC), and the Simulated Void Box Capsule (SVBC) are considered in this appendix. HEDL and ORNL recommended values for the SSC-1, the SSC-2, and the SPVC experiments are discussed and reported in Section 4.2, Appendix C, and Appendix B of NUREG/CR-3320, Vol. 1 (Mc86b). Values derived or used by other LWR-PV-SDIP participants are reported in Appendices A.1 through A.8 of NUREG/CR-3320, Vol. 1.

The HEDL and ORNL derived values of the PSF-SSC, -SPVC, and -SVBC neutron exposure parameter values are based on the use of the FERRET-SAND II and LSL codes, respectively; see ASTM Standard E944 (As85b). The procedures used for the ORNL-LSL analyses have been documented by Stallmann (St84).

This appendix provides reference information and documentation on the procedures used for the HEDL FERRET-SAND II analyses of the dosimetry from the four PSF SSC-1, SSC-2, SPVC, and SVBC experiments. FERRET-SAND II code input and output analysis results are given for the capsule center position for each of these four experiments. Appendix A of this report provides a discussion and documentation of the results of the HEDL radiometric measurements and conversion of individual sensor activities to reaction rates. The HEDL and ORNL procedures used for obtaining sensor gradient corrections to specified (x,y,z) locations are discussed in Appendix C [Appendix B of NUREG/CR-3320, Vol. 1 (Li86)] and Reference (St84).

Results obtained from the SVBC (Pe86) experiment were intended to provide supporting data that could be used together with ASTM Standard E1035-84, Determining Radiation Exposures for Nuclear Reactor Vessel Support Structures (As85f), to make plant-specific end-of-life projections of a shield tank or support structure steel's adjusted nil-ductility temperature.

As stated by Perrin (Pe86):

> "The materials included in the SVBC included two base metal and two weld metal conditions of A537-2 of direct relevance to neutron shield tanks. Also included were A36 and A516, materials used in support structures. Other materials included A540 and A508."
>
> "Seven of the eight materials showed essentially no shift in the Charpy curves or drop in the upper-shelf energy levels. One of the eight materials, the bulk weld material, showed an apparent

increase (42°F) in the transition temperature region of the curve to higher temperature, and a possible drop in the upper-shelf energy level."

Because of the water flooding of the void box during the early part of the irradiation, the SVBC target neutron exposure of ~5 x 10^{17} n/cm^2 (E > 1 MeV) was never achieved. It was estimated by ORNL that the actual fluence (E > 1 MeV) was a factor of 20 to 40 times lower than the target fluence based on an early assessment of preliminary results of the HEDL dosimetry measurements. The SVBC irradiation temperature was estimated to be ~37°C by ORNL.

The HEDL FERRET-SAND II results reported herein indicate that the actual neutron exposure values for the center location of the SVBC were 6.1 x 10^{-5} dpa and 4.8 x 10^{16} n/cm^2 (E > 1 MeV), with (1σ) uncertainties in the range of 14 to 22%.

These SVBC physics-dosimetry results are of additional interest because of the need to verify the ORNL estimates of the effect of the water flooding and voidage on the perturbation of the neutron exposure and exposure rates in the SPVC. Such perturbations could be contributing to some of the observed systematic biases between calculated and measured neutron exposure and dosimeter sensor reaction rates, particularly at the 1/2T position of the SPVC (see Figures A3-A6). The information of interest here is that associated with the HEDL determinations of individual sensor reaction rates gradients as reported in Appendix A by Kellogg et al. It is important to observe that the integrated effects of the SPVC perturbations resulting from the void box flooding are included in the HEDL and ORNL reported exposure values for the SSC-1, SSC-2, and SPVC (OT, 1/4T, 1/2T). What may not have been properly assessed by ORNL, however, would be small, but perhaps, non-negligible changes associated with the exposure rates.

Another reason for placing emphasis on the effects of the flooding of the void box, is to better define what the actual exposure rates were for the eight steel materials irradiated in the SVBC. Here, knowing the effect of flux level could be important for the future interpretation and use of the 42°F Charpy shift data point for the bulk weld material and the setting of upper bound limits for the observed shifts (≤15°F) for the other seven materials (Mc86). The high shift of 42°F for the low-temperature (~67°F) irradiation of the bulk weld material for a neutron fluence in the low 10^{16} n/cm^2 (E > 1 MeV) exposure range was unexpected. This is partly why Perrin qualified this measured change as an "apparent increase in the transition temperature region and a possible drop in the upper-shelf energy level." Another important reason for the more careful quantification of the environmental exposure conditions for the eight SVBC steel materials is to provide documented-reference data that can be used in the event any of these irradiated materials were to be reused in future metallurgical testing programs related to end-of-life and plant life extension studies associated with shield tanks and support structure steel components (Go86,Mc86).

B2 DESCRIPTION OF THE FERRET-SAND II ANALYSIS AND INPUT DATA

B2.1 HEDL National Dosimetry Center Procedures

B2.1.1 Introduction

As part of the process of determining the neutron flux-spectra, exposure and their accuracies, analytical studies are performed with the FERRET and SAND-II codes (Mc67,Sc79). The FERRET code compares integral measurements and calculated group fluxes, using covariance information. At this time, the SAND-II code has been used primarily to process data that was input to the FERRET code.

B2.1.2 Description of the FERRET-SAND II Analysis and Input Data

The FERRET code uses both integral and differential data to adjust a priori group fluxes, ϕ_g, which are typically obtained from calculations. A lognormal least-squares algorithm weights both the a priori values and the measured data in accordance with assigned uncertainties and correlations. In general, the measured values f are linearly related to the flux ϕ by some response matrix A:

$$f_i^{(s,\alpha)} = \sum_g A_{ig}^{(s)} \phi_g^{(\alpha)} \qquad (1)$$

where i indexes the measured values belonging to a single data set s, g designates the energy group, and α delineates separate spectra that may be simultaneously adjusted. For example,

$$R_i = \sum_g \sigma_{ig} \phi_g \qquad (2)$$

relates a set of measured reaction rates R_i to a single spectrum ϕ_g by the multigroup cross sections σ_{ig}. (In this case, FERRET also adjusts the cross sections.) Differential flux measurements have the particularly simple response, $A_{gg'} = \delta_{gg'}$, where $\delta_{gg'}$ is the Kronecker delta. The lognormal approach automatically accounts for the physical constraint of positive fluxes, even with large assigned uncertainties.

For the analysis of dosimetry data, the continuous quantities (i.e., fluxes and cross sections) were approximated in 53 groups. The group structure is given in Table B1.1. The calculated flux-spectra were expanded or contracted into this group structure using the SAND II code. This procedure is carried out by first expanding the spectrum into the SAND II 620-group structure using a SPLINE interpolation procedure for interpolation in

TABLE B1.1

NEUTRON ENERGY GROUP STRUCTURE

	Group Upper Bound (UB) (MeV)
1	.16905+002
2	.14918+002
3	.13499+002
4	.11618+002
5	.10000+002
6	.86071+001
7	.74082+001
8	.60653+001
9	.49659+001
10	.36788+001
11	.28650+001
12	.22313+001
13	.17377+001
14	.13534+001
15	.11080+001
16	.82085+000
17	.63928+000
18	.49787+000
19	.38774+000
20	.30197+000
21	.18316+000
22	.11109+000
23	.67379-001
24	.40868-001
25	.25540-001
26	.19890-001
27	.15034-001
28	.91188-002
29	.55308-002
30	.33546-002
31	.28395-002
32	.24038-002
33	.20347-002
34	.12341-002
35	.74852-003
36	.45400-003
37	.27536-003
38	.16702-003
39	.10130-003
40	.61442-004
41	.37267-004
42	.22603-004
43	.13710-004
44	.83153-005
45	.50435-005
46	.30590-005
47	.18554-005
48	.11254-005
49	.68256-006
50	.41399-006
51	.25110-006
52	.15230-006
53	.92370-007
E_{LB}	10000-009*

*Group 53 Lower Bound (LB)

regions where group boundaries do not coincide. The high end of the spectrum is extrapolated using a fission spectrum form. The 620-point spectrum is then easily collapsed to 53 groups. This procedure is, in some cases, sensitive to differences in group boundaries; and energy-groups must be chosen to minimize variations in results. For many applications, the boundary effects can be ignored.

The cross sections were also collapsed into the 53 energy-group structure using SAND II with calculated spectra (as expanded to 620 groups) as weighting functions. The cross sections were taken from the ENDF/B-V dosimetry file. Uncertainty estimates and 53 x 53 covariance matrices were constructed for each cross section. Correlations between cross sections were neglected due to data and code limitations, but are expected to be unimportant.

For each set of data or a priori values, the inverse of the corresponding relative covariance matrix M is used as a statistical weight. In some cases, as for the cross sections, a multigroup covariance matrix is used. More often, a simple parameterized form, Equation 3, is used:

$$M_{gg'} = F_N^2 + R_g R_{g'} \rho_{gg'} \qquad (3)$$

where R_N specifies an overall fractional normalization uncertainty (i.e., complete correlation) for the corresponding set of values. The fractional uncertainties R_g specify additional random uncertainties for group g that are correlated with a correlation matrix, Equation 4:

$$\sigma_{gg'} = (1 - \theta)\, \sigma_{gg'} + \theta \exp\left(-\frac{(g-g')^2}{2\gamma^2}\right) \qquad (4)$$

The first term specifies purely random uncertainties while the second term describes short-range correlations over a range γ (θ specifies the strength of the latter term).

For the a priori calculated fluxes, a short-range correlation of $\gamma = 6$ groups was used. This choice implies that neighboring groups are strongly correlated. Strong long-range correlations (or anticorrelations) were justified based on information presented by R. A. Maerker (St82). Maerker's results are closely duplicated when $\gamma = 6$. For the integral reaction rate covariances, simple normalization and random uncertainties were combined as deduced from experimental uncertainties. Specific assignments of uncertainty values were made, as described in the following sections.

B2.1.3 Calculated Flux-Spectral Data

The FERRET adjusted spectra were found to be only slightly dependent on the input calculated spectra. The calculated spectra were assumed to have a normalization uncertainty of 100%. This estimate was assumed so that the reaction ratio would establish the flux magnitude. The value of group uncertainties was chosen to be 50% for all groups correlated as detailed in Table B1.2.

B2.1.4 Cross-Section Data

The cross-section uncertainties and errors associated with the ENDF-V and other values are included in the cross-section covariance matrices. The uncertainties and errors reflected in these matrices appear to be conservative.

Intercorrelations between sets of data (i.e., between spectra at different positions, etc.) are not included in the FERRET analysis at this time. These neglected correlations are not expected to significantly affect the adjusted flux-spectra.

B2.1.5 Comparison of FERRET-SAND II Analysis and Individual Detectors

In Section 4.1.1 of Reference (Mc87e), the NBS method of examining individual detector responses was used by Grundl and McGarry to predict the flux for a surveillance capsule location for a generic two-loop Westinghouse pressurized water reactor. That method did not include uncertainties in the measured reaction rates because explicit estimates were not available. For comparison with the NBS results, the FERRET code exposure parameter derived values used a generic set of estimated uncertainties (Table B1.2). Using the same reactions selected by NBS and the reaction rate standard deviations from Simons' work (Si82a), multiple-foil adjusted values of flux-spectrum were determined with the FERRET code. Results are shown in Table B2 along with results derived from single-foil response analysis. In general, the two methods yielded similar results.

The uniqueness of the Eq. 2 solution flux-spectrum, ϕg, is bounded by a set of assigned uncertainties, such as those given in Table B1.2. The proper assignment of these uncertainties to the calculated (a priori) flux-spectrum is a critical consideration for the application of any least-squares adjustment code. It is very important, therefore, to make careful comparisons of the adjusted multiple-foil with single-foil results to help test and verify the validity of the error assignments for the a priori calculated flux-spectrum. The results in Table B2 provide an example of such a test and verification for a PWR simulated surveillance capsule (SSC) irradiation experiment.

TABLE B1.2

FERRET INPUT UNCERTAINTIES AND
CORRELATION PARAMETER VALUES*

Data Set	Normalization Uncertainty R	Random Uncertainty R	Correlation Strength	Correlation Width
Calculated Flux $E = 10^{-10}$ - 18 MeV	1.00	0.50	0.8	6.0
Cross Sections (Input as full covariance matrix)				
Reaction Rates [Values were based on data given in Reference (Si82a)]				

Correlation Matrix Format

$$M_{ij} = (R_N)^2 + (R_g)_i \cdot (R_g)_j \cdot P_{ij}$$

$$P_{ij} = (1 - \theta) \cdot \sigma_{ij} + \theta \cdot \exp\left[-(i - j)^2/2\gamma^2\right]$$

(i and j denote energy groups)

* Uncertainty expressed as a fraction (e.g., 0.50 = 50%).

TABLE B2

COMPARISON OF SURVEILLANCE CAPSULE MULTIPLE- AND SINGLE-FOIL
INTEGRAL FLUX/s AND dpa/s

Integral Value	Multiple-Foil	Single-Foil
Flux, E > 0.1 MeV (n/cm^2-s)	$(5.6 \pm 0.85) \times 10^{11}$	$(5.34 \pm 0.9) \times 10^{11}$
Flux, E > 1.0 MeV (n/cm^2-s)	$(1.44 \pm 0.13) \times 10^{11}$	$(1.38 \pm 0.18) \times 10^{11}$
dpa/s	$(2.53 \pm 0.25) \times 10^{-10}$	$(2.46 \pm 0.4) \times 10^{-10}$

Lippincott et al. (Li87) have discussed this problem of the dependence of the FERRET-SAND II solution on the input uncertainties surveillance capsule and cavity (Void Box) dosimetry measurements for the H. B. Robinson Unit 2, Cycle 9, PWR benchmark experiment. A comparison was made of the derived exposure parameter values using the adjustment approach and the spectrum-averaged cross-section $\bar{\sigma}$ (single foil) approach. Table B3 presents the comparative results for both the 290° surveillance capsule and the 270° cavity midplane positions. Good agreement was obtained between the two methods at the surveillance position although the 11% difference for dpa is slightly larger than the 1σ uncertainty as evaluated by FERRET-SAND II. The FERRET-SAND II value is slightly biased by the calculated flux spectrum in the region where little detector response is present.

At the cavity position, a larger difference is observed between the two methods for $\phi(E > 1\ MeV)$. The difference is due to the fact that the ^{237}Np and ^{238}U responses indicate a relative underprediction of flux in the energy range of 0.5 to 2 MeV. Since most of the neutron flux above 1 MeV falls below 2 MeV, FERRET-SAND II weights the solution results with these two sensors. In some cases, it is clear that the flux is definitely overestimated. In the $\bar{\sigma}$ method, no spectral adjustment is made which results in all sensor responses being weighted equally. The latter method is perhaps more appropriate for extrapolating back into the vessel since the higher energy neutrons are more closely tied to those being transported directly from the vessel inner radius.

Additional differences between the two methods as applied here involve the use of different dosimetry cross sections (ENDF/B-V for FERRET and ENDF/B-IV for $\bar{\sigma}$) and different group structures. It was recommended in Reference (Li87) that the results from the two methods be averaged to produce a final result.

Because of the VB flooding and the associated complexity of the dosimetry analysis for the SVBC, no attempt has been made to compare the $\bar{\sigma}$ method and FERRET-SAND II results. The comparison of the results of these two methods for HBR-2 suggests, however, that the FERRET-SAND II error assignments for the SVBC exposure parameter values of dpa and $\phi t > 1MeV$, Table B4, may be too conservative and that the actual uncertainties could be a factor of up to two or more higher.

TABLE B3

COMPARISON OF DERIVED EXPOSURE PARAMETERS USING THE ADJUSTMENT AND SPECTRUM AVERAGED CROSS-SECTION METHODS

Parameter	$\bar{\sigma}$ Method	FERRET-SAND II	FERRET-SAND II / $\bar{\sigma}$ Method
		290° Surveillance Capsule	
ϕ(E > 1.0 MeV)	4.98×10^{10}	4.78×10^{10}	0.96
dpa/s	8.07×10^{-11}	7.15×10^{-11}	0.89
		270° Cavity Capsule	
ϕ(E > 1.0 MeV)	9.68×10^{8}	11.55×10^{8}	1.19
dpa/s	4.83×10^{-12}	5.28×10^{-12}	1.09

B3 SSC-1 AND SSC-2 CAPSULE CENTER FERRET-SAND II RESULTS

In Appendix C [Appendix B of Reference (Mc86b)], Lippincott and Simons have discussed and reported on the HEDL determination of the FERRET-SAND II derived exposure parameter values [$\phi t(E > 1\ MeV)$, $\phi t(E > 0.1\ MeV)$, $\phi t(thermal)$, and dpa] for the capsule center locations for the PSF experiment. Documentation of the detailed FERRET-SAND II results were not provided. The detailed FERRET-SAND II adjusted flux-spectra for the SSC-1 and SSC-2 experiments' capsule center location are given in Tables B5.1 and B6.1, respectively. Tables B5.2 and B6.2 compare calculated, measured, and adjusted reaction rates.

B4 SPVC CAPSULE CENTER FERRET-SAND II RESULTS

In Appendix C [Appendix B of Reference (Mc86b)], Lippincott and Simons have discussed and reported on the HEDL determination of the FERRET-SAND II derived exposure parameter values [$\phi t(E > 1MeV)$, $\phi t(E > 0.1MeV)$, $\phi t(thermal)$, and dpa] for the capsule center location for the SPVC experiment. Documentation of the detailed FERRET-SAND II results were not provided. The detailed FERRET-SAND II adjusted flux-spectra for the SPVC-0T, -1/4T and -1/2T capsule center locations are given in Tables B7.1, B8.1, and B9.1 respectively. Tables B7.2, B8.2 and B9.2 compare calculated, measured, and adjusted reaction rates.

B5 SVBC CAPSULE CENTER FERRET-SAND II RESULTS

For the SSC and the SPVC, and the other experiments in the Pool Side Facility (PSF) of the Oak Ridge Research Reactor (ORR), the reactor power time- history was used in the analysis of dosimetry to convert the time of removal reaction activities to the saturated reaction rates at a specific reactor power level (see Appendix A). This assumed that the local flux-history followed the reactor power history and the neutron spectrum did not change significantly during the irradiation.

During the two-year irradiation of the SPVC and SVBC experiments, the void box (VB) was inadvertently flooded with water. Some members of the ORNL staff believe that the flooding occured some time during the first month of irradiation and that it took only a short time for the VB to fill. Calculations by ORNL indicate that the flooded void box depressed the flux and hardened the neutron spectrum enough to reduce the $^{54}Fe(n,p)^{54}Mn$ reaction rate by over an order of magnitude. In some neutron energy regions, the calculations showed up to a factor of 33 reduction in the group flux values. The exact time-history of the VB local flux changes due to flooding is unknown, and it is clear that the reactor power time-history was inadequate for the analysis of the SVBC dosimetry. This was clearly shown in an initial attempt to adjust the SVBC flux spectrum using the derived reaction rates from Capsule HB-12, (see Appendix A), based on reactor power time-history. For the SVBC, the long- and short-lived reaction products produced very different and inconsistent FERRET-SAND II adjustments in the flux-spectrum.

Because of radioactive decay, the short half-life reaction products (30 to 70 day half-life) do not reflect the neutron exposure from the voided condition (i.e., high flux). Consequently, the short half-life reaction was used to determine the flux spectrum during the VB flooded condition. However, multiplying by the effective full-power exposure time does not give the correct neutron exposures to the metallurgical specimens because it is now believed that most of the exposure occurred during the voided condition.

The long half-life reaction can be used as neutron flux time integrators without knowing the actual flux time-history scenario. Two possible scenarios, A and B, are shown in Figure B1. Consider the two step constant flux time-history Scenario A. The reaction saturation activity, A (dps/nucleus), at the end of the irradiation is given by Equation 5:

$$A = \phi_1\bar{\sigma}_1 \quad (1 - e^{-\lambda t_1}) \cdot e^{-\lambda t_2} + \phi_2\bar{\sigma}_2 \cdot (1 - e^{-\lambda t_2}) \qquad (5)$$

where:

ϕ_i $(i = 1,2)$ = flux,
$\bar{\sigma}_i$ $(i = 1,2)$ = spectrum average cross sections,
t_1 = irradiation time for the voided condition,
t_2 = irradiation time for the flooded condition
λ = decay constant.

The subscripts 1 and 2 refer to the first and second time steps. For long half-life reaction products, a Taylor Series expansion and division by λ gives Equation 6:

$$\frac{A}{\lambda} = \phi_1\bar{\sigma}_1\lambda t_1 \cdot (1 - \lambda t_2) + \phi_2\bar{\sigma}_2 t_2. \qquad (6)$$

The $(1 - \lambda t_2)$ term is approximately 1 for long half-life reaction products and thus A/λ is the total number of reaction products. Analysis of the A/λ data with the SAND-FERRET code yields the effective fluence-spectrum. Four sources of uncertainties were considered in the analysis: 1) Those due to counting statistics and associated radiometric parameters, 2) sensor self-shielding corrections, 3) time-history, and 4) the a priori neutron spectrum. The radiometric sources of uncertainty were generally on the order of 5%, see Appendix A. Some of the shorter half-life fission products had radiometric-based uncertainties as high as 16%.* Some additional uncertainty in the $^{235}U(n,f)$ fission rate is expected because of neutron resonance self-shielding. Assumming an exponential attentuation of flux through the U_3O_8 sensor (16% of the true density), the self-shielding correction factor was estimated to be at most 0.9. Rather than making this correction with its associated large uncertainty, the uncertainty for this

---

*It appears that the $^{238}U(n,f)^{95}Zr$ reaction rate is about a factor of 10 low; and, therefore, it was not used in the present analysis.

sensor was just increased from 5 to 12%. Because of the low-energy response of ^{235}U, this had little impact on the resultant FERRET-SAND II fluences $E > 1$ MeV.

The major time-history uncertainty for the long half-lived reactions is due to the $(1 - \lambda t_2)$ term in Equation 6. For ^{137}Cs, this is <3%. However, up to 20% of ^{60}Co produced in the voided condition was lost by decay during the water-filled condition. Consequently, the uncertainty in the reaction rate for ^{60}Co was set at 21%.

A priori neutron spectra were obtained from Maerker [see references (Ma84a, Ma84b)]. Reference (Ma84a) gives the neutron spectra for the voided condition, while in Reference (Mc86b) Miller gives the correction factors needed to adjust the former group fluxes to account for the water flooding. The corrected spectrum is appropriate for the short half-life reactions. However, since the long half-life reactions saw some portion of both the voided and flooded conditions, the appropriate a priori spectrum here is some type of synthesis of both.

In order to handle solution uniqueness problems (see Section B2.1.5) and to accommodate large changes in the group fluxes, the group flux uncertainty was set at 300%. This was, in part, selected because the water caused up to a factor of 33 changes in some group fluxes. This large uncertainty allowed the FERRET code to adjust the group fluxes so that the integral fluxes and dpa gave, approximately, the same values independent of the a priori input flux-spectrum.

The results of the FERRET-SAND analysis for the SVBC are summarized in Table B4. Only one set of exposure parameter values is reported for the central location of the void box capsule because of the very low total neutron exposure.

The SVBC central location recommended damage exposure parameter values are 6.1×10^{-5} dpa and a fluence ($E > 1$ MeV) of 4.8×10^{16} n/cm^2. The calculated fluences ($E > 1$ MeV) and dpa for the voided and flooded conditions are given in Table B4 for comparison. The exposures for the short half-life reactions are based on the adjusted fluxes and the effective full-power exposure time of 5.097×10^7 seconds. It is apparent that the short half-life reactions under-determined the actual neutron exposures by a factor of approximately 6.4. The value of 4.7×10^{16} n/cm^2 based on the long half-life reactions indicates that most of the exposure of the eight steels may have occured within the first month of the irradiation and at a much higher flux level than the flooded condition.

The detailed adjusted flux-spectra for the cases with long- and short-life reactions are shown in Tables B10.1, B11.1, and B12.1. The a priori spectrum for the long half-life reaction rate case is the calculated spectrum for the voided box. The results starting from the spectrum with the flooded condition are nearly identical. The uncertainties in the group fluxes are large, but the cross-correlations allow prediction of integral neutron exposure values with modest uncertainties of only 14-22%. These

TABLE B4

SUMMARY OF DPA AND $\phi t > 1$ MeV FOR PSF/SVBC

Reaction Set	dpa	$\phi t > 1$ MeV (n/cm^2)
Calculation		
• Without Water Flooding	0.00129	5.00×10^{17}
• With Water Flooding	0.0000877	5.93×10^{16}
FERRET-SAND II		
• 6 long-lived reactions*	0.000064 (±22%)	4.7×10^{16} (±15%)
• 6 short-lived reactions**	0.0000096 (±15%)	7.5×10^{15} (±14%)

* Based on the long-lived reactions:	$^{235}U(n,f)^{137}Cs$	Gd Cover
	$^{237}Np(n,p)^{137}Cs$	"
	$^{238}U(n,f)^{137}Cs$	"
	$^{63}Cu(n,\alpha)^{60}Co$	"
	$^{59}Co(n,\gamma)^{60}Co$	"
	$^{59}Co(n,\gamma)^{60}Co$	Bare
** Based on the short-lived reactions:	$^{235}U(n,f)^{95}Zr$(a)	Gd Cover
	$^{237}Np(n,f)^{95}Zr$(b)	"
	$^{238}U(n,f)^{103}Ru$(c)	"
	$^{46}Ti(n,p)^{46}Sc$	"
	$^{58}Ni(n,p)^{58}Co$	"
	$^{45}Sc(n,\gamma)^{46}Sc$	"

a) The ^{103}Ru result was consistent with the ^{95}Zr result.

b) No ^{103}Ru result was reported.

c) The ^{95}Zr result was inconsistent with the ^{103}Ru result, and it appeared to be in error.

uncertainties, however, may be too low by a factor of two or more, see Section B2.1.5. Tables B10.2, B11.2 and B12.2 compare calculated, measured, and adjusted reaction rates.

The HEDL measured spectral set and gradient sensor reaction rates for the SVBC are given in Appendix A. As indicated by Kellogg et al., the flooding of the void box caused some very serious perturbations (from a cosine to a near linear axial distribution) of the measured reaction rate gradients. These gradient results should be used to make any off-midplane estimates of the expected variation of Table B4 dpa and $\Phi t > 1$ MeV exposure parameter values for individual SVBC Charpy specimens for the eight irradiated steels.

TABLE B5.1

FERRET-SANDII RESULTS FOR (AVERAGE FOR CAPSULE)
SIMULATED SURVEILLANCE CAPSULE - 1 (SSC-1)

GROUP	ENERGY (MEV) [a]	A PRIORI FLUX* (N/CM**2/SEC)	ADJUSTED FLUX (N/CM**2/SEC)	% UNCERTAIN (1 STD)
1	1.492+001	1.047+008	1.131+008	20.
2	1.350+001	3.346+008	3.661+008	19.
3	1.162+001	1.615+009	1.791+009	17.
4	1.000+001	5.014+009	5.639+009	15.
5	8.607+000	1.319+010	1.506+010	13.
6	7.408+000	2.747+010	3.183+010	12.
7	6.065+000	7.531+010	8.863+010	11.
8	4.966+000	1.309+011	1.556+011	11.
9	3.679+000	3.274+011	3.912+011	10.
10	2.865+000	4.629+011	5.519+011	11.
11	2.231+000	8.368+011	1.005+012	11.
12	1.738+000	1.011+012	1.219+012	12.
13	1.353+000	1.251+012	1.506+012	13.
14	1.108+000	1.335+012	1.595+012	14.
15	8.208-001	1.941+012	2.296+012	14.
16	6.393-001	2.073+012	2.408+012	16.
17	4.979-001	1.985+012	2.254+012	17.
18	3.877-001	1.324+012	1.466+012	19.
19	3.020-001	1.741+012	1.879+012	20.
20	1.832-001	2.195+012	2.307+012	21.
21	1.111-001	1.914+012	1.959+012	22.
22	6.738-002	9.045+011	9.029+011	23.
23	4.087-002	8.322+011	8.108+011	24.
24	2.554-002	7.451+011	7.101+011	24.
25	1.989-002	3.826+011	3.586+011	24.
26	1.503-002	4.178+011	3.859+011	24.
27	9.119-003	7.206+011	6.538+011	24.
28	5.531-003	6.910+011	6.273+011	24.
29	3.355-003	6.650+011	6.083+011	23.
30	2.839-003	2.166+011	1.999+011	22.
31	2.404-003	2.142+011	2.005+011	21.
32	2.035-003	2.121+011	2.024+011	20.
33	1.234-003	6.245+011	6.089+011	19.
34	7.485-004	6.099+011	6.088+011	18.
35	4.540-004	5.991+011	6.113+011	17.
36	2.754-004	5.920+011	5.633+011	12.
37	1.670-004	5.886+011	6.058+011	14.
38	1.013-004	5.891+011	7.402+011	8.
39	6.144-005	5.933+011	6.258+011	14.
40	3.727-005	6.013+011	6.217+011	14.

a) Lower Energy Bound

TABLE B5.1 (Cont'd)

FERRET-SANDII RESULTS FOR (AVERAGE FOR CAPSULE)
SIMULATED SURVEILLANCE CAPSULE - 1 (SSC-1)

GROUP	ENERGY (MEV)	A PRIORI FLUX* (N/CM**2/SEC)	ADJUSTED FLUX (N/CM**2/SEC)	% UNCERTAIN (1 STD)
41	2.260-005	6.131+011	6.196+011	14.
42	1.371-005	6.285+011	6.160+011	14.
43	8.315-006	6.478+011	6.118+011	14.
44	5.043-006	6.708+011	6.181+011	14.
45	3.059-006	6.977+011	6.248+011	14.
46	1.855-006	7.282+011	6.398+011	14.
47	1.125-006	7.625+011	6.571+011	13.
48	6.826-007	8.007+011	6.835+011	13.
49	4.140-007	8.420+011	7.231+011	13.
50	2.511-007	7.889+011	6.930+011	13.
51	1.523-007	6.708+011	6.119+011	13.
52	9.237-008	5.709+011	5.364+011	13.
53	1.000-010	1.598+012	1.587+012	7.
FLUX, E> 0.0 MEV		3.947+013	4.100+013	7.
FLUX, E< 0.414 EV		3.629+012	3.429+012	6.
FLUX, E> 0.1 MEV		1.884+013	2.132+013	11.
FLUX, E> 1.0 MEV		6.141+012	7.352+012	6.
DPA/SECOND		9.467-009	1.099-008	7.
FLUENCE+, E> 1.0 MEV		2.186+019	2.616+019	6.
DPA+		3.369-002	3.910-002	7.

* ABSOLUTE CALCULATED FLUX (OR NORMALIZED TO FE54(N,P)MN54 REACTION RATE).

\+ BASED ON 3.559+006 EFFECTIVE FULL POWER SECONDS OF EXPOSURE; UNITS OF N/CM**2 FOR FLUENCE AND TOTAL NUMBER OF DISPLACED ATOMS OF IRON PER TARGET ATOM OF IRON FOR DPA.

TABLE B5.2

COMPARISON OF MEASURED AND CALCULATED
REACTION RATES USED IN THE ANALYSIS OF
SIMULATED SURVEILLANCE CAPSULE - 1 (SSC-1)

		REACTION RATE (DPS/NUCLEUS)			RATIO MEAS/CALC	
REACTION	COVER	MEAS (a)	A PRIORI CALC	ADJ CALC	A PRIORI	ADJ CALC
FE54(N,P)MN54	BARE	4.52-013(4)	3.86-013	4.56-013	1.17	.99
FE58(N,G)FE59	"	3.77-012(4)	4.36-012	3.76-012	.87	1.00
NI58(N,P)CO58	"	6.35-013(4)	5.22-013	6.31-013	1.22	1.01
CU63(N,A)CO60	"	3.07-015(4)	2.65-015	3.07-015	1.16	1.00
TI46(N,P)SC46	"	5.94-014(4)	4.90-014	5.91-014	1.21	1.01
CO59(N,G)CO60	"	2.05-010(4)	1.79-010	1.96-010	1.15	1.05
SC45(N,G)SC46	"	7.21-011(4)	8.03-011	7.37-011	.90	.98
U235(N,F)CS137	Gd	3.99-010(5)	4.30-010	4.06-010	.93	.98
U238(N,F)CS137	"	2.51-012(10)	2.10-012	2.52-012	1.19	1.00
NP237(N,F)CS137	"	2.05-011(5)	1.65-011	2.03-011	1.24	1.01
CO59(N,G)CO60	"	1.09-010(4)	9.12-011	1.09-010	1.19	1.00
SC45(N,G)SC46	"	1.72-011(4)	1.97-011	1.71-011	.87	1.00
FE58(N,G)FE59	"	1.47-012(4)	1.76-012	1.52-012	.84	.97

a) The bracketed values are the one-sigma % uncertainty estimates.

TABLE B6.1

FERRET-SANDII RESULTS FOR (AVERAGE FOR CAPSULE)
SIMULATED SURVEILLANCE CAPSULE - 2 (SSC-2)

GROUP	ENERGY (MEV) [a]	A PRIORI FLUX* (N/CM**2/SEC)	ADJUSTED FLUX (N/CM**2/SEC)	% UNCERTAIN (1 STD)
1	1.492+001	1.047+008	9.523+007	20.
2	1.350+001	3.346+008	3.051+008	19.
3	1.162+001	1.615+009	1.482+009	17.
4	1.000+001	5.014+009	4.636+009	15.
5	8.607+000	1.319+010	1.235+010	13.
6	7.408+000	2.747+010	2.637+010	12.
7	6.065+000	7.531+010	7.425+010	11.
8	4.966+000	1.309+011	1.338+011	11.
9	3.679+000	3.274+011	3.451+011	10.
10	2.865+000	4.629+011	4.952+011	11.
11	2.231+000	8.368+011	9.203+011	11.
12	1.738+000	1.011+012	1.136+012	12.
13	1.353+000	1.251+012	1.405+012	13.
14	1.108+000	1.335+012	1.466+012	14.
15	8.208-001	1.941+012	2.105+012	14.
16	6.393-001	2.073+012	2.217+012	16.
17	4.979-001	1.985+012	2.089+012	17.
18	3.877-001	1.324+012	1.370+012	19.
19	3.020-001	1.741+012	1.767+012	20.
20	1.832-001	2.195+012	2.188+012	21.
21	1.111-001	1.914+012	1.877+012	22.
22	6.738-002	9.045+011	8.759+011	23.
23	4.087-002	8.322+011	7.977+011	24.
24	2.554-002	7.451+011	7.093+011	24.
25	1.989-002	3.826+011	3.631+011	25.
26	1.503-002	4.178+011	3.963+011	25.
27	9.119-003	7.206+011	6.843+011	25.
28	5.531-003	6.910+011	6.605+011	25.
29	3.355-003	6.650+011	6.418+011	25.
30	2.839-003	2.166+011	2.114+011	24.
31	2.404-003	2.142+011	2.117+011	23.
32	2.035-003	2.121+011	2.124+011	22.
33	1.234-003	6.245+011	6.331+011	21.
34	7.485-004	6.099+011	6.248+011	20.
35	4.540-004	5.991+011	6.179+011	19.
36	2.754-004	5.920+011	6.009+011	17.
37	1.670-004	5.886+011	6.039+011	16.
38	1.013-004	5.891+011	6.485+011	8.
39	6.144-005	5.933+011	5.960+011	15.
40	3.727-005	6.013+011	5.881+011	14.

a) Lower Energy Bound

TABLE B6.1 (Cont'd)

FERRET-SANDII RESULTS FOR (AVERAGE FOR CAPSULE)
SIMULATED SURVEILLANCE CAPSULE - 2 (SSC-2)

GROUP	ENERGY (MEV)	A PRIORI FLUX* (N/CM**2/SEC)	ADJUSTED FLUX (N/CM**2/SEC)	% UNCERTAIN (1 STD)
41	2.260-005	6.131+011	5.832+011	14.
42	1.371-005	6.285+011	5.785+011	14.
43	8.315-006	6.478+011	5.745+011	14.
44	5.043-006	6.708+011	5.789+011	15.
45	3.059-006	6.977+011	5.841+011	15.
46	1.855-006	7.282+011	5.948+011	15.
47	1.125-006	7.625+011	6.086+011	15.
48	6.826-007	8.007+011	6.282+011	14.
49	4.140-007	8.420+011	6.567+011	14.
50	2.511-007	7.889+011	6.179+011	13.
51	1.523-007	6.708+011	5.341+011	13.
52	9.237-008	5.709+011	4.615+011	13.
53	1.000-010	1.598+012	1.311+012	8.
FLUX, E> 0.0 MEV		3.947+013	3.862+013	8.
FLUX, E< 0.414 EV		3.629+012	2.924+012	6.
FLUX, E> 0.1 MEV		1.884+013	1.982+013	11.
FLUX, E> 1.0 MEV		6.141+012	6.741+012	6.
DPA/SECOND		9.467-009	1.011-008	7.
FLUENCE+, E> 1.0 MEV		5.171+019	5.676+019	6.
DPA+		7.971-002	8.511-002	7.

* ABSOLUTE CALCULATED FLUX (OR NORMALIZED TO FE54(N,P)MN54 REACTION RATE).

\+ BASED ON 8.420+006 EFFECTIVE FULL POWER SECONDS OF EXPOSURE; UNITS OF N/CM**2 FOR FLUENCE AND TOTAL NUMBER OF DISPLACED ATOMS OF IRON PER TARGET ATOM OF IRON FOR DPA.

TABLE B6.2

COMPARISON OF MEASURED AND CALCULATED
REACTION RATES USED IN THE ANALYSIS OF
SIMULATED SURVEILLANCE CAPSULE - 2 (SSC-2)

		REACTION RATE (DPS/NUCLEUS)			RATIO MEAS/CALC	
REACTION	COVER	MEAS (a)	A PRIORI CALC	ADJ CALC	A PRIORI	ADJ CALC
FE54(N,P)MN54	BARE	4.02-013(4)	3.86-013	4.04-013	1.04	.99
CU63(N,A)CO60	"	2.45-015(4)	2.65-015	2.48-015	.93	.99
TI46(N,P)SC46	"	5.20-014(4)	4.90-014	5.15-014	1.06	1.01
CO59(N,G)CO60	"	1.75-010(4)	1.79-010	1.67-010	.98	1.05
SC45(N,G)SC46	"	6.26-011(4)	8.03-011	6.37-011	.78	.98
FE58(N,G)FE59	"	3.40-012(4)	4.36-012	3.44-012	.78	.99
NI58(N,P)CO58	"	5.47-013(4)	5.22-013	5.48-013	1.05	1.00
CO59(N,G)CO60	Gd	9.32-011(4)	9.12-011	9.45-011	1.02	.99
U235(N,F)CS137	"	3.75-010(5)	4.30-010	3.80-010	.87	.99
U238(N,F)CS137	"	2.55-012(10)	2.10-012	2.33-012	1.21	1.10
NP237(N,F)CS137	"	1.74-011(5)	1.65-011	1.75-011	1.05	.99

a) The bracketed values are the one-sigma % uncertainty estimates.

TABLE B7.1

FERRET-SANDII RESULTS FOR (AVERAGE FOR CAPSULE)
SIMULATED PRESSURE VESSEL CAPSULE - 0T (SPVC-0T)

GROUP	ENERGY (MEV) [a]	A PRIORI FLUX* (N/CM**2/SEC)	ADJUSTED FLUX (N/CM**2/SEC)	% UNCERTAIN (1 STD)
1	1.492+001	2.218+007	2.078+007	20.
2	1.350+001	7.414+007	6.941+007	19.
3	1.162+001	3.473+008	3.261+008	17.
4	1.000+001	1.023+009	9.652+008	15.
5	8.607+000	2.574+009	2.453+009	13.
6	7.408+000	5.015+009	4.869+009	12.
7	6.065+000	1.298+010	1.285+010	11.
8	4.966+000	2.031+010	2.061+010	11.
9	3.679+000	4.488+010	4.661+010	11.
10	2.865+000	5.787+010	6.164+010	11.
11	2.231+000	1.077+011	1.188+011	11.
12	1.738+000	1.245+011	1.411+011	12.
13	1.353+000	1.487+011	1.692+011	13.
14	1.108+000	1.503+011	1.679+011	14.
15	8.208-001	2.086+011	2.312+011	15.
16	6.393-001	2.363+011	2.585+011	16.
17	4.979-001	2.408+011	2.592+011	18.
18	3.877-001	1.686+011	1.781+011	19.
19	3.020-001	2.189+011	2.266+011	20.
20	1.832-001	2.784+011	2.823+011	22.
21	1.111-001	2.518+011	2.509+011	23.
22	6.738-002	1.239+011	1.218+011	24.
23	4.087-002	1.136+011	1.106+011	24.
24	2.554-002	1.011+011	9.797+010	25.
25	1.989-002	5.154+010	5.009+010	25.
26	1.503-002	5.595+010	5.484+010	25.
27	9.119-003	9.547+010	9.498+010	25.
28	5.531-003	9.002+010	9.162+010	25.
29	3.355-003	8.484+010	8.890+010	25.
30	2.839-003	2.719+010	2.953+010	25.
31	2.404-003	2.664+010	3.005+010	24.
32	2.035-003	2.613+010	3.063+010	23.
33	1.234-003	7.537+010	9.130+010	22.
34	7.485-004	7.109+010	8.854+010	21.
35	4.540-004	6.709+010	8.485+010	20.
36	2.754-004	6.338+010	8.012+010	19.
37	1.670-004	5.996+010	7.480+010	18.
38	1.013-004	5.685+010	8.182+010	11.
39	6.144-005	5.402+010	6.202+010	17.
40	3.727-005	5.149+010	5.469+010	17.

a) Lower Energy Bound

TABLE B7.1 (Cont'd)

FERRET-SANDII RESULTS FOR (AVERAGE FOR CAPSULE)
SIMULATED PRESSURE VESSEL CAPSULE - 0T (SPVC-0T)

GROUP	ENERGY (MEV)	A PRIORI FLUX* (N/CM**2/SEC)	ADJUSTED FLUX (N/CM**2/SEC)	% UNCERTAIN (1 STD)
41	2.260-005	4.926+010	4.837+010	17.
42	1.371-005	4.752+010	4.271+010	17.
43	8.315-006	5.185+010	4.230+010	16.
44	5.043-006	6.832+010	5.226+010	16.
45	3.059-006	9.732+010	6.968+010	16.
46	1.855-006	1.387+011	9.507+010	16.
47	1.125-006	1.926+011	1.273+011	15.
48	6.826-007	2.590+011	1.657+011	13.
49	4.140-007	3.377+011	2.181+011	13.
50	2.511-007	3.500+011	2.339+011	12.
51	1.523-007	2.996+011	2.276+011	13.
52	9.237-008	2.568+011	2.123+011	14.
53	1.000-010	7.295+011	7.107+011	8.
FLUX, E> 0.0 MEV		6.454+012	6.100+012	7.
FLUX, E< 0.414 EV		1.636+012	1.385+012	6.
FLUX, E> 0.1 MEV		2.306+012	2.460+012	11.
FLUX, E> 1.0 MEV		7.476+011	8.265+011	7.
DPA/SECOND		1.187-009	1.277-009	7.
FLUENCE+, E> 1.0 MEV		3.811+019	4.212+019	7.
DPA+		6.050-002	6.509-002	7.

* ABSOLUTE CALCULATED FLUX (OR NORMALIZED TO FE54(N,P)MN54 REACTION RATE).

\+ BASED ON 5.097+007 EFFECTIVE FULL POWER SECONDS OF EXPOSURE; UNITS OF N/CM**2 FOR FLUENCE AND TOTAL NUMBER OF DISPLACED ATOMS OF IRON PER TARGET ATOM OF IRON FOR DPA.

TABLE B7.2

COMPARISON OF MEASURED AND CALCULATED
REACTION RATES USED IN THE ANALYSIS OF
SIMULATED PRESSURE VESSEL CAPSULE - 0T (SPVC-0T)

		REACTION RATE (DPS/NUCLEUS)			RATIO MEAS/CALC	
REACTION	COVER	MEAS (a)	A PRIORI CALC	ADJ CALC	A PRIORI	ADJ CALC
FE54(N,P)MN54	BARE	5.54-014(6)	5.46-014	5.65-014	1.02	.98
FE58(N,G)FE59	"	1.20-012(9)	1.48-012	1.24-012	.81	.97
NI58(N,P)CO58	"	7.46-014(9)	7.28-014	7.58-014	1.02	.98
CU63(N,A)CO60	"	4.51-016(6)	4.75-016	4.57-016	.95	.99
TI46(N,P)SC46	"	8.28-015(9)	7.95-015	8.10-015	1.04	1.02
SC45(N,G)SC46	"	2.73-011(9)	3.24-011	2.79-011	.84	.98
CO59(N,G)CO60	"	5.37-011(6)	5.11-011	4.92-011	1.05	1.09
CO59(N,G)CO60	Gd	1.53-011(6)	1.36-011	1.45-011	1.12	1.05
U235(N,F)CS137	"	6.00-011(6)	9.23-011	6.91-011	.65	.87
U238(N,F)CS137	"	3.30-013(10)	2.70-013	2.99-013	1.22	1.10
NP237(N,F)CS137	"	2.17-012(6)	1.98-012	2.17-012	1.10	1.00

a) The bracketed values are the one-sigma % uncertainty estimates.

TABLE B8.1

FERRET-SANDII RESULTS FOR (AVERAGE FOR CAPSULE)
SIMULATED PRESSURE VESSEL CAPSULE - 1/4T (SPVC-1/4T)

GROUP	ENERGY (MEV) [a]	A PRIORI FLUX* (N/CM**2/SEC)	ADJUSTED FLUX (N/CM**2/SEC)	% UNCERTAIN (1 STD)
1	1.492+001	9.642+006	9.022+006	20.
2	1.350+001	3.358+007	3.159+007	19.
3	1.162+001	1.570+008	1.489+008	17.
4	1.000+001	4.542+008	4.346+008	15.
5	8.607+000	1.130+009	1.095+009	13.
6	7.408+000	2.151+009	2.129+009	12.
7	6.065+000	5.360+009	5.425+009	11.
8	4.966+000	8.094+009	8.422+009	11.
9	3.679+000	1.797+010	1.917+010	11.
10	2.865+000	2.447+010	2.643+010	11.
11	2.231+000	4.906+010	5.378+010	11.
12	1.738+000	6.389+010	7.057+010	12.
13	1.353+000	8.333+010	9.200+010	13.
14	1.108+000	9.766+010	1.068+011	14.
15	8.208-001	1.497+011	1.623+011	14.
16	6.393-001	1.765+011	1.890+011	15.
17	4.979-001	2.002+011	2.115+011	17.
18	3.877-001	1.394+011	1.451+011	18.
19	3.020-001	1.982+011	2.029+011	20.
20	1.832-001	2.237+011	2.252+011	21.
21	1.111-001	2.089+011	2.069+011	22.
22	6.738-002	8.060+010	7.856+010	23.
23	4.087-002	7.266+010	6.980+010	24.
24	2.554-002	6.591+010	6.248+010	24.
25	1.989-002	3.414+010	3.203+010	24.
26	1.503-002	3.749+010	3.484+010	25.
27	9.119-003	6.510+010	5.972+010	25.
28	5.531-003	6.283+010	5.759+010	24.
29	3.355-003	6.067+010	5.581+010	24.
30	2.839-003	1.977+010	1.824+010	24.
31	2.404-003	1.954+010	1.817+010	23.
32	2.035-003	1.933+010	1.821+010	22.
33	1.234-003	5.672+010	5.446+010	21.
34	7.485-004	5.493+010	5.391+010	19.
35	4.540-004	5.325+010	5.365+010	18.
36	2.754-004	5.170+010	4.996+010	16.
37	1.670-004	5.026+010	5.251+010	15.
38	1.013-004	4.895+010	5.608+010	8.
39	6.144-005	4.775+010	5.280+010	14.
40	3.727-005	4.668+010	5.219+010	14.

a) Lower Energy Bound

TABLE B8.1 (Cont'd)

FERRET-SANDII RESULTS FOR (AVERAGE FOR CAPSULE)
SIMULATED PRESSURE VESSEL CAPSULE - 1/4T (SPVC-1/4T)

GROUP	ENERGY (MEV)	A PRIORI FLUX* (N/CM**2/SEC)	ADJUSTED FLUX (N/CM**2/SEC)	% UNCERTAIN (1 STD)
41	2.260-005	4.573+010	5.084+010	14.
42	1.371-005	4.489+010	4.922+010	14.
43	8.315-006	4.417+010	4.750+010	14.
44	5.043-006	4.343+010	4.430+010	15.
45	3.059-006	4.267+010	4.147+010	16.
46	1.855-006	4.187+010	3.848+010	16.
47	1.125-006	4.105+010	3.572+010	16.
48	6.826-007	4.020+010	3.319+010	15.
49	4.140-007	3.929+010	3.067+010	15.
50	2.511-007	3.537+010	2.629+010	15.
51	1.523-007	2.999+010	2.131+010	15.
52	9.237-008	2.545+010	1.759+010	16.
53	1.000-010	7.082+010	4.577+010	13.
FLUX, E> 0.0 MEV		3.144+012	3.143+012	9.
FLUX, E< 0.414 EV		1.616+011	1.110+011	11.
FLUX, E> 0.1 MEV		1.667+012	1.746+012	12.
FLUX, E> 1.0 MEV		4.050+011	4.419+011	7.
DPA/SECOND		7.258-010	7.704-010	8.
FLUENCE+, E> 1.0 MEV		2.064+019	2.252+019	7.
DPA+		3.700-002	3.927-002	8.

* ABSOLUTE CALCULATED FLUX (OR NORMALIZED TO FE54(N,P)MN54 REACTION RATE).

\+ BASED ON 5.097+007 EFFECTIVE FULL POWER SECONDS OF EXPOSURE; UNITS OF N/CM**2 FOR FLUENCE AND TOTAL NUMBER OF DISPLACED ATOMS OF IRON PER TARGET ATOM OF IRON FOR DPA.

TABLE B8.2

COMPARISON OF MEASURED AND CALCULATED
REACTION RATES USED IN THE ANALYSIS OF
SIMULATED PRESSURE VESSEL CAPSULE - 1/4T (SPVC-1/4T)

		REACTION RATE (DPS/NUCLEUS)			RATIO MEAS/CALC	
REACTION	COVER	MEAS (a)	A PRIORI CALC	ADJ CALC	A PRIORI	ADJ CALC
FE54(N,P)MN54	BARE	2.44-014(6)	2.30-014	2.44-014	1.06	1.00
FE58(N,G)FE59	"	1.53-013(9)	2.46-013	1.79-013	.62	.86
NI58(N,P)CO58	"	3.38-014(9)	3.13-014	3.35-014	1.08	1.01
CU63(N,A)CO60	"	1.93-016(6)	2.02-016	1.96-016	.95	.98
TI46(N,P)SC46	"	3.48-015(9)	3.28-015	3.41-015	1.06	1.02
SC45(N,G)SC46	"	2.70-012(9)	3.83-012	2.80-012	.71	.96
CO59(N,G)CO60	"	1.06-011(6)	1.09-011	1.05-011	.97	1.01
CO59(N,G)CO60	Gd	7.62-012(6)	6.82-012	7.54-012	1.12	1.01
U235(N,F)CS137	"	2.81-011(5)	2.79-011	2.73-011	1.01	1.03
U238(N,F)CS137	"	1.46-013(9)	1.31-013	1.43-013	1.12	1.02
NP237(N,F)CS137	"	1.32-012(6)	1.24-012	1.32-012	1.07	1.00

a) The bracketed values are the one-sigma % uncertainty estimates.

TABLE B9.1

FERRET-SANDII RESULTS FOR (AVERAGE FOR CAPSULE)
SIMULATED PRESSURE VESSEL CAPSULE - 1/2T (SPVC-1/2T)

GROUP	ENERGY (MEV) [a]	A PRIORI FLUX* (N/CM**2/SEC)	ADJUSTED FLUX (N/CM**2/SEC)	% UNCERTAIN (1 STD)
1	1.492+001	3.751+006	3.582+006	20.
2	1.350+001	1.358+007	1.312+007	19.
3	1.162+001	6.332+007	6.198+007	17.
4	1.000+001	1.779+008	1.765+008	15.
5	8.607+000	4.328+008	4.369+008	13.
6	7.408+000	7.961+008	8.253+008	12.
7	6.065+000	1.890+009	2.014+009	11.
8	4.966+000	2.735+009	3.011+009	11.
9	3.679+000	6.069+009	6.880+009	11.
10	2.865+000	8.727+009	9.978+009	11.
11	2.231+000	1.861+010	2.141+010	11.
12	1.738+000	2.693+010	3.087+010	12.
13	1.353+000	3.812+010	4.346+010	12.
14	1.108+000	5.137+010	5.812+010	14.
15	8.208-001	8.851+010	9.901+010	14.
16	6.393-001	1.081+011	1.193+011	15.
17	4.979-001	1.371+011	1.494+011	16.
18	3.877-001	9.649+010	1.036+011	18.
19	3.020-001	1.462+011	1.546+011	19.
20	1.832-001	1.578+011	1.640+011	20.
21	1.111-001	1.474+011	1.503+011	21.
22	6.738-002	5.476+010	5.459+010	22.
23	4.087-002	4.744+010	4.641+010	23.
24	2.554-002	4.183+010	4.017+010	23.
25	1.989-002	2.119+010	2.007+010	24.
26	1.503-002	2.288+010	2.138+010	24.
27	9.119-003	3.873+010	3.536+010	24.
28	5.531-003	3.611+010	3.312+010	24.
29	3.355-003	3.363+010	3.125+010	23.
30	2.839-003	1.069+010	1.003+010	23.
31	2.404-003	1.043+010	1.001+010	22.
32	2.035-003	1.018+010	1.008+010	21.
33	1.234-003	2.911+010	3.018+010	20.
34	7.485-004	2.706+010	2.948+010	18.
35	4.540-004	2.515+010	2.907+010	17.
36	2.754-004	2.339+010	2.505+010	14.
37	1.670-004	2.176+010	2.731+010	14.
38	1.013-004	2.029+010	2.908+010	8.
39	6.144-005	1.895+010	2.670+010	14.
40	3.727-005	1.775+010	2.577+010	14.

a) Lower Energy Bound

TABLE B9.1 (Cont'd)

FERRET-SANDII RESULTS FOR (AVERAGE FOR CAPSULE)
SIMULATED PRESSURE VESSEL CAPSULE - 1/2T (SPVC-1/2T)

GROUP	ENERGY (MEV)	A PRIORI FLUX* (N/CM**2/SEC)	ADJUSTED FLUX (N/CM**2/SEC)	% UNCERTAIN (1 STD)
41	2.260-005	1.670+010	2.377+010	14.
42	1.371-005	1.579+010	2.176+010	14.
43	8.315-006	1.503+010	1.992+010	15.
44	5.043-006	1.436+010	1.673+010	16.
45	3.059-006	1.368+010	1.436+010	16.
46	1.855-006	1.298+010	1.209+010	17.
47	1.125-006	1.225+010	1.019+010	17.
48	6.826-007	1.151+010	8.580+009	16.
49	4.140-007	1.073+010	7.131+009	17.
50	2.511-007	9.313+009	5.608+009	17.
51	1.523-007	7.915+009	4.373+009	17.
52	9.237-008	6.733+009	3.528+009	17.
53	1.000-010	1.883+010	8.758+009	16.
FLUX, E> 0.0 MEV		1.715+012	1.809+012	9.
FLUX, E< 0.414 EV		4.279+010	2.227+010	13.
FLUX, E> 0.1 MEV		1.049+012	1.129+012	12.
FLUX, E> 1.0 MEV		1.862+011	2.111+011	7.
DPA/SECOND		3.995-010	4.367-010	9.
FLUENCE+, E> 1.0 MEV		9.490+018	1.076+019	7.
DPA+		2.036-002	2.226-002	9.

* ABSOLUTE CALCULATED FLUX (OR NORMALIZED TO FE54(N,P)MN54 REACTION RATE).

\+ BASED ON 5.097+007 EFFECTIVE FULL POWER SECONDS OF EXPOSURE; UNITS OF N/CM**2 FOR FLUENCE AND TOTAL NUMBER OF DISPLACED ATOMS OF IRON PER TARGET ATOM OF IRON FOR DPA.

TABLE B9.2

COMPARISON OF MEASURED AND CALCULATED
REACTION RATES USED IN THE ANALYSIS OF
SIMULATED PRESSURE VESSEL CAPSULE - 1/2T (SPVC-1/2T)

		REACTION RATE (DPS/NUCLEUS)			RATIO MEAS/CALC	
REACTION	COVER	MEAS (a)	A PRIORI CALC	ADJ CALC	A PRIORI	ADJ CALC
FE54(N,P)MN54	BARE	9.37-015(6)	8.26-015	9.26-015	1.13	1.01
FE58(N,G)FE59	"	5.17-014(9)	8.59-014	6.58-014	.60	.79
NI58(N,P)CO58	"	1.33-014(9)	1.15-014	1.30-014	1.16	1.02
CU63(N,A)CO60	"	7.37-017(6)	7.44-017	7.53-017	.99	.98
TI46(N,P)SC46	"	1.29-015(9)	1.16-015	1.26-015	1.12	1.02
SC45(N,G)SC46	"	5.79-013(9)	1.09-012	6.84-013	.53	.85
CO59(N,G)CO60	"	4.32-012(6)	3.82-012	4.38-012	1.13	.99
CO59(N,G)CO60	Gd	3.76-012(6)	2.68-012	3.65-012	1.40	1.03
U235(N,F)CS137	"	1.30-011(5)	1.06-011	1.19-011	1.23	1.09
U238(N,F)CS137	"	6.05-014(8)	5.33-014	6.05-014	1.14	1.00
NP237(N,F)CS137	"	7.15-013(7)	6.67-013	7.25-013	1.07	.99

a) The bracketed values are the one-sigma % uncertainty estimates.

TABLE B10.1

FERRET-SANDII RESULTS FOR (HB-12 LOCATION)
SIMULATED VOID BOX CAPSULE (SVBC)
(USING VOIDED BOX A PRIORI SPECTRUM & LONG HALF-LIFE REACTIONS)

GROUP	ENERGY (MEV) [a]	A PRIORI FLU* (N/CM**2)	ADJUSTED FLU (N/CM**2)	% UNCERTAIN (1 STD)
1	1.492+001	1.679+013	1.106+012	220.
2	1.350+001	4.551+013	2.788+012	199.
3	1.162+001	2.217+014	1.315+013	175.
4	1.000+001	5.935+014	3.458+013	148.
5	8.607+000	1.363+015	8.254+013	125.
6	7.408+000	2.326+015	1.685+014	121.
7	6.065+000	5.092+015	4.270+014	117.
8	4.966+000	6.955+015	7.767+014	134.
9	3.679+000	1.429+016	2.110+015	140.
10	2.865+000	1.992+016	3.320+015	140.
11	2.231+000	4.435+016	9.804+015	113.
12	1.738+000	6.587+016	1.469+016	90.
13	1.353+000	1.007+017	8.020+015	129.
14	1.108+000	1.296+017	5.098+015	130.
15	8.208-001	3.184+017	7.381+015	116.
16	6.393-001	4.136+017	7.620+015	123.
17	4.979-001	4.881+017	7.867+015	139.
18	3.877-001	3.349+017	5.562+015	165.
19	3.020-001	5.858+017	9.463+015	183.
20	1.832-001	6.058+017	1.075+016	204.
21	1.111-001	5.478+017	1.163+016	224.
22	6.738-002	1.951+017	5.369+015	243.
23	4.087-002	8.379+016	3.129+015	260.
24	2.554-002	3.213+016	1.666+015	273.
25	1.989-002	1.276+016	9.168+014	284.
26	1.503-002	1.381+016	1.341+015	291.
27	9.119-003	2.330+016	2.937+015	295.
28	5.531-003	2.134+016	3.326+015	296.
29	3.355-003	1.914+016	3.501+015	295.
30	2.839-003	5.853+015	1.194+015	290.
31	2.404-003	5.575+015	1.214+015	282.
32	2.035-003	5.286+015	1.185+015	271.
33	1.234-003	1.480+016	3.318+015	258.
34	7.485-004	1.470+016	3.250+015	242.
35	4.540-004	1.471+016	3.194+015	225.
36	2.754-004	1.474+016	3.129+015	209.
37	1.670-004	1.477+016	3.072+015	196.
38	1.013-004	1.481+016	2.621+015	54.
39	6.144-005	1.486+016	3.126+015	181.
40	3.727-005	1.491+016	3.127+015	181.

a) Lower Energy Bound

TABLE B10.1 (Cont'd)

FERRET-SANDII RESULTS FOR (HB-12 LOCATION)
SIMULATED VOID BOX CAPSULE (SVBC)
(USING VOIDED BOX A PRIORI SPECTRUM & LONG HALF-LIFE REACTIONS)

GROUP	ENERGY (MEV)	A PRIORI FLU* (N/CM**2)	ADJUSTED FLU (N/CM**2)	% UNCERTAIN (1 STD)
41	2.260-005	1.498+016	3.250+015	180.
42	1.371-005	1.503+016	3.343+015	177.
43	8.315-006	1.506+016	3.416+015	168.
44	5.043-006	1.509+016	3.329+015	169.
45	3.059-006	1.561+016	3.376+015	163.
46	1.855-006	2.159+016	4.494+015	159.
47	1.125-006	3.463+016	6.874+015	147.
48	6.826-007	5.459+016	1.052+016	123.
49	4.140-007	8.100+016	1.446+016	121.
50	2.511-007	8.445+016	1.397+016	135.
51	1.523-007	7.261+016	1.110+016	145.
52	9.237-008	6.249+016	9.249+015	146.
53	1.000-010	1.757+017	2.191+016	63.
FLUENCE+, E> 0.0 MEV		4.885+018	2.647+017	42.
FLUENCE, E< 0.414 EV		4.762+017	7.068+016	44.
FLUENCE, E> 0.1 MEV		3.727+018	1.059+017	59.
FLUENCE, E> 1.0 MEV		5.002+017	4.707+016	15.
DPA+		1.292-003	6.353-005	22.

* ABSOLUTE CALCULATED FLUENCE.
\+ BASED ON TOTAL REACTION PRODUCTS; UNITS OF N/CM**2 FOR FLUENCE AND TOTAL NUMBER OF DISPLACED ATOMS OF IRON PER TARGET ATOM OF IRON FOR DPA.

TABLE B10.2

COMPARISON OF MEASURED AND CALCULATED
REACTIONS USED IN THE ANALYSIS OF
SIMULATED VOID BOX CAPSULE (SVBC)
(USING VOIDED BOX A PRIORI SPECTRUM & LONG HALF-LIFE REACTIONS)

		REACTION PRODUCTS (ATOMS/NUCLEUS)			RATIO MEAS/CALC	
REACTION	COVER	MEAS (a)	A PRIORI CALC	ADJ CALC	A PRIORI	ADJ CALC
NP237(N,F)CS137	Gd	1.00-007(6)	2.11-006	1.01-007	.05	.99
U235(N,F)CS137	Gd	3.06-006(12)	2.03-005	3.05-006	.15	1.00
U238(N,F)CS137	Gd	2.01-008(6)	1.35-007	1.99-008	.15	1.01
CU63(N,A)CO60	Gd	1.60-011(21)	2.20-010	1.66-011	.07	.97
CO59(N,G)CO60	Gd	5.02-007(21)	2.79-006	5.04-007	.18	1.00
CO59(N,G)CO60	BARE	1.78-006(21)	1.23-005	1.80-006	.15	.99

a) The bracketed values are the one-sigma % uncertainty estimates.

TABLE B11.1

FERRET-SANDII RESULTS FOR (HB-12 LOCATION)
SIMULATED VOID BOX CAPSULE (SVBC)
(USING FLOODED BOX A PRIORI SPECTRUM & SHORT HALF-LIFE REACTIONS)

GROUP	ENERGY (MEV) [a]	A PRIORI FLU* (N/CM**2)	ADJUSTED FLU (N/CM**2)	% UNCERTAIN (1 STD)
1	1.492+001	1.952+005	3.921+004	215.
2	1.350+001	5.305+005	9.637+004	194.
3	1.162+001	2.549+006	4.255+005	172.
4	1.000+001	6.563+006	1.020+006	149.
5	8.607+000	1.454+007	2.138+006	127.
6	7.408+000	2.297+007	3.242+006	118.
7	6.065+000	4.643+007	5.743+006	111.
8	4.966+000	5.754+007	6.129+006	121.
9	3.679+000	9.678+007	9.671+006	109.
10	2.865+000	1.052+008	1.182+007	116.
11	2.231+000	1.637+008	2.392+007	116.
12	1.738+000	1.784+008	5.266+007	68.
13	1.353+000	1.924+008	1.729+007	135.
14	1.108+000	1.786+008	9.582+006	141.
15	8.208-001	2.827+008	1.165+007	141.
16	6.393-001	2.255+008	9.227+006	160.
17	4.979-001	2.472+008	9.627+006	177.
18	3.877-001	1.607+008	6.565+006	198.
19	3.020-001	2.602+008	1.062+007	216.
20	1.832-001	2.480+008	1.079+007	233.
21	1.111-001	1.978+008	9.566+006	249.
22	6.738-002	8.233+007	4.599+006	263.
23	4.087-002	8.201+007	5.377+006	274.
24	2.554-002	7.712+007	5.969+006	282.
25	1.989-002	4.102+007	3.721+006	287.
26	1.503-002	4.592+007	4.756+006	289.
27	9.119-003	8.203+007	9.352+006	289.
28	5.531-003	8.205+007	9.931+006	286.
29	3.355-003	8.205+007	1.014+007	280.
30	2.839-003	2.736+007	3.355+006	273.
31	2.404-003	2.734+007	3.171+006	260.
32	2.035-003	2.736+007	2.932+006	246.
33	1.234-003	8.207+007	7.808+006	226.
34	7.485-004	8.207+007	6.968+006	207.
35	4.540-004	8.208+007	6.154+006	186.
36	2.754-004	8.209+007	5.486+006	169.
37	1.670-004	8.209+007	4.869+006	154.
38	1.013-004	8.210+007	4.488+006	151.
39	6.144-005	8.210+007	4.186+006	152.
40	3.727-005	8.211+007	3.833+006	154.

a) Lower Energy Bound

TABLE B11.1 (Cont'd)

FERRET-SANDII RESULTS FOR (HB-12 LOCATION)
SIMULATED VOID BOX CAPSULE (SVBC)
(USING FLOODED BOX A PRIORI SPECTRUM & SHORT HALF-LIFE REACTIONS)

GROUP	ENERGY (MEV)	A PRIORI FLUX* (N/CM**2/SEC)	ADJUSTED FLUX (N/CM**2/SEC)	% UNCERTAIN (1 STD)
41	2.260-005	8.212+007	3.859+006	168.
42	1.371-005	8.211+007	3.825+006	172.
43	8.315-006	8.213+007	3.741+006	168.
44	5.043-006	8.213+007	4.256+006	175.
45	3.059-006	8.214+007	4.582+006	164.
46	1.855-006	8.214+007	5.022+006	154.
47	1.125-006	8.213+007	5.481+006	127.
48	6.826-007	8.215+007	5.793+006	118.
49	4.140-007	8.865+007	7.124+006	122.
50	2.511-007	1.109+008	1.020+007	161.
51	1.523-007	1.060+008	1.207+007	192.
52	9.237-008	1.013+008	1.345+007	216.
53	1.000-010	3.559+008	5.374+007	237.
FLUX, E> 0.0 MEV		5.422+009	4.521+008	58.
FLUX, E< 0.414 EV		7.627+008	9.658+007	180.
FLUX, E> 0.1 MEV		2.706+009	2.128+008	44.
FLUX, E> 1.0 MEV		1.163+009	1.478+008	14.
DPA/SECOND		1.721-012	1.882-013	15.
FLUENCE+, E> 1.0 MEV		5.928+016	7.531+015	14.
DPA+		8.770-005	9.591-006	15.

* ABSOLUTE CALCULATED FLUX (OR NORMALIZED TO FE54(N,P)MN54 REACTION RATE).

\+ BASED ON 5.097+007 EFFECTIVE FULL POWER SECONDS OF EXPOSURE; UNITS OF N/CM**2 FOR FLUENCE AND TOTAL NUMBER OF DISPLACED ATOMS OF IRON PER TARGET ATOM OF IRON FOR DPA.

TABLE B11.2

COMPARISON OF MEASURED AND CALCULATED
REACTIONS USED IN THE ANALYSIS OF
SIMULATED VOID BOX CAPSULE (SVBC)
(USING FLOODED BOX A PRIORI SPECTRUM & SHORT HALF-LIFE REACTIONS)

		REACTION RATE (DPS/NUCLEUS)			RATIO MEAS/CALC	
REACTION	COVER	MEAS (a)	A PRIORI CALC	ADJ CALC	A PRIORI	ADJ CALC
U235(N,F)ZR95	Gd	2.86-015(12)	4.44-014	2.89-015	.06	.99
NP237(N,F)ZR95	Gd	2.47-016(16)	2.75-015	2.74-016	.09	.90
TI46(N,P)SC46	Gd	3.52-018(5)	2.79-017	3.52-018	.13	1.00
U238(N,F)RU103	Gd	8.25-017(15)	4.86-016	7.36-017	.17	1.12
NI58(N,P)CO58	Gd	2.16-017(5)	1.75-016	2.18-017	.12	.99
SC45(N,G)SC46	Gd	1.26-016(6)	1.82-015	1.26-016	.07	1.00

a) The bracketed values are the one-sigma % uncertainty estimates.

TABLE B12.1

FERRET-SANDII RESULTS FOR (HB-12 LOCATION)
SIMULATED VOID BOX CAPSULE (SVBC)
(USING FLOODED BOX A PRIORI SPECTRUM & LONG HALF-LIFE REACTIONS)

GROUP	ENERGY (MEV) [a]	A PRIORI FLU* (N/CM**2)	ADJUSTED FLU (N/CM**2)	% UNCERTAIN (1 STD)
1	1.492+001	9.952+012	1.103+012	221.
2	1.350+001	2.704+013	2.740+012	200.
3	1.162+001	1.299+014	1.269+013	176.
4	1.000+001	3.345+014	3.279+013	150.
5	8.607+000	7.411+014	7.908+013	126.
6	7.408+000	1.171+015	1.617+014	122.
7	6.065+000	2.366+015	4.244+014	117.
8	4.966+000	2.933+015	8.262+014	133.
9	3.679+000	4.933+015	2.283+015	139.
10	2.865+000	5.361+015	3.741+015	138.
11	2.231+000	8.345+015	9.345+015	113.
12	1.738+000	9.092+015	1.329+016	95.
13	1.353+000	9.808+015	9.553+015	123.
14	1.108+000	9.103+015	6.088+015	124.
15	8.208-001	1.441+016	7.908+015	111.
16	6.393-001	1.150+016	6.075+015	132.
17	4.979-001	1.260+016	6.008+015	149.
18	3.877-001	8.190+015	3.657+015	175.
19	3.020-001	1.326+016	5.321+015	194.
20	1.832-001	1.264+016	4.751+015	215.
21	1.111-001	1.008+016	3.692+015	234.
22	6.738-002	4.197+015	1.558+015	252.
23	4.087-002	4.180+015	1.626+015	267.
24	2.554-002	3.931+015	1.638+015	279.
25	1.989-002	2.091+015	9.440+014	288.
26	1.503-002	2.341+015	1.145+015	294.
27	9.119-003	4.181+015	2.198+015	297.
28	5.531-003	4.182+015	2.330+015	297.
29	3.355-003	4.182+015	2.432+015	295.
30	2.839-003	1.394+015	8.323+014	290.
31	2.404-003	1.393+015	8.446+014	281.
32	2.035-003	1.395+015	8.529+014	270.
33	1.234-003	4.183+015	2.585+015	256.
34	7.485-004	4.183+015	2.627+015	240.
35	4.540-004	4.184+015	2.713+015	224.
36	2.754-004	4.184+015	2.840+015	208.
37	1.670-004	4.184+015	3.033+015	195.
38	1.013-004	4.185+015	2.720+015	57.
39	6.144-005	4.185+015	3.714+015	176.
40	3.727-005	4.185+015	4.214+015	171.

a) Lower Energy Bound

TABLE B12.1 (Cont'd)

FERRET-SANDII RESULTS FOR (HB-12 LOCATION)
SIMULATED VOID BOX CAPSULE (SVBC)
(USING FLOODED BOX A PRIORI SPECTRUM & LONG HALF-LIFE REACTIONS)

GROUP	ENERGY (MEV)	A PRIORI FLU* (N/CM**2)	ADJUSTED FLU (N/CM**2)	% UNCERTAIN (1 STD)
41	2.260-005	4.186+015	4.842+015	167.
42	1.371-005	4.185+015	5.625+015	158.
43	8.315-006	4.186+015	6.685+015	138.
44	5.043-006	4.186+015	6.860+015	152.
45	3.059-006	4.186+015	7.426+015	150.
46	1.855-006	4.186+015	7.794+015	153.
47	1.125-006	4.186+015	8.106+015	148.
48	6.826-007	4.187+015	8.496+015	138.
49	4.140-007	4.518+015	8.725+015	146.
50	2.511-007	5.653+015	1.017+016	149.
51	1.523-007	5.400+015	8.641+015	153.
52	9.237-008	5.163+015	7.554+015	152.
53	1.000-010	1.814+016	2.348+016	55.
FLUENCE+, E> 0.0 MEV		2.763+017	2.385+017	29.
FLUENCE, E< 0.414 EV		3.887+016	5.857+016	49.
FLUENCE, E> 0.1 MEV		1.379+017	8.358+016	39.
FLUENCE, E> 1.0 MEV		5.928+016	4.854+016	15.
DPA+		8.770-005	5.876-005	15.

* ABSOLUTE CALCULATED FLUENCE.
\+ BASED ON TOTAL REACTION PRODUCTS; UNITS OF N/CM**2 FOR FLUENCE AND TOTAL NUMBER OF DISPLACED ATOMS OF IRON PER TARGET ATOM OF IRON FOR DPA.

TABLE B12.2

COMPARISON OF MEASURED AND CALCULATED
REACTIONS USED IN THE ANALYSIS OF
SIMULATED VOID BOX CAPSULE (SVBC)
(USING FLOODED BOX A PRIORI SPECTRUM & LONG HALF-LIFE REACTIONS)

		REACTION PRODUCTS (ATOMS/NUCLEUS)			RATIO MEAS/CALC	
REACTION	COVER	MEAS (a)	A PRIORI CALC	ADJ CALC	A PRIORI	ADJ CALC
NP237(N,F)CS137	Gd	1.00-007(6)	1.40-007	1.01-007	.71	.99
U235(N,F)CS137	Gd	3.06-006(12)	2.26-006	3.05-006	1.35	1.01
U238(N,F)CS137	Gd	2.01-008(6)	2.48-008	1.99-008	.81	1.01
CU63(N,A)CO60	Gd	1.60-011(21)	1.12-010	1.65-011	.14	.97
CO59(N,G)CO60	Gd	5.02-007(21)	5.58-007	5.06-007	.90	.99
CO59(N,G)CO60	BARE	1.78-006(21)	1.51-006	1.79-006	1.18	1.00

a) The bracketed values are the one-sigma % uncertainty estimates.

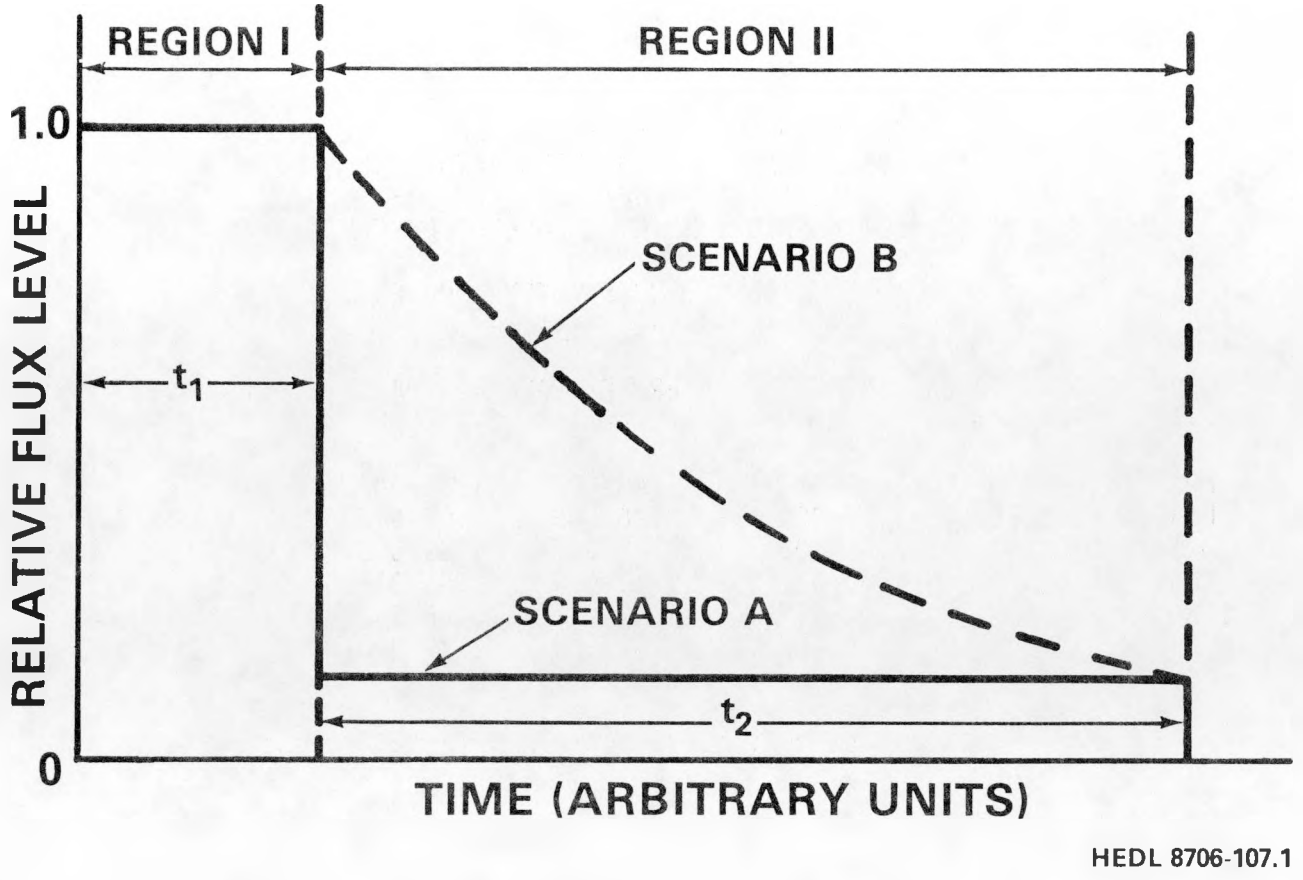

FIGURE B1. Two Flux Level Time-History Scenarios.

A P P E N D I X C

HEDL RECOMMENDED EXPOSURE PARAMETER VALUES FOR THE PSF BLIND TEST

CONTENTS

A P P E N D I X C

C1 HEDL RECOMMENDED EXPOSURE PARAMETER VALUES FOR THE PSF BLIND TEST

E. P. Lippincott and R. L. Simons (HEDL)

C1.1 Introduction

At the PSF Blind Test Workshop, detailed information and results for exposure parameter values for the PSF Metallurgical irradiations were provided by Fred Stallmann (ORNL) and Bob Simons (HEDL). [Reference is made to the Blind Test Workshop Minutes (Gu84d).] The HEDL and ORNL results (based on measured HEDL dosimetry data evaluated by Kellogg and Matsumoto and ORNL calculations by Maerker) were derived using two different, but similar, least-squares approaches. This Appendix presents the recommendation by HEDL for exposure parameter tabulation based on an average of the ORNL and HEDL evaluations. The ORNL data are those from Gu84d and not from the revised final version of St84 (see Section 4.2 and Appendix D).

Table C1 presents the HEDL and ORNL exposure parameter values at the center of each capsule. The HEDL results have been updated to include all reaction rates corrected for gradients to capsule center in the least squares analysis. The HEDL analysis includes the $^{238}U(n,f)$ reaction corrected for ^{239}Pu (build-in) fissions. The new HEDL results also include an evaluation of the thermal neutron exposure (normalized by assuming a 20°C Maxwellian; multiplication of these values by a factor of 1.384 will convert the values to a 288°C Maxwellian temperature for comparison with 288°C surveillance capsule thermal fluences).

The ORNL evaluation (Gu84d) was carried out similar to HEDL's except the $^{238}U(n,f)$ results were discarded. All the results agree within 4% except for the ϕt ($E > 0.1$) and dpa results at SSC-1, where a difference as large as 7.5% is observed. The HEDL and ORNL uncertainty estimates are in good agreement, these being 7% to 8% for $\phi t(E > 1)$, 11% to 12% for $\phi t(E > 0.1)$, and 8% to 9% for dpa. The HEDL thermal fluence uncertainty estimate is about 12%.

To obtain exposure values for the various specimens, corrections must be made for gradients in the x, y, and z directions. These gradient factors were obtained by Stallmann by fitting to a cosine function in the x and z directions and to an exponential in the y direction (away from the core). HEDL also fit the data to an exponential in the y direction but used hand-drawn curves through the data points in the x and z directions.

Since the workshop, Stallmann has modified his values for the y slope to account for changes in the gradient as a function of position. The HEDL gradient values have also been changed to include the effect of the change in the neutron spectrum with position. Using the revised values, the HEDL

C1.2 Tabulations

TABLE C1

EXPOSURE PARAMETERS AT CAPSULE CENTER

Location	$\phi t(E>1)$ $(10^{19} n/cm^2)$	$\phi t(E>0.1)$ $(10^{19} n/cm^2)$	dpa	ϕt(thermal) $(10^{19} n/cm^2)$
		HEDL VALUES		
SSC-1	2.62	7.59	0.0391	1.22
SSC-2	5.59	16.5	0.0842	2.46
0-T	4.21	12.5	0.0651	7.06
¼-T	2.25	8.90	0.0393	0.566
½-T	1.08	5.76	0.0223	0.114
		ORNL VALUES		
SSC-1	2.64	8.16	0.0408	N/A
SSC-2	5.50	16.8	0.0845	N/A
0-T	4.06	12.6	0.0648	N/A
¼-T	2.23	9.02	0.0397	N/A
½-T	1.07	5.90	0.0228	N/A
		COMPOSITE VALUES		
SSC-1	2.63	7.88	0.0400	1.22
SSC-2	5.55	16.7	0.0844	2.46
0-T	4.13	12.6	0.0649	7.06
¼-T	2.24	8.96	0.0395	0.566
½-T	1.08	5.83	0.0226	0.114

and ORNL y gradient correction agrees to within ~4% for the worst case. The largest gradient corrections are for the Charpy notch exposures; the tensile and CT specimens are located closer to the y capsule centerline. The maximum y gradient correction is 17% except for thermal neutrons where corrections are as large as a factor of 2.

HEDL and ORNL agreement of the x gradient values is similar to that observed for the y gradient. The x gradient is assumed to be independent of neutron energy because of lack of data to indicate any spectral dependence. The maximum x gradient correction is 15%.

Differences between ORNL and HEDL results of the z gradient corrections are, generally, also very small except at the extreme positions where the differences can be as large as 4%. The z gradient has a slight spectral dependence. A detailed evaluation of the thermal neutron z dependence is not presented here, but a number of perturbations exist to complicate the evaluation of the thermal exposure. The maximum z gradient correction is 20%.

Average exposure parameter values for the six groups of separate Charpy specimens are given in Table C2. These values may be used in place of the more detailed results in Table C5, if desired.

Examples of typical fits using a cosine function for SSC and SPVC data in the z direction are shown in Appendix A (Figures A3 to A6). These curves illustrate the substantial deviations from the cosine flux shape that exist in the PSF and serve to indicate the extreme care that must be used to obtain accurate gradient fits. The lack of any accurate function available to fit these data led to the HEDL decision to use empirical fits to the data in lieu of a fitting procedure as used at ORNL. It is recognized that the fitting procedure, while introducing inaccuracies due to the deviation of the true shape from the fitting function, also can improve accuracy by smoothing over unrecognized experimental statistical deviations. Thus, for the purposes of producing a recommended set of exposure values, it was decided to compute an average of the ORNL and HEDL results which, by averaging over the two independent evaluations (both spectral adjustment and gradient correction), produces a mean evaluation with potentially lower error.

The exposure parameter values for the CT specimens are given in Table C3 and C4. It should be noted that the top and bottom 1/2 CT specimens have the notch opening oriented away from the Z midplane (as shown on the as-built print) in contrast to the orientation shown on the earlier drawings that have been consistently reproduced. The notch tip for these specimens is thus at 10.83 cm from capsule centerline as opposed to 11.29 cm. All other specimen locations are correct on the drawings [see, for example, those in Ref. (St84)].

TABLE C2

EXPOSURE PARAMETERS FOR CHARPY GROUPS

Location	$\phi t(E>1)$ $(10^{19} n/cm^2)$	$\phi t(E>0.1)$ $(10^{19} n/cm^2)$	dpa	ϕt(thermal) $(10^{19} n/cm^2)$
		F23 PLATE (A302B)		
SSC-1	2.72	7.67	0.0400	1.30
SSC-2	5.73	16.2	0.0844	2.62
0-T	4.03	11.4	0.0615	12.5
¼-T	2.26	8.43	0.0383	0.855
½-T	1.12	5.63	0.0224	0.126
		3PT, 3PU PLATE (A533B)		
SSC-1	2.49	6.94	0.0365	1.20
SSC-2	5.24	14.7	0.0770	2.43
0-T	3.68	10.2	0.0556	11.5
¼-T	2.05	7.46	0.0343	0.786
½-T	1.01	4.94	0.0199	0.123
		CODE K FORGING (22NiMoCr37)		
SSC-1	1.73	5.42	0.0270	1.32
SSC-2	3.65	11.5	0.0569	2.66
0-T	2.84	9.2	0.0456	2.73
¼-T	1.52	6.30	0.0273	0.261
½-T	0.73	4.10	0.0157	0.081

TABLE C2 (Cont'd)

Location	$\phi t(E>1)$ $(10^{19} n/cm^2)$	$\phi t(E>0.1)$ $(10^{19} n/cm^2)$	dpa	ϕt(thermal) $(10^{19} n/cm^2)$
		CODE MO FORGING (A508-3)		
SSC-1	1.89	6.00	0.0294	1.42
SSC-2	3.98	12.7	0.0621	2.87
0-T	3.11	10.2	0.0504	2.96
$\frac{1}{4}$-T	1.67	7.11	0.0305	0.284
$\frac{1}{2}$-T	0.82	4.66	0.0177	0.083
		CODE EC WELD (A533B)		
SSC-1	1.75	5.53	0.0274	1.36
SSC-2	3.69	11.7	0.0578	2.74
0-T	2.97	9.7	0.0480	2.85
$\frac{1}{4}$-T	1.62	6.85	0.0295	0.275
$\frac{1}{2}$-T	0.80	4.56	0.0173	0.083
		CODE R WELD (A533B)		
SSC-1	2.52	7.08	0.0370	1.24
SSC-2	5.31	15.0	0.0782	2.50
0-T	3.85	10.8	0.0585	12.0
$\frac{1}{4}$-T	2.19	8.13	0.0370	0.827
$\frac{1}{2}$-T	1.10	5.50	0.0220	0.126

TABLE C3

EXPOSURE PARAMETERS FOR ICT SPECIMENS

Location	Sample Identification	$\phi t(E>1)$ $10^{19}n/cm^2$	$\phi t(E>0.1)$ $10^{19}n/cm^2$	dpa
		F23 PLATE (A302B)		
SSC-1	F23-9R	2.54	7.61	0.0386
	F23-21R	2.53	7.58	0.0385
	F23-13R	2.52	7.54	0.0383
	F23-5R	2.37	7.07	0.0360
	F23-17R	2.36	7.05	0.0358
SSC-2	F23-6R	5.35	16.1	0.0814
	F23-28R	5.34	16.1	0.0811
	F23-20R	5.32	16.0	0.0809
	F23-2R	5.00	15.0	0.0759
	F23-24R	4.98	14.9	0.0756
0-T	F23-19R	4.01	12.2	0.0630
	F23-1R	3.99	12.2	0.0628
	F23-23R	3.96	12.1	0.0622
	F23-15R	3.83	11.6	0.0601
	F23-27R	3.82	11.6	0.0599
$\frac{1}{4}$-T	F23-8R	2.18	8.71	0.0384
	F23-30R	2.17	8.68	0.0383
	F23-12R	2.13	8.49	0.0375
	F23-4R	2.10	8.34	0.0369
	F23-16R	2.09	8.32	0.0367
$\frac{1}{2}$-T	F23-7R	1.05	5.68	0.0220
	F23-29R	1.05	5.67	0.0220
	F23-11R	1.02	5.47	0.0213
	F23-3R	1.03	5.51	0.0215
	F23-25R	1.02	5.49	0.0214
		3P PLATE (A533B)		
SSC-1	3PS-12	2.52	7.52	0.0382
	3PS-11	2.33	6.92	0.0353
	3PS-14	2.33	6.90	0.0352
SSC-2	3PS-7	5.31	15.9	0.0806
	3PS-6	4.92	14.7	0.0746
	3PS-8	4.91	14.6	0.0743

TABLE C3 (Cont'd)

Location	Sample Identification	$\phi t(E>1)$ $10^{19}n/cm^2$	$\phi t(E>0.1)$ $10^{19}n/cm^2$	dpa
0-T	3PS-10	3.95	12.0	0.0620
	3PS-9	3.66	11.0	0.0571
	3PS-15	3.65	10.9	0.0570
$\frac{1}{4}$-T	3PS-16	2.13	8.47	0.0374
	3PS-13	1.97	7.68	0.0343
	3PT-1	1.96	7.66	0.0342
$\frac{1}{2}$-T	3PT-3	1.02	5.46	0.0212
	3PT-2	0.95	4.94	0.0194
	3PT-4	0.94	4.92	0.0194

TABLE C4

EXPOSURE PARAMETERS FOR ½CT SPECIMENS

Location	Sample Identification	$\phi t(E \geq 1)$ 10^{19}n/cm^2	$\phi t(E > 0.1)$ 10^{19}n/cm^2	dpa
		F23 PLATE (A302B)		
SSC-1	F23-30R	2.92	8.44	0.0435
	F23-25R	2.92	8.46	0.0437
	F23-20R	2.88	8.33	0.0430
	F23-15R	2.75	7.93	0.0410
	F23-10R	2.60	7.48	0.0387
	F23-66R	2.35	7.29	0.0364
	F23-63R	2.36	7.31	0.0365
	F23-52R	2.32	7.20	0.0359
	F23-42R	2.22	6.85	0.0342
	F23-40R	2.10	6.46	0.0324
SSC-2	F23-29R	6.15	17.9	0.0919
	F23-27R	6.17	17.9	0.0921
	F23-19R	6.07	17.7	0.0907
	F23-17R	5.80	16.8	0.0864
	F23-7R	5.50	15.8	0.0817
	F23-62R	4.96	15.5	0.0768
	F23-58R	4.97	15.5	0.0770
	F23-54R	4.89	15.3	0.0758
	F23-46R	4.67	14.5	0.0722
	F23-38R	4.43	13.7	0.0683
0-T	F23-31R	4.44	12.9	0.0685
	F23-21R	4.46	13.0	0.0687
	F23-11R	4.42	12.9	0.0682
	F23-5R	4.29	12.4	0.0660
	F23-1R	4.13	12.1	0.0634
	F23-67R	3.81	12.1	0.0609
	F23-59R	3.82	12.2	0.0611
	F23-51R	3.79	12.1	0.0606
	F23-43R	3.68	11.7	0.0587
	F23-39R	3.55	11.4	0.0564

TABLE C4 (Cont'd)

Location	Sample Identification	$\phi t(E>1)$ 10^{19}n/cm^2	$\phi t(E>0.1)$ 10^{19}n/cm^2	dpa
$\frac{1}{4}$-T	F23-23R	2.43	9.32	0.0418
	F23-18R	2.45	9.43	0.0423
	F23-13R	2.44	9.38	0.0421
	F23-8R	2.38	9.10	0.0409
	F23-3R	2.30	8.73	0.0394
	F23-61R	2.03	8.43	0.0366
	F23-55R	2.05	8.52	0.0369
	F23-53R	2.04	8.48	0.0367
	F23-47R	1.99	8.22	0.0357
	F23-45R	1.92	7.89	0.0345
$\frac{1}{2}$-T	F23-28R	1.17	6.06	0.0239
	F23-24R	1.18	6.16	0.0242
	F23-14R	1.18	6.16	0.0242
	F23-9R	1.17	6.04	0.0239
	F23-4R	1.13	5.78	0.0229
	F23-65R	0.97	5.42	0.0207
	F23-57R	0.98	5.51	0.0210
	F23-49R	0.98	5.51	0.0210
	F23-41R	0.97	5.40	0.0207
	F23-37R	0.94	5.17	0.0199

TABLE C4 (Cont'd)

Location	Sample Identification	$\phi t(E>1)$ 10^{19}n/cm^2	$\phi t(E>0.1)$ 10^{19}n/cm^2	dpa
		3P PLATE (A533B)		
SSC-1	3PU-1	2.86	8.26	0.0427
	3PU-9	2.71	7.78	0.0403
	3PU-13	2.56	7.32	0.0379
	3PU-21	2.31	7.14	0.0356
	3PU-29	2.18	6.72	0.0337
	3PU-33	2.06	6.32	0.0317
SSC-2	3PU-8	6.03	17.5	0.0900
	3PU-16	5.72	16.5	0.0851
	3PU-17	5.40	15.5	0.0801
	3PU-30	4.86	15.1	0.0752
	3PU-32	4.61	14.2	0.0711
	3PU-37	4.35	13.4	0.0669
0-T	3PU-2	4.36	12.6	0.0671
	3PU-10	4.13	11.8	0.0632
	3PU-26	3.89	11.0	0.0592
	3PU-18	3.74	11.9	0.0597
	3PU-14	3.54	11.1	0.0562
	3PU-34	3.33	10.4	0.0527
$\frac{1}{4}$-T	3PU-3	2.37	9.07	0.0408
	3PU-11	2.25	8.46	0.0383
	3PU-19	2.12	7.86	0.0358
	3PU-27	1.98	8.20	0.0356
	3PU-15	1.88	7.64	0.0335
	3PU-35	1.77	7.11	0.0313
$\frac{1}{2}$-T	3PU-4	1.14	5.87	0.0232
	3PU-12	1.08	5.47	0.0218
	3PU-20	1.02	5.08	0.0204
	3PU-24	0.95	5.26	0.0202
	3PU-31	0.90	4.89	0.0189
	3PU-36	0.85	4.55	0.0177

TABLE C5

EXPOSURE PARAMETERS FOR CHARPY SPECIMENS

Location	Sample Identification	$\phi t(E>1)$ 10^{19}n/cm^2	$\phi t(E>0.1)$ 10^{19}n/cm^2	dpa
		F23 PLATE (A302B)		
SSC-1 (Left)	F23-1	2.69	7.58	0.0396
	F23-8	2.73	7.72	0.0402
	F23-25	2.74	7.75	0.0404
	F23-45	2.75	7.76	0.0405
	F23-77	2.75	7.76	0.0405
	F23-84	2.74	7.73	0.0404
	F23-91	2.71	7.62	0.0398
	F23-138	2.68	7.55	0.0394
	F23-145	2.65	7.44	0.0389
SSC-1 (Right)	F23-11	2.68	7.57	0.0395
	F23-18	2.72	7.70	0.0401
	F23-50	2.74	7.73	0.0404
	F23-70	2.74	7.75	0.0404
	F23-102	2.74	7.74	0.0404
	F23-109	2.73	7.71	0.0403
	F23-116	2.70	7.61	0.0397
	F23-163	2.67	7.53	0.0393
	F23-170	2.64	7.42	0.0389
SSC-2 (Left)	F23-5	5.67	16.1	0.0835
	F23-22	5.76	16.4	0.0849
	F23-42	5.79	16.4	0.0853
	F23-74	5.80	16.5	0.0855
	F23-81	5.80	16.4	0.0854
	F23-88	5.78	16.4	0.0852
	F23-95	5.71	16.2	0.0841
	F23-142	5.65	16.0	0.0832
	F23-76	5.59	15.8	0.0822
SSC-2 (Right)	F23-15	5.66	16.0	0.0833
	F23-47	5.75	16.3	0.0847
	F23-67	5.78	16.4	0.0851
	F23-99	5.79	16.4	0.0853
	F23-106	5.78	16.4	0.0852
	F23-113	5.77	16.4	0.0850
	F23-120	5.70	16.1	0.0839
	F23-167	5.64	16.0	0.0830
	F23-101	5.57	15.7	0.0820

TABLE C5 (Cont'd)

Location	Sample Identification	$\phi t(E > 1)$ $10^{19} n/cm^2$	$\phi t(E > 0.1)$ $10^{19} n/cm^2$	dpa
0-T (Left)	F23-2	4.12	11.6	0.0627
	F23-9	4.16	11.8	0.0634
	F23-39	4.16	11.8	0.0635
	F23-71	4.17	11.8	0.0636
	F23-78	4.16	11.8	0.0634
	F23-95	4.15	11.7	0.0632
	F23-92	4.10	11.6	0.0624
	F23-139	4.06	11.4	0.0618
	F23-7	4.01	11.3	0.0609
0-T (Right)	F23-12	3.93	11.1	0.0598
	F23-19	3.96	11.2	0.0604
	F23-64	3.97	11.2	0.0606
	F23-96	3.98	11.2	0.0606
	F23-103	3.97	11.2	0.0605
	F23-110	3.96	11.2	0.0603
	F23-117	3.91	11.0	0.0595
	F23-164	3.87	10.9	0.0589
	F23-17	3.83	10.7	0.0581
$\frac{1}{4}$-T (Left)	F23-3	2.32	8.67	0.0393
	F23-10	2.33	8.74	0.0396
	F23-40	2.33	8.74	0.0397
	F23-72	2.33	8.74	0.0396
	F23-79	2.33	8.69	0.0395
	F23-86	2.32	8.65	0.0393
	F23-93	2.28	8.49	0.0386
	F23-140	2.26	8.38	0.0381
	F23-24	2.23	8.25	0.0376
$\frac{1}{2}$-T (Right)	F23-13	2.22	8.32	0.0377
	F23-20	2.24	8.38	0.0380
	F23-65	2.24	8.38	0.0380
	F23-97	2.24	8.38	0.0380
	F23-104	2.23	8.33	0.0379
	F23-111	2.22	8.29	0.0377
	F23-118	2.19	8.14	0.0370
	F23-165	2.16	8.03	0.0366
	F23-49	2.14	7.91	0.0361

TABLE C5 (Cont'd)

Location	Sample Identification	$\phi t(E>1)$ $10^{19}n/cm^2$	$\phi t(E>0.1)$ $10^{19}n/cm^2$	dpa
½-T (Left)	F23-4	1.15	5.85	0.0233
	F23-21	1.16	5.86	0.0233
	F23-41	1.16	5.86	0.0233
	F23-73	1.16	5.85	0.0233
	F23-80	1.15	5.80	0.0231
	F23-87	1.14	5.76	0.0229
	F23-94	1.12	5.64	0.0225
	F23-141	1.11	5.56	0.0222
	F23-44	1.10	5.47	0.0219
½-T (Right)	F23-14	1.10	5.60	0.0222
	F23-46	1.11	5.61	0.0223
	F23-66	1.11	5.61	0.0223
	F23-98	1.10	5.60	0.0222
	F23-105	1.10	5.55	0.0221
	F23-112	1.09	5.51	0.0219
	F23-119	1.07	5.39	0.0215
	F23-166	1.06	5.32	0.0212
	F23-69	1.05	5.23	0.0209
		3P PLATE (A533B)		
SSC-1 (Left)	3PU-1	2.61	7.32	0.0383
	3PU-2	2.56	7.19	0.0377
	3PU-3	2.46	6.86	0.0361
	3PU-4	2.40	6.71	0.0352
	3PU-5	2.34	6.47	0.0342
SSC-1 (Right)	3PU-17	2.60	7.30	0.0382
	3PU-18	2.56	7.17	0.0376
	3PU-19	2.46	6.85	0.0360
	3PU-20	2.40	6.69	0.0351
	3PU-21	2.33	6.45	0.0341
SSC-2 (Left)	3PT-6	5.51	15.5	0.0809
	3PT-7	5.41	15.2	0.0796
	3PT-8	5.20	14.5	0.0762
	3PT-9	5.07	14.2	0.0742
	3PT-10	4.94	13.7	0.0721

TABLE C5 (Cont'd)

Location	Sample Identification	$\phi t(E>1)$ 10^{19}n/cm^2	$\phi t(E>0.1)$ 10^{19}n/cm^2	dpa
SSC-2 (Right)	3PT-22	5.49	15.5	0.0807
	3PT-23	5.40	15.2	0.0794
	3PT-24	5.19	14.5	0.0760
	3PT-25	5.06	14.2	0.0740
	3PT-26	4.93	13.7	0.0719
0-T (Left)	3PU-6	3.95	11.1	0.0600
	3PU-7	3.89	10.8	0.0589
	3PU-8	3.73	10.3	0.0562
	3PU-9	3.63	10.0	0.0547
	3PU-10	3.53	9.7	0.0531
0-T (Right)	3PU-22	3.77	10.6	0.0572
	3PU-23	3.71	10.3	0.0562
	3PU-24	3.55	9.8	0.0536
	3PU-25	3.46	9.5	0.0522
	3PU-26	3.37	9.2	0.0506
$\frac{1}{4}$-T (Left)	3PU-11	2.20	8.09	0.0370
	3PU-12	2.16	7.92	0.0363
	3PU-13	2.07	7.52	0.0346
	3PU-14	2.02	7.29	0.0337
	3PU-15	1.97	7.04	0.0326
$\frac{1}{4}$-T (Right)	3PU-27	2.11	7.75	0.0355
	3PU-28	2.07	7.60	0.0348
	3PU-29	1.99	7.21	0.0332
	3PU-30	1.94	6.99	0.0323
	3PU-31	1.89	6.75	0.0313
$\frac{1}{2}$-T (Left)	3PT-1	1.08	5.37	0.0215
	3PT-2	1.06	5.25	0.0211
	3PT-3	1.02	4.99	0.0201
	3PT-4	1.00	4.84	0.0196
	3PT-5	0.98	4.68	0.0190
$\frac{1}{2}$-T (Right)	3PT-17	1.03	5.13	0.0206
	3PT-18	1.02	5.02	0.0202
	3PT-19	0.98	4.77	0.0192
	3PT-20	0.96	4.63	0.0187
	3PT-21	0.93	4.47	0.0182

TABLE C5 (Cont'd)

Location	Sample Identification	$\phi t(E>1)$ 10^{19}n/cm^2	$\phi t(E>0.1)$ 10^{19}n/cm^2	dpa
		CODE K FORGING (22NiMoCr37)		
SSC-1 (Left)	K-512	1.86	5.90	0.0292
	K-513	1.84	5.81	0.0288
	K-514	1.81	5.72	0.0283
	K-62	1.71	5.36	0.0267
	K-63	1.67	5.24	0.0260
	K-64	1.63	5.05	0.0253
SSC-1 (Right)	K-65	1.86	5.88	0.0291
	K-66	1.84	5.80	0.0287
	K-67	1.81	5.71	0.0283
	K-515	1.78	5.61	0.0278
	K-610	1.74	5.48	0.0272
	K-611	1.71	5.35	0.0266
	K-612	1.67	5.23	0.0259
	K-613	1.62	5.04	0.0252
SSC-2 (Left)	K-614	3.93	12.5	0.0615
	K-615	3.88	12.3	0.0608
	K-72	3.83	12.1	0.0598
	K-74	3.61	11.4	0.0563
	K-75	3.52	11.1	0.0549
	K-76	3.43	10.7	0.0533
SSC-2 (Right)	K-77	3.92	12.5	0.0614
	K-710	3.87	12.3	0.0606
	K-711	3.82	12.1	0.0597
	K-73	3.75	11.9	0.0587
	K-712	3.68	11.6	0.0575
	K-713	3.60	11.3	0.0562
	K-714	3.52	11.1	0.0547
	K-715	3.42	10.7	0.0532
0-T (Left)	K-410	3.13	10.3	0.0507
	K-411	3.09	10.1	0.0500
	K-412	3.05	9.9	0.0492
	K-414	2.88	9.3	0.0462
	K-415	2.80	9.0	0.0449
	K-52	2.72	8.7	0.0435

TABLE C5 (Cont'd)

Location	Sample Identification	$\phi t(E>1)$ 10^{19}n/cm^2	$\phi t(E>0.1)$ 10^{19}n/cm^2	dpa
0-T (Right)	K-53	2.99	9.8	0.0484
	K-54	2.95	9.7	0.0477
	K-55	2.91	9.5	0.0470
	K-413	2.86	9.3	0.0461
	K-56	2.80	9.1	0.0451
	K-57	2.74	8.8	0.0440
	K-510	2.67	8.6	0.0428
	K-511	2.60	8.3	0.0415
¼-T (Left)	K-36	1.67	7.07	0.0304
	K-37	1.65	6.96	0.0300
	K-310	1.62	6.82	0.0295
	K-312	1.53	6.35	0.0276
	K-313	1.49	6.15	0.0268
	K-314	1.45	5.94	0.0260
¼-T (Right)	K-315	1.60	6.78	0.0291
	K-42	1.58	6.67	0.0287
	K-43	1.56	6.54	0.0282
	K-311	1.53	6.41	0.0277
	K-44	1.50	6.25	0.0271
	K-45	1.47	6.08	0.0264
	K-46	1.43	5.90	0.0257
	K-47	1.39	5.69	0.0249
½-T (Left)	K-24	0.813	4.61	0.0175
	K-25	0.803	4.53	0.0173
	K-26	0.791	4.45	0.0170
	K-210	0.749	4.14	0.0159
	K-211	0.732	4.01	0.0154
	K-212	0.714	3.88	0.0150
½-T (Right)	K-213	0.777	4.41	0.0168
	K-214	0.768	4.34	0.0165
	K-215	0.756	4.25	0.0162
	K-27	0.744	4.16	0.0159
	K-32	0.730	4.06	0.0156
	K-33	0.716	3.95	0.0152
	K-34	0.700	3.83	0.0148
	K-35	0.683	3.71	0.0143

TABLE C5 (Cont'd)

Location	Sample Identification	$\phi t(>1)$ $10^{19}n/cm^2$	$\phi t(E>0.1)$ $10^{19}n/cm^2$	dpa
	CODE MO FORGING (A508-3)			
SSC-1 (Left)	MO-01	1.91	6.07	0.0300
	MO-02	1.91	6.06	0.0299
	MO-03	1.90	6.04	0.0298
	MO-04	1.89	6.01	0.0297
	MO-05	1.88	5.96	0.0295
SSC-1 (Right)	MO-06	1.89	6.02	0.0297
	MO-07	1.90	6.04	0.0298
	MO-08	1.91	6.05	0.0299
	MO-09	1.91	6.06	0.0299
	MO-10	1.90	6.05	0.0299
	MO-11	1.90	6.03	0.0298
	MO-12	1.89	5.99	0.0296
	MO-13	1.88	5.95	0.0294
SSC-2 (Left)	MO-53	4.04	12.9	0.0633
	MO-54	4.03	12.8	0.0632
	MO-55	4.02	12.8	0.0630
	MO-56	4.00	12.7	0.0627
	MO-57	3.97	12.6	0.0622
SSC-2 (Right)	MO-58	3.99	12.8	0.0626
	MO-59	4.01	12.8	0.0630
	MO-60	4.02	12.8	0.0631
	MO-61	4.03	12.8	0.0631
	MO-62	4.02	12.8	0.0630
	MO-63	4.01	12.8	0.0628
	MO-64	3.99	12.7	0.0625
	MO-65	3.96	12.6	0.0620
0-T (Left)	MO-14	3.21	10.6	0.0521
	MO-15	3.21	10.6	0.0521
	MO-16	3.20	10.5	0.0519
	MO-17	3.18	10.5	0.0516
	MO-18	3.16	10.4	0.0512

TABLE C5 (Cont'd)

Location	Sample Identification	$\phi t(E>1)$ $10^{19}n/cm^2$	$\phi t(E>0.1)$ $10^{19}n/cm^2$	dpa
0-T (Right)	MO-19	3.06	10.1	0.0496
	MO-20	3.06	10.1	0.0497
	MO-21	3.07	10.1	0.0497
	MO-22	3.06	10.1	0.0497
	MO-23	3.06	10.1	0.0496
	MO-24	3.05	10.0	0.0495
	MO-25	3.04	10.0	0.0492
	MO-26	3.02	9.9	0.0488
$\frac{1}{4}$-T (Left)	MO-27	1.72	7.36	0.0315
	MO-28	1.72	7.33	0.0314
	MO-29	1.71	7.30	0.0313
	MO-30	1.70	7.24	0.0311
	MO-31	1.69	7.16	0.0308
$\frac{1}{4}$-T (Right)	MO-32	1.65	7.07	0.0303
	MO-33	1.66	7.07	0.0303
	MO-34	1.66	7.07	0.0303
	MO-35	1.65	7.06	0.0302
	MO-36	1.65	7.03	0.0301
	MO-37	1.64	7.00	0.0300
	MO-38	1.63	6.94	0.0298
	MO-39	1.62	6.87	0.0295
$\frac{1}{2}$-T (Right)	MO-40	0.843	4.84	0.0183
	MO-41	0.840	4.81	0.0182
	MO-42	0.835	4.78	0.0181
	MO-43	0.829	4.73	0.0179
	MO-44	0.821	4.67	0.0178
$\frac{1}{2}$-T (Left)	MO-45	0.809	4.65	0.0176
	MO-46	0.809	4.65	0.0176
	MO-47	0.808	4.64	0.0175
	MO-48	0.806	4.63	0.0175
	MO-49	0.803	4.60	0.0174
	MO-50	0.798	4.57	0.0173
	MO-51	0.793	4.53	0.0172
	MO-52	0.785	4.47	0.0170

TABLE C5 (Cont'd)

Location	Sample Identification	$\phi t(E > 1)$ $10^{19} n/cm^2$	$\phi t(E > 0.1)$ $10^{19} n/cm^2$	dpa
		CODE EC WELD (A533B)		
SSC-1 (Left)	EC-1	1.73	5.44	0.0270
	EC-2	1.76	5.56	0.0275
	EC-3	1.82	5.77	0.0285
	EC-4	1.85	5.86	0.0289
	EC-5	1.87	5.93	0.0293
	EC-6	1.88	5.99	0.0295
SSC-1 (Right)	EC-7	1.72	5.43	0.0269
	EC-8	1.76	5.55	0.0275
	EC-9	1.82	5.76	0.0285
	EC-10	1.84	5.85	0.0289
	EC-11	1.86	5.91	0.0292
	EC-12	1.88	5.98	0.0295
SSC-2 (Left)	EC-49	3.64	11.5	0.0569
	EC-50	3.71	11.8	0.0581
	EC-51	3.84	12.2	0.0602
	EC-52	3.90	12.4	0.0610
	EC-53	3.94	12.6	0.0618
	EC-54	3.98	12.7	0.0623
SSC-2 (Right)	EC-55	3.63	11.5	0.0568
	EC-56	3.70	11.8	0.0580
	EC-57	3.83	12.2	0.0601
	EC-58	3.89	12.4	0.0609
	EC-59	3.93	12.5	0.0616
	EC-60	3.97	12.7	0.0622
0-T (Left)	EC-13	3.01	9.8	0.0486
	EC-14	3.06	10.0	0.0493
	EC-15	3.13	10.3	0.0506
	EC-16	3.15	10.4	0.0511
	EC-17	3.18	10.4	0.0515
	EC-18	3.19	10.5	0.0518
0-T (Right)	EC-19	2.87	9.4	0.0464
	EC-20	2.91	9.5	0.0471
	EC-21	2.98	9.8	0.0483
	EC-22	3.01	9.9	0.0487
	EC-23	3.03	10.0	0.0491
	EC-24	3.05	10.0	0.0494

TABLE C5 (Cont'd)

Location	Sample Identification	$\phi t(E > 1)$ $10^{19} n/cm^2$	$\phi t(E > 0.1)$ $10^{19} n/cm^2$	dpa
¼-T (Left)	EC-25	1.64	6.91	0.0298
	EC-26	1.66	7.02	0.0302
	EC-27	1.69	7.20	0.0309
	EC-28	1.70	7.27	0.0311
	EC-29	1.71	7.32	0.0313
	EC-30	1.72	7.35	0.0315
¼-T (Right)	EC-31	1.57	6.63	0.0285
	EC-32	1.59	6.73	0.0289
	EC-33	1.62	6.90	0.0296
	EC-34	1.63	6.97	0.0298
	EC-35	1.64	7.02	0.0300
	EC-36	1.65	7.05	0.0302
½-T (Left)	EC-37	0.814	4.62	0.0176
	EC-38	0.824	4.70	0.0179
	EC-39	0.838	4.81	0.0182
	EC-40	0.842	4.84	0.0183
	EC-41	0.844	4.85	0.0183
	EC-42	0.846	4.85	0.0184
½-T (Right)	EC-43	0.778	4.42	0.0168
	EC-44	0.788	4.49	0.0171
	EC-45	0.802	4.60	0.0174
	EC-46	0.806	4.62	0.0175
	EC-47	0.807	4.64	0.0175
	EC-48	0.809	4.64	0.0176
		CODE R WELD (A533B)		
SSC-1 (Left)	R1	2.42	6.78	0.0356
	R2	2.48	6.96	0.0365
	R3	2.53	7.12	0.0372
	R4	2.58	7.27	0.0380
	R6	2.62	7.38	0.0386
	R7	2.66	7.50	0.0391

TABLE C5 (Cont'd)

Location	Sample Identification	$\phi t(E > 1)$ $10^{19} n/cm^2$	$\phi t(E > 0.1)$ $10^{19} n/cm^2$	dpa
SSC-1 (Right)	R8	2.42	6.76	0.0355
	R9	2.48	6.95	0.0364
	R11	2.53	7.10	0.0372
	R12	2.58	7.25	0.0379
	R13	2.61	7.37	0.0385
	R14	2.65	7.48	0.0390
SSC-2 (Left)	R31	5.11	14.4	0.0751
	R32	5.24	14.8	0.0769
	R33	5.34	15.1	0.0786
	R34	5.45	15.4	0.0801
	R36	5.53	15.6	0.0814
	R37	5.61	15.9	0.0825
SSC-2 (Right)	R38	5.10	14.3	0.0749
	R39	5.23	14.7	0.0768
	R41	5.33	15.1	0.0784
	R42	5.43	15.4	0.0799
	R43	5.52	15.6	0.0812
	R44	5.60	15.9	0.0823
0-T (Left)	R46	3.84	10.7	0.0582
	R47	3.90	10.9	0.0592
	R48	3.96	11.1	0.0601
	R49	4.01	11.3	0.0609
	R51	4.05	11.4	0.0616
	R52	4.09	11.5	0.0622
0-T (Right)	R53	3.67	10.2	0.0555
	R54	3.72	10.4	0.0565
	R56	3.78	10.6	0.0573
	R57	3.83	10.8	0.0581
	R58	3.86	10.9	0.0588
	R59	3.90	11.0	0.0593
$\frac{1}{4}$-T (Left)	R16	2.18	8.04	0.0368
	R17	2.22	8.19	0.0374
	R18	2.24	8.32	0.0379
	R19	2.27	8.44	0.0384
	R21	2.29	8.53	0.0388
	R22	2.30	8.61	0.0391

TABLE C5 (Cont'd)

Location	Sample Identification	$\phi t(E > 1)$ $10^{19} n/cm^2$	$\phi t(E > 0.1)$ $10^{19} n/cm^2$	dpa
¼-T (Right)	R23	2.09	7.71	0.0353
	R24	2.12	7.86	0.0358
	R26	2.15	7.98	0.0363
	R27	2.17	8.09	0.0368
	R28	2.19	8.18	0.0372
	R29	2.21	8.26	0.0375
½-T (Left)	R68	1.10	5.45	0.0219
	R69	1.11	5.57	0.0223
	R71	1.13	5.67	0.0227
	R72	1.14	5.75	0.0229
	R73	1.15	5.80	0.0231
	R74	1.15	5.83	0.0232
½-T (Right)	R76	1.05	5.22	0.0209
	R77	1.06	5.33	0.0213
	R78	1.08	5.42	0.0217
	R79	1.09	5.50	0.0219
	R81	1.10	5.55	0.0221
	R82	1.10	5.58	0.0222

Table C5 presents the exposure parameter values for all the individual Charpy specimens organized by groups. The values are given at the notch tip. The tensile specimens are presented separately in Table C6. Each tensile specimen exposure parameter value is calculated at the center of the specimen, 0.77 cm from the capsule y centerline.

As indicated above, the values in Tables C2 through C6 are obtained by taking the composit centerline values given in Table C1 and multiplying by the x, y, and z composite gradient factors obtained by averaging the ORNL and HEDL factors. The additional uncertainty contributed by uncertainties in the gradient factors is relatively small. Overall uncertainties on the values in Tables C2 through C6 can be conservatively estimated to be ±8% for $\phi t(E > 1)$, ±12% for $\phi t(E > 0.1)$, and ±9% for dpa. The uncertainties in the thermal values in Table C2 are about ±16%.

The exposure parameter values in this Appendix are the final HEDL recommended values, as evaluated using the preliminary ORNL evaluation and the final HEDL evaluation. As stated above this set of recommended values was adopted in order to minimize the impact of the various assumptions made by the two evaluations. Since this composite evaluation was completed, ORNL has updated their evaluation as is detailed in Section 4.2. This final ORNL analysis shows better agreement for some parameters and worse agreement for others, but overall agreement (except for thermal fluence which ORNL now includes) is not much changed from the values discussed above. Therefore, the statement in Section 4.2 that the difference between the evaluations is of little consequence for damage correlations is agreed with here and experimenters are free to use either the composit HEDL recommendation as tabulated in this appendix or the revised ORNL values in Section 4.2.

One other change between the revised ORNL values and those reported in this appendix should be noted, however. The revised values are assigned generally lower uncertainty values [in the case of $\phi t(E > 0.1$ MeV) a factor of two lower]. Agreement between the two PSF evaluations notwithstanding, the ORNL uncertainty estimates must be regarded as non-conservative unless the Lepricon-LSL technique used can be validated over a suitable range of environments.

The thermal flux uncertainty estimates seem to be particularly low in both evaluations. A revised co-variance matrix* for the low energy flux spectrum has recently been introduced into the FERRET code and this more conservative uncertainty assumption indicates typical uncertainties in thermal fluence evaluations to be ±30%, which appears more realistic.

---

* In this revised co-variance matrix, the calculated a priori thermal flux values are assigned an additional 100% uncertainty.

TABLE C6

EXPOSURE PARAMETERS FOR TENSILE SPECIMENS

Location	Sample Identification	$\phi t(E > 1)$ $10^{19} n/cm^2$	$\phi t(E > 0.1)$ $10^{19} n/cm^2$	dpa
		F23 PLATE (A302B)		
SSC-1	F23-T1	2.58	7.41	0.0383
	F23-T6	2.61	7.51	0.0389
	F23-T7	2.59	7.43	0.0385
	F23-T23	2.57	7.39	0.0382
	F23-T16	2.58	7.41	0.0384
SSC-2	F23-T5	5.43	15.7	0.0808
	F23-T13	5.52	15.9	0.0821
	F23-T11	5.46	15.7	0.0812
	F23-T27	5.42	15.7	0.0806
	F23-T20	5.45	15.7	0.0811
0-T	F23-T2	3.99	11.5	0.0613
	F23-T28	4.02	11.6	0.0617
	F23-T8	3.98	11.5	0.0611
	F23-T24	3.81	11.0	0.0585
	F23-T17	3.80	11.0	0.0583
$\frac{1}{4}$-T	F23-T3	2.23	8.51	0.0383
	F23-T12	2.24	8.53	0.0384
	F23-T9	2.21	8.38	0.0378
	F23-T25	2.14	8.16	0.0367
	F23-T18	2.12	8.04	0.0362
$\frac{1}{2}$-T	F23-T4	1.11	5.71	0.0225
	F23-T21	1.10	5.69	0.0225
	F23-T10	1.08	5.57	0.0220
	F23-T26	1.06	5.46	0.0215
	F23-T19	1.04	5.32	0.0210
		3P PLATE (A533B)		
SSC-1	3PT-T1	2.39	6.80	0.0354
	3PT-T12	2.38	6.78	0.0353
SSC-2	3PT-T5	5.04	14.4	0.0747
	3PT-T8	5.03	14.4	0.0745

TABLE C6 (Cont'd)

Location	Sample Identification	$\phi t(E > 1)$ $10^{19} n/cm^2$	$\phi t(E > 0.1)$ $10^{19} n/cm^2$	dpa
0-T	3PT-T2	3.68	10.4	0.0560
	3PT-T11	3.51	9.9	0.0534
¼-T	3PT-T3	2.03	7.55	0.0344
	3PT-T12	1.95	7.24	0.0330
½-T	3PT-T4	1.000	4.99	0.0200
	3PT-T13	0.956	4.78	0.0191
	CODE K FORGING (22NiMoCr37)			
SSC-1	K-98	1.87	5.82	0.0291
	K-99	1.84	5.75	0.0285
SSC-2	K-910	3.96	12.3	0.0614
	K-911	3.88	12.2	0.0601
0-T	K-96	3.11	9.9	0.0497
	K-97	3.05	9.8	0.0487
¼-T	K-93	1.67	6.85	0.0298
	K-95	1.63	6.69	0.0292
½-T	K-91	0.814	4.47	0.0172
	K-92	0.799	4.36	0.0168
	CODE MO FORGING (A508-3)			
SSC-1	MO-1	2.00	6.24	0.0310
	MO-2	2.01	6.27	0.0312
	MO-3	2.01	6.28	0.0313
SSC-2	MO-13	4.21	13.2	0.0655
	MO-14	4.23	13.3	0.0658
	MO-15	4.24	13.3	0.0660
0-T	MO-4	3.33	10.7	0.0535
	MO-5	3.33	10.7	0.0536
	MO-6	3.34	10.8	0.0537
¼-T	MO-7	1.80	7.56	0.0326
	MO-8	1.80	7.56	0.0326
	MO-9	1.80	7.56	0.0326

TABLE C6 (Cont'd)

Location	Sample Identification	$\phi t(E > 1)$ $10^{19} n/cm^2$	$\phi t(E > 0.1)$ $10^{19} n/cm^2$	dpa
½-T	MO-10	0.884	4.99	0.0190
	MO-11	0.884	4.99	0.0190
	MO-12	0.884	4.98	0.0190
		CODE EC WELD (A533B)		
SSC-1	ET-1	1.89	5.88	0.0293
	ET-2	1.88	5.87	0.0292
SSC-2	ET-10	3.98	12.5	0.0618
	ET-11	3.97	12.4	0.0616
0-T	ET-3	3.21	10.3	0.0515
	ET-4	3.06	9.8	0.0491
¼-T	ET-5	1.75	7.30	0.0316
	ET-6	1.68	7.00	0.0303
½-T	ET-7	0.870	4.89	0.0187
	ET-9	0.832	4.68	0.0179
		CODE R WELD (A533B)		
SSC-1	R88T	2.24	6.37	0.0332
	R89T	2.24	6.35	0.0331
SSC-2	R64T	4.73	13.5	0.0701
	R65T	4.72	13.5	0.0699
0-T	R62T	3.64	10.3	0.0555
	R63T	3.47	9.9	0.0529
¼-T	R86T	2.06	7.70	0.0350
	R87T	1.98	7.38	0.0335
½-T	R84T	1.031	5.18	0.0206
	R85T	0.986	4.95	0.0197

A P P E N D I X D

ORNL RECOMMENDED EXPOSURE PARAMETER VALUES FOR THE PSF BLIND TEST

A P P E N D I X D

D1 ORNL RECOMMENDED EXPOSURE VALUES FOR THE PSF BLIND TEST

F. W. Stallmann

The original ORNL data that are used in Appendix C were revised and are published in Reference (St84). A discussion of the differences between the final ORNL and the HEDL evaluation is given in Section 2.2 of (Mc86b). This section also contains a complete tabulation of the ORNL recommended exposure parameter values; and they need not, therefore, be repeated here.

DISTRIBUTION

DOE-HQ/Office of Asst Secretary
for Nuclear Energy
NE-1, FORS
Washington, DC 20585

AD Rossin, Asst Secretary

DOE-RL/AMF
Laboratory Management & Technology
Services Branch
P.O. Box 550, FED/513
Richland, WA 99352

DK Jones, Chief

American Society
for Testing & Materials
1916 Race Street
Philadelphia, PA 19103

M. Lieff

Ames Laboratory
Iowa State University
Ames, IA 50010

MS Wechsler

APTECH Engineering Services
795 San Antonio Road
Palo Alto, CA 94303

PD Hedgecock

Argonne National Laboratory-East
9700 South Cass Avenue
Argonne, IL 60439

LR Greenwood

Arizona State University (2)
College of Eng & Applied Science
Tempe, AZ 85287

JW McKlveen
G. Stewart

Arkansas Power and Light
P.O. Box 551
Little Rock, AK 72203

O. Cypret

Babcock & Wilcox Co (6)
Lynchburg Research Center
P.O. Box 11165
Lynchburg, VA 24506-1165

LL Collins
SQ King
AA Lowe Jr
DA Nitti
N. Snidow
F. Walters

Baltimore Gas & Electric Co
Lexington and Liberty Streets
P.O. Box 1475
Baltimore, MD 21203

E. Titland

DISTRIBUTION (Cont'd)

Battelle
Pacific Northwest Laboratory (35)
P.O. Box 999
Richland, WA 99352

R. Allen
J. Barner
A. Burtron
TT Claudson
DG Doran
M. Freshley
R. Gold
GL Guthrie
B. Johnson
LS Kellogg
WN McElroy (20)
WC Morgan
CC Preston
JTA Roberts
LC Schmid
J. Straalsund

Battelle Memorial Institute
Office of Nuclear Waste Isolation
505 King Avenue
Columbus, OH 43201

MP Manahan
JS Perrin

Bechtel Power Corporation
15740 Shady Grove Road
Gaithersburg, MD 20760

WC Hopkins

Boeing Computer
Services Richland, Inc. (2)
P.O. Box 300
Richland, WA 99352

JM Dahlke
NE Kenny

Brookhaven National Laboratory
Upton, Long Island, NY 11973

J. Carew

Carolina Power & Light Co
P.O. Box 1551
Raleigh, SC 27602

SP Grant

Central Electricity Generating Board (4)
Research Division
Berkeley Nuclear Laboratories
Berkeley, Gloucestershire GL13 9PB, UK

BJ Darlaston
TE Lewis
PJ Heffer
J. Young

Centre d'Etude de l'Energie Nucléaire
Studiecentrum voor Kernenergie (7)
Boeretang 200
B-2400 Mol, Belgium

J. Debrue
G. DeLeeuw
S. DeLeeuw
PJ D'hondt
A. Fabry
G. Minsart
Ph Van Asbroeck

CNEA
DPTO de Materiales, C.A.C.
Avda del Libertador 8250
1429 Buenos Aires, Argentina

M. Mondino

Combustion Engineering Inc (2)
1000 Prospect Hill Road
Windsor, CT 06095

S. Byrne
G. Cavanaugh

DISTRIBUTION (Cont'd)

Comitato Nazional per l'Energia Nuclere
Centro di Studi Nucleari della Casaccia
Casella Postale 2400
I-00060 Santa Maria di Galeria
Rome, Italy

M. Petille

Commissariat a l'Energie Atomique
Centre d'Etudes Nucleaires de Saclay (2)
Boite Postale 2
F-91190 Gif-sur-Yvette, France

AA Alberman
P. Soulat

Commissariat a l'Energie Atomique
Centre d'Etudes Nucleaires de Cadarache
F-13115 St Paul Lez Durance, France

JP Genthon

Commissariat a l'Energie Atomique
Service des Transfers Thermiques
F-38401 Grenoble, France

P. Mas

Commonwealth Edison
P.O. Box 767
Chicago, IL 60690

E. Steeve

Consolidated Edison of NY
4 Irving Place
Room 1515S
New York, NY 10003

S. Rothstein

Consumers Power
1945 W. Parnall Road
Jackson, MI 49201

H. Slager

EG&G Idaho, Inc (2)
P.O. Box 1625
Idaho Falls, ID 83415

CW Frank
JW Rogers

Electric Power Research Institute (4)
3412 Hillview Avenue
P.O. Box 10412
Palo Alto, CA 94304

T. Griesbach O. Ozer
TU Marston JJ Taylor

Energieonderzoek Centrum Nederland (2)
Netherlands Energy Research Foundation
Westerdionweg 3
Postfach 1
NL-1755 ZG, Petten, The Netherlands

H. Rottger
WL Zijp

Ente Nazionale per l'Energia Elettica
Italian Atomic Power Authority
National Electric Energy Agency
Viale Regina Margherita 137
Rome, Italy

M. Galliani

DISTRIBUTION (Cont'd)

EURATOM
European Atomic Energy Community
Materials Science Division
Joint Research Center Ispra
I-21020 Ispra, Varese, Italy

R. Dierckx

Florida Power & Light (2)
9250 W. Flager Street
P.O. Box 52100
Miami, FL 33152

S. Collard
JB Sun

GKSS-Forschungszentrum Geesthacht GmbH (3)
Max-Planck-Strasse
Postfach 1160
D-2054 Geesthacht,
Federal Republic of Germany

J. Ahlf W. Spalthoff
GM Richter

General Electric Company
Vallecitos Nuclear Center-103
P.O. Box 460
Vallecitos Road
Pleasanton, CA 94566

GC Martin

General Public Utilities
100 Interpace Parkway
Parsippany, NJ 07054

AP Rochina

Grove Engineering
P.O. Box 720
Washington Grove, MD 20880

CA Negin

Helgeson Scientific Services
5587 Sunol Blvd
Pleasanton, CA 94566

WH Zimmer

Institut für Kernenergetik
und Energiesysteme (2)
Pfaffenwaldring 31
Postfach 801140
D-7000 Stuttgart 80 (Vaihingen),
Federal Republic of Germany

G. Hehn
G. Prillinger

International Atomic Energy Agency (3)
Wagramerstrasse 5, Postfach 100
A-1400 Vienna, Austria

A. Sinev JJ Schmidt
NA Titkov

IRT Corporation (2)
P.O. Box 80817
San Diego, CA 92183

NL Lurie
WE Selph

DISTRIBUTION (Cont'd)

Japan Atomic Energy Research Institute
Tokai Research Establishment
Tokai-mura, Naka-gun
Ibaraki-ken, 319-11 Japan

S. Mizazono

Institut für Festkorperforschung der
Kernforschungsanlage Jülich GmbH (3)
Postfach 1913
D-517 Jülich 1,
Federal Republic of Germany

G. Borchardt L. Weise
D. Pachur

Kraftwerk Union Aktiengesellschaft (3)
Postfach 3220
D-8520 Erlangen,
Federal Republic of Germany

A. Gerscha C. Leitz
J. Koban

La Societe FRAMATOME
Tour Fiat-Cedex 16
92084 Paris La Defense, France

C. Buchalet

Lawrence Livermore National Laboratory (2)
P.O. Box 808
Livermore, CA 94550

M. Guinan
R. Van Konynenburg

Los Alamos National Laboratory (2)
P.O. Box 1663
Los Alamos, NM 87545

GE Hansen
L. Stewart

Maine Yankee Atomic Power Company
Edison Drive
Augusta, MA 04336

HF Jones

Materials Engineering Associates Inc (2)
111 Mel-Mara Drive
Oxen Hill, MD 20745

JR Hawthorne
FJ Loss

Metrology Control Corporation
P.O. Box 944
Richland, WA 99352

JH Roberts

National Bureau of Standards (3)
Gaithersburg, MD 20899

JA Grundl ED McGarry
G. Lamaze

Naval Research Laboratory
Engineering Materials Division
Thermostructural Materials Branch
Code 6390
Washington, DC 20375

LE Steele

DISTRIBUTION (Cont'd)

Northeast Utilities Service Co (3)
P.O. Box 270
Hartford, CT 06101

MF Ahern
JF Ely
M. Kupinski

Northern States Power
414 Nicollet Mall
Minneapolis, MN 55401

G. Neils

Nuclear Regulatory Commission
Office of Nuclear Regulatory Research (7)
Division of Engineering Technology
Materials Engineering Branch
NL-5650
Washington, DC 20555

R. Alexander
W. Hazelton
L. Lois
PN Randall
CZ Serpan, Chief
A. Toboada
M. Vagin

Nuclear Regulatory Commission
Office of Nuclear Reactor Regulation
Division of Safety Review and Oversight
Engineering Issues Branch
Washington, DC 20555

RE Johnson

Oak Ridge National Laboratory (4)
P.O. Box X
Oak Ridge, TN 37830

FBK Kam
RE Maerker
LS Miller
FW Stallmann

Omaha Public Power District
1623 Harney Street
Omaha, NE 68102

J. Gasper

RACAH Institute of Physics
The Hebrew University
91904 Jerusalam, Israel

JJ Wagschal

Radiation Research Associates
3550 Hulen Street
Fort Worth, TX 76107

RM Rubin

Rochester & Electric Corp
Supervisor of Material Engineering
89 East Avenue
Rochester, NY 14649

AE Curtiss III

Rockwell International
Rocketdyne Division (2)
6633 Canoga Avenue
Canoga Park, CA 91304

H. Farrar
BM Oliver

Rolls-Royce & Associates Ltd (4)
P.O. Box 31
Derby DE2 8BJ, UK

M. Austin
R. Squires
AF Thomas
TJ Williams

DISTRIBUTION (Cont'd)

Royal Naval College
Dept of Nucl Science & Technology
Greenwich, London SE10 9NN, UK

JRA Lakey

S.A. Cockerill-Ougree
Recherches et Developments
Division de la Construction Mecanique
B-4100 Serraing, Belgium

J. Widart

Sandia National Laboratory
P.O. Box 5800, MS-6446
Albuquerque, NM 87059

L. Bustard

Science Applications, Inc
P.O. Box 2351
La Jolla, CA 92037

GL Simmons

Ship Research Institute
Tokai Branch Office
Tokai-mura, Naka-gun
Ibaraki-ken, 319-11 Japan

K. Takeuchi

Southwest Research Institute
6220 Calebra Road
P.O. Box 28510
San Antonio, TX 78284

PK Nair

Swiss Federal Institute
for Reactor Research
CH-5303 Würenlingen, Switzerland

F. Hegedus

United Kingdom Atomic Energy Authority
Atomic Energy Research Establishment
Harwell, Oxon OX11 ORA, UK

AJ Fudge

United Kingdom Atomic Energy Authority
Atomic Energy Establishment (5)
Winfrith, Dorchester, Dorset, UK

J. Butler
MD Carter
I. Curl
P. Miller
A. Packwood

United Kingdom
Nuclear Installations Inspectorate
Health and Safety Executive
Thames House North
Millbank, London SWIP 4QJ, UK

T. Currie

University of Arkansas (2)
Dept of Mechanical Engineering
Fayetteville, AR 72701

CO Cogburn
L. West

DISTRIBUTION (Cont'd)

University of California
at Santa Barbara (2)
Dept of Chem & Nucl Engineering
Santa Barbara, CA 93106

G. Lucas
GR Odette

University of Illinois
Urbana, IL 61801

JG Williams

University of London Research Center
Silwood Park
Sunnyhill, Ascot,
Berkshire SL5 7PY, UK

JA Mason

University of Tokyo
Dept of Nuclear Engineering
7-3-1, Hongo,
Bunkyo-ku, Tokyo, 113 Japan

M. Nakazawa

University of Virginia
Dept of Nuclear Engineering
Dept of Material Science
Charlottesvill, VA 22901

TG Williamson

Virginia Power and Light
P.O. Box 26666
Richmond, VA 23261

D. Hostetler

Westinghouse
Nuclear Energy Systems (6)
P.O. Box 355
Pittsburgh, PA 15230

SL Anderson
AH Fero
EP Lippincott
F. Lau
TR Mager
SE Yanichko

Westinghouse
Research and Development Center
1310 Beulah Road
Pittsburgh, PA 15235

FH Ruddy

Yankee Atomic Electric Co
1671 Worchester Road
Framingham, MA 01701

E. Biemiller

WHC (10)
P.O. Box 1970, W/C-123
Richland, WA 99352

HJ Anderson	W/C-28
RL Knecht	W/A-40
WF Sheely	W/C-44
FR Shober	W/E-3
RL Simons	W/A-57
HH Yoshikawa	W/C-44
Central Files	W/C-110
Documentation (3)	W/C-123

NRC FORM 335 (2:84) NRCM 1102 3201, 3202

U.S. NUCLEAR REGULATORY COMMISSION

BIBLIOGRAPHIC DATA SHEET

SEE INSTRUCTIONS ON THE REVERSE

1. REPORT NUMBER (Assigned by TIDC, add Vol. No., if any)
NUREG/CR-3320, VOL. 3
HEDL-TME 87-3

2. TITLE AND SUBTITLE
LWR PRESSURE VESSEL SURVEILLANCE DOSIMETRY IMPROVEMENT PROGRAM: PSF PHYSICS-DOSIMETRY PROGRAM

3. LEAVE BLANK

4. DATE REPORT COMPLETED
MONTH: July YEAR: 1987

5. AUTHOR(S)
Edited by W. N. McElroy and R. Gold

6. DATE REPORT ISSUED
MONTH: October YEAR: 1987

7. PERFORMING ORGANIZATION NAME AND MAILING ADDRESS (Include Zip Code)
Hanford Engineering Development Laboratory
P.O. Box 1970
Richland, WA 99352

8. PROJECT/TASK/WORK UNIT NUMBER

9. FIN OR GRANT NUMBER
B5988

10. SPONSORING ORGANIZATION NAME AND MAILING ADDRESS (Include Zip Code)
Division of Engineering
Office of Nuclear Regulatory Research
U.S. Nuclear Regulatory Commission
Washington, DC 20555

11a. TYPE OF REPORT
Technical

b. PERIOD COVERED (Inclusive dates)

12. SUPPLEMENTARY NOTES

13. ABSTRACT (200 words or less)

The metallurgical irradiation experiment at the Oak Ridge Research Reactor Poolside Facility (ORR-PSF) is one of the series of benchmark experiments in the framework of the Light Water Reactor Pressure Vessel Surveillance Dosimetry Improvement Program (LWR-PV-SDIP). The goal of this program is to test, against well-established benchmarks, the methodologies and data bases that are used to predict the irradiation embrittlement and fracture toughness of pressure vessel and support structure steels. The prediction methodology includes procedures for neutron physics calculations, dosimetry and spectrum adjustment methods, metallurgical tests, and damage correlations. The benchmark experiments serve to validate, improve, and standardize these procedures. The results of this program are implemented in a set of ASTM Standards on pressure vessel surveillance procedures. These, in turn, may be used as guides for the nuclear industry and for the Nuclear Regulatory Commission (NRC).

To serve as a benchmark, a very careful characterization of the ORR-PSF experiment is necessary, both in terms of neutron flux-fluence spectra and of metallurgical test results. Statistically determined uncertainties must be given in terms of variances and covariances to make comparisons between predictions and experimental results meaningful. Detailed descriptions of the PSF physics-dosimetry program and its results are reported.

14. DOCUMENT ANALYSIS – a. KEYWORDS/DESCRIPTORS
LWR pressure vessel surveillance
Physics-dosimetry
Dosimetry data base

b. IDENTIFIERS/OPEN-ENDED TERMS

15. AVAILABILITY STATEMENT
Unlimited

16. SECURITY CLASSIFICATION
(This page) Unclassified
(This report) Unclassified

17. NUMBER OF PAGES

18. PRICE

☆U.S. GOVERNMENT PRINTING OFFICE:1987-202-292:60231